Pathophysiological Characterization

of intra- and extracellularly aggregated

Amyloid Peptides in Dementias

Doctoral Thesis

In partial fulfillment of the requirements for the degree

"Doctor rerum naturalium (Dr. rer. nat.)"

in the Molecular Medicine Study Program

at the Georg-August-University Göttingen

submitted by

Anika Saul

born in Heilbad Heiligenstadt, Germany

Göttingen, April 2013

Members of the Thesis Committee

Supervisor

Prof. Dr. Thomas Bayer

Department of Psychiatry

University Medical Center, Georg-August-University, Göttingen

Second Member of the Thesis Committee

Prof. Dr. Mikael Simons

Department of Cellular Neuroscience

Max-Planck-Institute for Experimental Medicine, Göttingen

Third Member of the Thesis Committee

Prof. Dr. Alexander Flügel

Department of Neuroimmunology

University Medical Center, Georg-August-University, Göttingen

Date of disputation:

For

my family

Affidavit

I hereby declare that my doctoral thesis entitled **"Pathophysiological Characterization of intra- and extracellularly aggregated Amyloid Peptides in Dementias"** has been written independently with no other sources and aids than quoted.

Anika Saul

Göttingen, April 2013

List of Publications

Original Articles:

- **Saul, A.**, Lashley, T., Revesz, T., Holton, J., Ghiso, J. A., Coomaraswamy, J. & Wirths, O. 2013. Abundant pyroglutamate-modified ABri and ADan peptides in extracellular and vascular amyloid deposits in familial British and Danish dementias. *Neurobiol Aging*, 34, 1416-25.

- Härtig, W., **Saul, A.**, Kacza, J., Grosche, J., Goldhammer, S., Michalski, D. & Wirths, O. 2013. Immunolesion-induced loss of cholinergic projection neurons promotes beta-amyloidosis and tau hyperphosphorylation in the hippocampus of triple-transgenic mice. *Neuropathol Appl Neurobiol*, 9, 12050.

- **Saul, A.**, Sprenger, F., Bayer, T. A. & Wirths, O. 2013. Accelerated tau pathology with synaptic and neuronal loss in a novel triple transgenic mouse model of Alzheimer's disease. *Neurobiol Aging*, 5, 201-7.

Abstracts:

- **Saul A.**, Lashley T., Revesz T., Ghiso J., Coomaraswamy J., Bayer T.A. & Wirths O. 2011: Analysis of pyroglutamate-modified amyloid peptides in Familial British and Familial Danish dementia. *Neurodegenerative Diseases*, Vol. 8, Suppl. 1.

- Wirths O., Bayer T.A. & **Saul A.** 2013: ApoE Fragmentation is linked to Neuritic Dystrophy in Transgenic Mouse Models of Alzheimer's Disease. *Neurodegenerative Diseases*, Vol. 11, Suppl. 1.

Contents

3 Results   62

4 Discussion 111

Acknowledgement

Abstract

Alzheimer's Disease (AD) is the most common form of dementia in the elderly population and is neuropathologically characterized by hippocampal neurofibrillary degeneration, chronic inflammation as well as widespread parenchymal and vascular amyloid deposits. These features are remarkably similar to those seen in the heritable disorders Familial British (FBD) and Danish Dementias (FDD). Like β-amyloid (Aβ) in AD, ABri and ADan peptides are the main components of amyloid deposits in FBD and FDD, respectively, and are produced by proteolytic processing of mutant BRI2. These peptides start with an N-terminal glutamate, which can be post-translationally converted into a pyroglutamate- (pGlu-) modified form, a mechanism which is also valid for Aβ peptides in AD.

Like pGlu-Aβ, pGlu-ABri peptides showed an increased aggregation propensity and both pGlu-modified ABri and ADan exhibited a higher toxicity on human neuroblastoma cells as compared to their non-modified counterparts.

Novel antibodies, detecting the pGlu-modified forms of ABri and ADan peptides, were generated. Using these antibodies, abundant extracellular amyloid plaques, as well as vascular and parenchymal deposits were detected in human FBD and FDD brain tissue, as well as in a mouse model for FDD. Further immunostainings of human samples revealed that highly aggregated pGlu-ABri and pGlu-ADan peptides are mainly present in plaque cores and central vascular deposits, suggesting that these peptides have seeding properties. Furthermore, ADan peptides were detected in pre-synaptic terminals of the hippocampus from an FDD mouse model, where they might contribute to impaired synaptic transmission.

To investigate the direct role of ADan peptides on neuronal integrity, a novel mouse model was generated, expressing ADan1Q-34, that showed abundant intracellular transgene expression, especially in hippocampal and cortical regions. Animals obtained from different ADan1Q-34 transgenic lines showed an impaired spatial reference memory and changes in anxiety comparable to AD mouse models.

In addition to the pGlu-modification of Aβ peptides, another possible mechanism for enhanced amyloid aggregation in AD might be Apolipoprotein E (ApoE) proteolysis. The ApoE4 allele represents the most important risk factor for AD and due to its unique biochemical properties, ApoE4 is more susceptible to proteolysis resulting in the release of toxic fragments. So far, there is a mass of reports discussing the influence of ApoE and its

fragments on Aβ clearance and deposition, whereas the impact of Aβ on ApoE fragmentation has not been studied.

It could be shown that endogenous, murine ApoE becomes proteolytically processed in several dementia mouse models with amyloid pathology in a manner completely reflecting the human pattern. The major portion of murine ApoE fragments was found in synaptosomal fractions of AD mouse models coinciding with intracellular Aβ aggregation, accumulation of autophagic vacuoles, axonopathy and synaptic loss. *In vitro* experiments using SH-SY5Y, Ntera2 and Neuro2a cells suggest that human and murine ApoE fragmentation is putatively driven by intracellular Aβ, whereas exogenous Aβ exclusively leads to increased full-length ApoE expression.

Furthermore, crossing 5XFAD with tau transgenic PS19 mice resulted in drastically enhanced tau pathology, astrocytosis, loss of synapto-dendritic connections and neurons as well as hippocampal atrophy. This indicates that Aβ and Aβ-induced ApoE fragments trigger tau phosphorylation either in concert or independently from each other in an upstream event, leading to an accelerated progression of AD pathology.

In conclusion, the similarities of ABri and ADan peptides to Aβ in AD suggest that the post-translational pGlu-modification of amyloid peptides might represent a general pathological mechanism leading to increased aggregation and toxicity in these forms of degenerative dementias. Moreover, it could be demonstrated that in addition to the well-known effects of ApoE on Aβ levels, increased amounts of Aβ (and ADan) peptides in turn promote ApoE proteolysis, which might result in a vicious circle leading to neurodegeneration in dementias.

List of Figures

List of Tables

List of Abbreviations

AAV: Adeno-Associated-Virus

ABri: British amyloid

ABriPP: British mutant form of BRI

AD: Alzheimer's Disease

ADAM10: disintegrin and metalloproteinase domain 10

ADan: Danish amyloid

ADanPP: Danish mutant form of BRI2

ApoE: Apolipoprotein E

APP: amyloid precursor protein

AVs: autophagic vacuoles

Aβ: β-amyloid

BACE1: β-site APP cleaving enzyme 1

CAA: cerebral amyloid angiopathy

COX: cyclooxygenase

CSF: cerebrospinal fluid

CTF23: C-terminal fragment of ITM2B/BRI2

Ctrl: control

DAB: diaminobenzidine

fAD: familial Alzheimer's Disease

FBD: Familial British Dementia

FDD: Familial Danish dementias

FTD: Frontotemporal Dementia

he: hemizygous

ho: homozygous

ICD: intracellular domain

ITM2B/BRI2: integral transmembrane protein 2B

KI: knock-in

LDH-assay: cytotoxicity assay

LDL: low-density lipoprotein

mApoE: murine ApoE

MAPT: microtubule-associated protein tau

MCI: mild cognitive impairment

MTT-assay: cell proliferation assay

NAC: N-acetyl-L-Cysteine

NFTs: neurofibrillary tangles

PFA: paraformaldehyde

pGlu: pyroglutamate

PHFs: paired helical filaments

PS1/2: Presenilin-1/2

PSD95: postsynaptic density protein 95

QC: glutaminyl cyclase

ROS: reactive oxygen species

rpm: rounds per minute

RT: room temperature

sAD: sporadic Alzheimer's Disease

SEM: standard error of the mean

Thio-S: Thioflavin S

ThT: Thioflavin T

TRH: thyrotropin-releasing hormone

WT: wild-type

1 Introduction

1.1 Alzheimer´s Disease

Morbus Alzheimer or Alzheimer´s Disease (AD) is a neurodegenerative disease and represents the most common form of dementia in the elderly population. Approximately 10 % of the human population over 65 years and 25 to 45 % of people over 85 years are affected. Currently, there are 36 million people suffering from this disease and due to demographic development, this number is estimated to triple in the year 2050 (Report 2011). The characteristic clinical features of AD are declined cognitive abilities, inactivity, personality changes and neuropsychological symptoms. AD is neuropathologically characterized by the formation of plaques *inter alia*, consisting of β-amyloid (Aβ), cerebral amyloid angiopathy (CAA), neurofibrillary tangles (NFTs), brain atrophy and inflammation.

1.1.1 Etiopathology

The course of AD is subdivided into four stages, described chronologically here.

In the preclinical stage, mild cognitive difficulties and first deficits of the short-term memory occur that can affect daily living activities. These symptoms can arise several years before a person gets diagnosed (Bäckman et al. 2004).

In the mild cognitive impairment (MCI) stage, a preliminary phase of AD, the patient's ability to learn and to memorize further decline. Difficulties with language, executive functions, agnosia or apraxia are also possible (Förstl and Kurz 1999). In addition, first deficits of episodic, semantic and implicit memory recall can be observed in patients (Carlesimo and Oscar-Berman 1992, Jelicic et al. 1995).

The moderate stadium of AD includes progressive disability to perform common activities of daily living. Impairment of language, disorientation, motor deficits and memory decline exhibit an increase. Furthermore, behavioral changes and neuropsychiatric symptoms become more prominent (Förstl and Kurz 1999).

Finally, patients with advanced dementia completely lose their autonomy. Language skills are minimized; ranging from single phrases and words to complete loss of speech

(Frank 1994). Extreme lethargy and apathy are common symptoms beside absent mobility. The advanced dementia is not the primary cause of death, but facilitates infections like pneumonia and cardiac infarction (Förstl and Kurz 1999).

1.1.2 Diagnosis

Since the German neuropathologist Alois Alzheimer described the first dementia case in 1901, diagnosing AD nowadays is still difficult and can only be definitely confirmed *post mortem*, because diagnosis is based on neuropathological hallmarks. The main histopathological criteria is the progression of NFT formation, which is classified into so-called Braak stages I to VI, in addition to the analysis of amyloid plaques (Braak and Braak 1991, Mirra et al. 1991).

Prior to death, a relative solid diagnosis is only possible when patients reach the stadium of MCI. In this state, neuropsychological tests like the Mini-Mental State Examination (MMSE) (Folstein et al. 1975) or the Clock-drawing test (Sunderland et al. 1989) in combination with neuroimaging methods like magnetic resonance imaging (MRI), computed tomography (CT), single photon emission computed tomography (SPECT) and positron emission tomography using an amyloid-binding dye (PiB-PET) or with radiolabeled glucose (FDG-PET) could give some indications and may also predict the conversion from MCI to AD (Perrin et al. 2009, Schroeter et al. 2009). Additionally, decreased levels of $A\beta_{x-42}$ as well as elevated amounts of total tau and hyperphosphorylated tau in the cerebrospinal fluid (CSF) also correlate with the severity of the disease (Mattsson et al. 2009, Perrin et al. 2009).

1.1.3 Neuropathological Hallmarks

1.1.3.1 Aβ Deposits

AD belongs to the family of proteopathies along with the diseases like Parkinson´s Disease, frontotemporal dementia, Prion disease or Huntington´s disease. Extracellular deposits consisting of Aβ peptides are one of the most prominent characteristics in AD brains. Aβ peptides are generated by enzymatic cleavage of the amyloid precursor protein (APP) by β- and γ-secretases (Haass et al. 2012). Under normal conditions, Aβ is continuously produced and degraded, but in AD brains peptide turnover is impaired leading to depositions in the

vascular and parenchymal tissue of the grey matter. Especially the putatively neurotoxic Aβ$_{x-42}$ species are elevated in AD that may lead to neurodegeneration. Due to their different morphology and biochemical composition, senile amyloid plaques can be divided into two subclasses (Fig. 1.1): Neuritic plaques consist of highly aggregated fibrillary Aβ and are detectable with β-sheet binding dyes like Thioflavin-S/T, Congo Red or silver staining. The focal or stellate deposits are often primarily formed in neocortex and later spread to the amygdala, hippocampus, subcortical layers and brainstem. These plaques are associated with degenerated neurons, neurofilament-positive dystrophic neurites, as well as micro- and astrogliosis (Selkoe 2001, Duyckaerts et al. 2009). On the other hand, diffuse plaques are the most common type of senile plaques found in cortical tissue of AD patients, but also to a lesser extent in normal aged people. This kind of plaques is not recognized by antibodies against neurofilaments, tau and paired helical filaments (PHF) that are associated with dystrophic neurites and disruption of axonal transport (Joachim et al. 1989, Duyckaerts et al. 2009).
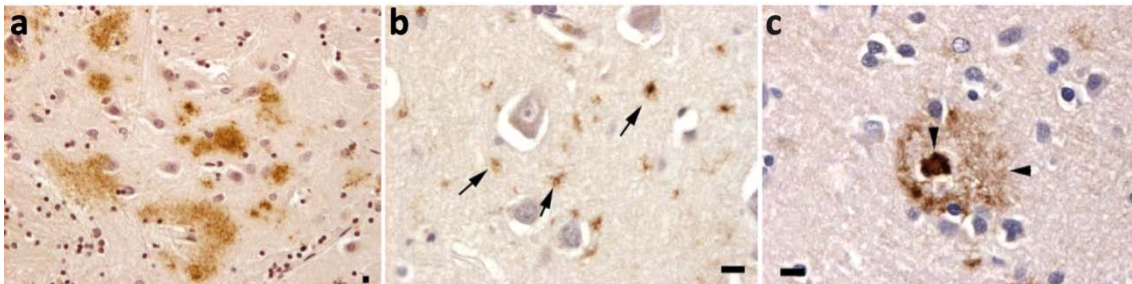
Figure 1.1. Diffuse plaques are not associated with neuritic dystrophy (a), whereas focal (b) and stellate (c) amyloid plaques also contain ubiquitin, tau and PHFs. Adapted from (Duyckaerts et al. 2009)

1.1.3.2 Cerebral Amyloid Angiopathy

Amyloidogenic peptides can also highly aggregate in vascular tissues of the brain, which is known as CAA (Fig. 1.2). These deposits can be observed in over 80 % of all AD cases and lead to a constriction of blood vessels, which causes subsequent degenerative vascular changes, resulting in cerebral hemorrhage, ischemic lesions and dementia. CAA was first described in senile plaques of an AD patient in 1938, but it is also associated with other diseases. It is classified according to deposited amyloid peptide, but the most common forms are sporadic CAA and CAA associated with AD. CAA also has a hereditary component. For instance, the Dutch mutation of *APP* (E693Q or E22Q) leads to an enhanced aggregation

propensity of Aβ and mutations of *Presenilin-1* (*PS1*) and *Presenilin-2* (*PS2*) also facilitate severe CAA (Revesz et al. 2003).
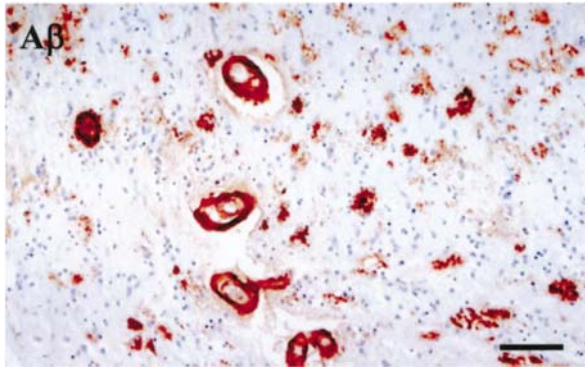
Figure 1.2. CAA is present in more than 80 % of all AD cases. Aβ deposits in vessel walls cause degenerative vascular changes (Revesz et al. 2003).

1.1.3.3 Neurofibrillary Tangles

NFTs composed of hyperphosphorylated tau protein are another major hallmark of AD. Tauopathy is widespread in a variety of diseases like Familial British and Danish dementias, frontotemporal dementia or Pick´s disease. The spreading of NFTs, ranked in Braak stages, correlates well with AD progression (transentorhinal stages I-II: clinically silent cases; limbic stages III-IV: incipient AD; neocortical stages V-VI: fully developed AD; (Braak and Braak 1995)). Under normal conditions, the microtubule-associated protein tau has a physiological function as a regulator of microtubule plasticity. Tau stabilizes the cytoskeleton by the binding of its repetitive sequences to microtubules. If tau becomes phosphorylated by diverse kinases, it detaches from microtubules and starts to aggregate into neurofibrils leading to microtubule instability and disintegration (Lee et al. 2005). Under pathological conditions, tau is massively phosphorylated and aggregates to NFTs (Fig. 1.3) causing several cellular dysfunctions like mistrafficking of proteins or loss of neuronal integrity and mediates Aβ-induced toxicity (Ittner and Götz 2011).
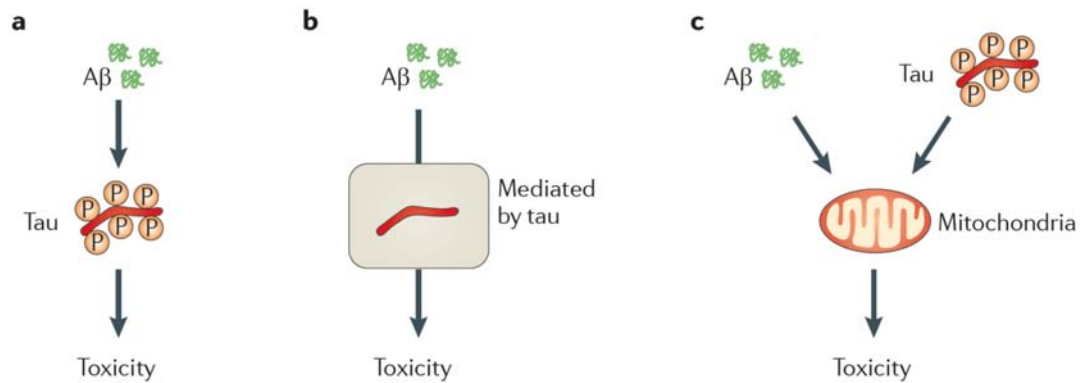
Figure 1.3. Hyperphosphorylation of tau leads to the formation of NFTs resulting in destabilization of microtubules. Tau aggregates act toxic *per se* but also mediate Aβ toxicity (Ittner and Götz 2011).

1.1.3.4 Brain Atrophy

Neuron loss in specific regions is the main reason for brain atrophy. As described before for diagnosing AD, CT and MRI imaging methods are used to visualize enlarged ventricles and widened cortical sulci that are characteristic features for brain atrophy in the progression of the dementia (Fig. 1.4). Thus, the medial temporal lobe including the hippocampus and the entorhinal cortex are primarily affected (Braak et al. 1999). It has been shown that MRI measurements of hippocampal atrophy have an accuracy of 80 to 90 % in diagnosing AD (Jagust 2006) and give some indications about the progression from MCI to AD (Jack et al. 2005). It is supposed that entorhinal cortex volume decrease might precede hippocampal atrophy in AD, which is also highly predictable for incipient disease in MCI (Detoledo-Morrell et al. 2004, Pennanen et al. 2004).
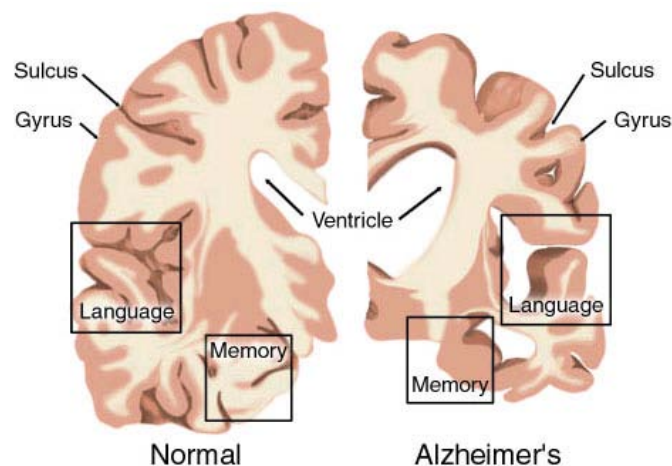
Figure 1.4. Brain atrophy is highly represented in AD. Shrinkage of hippocampus and entorhinal cortex leads *inter alia* to memory and cognitive decline as well as speech impairment. Adapted from http://www.ahaf.org

5

1.1.3.5 Inflammation

Chronic inflammatory processes including astro- and microgliosis leading to detrimental processes are also prominent hallmarks of AD. It has been found that in the CA1 region of the hippocampus of AD patients cyto- and chemokines as well as other inflammatory related proteins like interleukin (IL)-1α, IL-1β, cyclooxygenase (COX)-2 and NF-κB1 are abnormally expressed as compared to non-demented controls (Colangelo et al. 2002). Thereby, the activation of astrocytes (Fig 1.5) and microglia is driven by highly aggregated Aβ found in neuritic plaques (Itagaki et al. 1989). Contrariwise, Aβ accumulation and deposition is also accelerated by glial dysfunction to clear amyloid peptides (Nagele et al. 2003, Hickman et al. 2008).
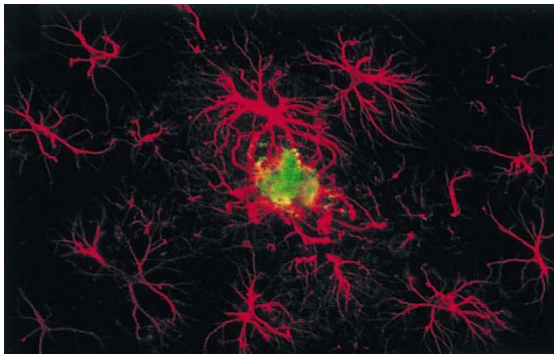
Figure 1.5. Astrogliosis in Tg2576 mice expressing APP_{695} with the Swedish mutation (Apelt and Schliebs 2001). Activated astrocytes (GFAP, red) are arranged in close proximity to a neuritic Aβ plaque (green).

1.1.4   The Amyloid Precursor Protein

The amyloid precursor protein (APP) is ubiquitously expressed and is the source of Aβ peptides after distinct proteolysis. In humans, several alternative splicing isoforms are expressed with APP carrying 365 to 770 amino acids, whereas certain isoforms like the encoding proteins APP_{695}, APP_{751} and APP_{770} are predominantly expressed by neurons (Zheng and Koo 2006).

APP is a type-I transmembrane glycoprotein with extracellularly located N-terminal amino acids and a cytosolic positioned C-terminus (Kang et al. 1987, Dyrks et al. 1988). APP enters the secretory pathway with transition from the endoplasmic reticulum to the cell membrane and becomes modified by glycosylations, phoshorylations of ecto- and intracellular domain as well as tyrosine sulphation. Based on *in vitro* studies, major portion of APP remains in the Golgi apparatus and *trans*-Golgi network. After APP reaches the cell

surface, it becomes rapidly internalized again by its "YENPTY" internalization motif (APP$_{682-687}$) and enters either endocytic, recycling and lysosomal pathways or it is trafficked back to the cytoplasmic membrane (Haass et al. 1992, Lai et al. 1995, Marquez-Sterling et al. 1997).

1.1.4.1 Biological Functions of APP and its Fragments

Currently, the primary function of APP is not known. It is supposed to be a regulator of synapse function and formation (Priller et al. 2006), neuronal plasticity (Turner et al. 2003) and iron export (Duce et al. 2010). *In vitro* studies have shown that APP is able to form anti-parallel dimers indicating a cell adhesion function (Wang and Ha 2004). A role for APP in neurite outgrowth and synaptogenesis may be linked to its adhesive properties, whereas the extracellular APP domain may exert these activities in auto- and paracrine manners. The expression of APP is not only up-regulated during neuronal maturation and differentiation (Hung et al. 1992, Bibel et al. 2004), but also during traumatic brain injury in mammals (Murakami et al. 1998). APP undergoes rapid anterograde transport in highly polarized neurons (Koo et al. 1990) and is targeted to synapses, where secreted APP putatively regulates synaptogenesis (Moya et al. 1994).

Furthermore, one fragment derived from the non-amyloidogenic processing pathway, the secreted soluble APPα (sAPPα), is considered to be neuroprotective and neurotrophic as well as a regulator of cell excitability and synaptic plasticity. In contrast, Aβ seems to have opposing effects and, therefore, it may regulate neural functions including cell excitability, synaptic transmission and long-term potentiation. In fact, the accumulation of Aβ combined with reduced levels of specific APP fragments is likely directly linked to cognitive decline in early AD (Turner et al. 2003). In contrast to its associations to AD pathology, it has been recently found that Aβ also has antiseptic properties and, therefore, may play a role in the innate immune system (Soscia et al. 2010). Further possible physiological roles of Aβ are the reduction of oxidative stress (Zou et al. 2002, Baruch-Suchodolsky and Fischer 2009, Sinha et al. 2012), acting as a transcription factor (Bailey et al. 2011, Maloney and Lahiri 2011), activation of kinases (Bogoyevitch et al. 2004, Tabaton et al. 2010), regulation of the sleep-wake cycle by controlling neuronal activity (Kang et al. 2009) and regulation of cholesterol transport (Yao and Papadopoulos 2002, Igbavboa et al. 2009).

1.1.4.2 Amyloidogenic and Non-Amyloidogenic Processing

As already indicated, APP is physiologically processed by multiple secretases at several different subcellular sites in either amyloidogenic or non-amyloidogenic fashion (Fig. 1.6).

In the non-amyloidogenic pathway, APP is first cleaved within the Aβ sequence (between leucine-16 and leucine-17) by a set of α-secretases leading to the release of the soluble sAPPα fragment into the extracellular space (Sisodia et al. 1990, Anderson et al. 1991). A-secretases are supposed to be membrane-bound and are predominantly active at the cell surface (Sisodia 1992). Several zinc metalloproteases have been found that could function as α-secretases, whereas the enzymatic activity can be shared by a set of these disintegrin and metalloproteases like ADAM9, ADAM10, TACE or ADAM17 and ADAM19 (Allinson et al. 2003, Haass et al. 2012). The remaining, membrane-bound C-terminal fragment (C83) is further cleaved by γ-secretase within the trans-membrane region of APP, resulting in the liberation of the soluble, 3 kDa P3 fragment and the production of the membrane-bound APP intracellular domain (AICD), which is a potential transcriptional regulator (Haass et al. 1993, Hartmann 1999, Cao and Sudhof 2001). In contrast to Aβ, P3 peptide is rapidly degraded and does not play a role in AD pathogenesis.

In the amyloidogenic pathway, APP is first cleaved within the extracellular domain at the N-terminus of the Aβ sequence (at aspartate-1 or aspartate-11) by the aspartyl protease β-site APP cleaving enzyme 1 (BACE1), after which the soluble N-terminal ecto-domain sAPPβ becomes liberated (Vassar et al. 1999). The membrane-bound, 99-residue C-terminal rest (C99) is subsequently processed by γ-secretase mediated intra-membrane proteolysis leading to the liberation of Aβ and AICD (Annaert and De Strooper 2002). The length of Aβ peptides can vary from 37 to 43 amino acids, where $Aβ_{1-40}$ is the most common isoform under normal physiological conditions. $Aβ_{1-42}$ represents the main portion in amyloid plaques and is considered to be neurotoxic and affects memory as well as neuronal survival (Haass and Selkoe 2007). The γ-secretase is a multi-protein complex consisting of several trans-membrane proteins: PS1 or PS2, nicastrin, anterior pharynx defective-1 (Aph-1), presenilin enhancer protein (PEN-2) and the recently found cluster of differentiation 147 protein (CD147) that functions as negative regulator of the complex (Kaether et al. 2006, Zhou et al. 2006b). PS1 and PS2 are aspartyl proteases in the catalytic subunit of the γ-secretase complex with mutations in their sequences leading to enhanced Aβ production and the development of AD.

As previously mentioned, non-amyloidogenic processing mainly occurs at the cell surface, whereas amyloidogenic cleavage involves transit through the endocytic organelles where APP encounters β- and γ-secretases (Thinakaran and Koo 2008). However, enhancement of α-secretase activity leads to significantly reduced Aβ generation and plaque formation *in vivo* and *in vitro*, suggesting that both pathways compete with each other at least in some subcellular compartments (Nitsch et al. 1992, Postina et al. 2004). Therefore, the homeostasis of APP processing plays an important role in the development and progression of AD.
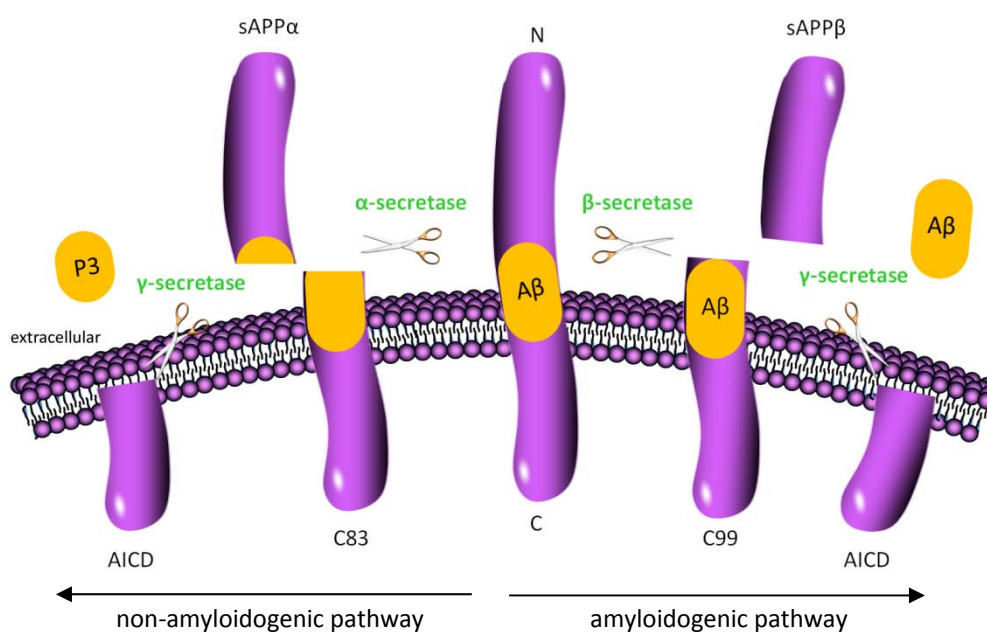
Figure 1.6. APP can be processed in non-amyloidogenic and amyloidogenic manner. Homeostasis of both pathways plays an important role for developing AD. Figure generated after (Haass et al. 2012).

1.1.4.3 The Amyloid Hypothesis

The β-amyloid cascade hypothesis was first introduced by Hardy and Allsop in 1991 and is based originally on a central role of Aβ peptides in the pathological cascade leading to neuropathological changes and the formation of NFTs (Fig. 1.7a) (Hardy and Allsop 1991). It states that elevated levels of extracellular Aβ, which are the result of several risk factors, lead to increased extracellular plaque deposition resulting in neuronal and synaptic dysfunction. Brain atrophy of distinct areas follows as a consequence of neuron and synapse loss, leading in the end to memory loss and other clinical symptoms. This hypothesis was

controversial for some time, because amyloid plaque load poorly correlates with cognitive decline and dementia severity (Arnold et al. 1991, Arriagada et al. 1992). Furthermore, massive plaque pathology could be also detected *post mortem* (Strittmatter et al. 1993, Savva et al. 2009, Wirths et al. 2010a) and in PiB-PET (Chetelat et al. 2010) in non-demented people without any evidence of dementia. In addition, anti-Aβ vaccination trials (AN1792) in patients led, indeed, to significantly reduced plaque pathology, but cognitive improvement was still absent (Holmes et al. 2008). On the other hand, there are several arguments supporting the amyloid hypothesis. For example, mutations in *APP*, *PS1* or *PS2* genes, which encode both the substrate and the key enzyme for the generation of Aβ, increases a person´s chance to 100 % to get the familial early onset form of AD due to significantly enhanced levels of $Aβ_{42}$ and faster amyloid aggregation (Rademakers and Rovelet-Lecrux 2009). Furthermore, in the case of Down-Syndrome that based on a triplication of chromosome 21, on which *APP* is localized, patients also develop AD pathology at young ages (Heston and Mastri 1977). Moreover, mouse models that rely on mutations in *APP*, *PS1* and *PS2* genes recapitulate some aspects of AD. Aβ immunization led also to reduced amyloid pathology and rescued cognitive impairment in AD mouse models (Bard et al. 2000, Sigurdsson et al. 2001, Tampellini et al. 2007, Wirths and Bayer 2008). An additional proof of concept has been recently discovered; scientists identified a protective APP mutation (A673T) resulting in less production of toxic Aβ fragments. Humans harboring this mutation do not only produce about 20 % less Aβ their whole life, they also achieved better scores in cognitive tests compared to age-matched, non-demented controls (Jonsson et al. 2012).

Some controversies against this classical amyloid hypothesis may be explained by the modified amyloid hypothesis (Fig. 1.7b), in which intracellular accumulated Aβ peptides play a significant role (Wirths et al. 2004). It is hypothesized that diverse risk factors induce elevated levels of intracellular Aβ, which further accumulate to oligomers and cause neuronal and synaptosomal dysfunction leading to AD symptoms. On the other hand, elevated soluble, intracellular Aβ could be secreted and taken up again from the cells, which also contributes to intracellular accumulation, or Aβ further aggregates to amyloid plaques (Wirths et al. 2004). Intracellular Aβ could be found in patients with Down-Syndrome at a young age, before extracellular plaque pathology initiated, whereas the amount of intracellular accumulations was decreased together with increasing plaques at an older age (Gyure et al. 2001). Furthermore, the majority of AD mouse models, which carry explicit

plaque pathology, develop inflammatory reactions that reflects human AD pathology but with lacking neuron loss (Wirths et al. 2004). In contrast, recently generated mouse models like the APP/PSKI (Casas et al. 2004), 5XFAD (Oakley et al. 2006) or TBA2 mouse models (Wirths et al. 2009) harbor early intracellular Aβ accumulations and show neuron loss in correlation with behavior deficits. All of these aspects imply that soluble intracellular and extracellular Aβ oligomers are connected upstream of the formation of NFTs and that they play an important role in the early progression of AD.
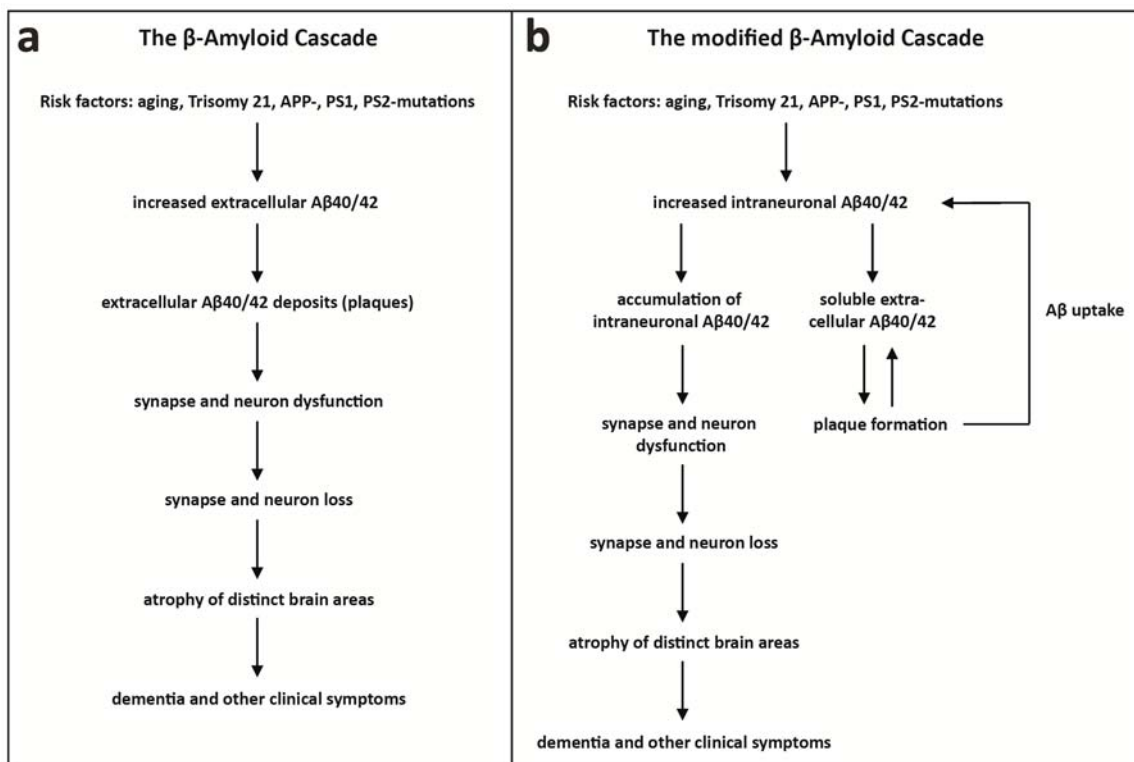
Figure 1.7. The amyloid cascade hypothesis (a) that exists for over 20 years is an important pillar of AD research. Later on, soluble intracellular and extracellular Aβ oligomers were identified to cause neuron loss (b). Figure adapted from (Wirths et al. 2004)

1.1.5   Inheritance

AD is a heterogeneous disorder with both familial and sporadic forms (fAD and sAD, respectively), where the prevalence of all familial, autosomal dominant AD cases is below 0.1 % (Blennow et al. 2006). FAD relies on point mutations that have been discovered in three different genes (Fig. 1.8): *APP* on chromosome 21 (32 mutations), *PS1* on chromosome 14 (182 mutations) and *PS2* on chromosome 1 (13 mutations). These mutations cause early-onset of AD, with disease onset ranging from 29 to 50 years of age. Mutations in *APP* increase the production of total Aβ or specifically elevate $A\beta_{42}$, which is the main component of senile plaques, whereby for instance mutations near the BACE1 site accelerate β-secretase cleavage and increase general Aβ levels (Citron et al. 1992, Haass et al. 1994). Mutations near the γ-secretase site specifically increase $A\beta_{42}$ production, which is inversely correlated with $A\beta_{40}$ generation (Suzuki et al. 1994). The Dutch (E693Q) and London (V717I) mutations of the *APP* gene (Fig. 1.8a) were the first mutations described within and outside of the Aβ sequence (Levy et al. 1990, Suzuki et al. 1994). Due to increased total Aβ production or elevated $A\beta_{42}$ generation, several mutations in *APP* are also associated with an increased risk of CAA (Revesz et al. 2009). Some fAD mutations also affect AICD production, but this does not correlate with an increase or decrease in Aβ levels indicating that fAD mutations exert their pathogenic effect by altering Aβ processing and not APP signaling (Hecimovic et al. 2004). Mutations in *PS1* and *PS2* genes are the most common cause of fAD (Fig. 1.8b). These genes encode the catalytic part of the γ-secretase complex and mutations primarily result in an increased ratio of $A\beta_{42}/A\beta_{40}$, which is caused by a shift towards the production of the longer $A\beta_{42}$ variant (Scheuner et al. 1996, Citron et al. 1997).

a

b
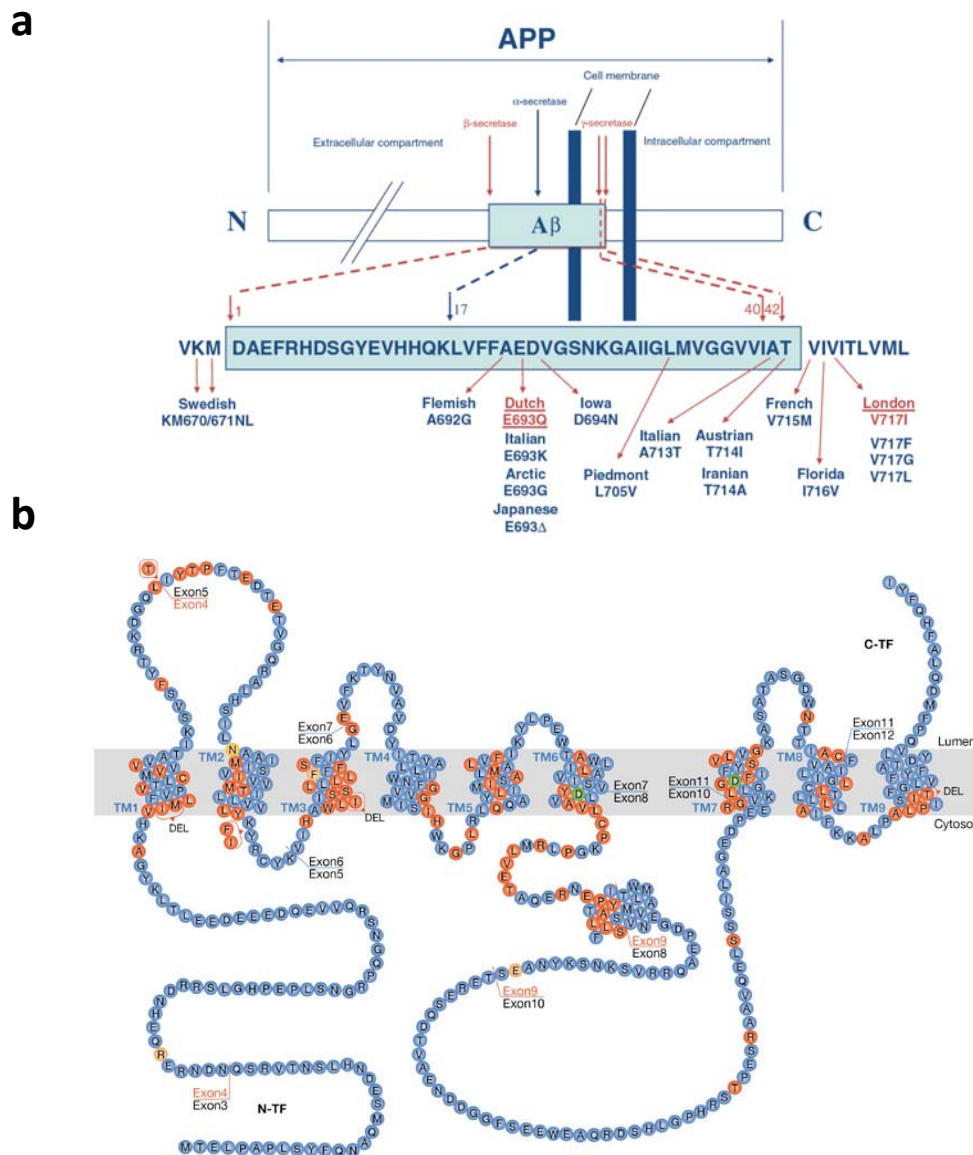
Figure 1.8. (a) More than 30 mutations in *APP* have been identified over the last decades within or outside the Aβ sequence that influence β- and γ-secretase activity. (b) Almost 200 known mutations (red) in *PS1* and *PS2*, which affect the γ-secretase activity, are accountable for the most cases of fAD. Figures from (Revesz et al. 2009) and http://www.nature.com

1.1.6 Risk Factors

The main risk factor for getting AD is aging. Epidemiological studies have suggested that AD risk is also elevated by a decreased reserve capacity of the brain. This is defined as the number of neurons and their synaptic and dendritic arborization in combination with lifestyle-related cognitive strategies. Therefore, low educational and occupational skills as well as low mental ability at young ages and reduced mental and physical activity during late life can increase the chance getting the disease (Mayeux 2003, Mortimer et al. 2003). Further studies have shown, that brain trauma caused by head injury could also increase the

risk for AD, but it is still unclear if and how trauma induces the pathological cascade (Jellinger 2004). Other risk factors that are also associated with AD and vascular dementia are hypercholesterolemia, obesity, coronary heart disease, hypertension, atherosclerosis, smoking and diabetes type II (Mayeux 2003).

Most cases of AD do not exhibit familial inheritance, but genes may act as risk factors. The best known and strongest genetic risk factor for sAD is the inheritance of the ε4 allele of the apolipoprotein E (*APOE*). Carrying one ApoE ε4 (ApoE4) allele almost quadruples the chance of getting the disease, while harboring two alleles increases the risk by 12 to 15 fold (Corder et al. 1993) (see also section 1.4). Genome-wide association studies (GWAS) revealed over 695 further genetic risk factors that are possibly responsible for increased risk to develop AD. Genes with the major disease relevance are listed in Fig. 1.9.

Gene/locus	Protein	Polymorphism	Candidate gene, locus or GWAS[a]	Grade	Effect estimate[b]	Pathway		
						Amyloid β	Inflammatory response	Cardiovascular risk factors
APOE	Apolipoprotein E	apoe ε2/3/4	Candidate gene	A	3.57 (3.21, 3.97)	Clearance, fibril formation	Modulation of immune response	Lipid metabolism, atherosclerosis
CLU	Clusterin	rs11136000	GWAS	A	0.85 (0.82, 0.89)	Clearance, fibril formation	Modulation of immune response	Lipid metabolism, atherosclerosis
PICALM	Phosphatidylinositol-binding clathrin assembly protein	rs541458	GWAS	A	0.87 (0.83, 0.91)	Recycling of APP?		
TNK1	Tyrosine kinase, non-receptor, 1	rs1554948	GWAS	A	0.86 (0.8, 0.93)			Phospholipid signal transduction
ACE	Angiotensin-converting enzyme	rs1800764	Candidate gene	A	0.83 (0.72, 0.95)			Cardiovascular pathophysiology
TFAM	Transcription factor a, mitochondrial	rs2306604	Candidate gene	A	0.82 (0.72, 0.94)			
CST3	Cystatin c	rs1064039	Candidate gene	A	1.13 (1, 1.28)	Amyloid angiopathy		Decreased expression in atherosclerosis
IL1B	Interleukin 1, beta	rs1143634	Candidate gene	A	1.17 (1.02, 1.36)		Cytokine	
CR1	Complement component (3b/4b) receptor 1	rs6656401	GWAS	B	1.18 (1.07, 1.29)	Clearance of Aβ	Complement receptor	
hCG2039140	[Predicted]	rs1903908	Locus	B	1.2 (1, 1.43)			
SORL1	Sortilin-related receptor	rs12285364	Candidate gene	B	1.21 (1, 1.45)	APP trafficking		Uptake of lipoproteins
CHRNB2	Cholinergic receptor, nicotinic, beta polypeptide 2 (neuronal)	rs4845378	Candidate gene	B	0.67 (0.5, 0.9)			
SORCS1	Sortilin-related vps10 domain containing receptor 1	rs600879	Candidate gene	B	1.24 (1.04, 1.48)	APP trafficking		Uptake of lipoproteins

Figure 1.9. Ranking of genes associated with sAD that harbor strong (Grade A) or moderate (Grade B) epidemiological impact (Sleegers et al. 2010).

1.2   Familial British and Danish Dementias

Familial British and Danish dementias (FBD and FDD, respectively) are rare, early-onset, autosomal dominant disorders that were first described by Worster-Drought et al. and Strömgren and colleagues (Worster-Drought et al. 1933, Strömgren et al. 1970). FBD and FDD are summarized as chromosome 13-linked amyloidopathies. On chromosome 13, the *integral transmembrane protein 2B* (*ITM2B* also known as *BRI2*) is located. Mutations in this gene cause the development of these dementias. In both diseases, male and females are

equally affected, with median ages of onset and death at 48 and 56 years in FBD and 27 and 58 years in FDD, respectively (Plant et al. 1990). The main neuropathological lesions in both dementias are hippocampal neurofibrillary degeneration as well as widespread parenchymal and vascular amyloid deposits. These features are remarkably similar to those seen in AD. Characteristic clinical features are progressive cognitive impairment, spasticity and cerebellar ataxia (Garringer et al. 2010).

1.2.1 Clinical Features

Patients with FBD develop marked memory impairment progressing to global dementia. So far, 343 individuals over nine generations since ca. 1780 have been identified (Griffiths et al. 1982, Love and Duchen 1982, Plant et al. 1990, Mead et al. 2000). Earliest etiopathology symptoms are personality changes, followed by cerebellar ataxia and spastic tetraparesis that are more drastic than in AD. Further common disease features are brainstem signs, pseudobulbar palsy, dysarthria and cerebral hemorrhage, although this occurs rarely for a familial cerebrovascular amyloidosis. Like in AD, patients get into a vegetative state with loss of speech, lethargy, paraplegy and incontinence.

Heredopathia ophthalmootoencephalica is a synonym for FDD. From 5 generations of one family, 13 individuals are/were affected. Etiopathology of this progressive dementia includes deafness and cataracts that usually start in the 20's and severe deafness that occurs almost simultaneously with cerebellar ataxia accompanied by intention tremor at the age of 45 years. In contrast to FBD patients, cerebellar ataxia does not induce spastic tetraparesis. Dementia associated with paranoid psychosis and temporal disturbances of consciousness are the final stages of FDD (Strömgren et al. 1970, Holton et al. 2002).

1.2.2 The Integral Membrane Protein 2B (BRI2)

Different mutations in the *BRI2* gene cause FBD and FDD (Vidal et al. 1999, Vidal et al. 2000). The *BRI2* gene is localized on the long arm of chromosome 13 (13q14) and encodes under wild-type conditions the BRI2 protein, which is a 266-amino acid long, type-II transmembrane protein (Vidal et al. 1999). *BRI2* is a member of an evolutionarily conserved multigene family with at least three homologues in mice and humans: *BRI1* (*ITM2A* or *E25A*), *BRI2* (*ITM2B* or *E25B*) and *BRI3* (*ITM2C* or *E25C*) (Deleersnijder et al. 1996, Pittois et al. 1998, Vidal et al. 1999, Vidal et al. 2001). *BRI2* is ubiquitously expressed in peripheral organs with

high levels of expression in brain, heart, kidney, pancreas, liver and placenta. Within the brain, it is ubiquitously present in white and gray matter, where it is more abundant in the hippocampus and the cerebellum compared with the cerebral cortex. *In situ* hybridizations revealed that mRNA of *BRI2* is present in a variety of different cell types in the brain like neurons, astrocytes, microglia, smooth muscle and cerebral endothelial cells (Vidal et al. 1999, Rostagno et al. 2005).

The BRI2 protein contains a transmembrane domain, a single conserved BRICHOS domain (Fig. 1.10) within the pro-peptide region and a N-glycosylation site at position 170. Its C-terminal region is extracellularly/lumenally located and its N-terminal domain is intracellularly/cytoplasmatically located (Vidal et al. 1999). The protein has been detected in pyramidal cells of the hippocampus and in Purkinje cells of the cerebellum. Under pathological conditions, BRI2 is also present in dystrophic neurites associated with amyloid plaques in AD patients and in Lewy neurites of patients with Lewy Body Dementia and Morbus Parkinson (Akiyama et al. 2004).

1.2.2.1 Biological Function of BRI2

So far, the function of BRI2 is relatively unknown, but due to its broad systemic expression pattern a wide-ranging function in general mechanisms is very likely. Its presence in transfected neurons as well as in dystrophic neurites *in vivo* suggests that BRI2 is axonally transported via secretory vesicles and possibly harbors a function in synaptic terminals, neuritic outgrowth and neuronal differentiation (Akiyama et al. 2004, Choi et al. 2004). A short form of BRI2, which is generated by alternative splicing, has been demonstrated to promote apoptosis, whereas this property also plays a role in the detrimental effects of amyloid peptides like Aβ (Davis et al. 1999, Miravalle et al. 2000, Fleischer et al. 2002). *In vitro* data and the genetic localization on chromosome 13 indicate a tumor suppressor function of BRI2, especially during initiation and progression of prostate carcinoma (Nupponen et al. 1998, Latil et al. 2003). Furthermore, BRI2 was identified as a ligand of APP, inhibiting Aβ production through the suppression of α- and β-secretases by masking their docking sites. It also inhibits the binding of nicastrin, which is part of the γ-secretase complex, to APP C-terminal fragments (Fotinopoulou et al. 2005, Matsuda et al. 2005, Matsuda et al. 2008). In addition, studies suggest that the 23-amino acid long C-terminal fragment, which is released after furin processing (see section 1.2.2.2), is able to block Aβ

aggregation *in vitro* and *in vivo* (Kim et al. 2008). Therefore, BRI2 plays a significant role in the physiological regulation of amyloidogenic and non-amyloidogenic processing of APP and in the formation of amyloid deposits.

1.2.2.2 Processing of the Integral Membrane Protein 2B

Like APP, BRI2 undergoes cleavage by several secretases (Fig. 1.10). Under normal physiological conditions, cleavage by the pro-protein convertase furin between arginine-243 and glutamate-244 leads to the secretion of a 23-amino acids long C-terminal fragment (here referred to as CTF23) (Kim et al. 1999, Kim et al. 2002, Choi et al. 2004). Furin is the most likely pro-hormone convertase to exert this cleavage, but there are some doubts if it is the actual BRI2 cleaving enzyme, because furin was mainly detected in the *trans*-Golgi network whereas BRI2 cleavage takes place in *cis/medial*-Golgi (Choi et al. 2004). BRI2 undergoes another extracellular proteolytic cleavage by a disintegrin and metalloproteinase domain 10 (ADAM10), which is an α-secretase candidate also involved in the processing of several other transmembrane proteins like APP (see section 1.1.4.2), Notch1 as well as N- and E-cadherins (Pan and Rubin 1997, Maretzky et al. 2005, Reiss et al. 2005, Martin et al. 2008). This processing liberates a 25 kDa fragment containing the highly conserved BRICHOS domain, which is also present in other type-II transmembrane proteins and is putatively involved in protein processing and targeting to the secretory pathway (Sanchez-Pulido et al. 2002). The remaining 22 kDa membrane-bound N-terminal fragment (NTF) becomes subsequently cleaved by intramembrane proteolysis of signal peptide peptidase-like proteases (sPPLa/b) resulting in the production of a low-molecular-weight secreted fragment and a 10 kDa intracellular domain (ICD) (Martin et al. 2008, Martin et al. 2009). This ICD possibly mediates signals to the nucleus as it is known for the Notch1-ICD that is generated by ADAM10 and γ-secretase cleavage (Artavanis-Tsakonas et al. 1999). BRI2 processing by ADAM10 and sPPL2a/b is independent from furin processing.
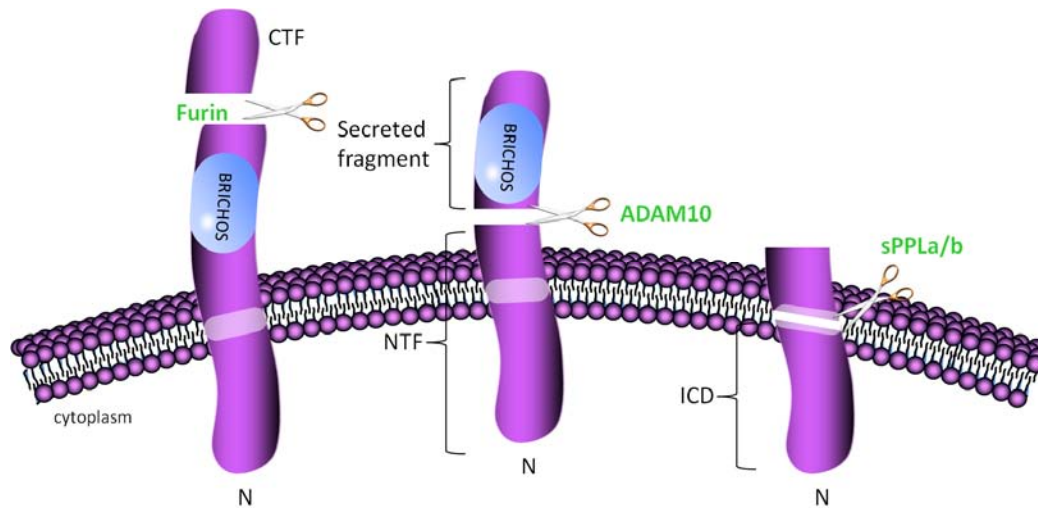
Figure 1.10. The proteolytical processing of BRI2 is quite similar to APP cleavage. BRI2 is first cleaved by furin leading to the secretion of a 3 kDa C-terminal fragment with 23 amino acids. Subsequently cleavage of the remaining N-terminal residue is carried out by ADAM10 and sPPLa/b. Figure generated after (Tsachaki et al. 2008)

1.2.3   Genetics

In contrast to AD, there are no sporadic forms of FBD and FDD. The cloning of the *BRI2* gene resulted in the identification of genetic defects underlying the novel cerebral amyloid diseases. A stop-codon to arginine mutation at position 267 in FBD (Vidal et al. 1999) and a 10-nucleotide duplication insertion at the same position in FDD (Vidal et al. 2000) result in elongated, 277-amino acid long precursor proteins ABriPP and ADanPP, respectively. Cleavage of these precursors results in the generation of two 34 amino acid-long C-terminal peptides called British amyloid (ABri) and Danish amyloid (ADan), respectively (Fig. 1.11). These amyloid peptides are 11 amino acids longer than the normal wild-type CTF23 and share homology in their first 22 amino acids although they completely differ at their C-termini. The additional amino acids change the aggregation propensity of these peptides from a non-amyloidogenic (CTF23) into an amyloidogenic form (ABri and ADan), leading to the formation of diffuse ADan deposits in FDD (Tomidokoro et al. 2005) and diffuse as well as compact ABri aggregations in FBD (Holton et al. 2001).
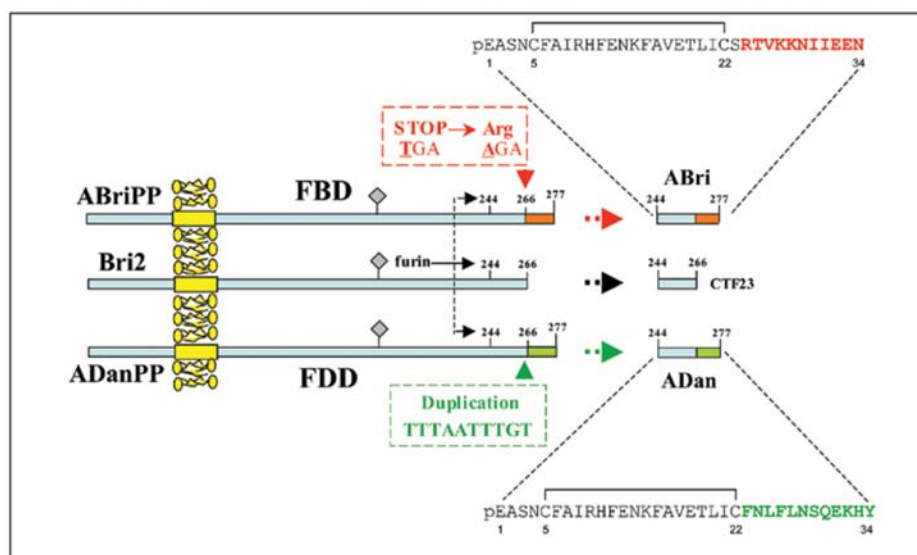
Figure 1.11. Different mutations in *BRI2* cause FBD and FDD. In both lesions, processing of precursors by a furin-like protease generates 34-amino acid long peptides (ABri or ADan, respectively) that have amyloidogenic properties in contrast to the wild-type CTF23. Figure from (Ghiso et al. 2006)

1.2.4   Neuropathological Hallmarks

As already indicated, FBD and FDD share some striking clinical and neuropathological similarities with AD as they also show parenchymal and vascular deposition of amyloid peptides, abundant tau phosphorylation, astro- and microgliosis as well as brain atrophy.

1.2.4.1 ABri and ADan Amyloid Deposits

As described above, ABri and ADan amyloid peptides are generated by furin cleavage of ABriPP or ADanPP precursor proteins in FBD and FDD, respectively. These peptides share no similar sequence to other known amyloid peptides, such as Aβ, but they also aggregate to non-fibrillary and fibrillary β-sheet structures leading to the development of plaques and CAA that are quite similar to Aβ deposits in AD (Holton et al. 2001, Tomidokoro et al. 2005) (Fig. 1.12). Interestingly, it has been shown that synthetic ABri and ADan peptides can undergo aggregation leading to fibril formation comparable to Aβ peptides in AD (Gibson et al. 2005, Ghiso et al. 2006). In FBD, ABri deposits are abundantly present in vascular and parenchymal tissues throughout the central nervous system (CNS) with the hippocampus, limbic system and cerebellum being mostly affected (Plant et al. 1990, Revesz et al. 1999, Holton et al. 2001). In FDD, ADan is mainly located in vascular and perivascular deposits,

parenchymal pre-amyloid lesions and in sparse neuritic plaques of the hippocampus and the cerebellum (Vidal et al. 2000). In both lesions, a widespread congophilic angiopathy is present that is comparable to CAA in AD (Weller et al. 1998). Highly aggregated fibrillar ABri and ADan lesions are Thio-S- and Congo red-positive and harbor a fibril bundle like shape, whereas Thio-S negative diffuse deposits are mainly structured as sparse, dispersed pre-fibrils with amorphous electron-dense material. In contrast to ABri in FBD, ADan deposits in the hippocampus of FDD patients contain predominantly pre-fibrillar amyloid, which are Thio-S and Congo-red negative (Vidal et al. 2000, Holton et al. 2002).
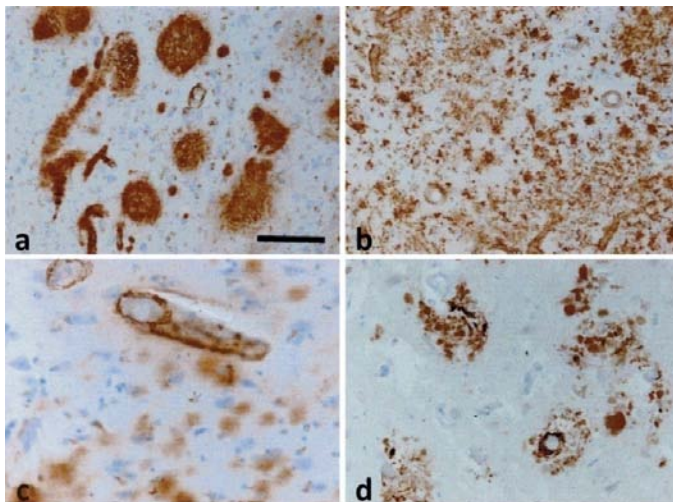
Figure 1.12. Amyloid lesions in FBD (a, c) and FDD (b, d) patients. In FBD, predominant compact fibrillar and sparse diffuse (a) as well as vascular ABri deposits (c) are abundant in the hippocampus and the cerebellum. ADan deposits in FDD are mainly seen in blood vessels (d), but also in mostly diffuse plaques located in the hippocampus (b). Picture adapted from (Rostagno et al. 2005)

A further similarity to AD is that dystrophic neurites surrounding ABri and ADan plaques can be found in patients of FBD and FDD, respectively, supporting an association between amyloid deposition and neuronal damage in these dementias (Vidal et al. 2000, Holton et al. 2001, Tomidokoro et al. 2005). Interestingly, it has been described in FDD patients that pre-amyloid and vascular deposits, especially in hippocampal and cerebral cortical regions, either contain Aβ alone or in combination with ADan suggesting a protein-protein interaction between those peptides. So far, this combination could not be detected in brains of FBD patients (Holton et al. 2002, Tomidokoro et al. 2005, Ghiso et al. 2006). In summary, compact plaques are absent in FDD and in certain brain areas in FBD, whereas parenchymal pre-amyloid deposits as well as vascular and perivascular lesions are present in this diseases.

1.2.4.2 Neurofibrillary Tangles and Chronic Inflammation

In FDD and FBD, neuropil threads and NFTs consisting of hyperphosphorylated tau are mainly present in limbic structures, which are affected by all types of ABri and ADan amyloid deposits (Plant et al. 1990, Revesz et al. 1999). But like in AD, there is no complete overlap between those neuropathological features. Although in FBD, FDD and AD different amyloid peptides are deposited, tau deposits are antigenically, ultrastructurally and biochemically indistinguishable (Ghetti et al. 1989, Giaccone et al. 1990, Holton et al. 2001, Holton et al. 2002, Giaccone et al. 2008).

A further neuropathological similarity to AD is inflammation in FBD and FDD (Rostagno et al. 2002). ABri and ADan peptides are able to induce pro-inflammatory processes comparable to $A\beta_{1-42}$ leading to activation of astrocytes and microglia.

1.3 Pyroglutamate-modified Amyloid Peptides

Another similarity of FDD and FBD to AD is the formation of pyroglutamate (pGlu)-modified amyloid peptides. In AD, this modification leads to a higher aggregation propensity, disturbed proteolytical degradation and increased toxicity of $A\beta$ peptides (Pike et al. 1995, Kuo et al. 1998, He and Barrow 1999, Russo et al. 2002). It has been reported that pGlu-modified $A\beta$ peptides represent a major fraction of plaque-associated $A\beta$ peptides in the AD brain (Harigaya et al. 2000) and biochemical analyses have shown that the majority of ABri and ADan peptides in FBD and FDD also contain a pGlu-modification at the N-terminus (Ghiso et al. 2006) (see Fig. 1.11). The pGlu-modification of $A\beta$ leads to an increased aggregation propensity *in vitro* (D'arrigo et al. 2009, Schilling et al. 2006) and similar findings have been reported for pGlu-modified ABri and ADan peptides (Schlenzig et al. 2009). The N-terminal pGlu-formation of $A\beta$ peptides can be catalyzed by glutaminyl cyclase (QC), an enzyme that can be pharmacologically inhibited by QC inhibitors *in vivo* (Schilling et al. 2008). Crossing the 5XFAD mouse model for AD with mice over-expressing human QC resulted in increased pGlu-$A\beta$ formation and an aggravation of behavioral deficits, whereas a knock-out of QC rescues the behavioral phenotype in 5XFAD mice (Jawhar et al. 2011b). In addition, over-expression of $A\beta_{3-42}$ peptides starting with an N-terminal glutamine, which leads to high pGlu-modified $A\beta$ levels, resulted in a severe neurological phenotype and neurodegeneration *in vivo* (Wirths et al. 2009), a finding that has been recently replicated

(Alexandru et al. 2011). It has also been previously reported that the formation of pGlu-residues at the N-termini of ABri peptides in patients suffering from FBD represents an early step in the process of amyloid deposition in this disorder. Using a combination of immunoprecipitation with a C-terminal antibody and subsequent mass spectrometry, it has been demonstrated that the majority of ABri peptides extracted from brain and peripheral organs harbored pGlu-residues at their N-termini, whereas ABri peptides in plasma were almost exclusively non-modified (Tomidokoro et al. 2010).

1.4 The Apolipoprotein E

The strongest genetic risk factor for late onset AD is the apolipoprotein E (ApoE) gene. Carrying one or two ApoE ε4 alleles (ApoE4) drastically increases the probability to develop AD (Corder et al. 1993). However, harboring ApoE4 does not only lead to an increased risk, but also results in a younger average age of onset and a more fatal disease progression. Aβ levels are highest in ApoE4 and lowest in ApoE ε2 allele (ApoE2) carriers, whereas total ApoE levels are inversely correlated to these Aβ levels with highest amounts in ApoE2 and lowest in ApoE4 genotype (Holtzman 2004). Human ApoE is a 299-amino acid protein, located on chromosome 19, with three different isoforms that only vary in two amino acids at positions 112 and 158 (Fig. 1.13). The most common form, the ApoE ε3 allele (ApoE3), has cysteine-112 and arginine-158, while the ApoE2 and the ApoE4 have on both positions either a cysteine or an arginine, respectively (Mahley et al. 2006).

1.4.1 Biochemical Properties of ApoE4

In humans, three different ApoE alleles are present that only differ in two amino acids at position 112 and 158 (Fig. 1.13a). Those small differences lead to changes in biochemical pattern between ApoE isoforms. ApoE consists of two structural domains: a 22 kDa N-terminal domain consisting of residues 1 to 191 that contains the low-density lipoprotein (LDL) receptor binding site and a 10 kDa C-terminal domain ranging from amino acids 216 to 299 that includes the major lipid binding site (Fig. 1.13b).
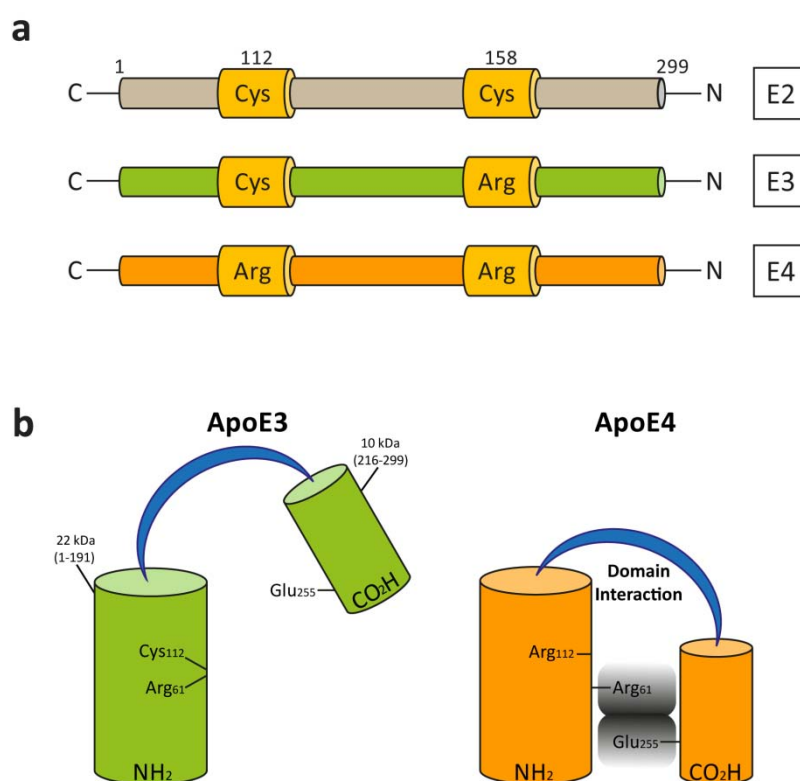
Figure 1.13. The three different ApoE isoforms only vary in two amino acids at position 112 and 158 (a). Due to the arginine-112 a domain interaction occurs in ApoE4 leading to a change of its biochemical properties (b). Figure generated after (Mahley et al. 2006)

ApoE4 has an arginine at position 112 that provides biochemical key properties that are putatively involved in ApoE4-associated AD pathology. Arginine at position 112 leads to conformational changes of ApoE4 resulting in the liberation of the side chain of arginine at position 61 from the helical bundle. This allows an interaction with glutamate at position 255 that causes a domain interaction of the LDL-receptor binding and the major lipid binding domain (Dong et al. 1994, Weisgraber 1990, Dong and Weisgraber 1996). In ApoE2 and ApoE3, the cysteine at position 112 inhibits this interaction, thus the domain interaction is much less frequent in these proteins. Furthermore, it has been shown that the domains, especially arginine-61 and glutamate-255, are located closer in lipid-free and phospholipid-bound ApoE4 than in ApoE3, which is also a result of the domain interaction (Hatters et al. 2005). The domain interaction provides a molten globule formation or reduced protein stability making ApoE4 more susceptible for proteolytic degradation (Weisgraber 1990, Morrow et al. 2002, Mahley et al. 2006).

1.4.2   Biological Functions

Throughout life and with increasing age, neurons need to be remodeled and repaired. Through its lipid transport function, ApoE plays an important role in these processes. ApoE redistributes lipids among cells, especially delivering lipids (including cholesterol) to injured cells for repair and protects from neurodegeneration and cognitive decline (Buttini et al. 1999, Buttini et al. 2002, Raber et al. 2004). Furthermore, ApoE is involved in maintaining synapto-dendritic connections, stimulates neurite outgrowth (Trommer et al. 2004), protects from oxidative stress (Miyata and Smith 1996) and plays a role in Aβ clearance (Ladu et al. 1995, Holtzman et al. 2000). ApoE also binds to tau protein and protects from hyperphosphorylation, whereby tau's ability to destabilize microtubules is inhibited (Strittmatter et al. 1994, Lovestone et al. 1996). In humans, there is an isoform-specific effect with ApoE4 being less effective to fulfill these tasks than ApoE2 or ApoE3. ApoE4 is also associated with impaired mitochondrial metabolism and CNS glucose utilization in non-demented carriers and AD patients (Small et al. 2000).

1.4.3   Aβ Regulation by ApoE

Under physiological conditions, levels of soluble Aβ are controlled by neuronal production and subsequent clearance via efflux into the peripheral circulation (Zlokovic et al. 2005), where lipidated ApoE regulates the proteolytic degradation of soluble Aβ (Jiang et al. 2008) (Fig. 1.14). ApoE is the main apolipoprotein in the brain and is predominantly synthesized and secreted by microglia as well as astrocytes (Pitas et al. 1987, Uchihara et al. 1995, Xu et al. 2006). Secreted ApoE becomes lipidated with phospholipids and cholesterol, which is mediated *inter alia* by the lipid transporter ATP-binding cassette transporter A1 (ABCA1) (Hirsch-Reinshagen et al. 2005, Wahrle et al. 2004), whose expression is regulated by activated Liver X receptors (LXR) that act as cellular cholesterol sensors (Beaven and Tontonoz 2006, Cao et al. 2007). Lipidation of ApoE leads to a conformation change of the protein resulting in an increased binding affinity of ApoE to Aβ and to membrane receptors (Fisher and Ryan 1999, Dergunov et al. 2000, Tokuda et al. 2000). Intra- and extracellular active proteolytic enzymes like insulin-degrading enzyme (IDE) (Kurochkin and Goto 1994) and neprilysin (NEP) (Iwata et al. 2000), which are also produced by microglia and astrocytes, work in concert with lipidated ApoE to clear soluble Aβ (Fig. 1.14).
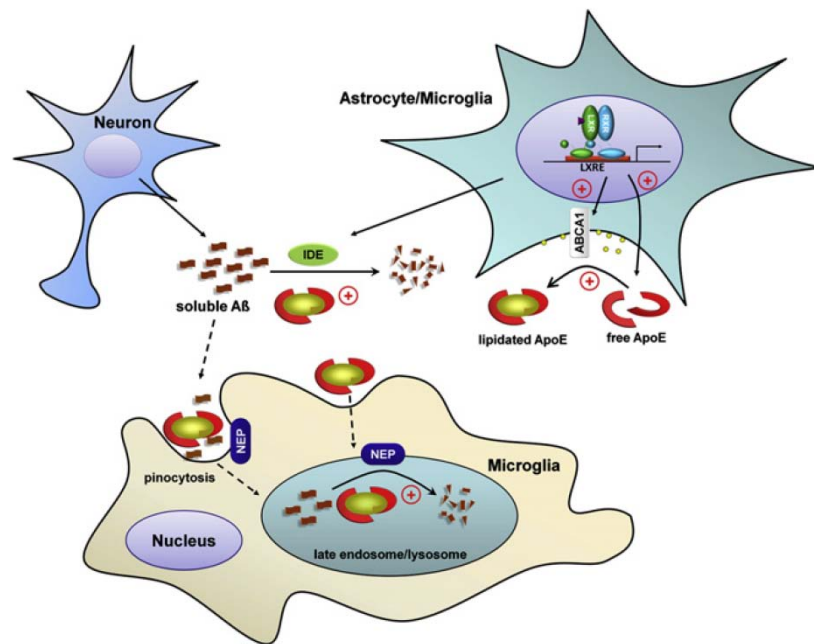
Figure 1.14. Lipidated ApoE binds to Aβ and contributes to its clearance in concert with Aβ degrading enzymes IDE and NEP. Picture from (Jiang et al. 2008)

Degradation of Aβ that is bound to lipidated ApoE takes place in the intercellular space or by glial cells via pinocytosis, where it enters autophagic pathways (Qiu et al. 1998, Jiang et al. 2008). As it has been shown that ApoE4 carriers harbor the highest Aβ levels (Holtzman 2004) and least lipidated ApoE (Tokuda et al. 2000, Jiang et al. 2008), it is suggested that structural differences between the different ApoE genotypes influence ApoE lipidation through conformation changes, thereby altering the efficiency of Aβ clearance. Therefore, the lipidation state of ApoE represents a critical determinant of the ability of ApoE to stimulate Aβ degradation.

1.4.4   Cellular Expression and Consequences

As already indicated, ApoE is normally synthesized by astrocytes and microglia, but also by oligodendrocytes and ependymal layer. Under certain physiological and pathological conditions, ApoE is also expressed by neurons (Han et al. 1994, Bao et al. 1996, Beffert et al. 1999, Aoki et al. 2003). This suggests that, in addition to its role as a lipid carrier, neuron-derived ApoE also functions as a stress-induced neuroprotective factor (Huang et al. 2004). Several mechanisms have been proposed to how apoE4 is linked to AD pathology. Due to the ApoE polymorphism in humans, there is an isoform-specific effect, with ApoE3 has a

protective impact on neurodegeneration while ApoE4 causes the opposite (Buttini et al. 1999). Furthermore, ApoE4 has also different effects when it is produced by astrocytes or by neurons. ApoE4 synthesized by astrocytes leads *inter alia* to increased Aβ production and deposition with simultaneously decreased ability of clearance leading to reduced neuritic outgrowth and memory impairment (Holtzman et al. 2000, Hartman et al. 2001, Vincent and Smith 2001). On the other hand, ApoE4 generated by neurons (Fig. 1.15) also causes reduced neurite outgrowth with decreased numbers of pre-synaptic terminals and loss of synapto-dendritic connections resulting in impaired long-term potentiation, which is in contrast to the neuroprotective characteristics of ApoE3. Additionally, enhanced phosphorylation of tau protein leading to the formation of NFTs is another effect of neuronal ApoE4. A possible cause for these effects is that ApoE4 accelerates lysosomal leakage that is induced by Aβ leading in the end to neurodegeneration and cognitive decline (Bellosta et al. 1995, Raber et al. 2000, Buttini et al. 2002, Ji et al. 2002, Brecht et al. 2004). Furthermore, ApoE in concert with Aβ is able to induce or accelerate impaired mitochondrial metabolism and oxidative stress, which is reflected in elevated levels of reactive oxygen species (ROS) that also contribute to neuronal death (Keller et al. 2000, Butterfield et al. 2002). Another important factor responsible for toxic effects is the unique biochemical property of ApoE4 to become proteolytically processed in neurons resulting in the conversion of a non-toxic full-length ApoE into toxic fragments (Huang et al. 2001, Harris et al. 2003).

1.4.5   Cellular Effects of ApoE Fragments

So far, one putative ApoE cleaving enzyme has been detected, which is a neuron-specific chymotrypsin-like serine protease that processes ApoE4 at methionine-272 and/or leucin-268. This leads to the liberation of an N-terminal 29 to 30 kDa fragment lacking the C-terminal 27 amino acids (Harris et al. 2003, Brecht et al. 2004). In brains of AD patients, further C-terminally truncated ApoE fragments with a size of 15 to 20 kDa have been also found. Hence, $ApoE_{1\text{-}272}$ has been demonstrated to be toxic in cell culture and inductive for neurodegenerative changes and the formation of NFTs in neurons of $ApoE4_{\Delta272\text{-}299}$ transgenic mice (Harris et al. 2003). Another fragment, the $ApoE4_{127\text{-}272}$, has been also reported to have neurotoxic properties in murine neuroblastoma cells (Chang et al. 2005). Key elements of the toxic action of fragmented ApoE are the receptor binding region, located in amino acids

136 to 150, and the lipid binding region, ranging from amino acids 240 to 270, whereby the deletion or mutation of one of those sequences resulted in a loss of toxicity.

Under normal conditions, ApoE enters the secretory pathway via crossing the endoplasmatic reticulum and Golgi apparatus and becomes secreted into the extracellular space (Chang et al. 2005) (Fig. 1.15). In contrast to ApoE3, large quantities of fragmented ApoE4 are translocated via its receptor binding domain into the cytosol, where fragments interact with the neuronal mitochondria and cytoskeleton. ApoE is able to bind, using its lipid-binding region, to α- and β-subunits of the mitochondrial F1-ATPase (Mahley et al. 1989), where accumulated fragments induce a disruption of energy metabolism mediated by mitochondrial regulation, electropotential impairment and trafficking failure of mitochondria to appropriate neuronal compartments as well as mitochondrial-apoptotic pathways (Mahley et al. 2006). Furthermore, the N-terminally truncated $ApoE4_{1-165}$ promotes cellular uptake of extracellular $A\beta_{42}$ leading to oxidative stress, whereupon, like in a vicious circle, neurons express more ApoE4 that is not as effective as ApoE3 in its antioxidant action and further accelerates mitochondrial dysfunction (Lauderback et al. 2002, Dafnis et al. 2011).
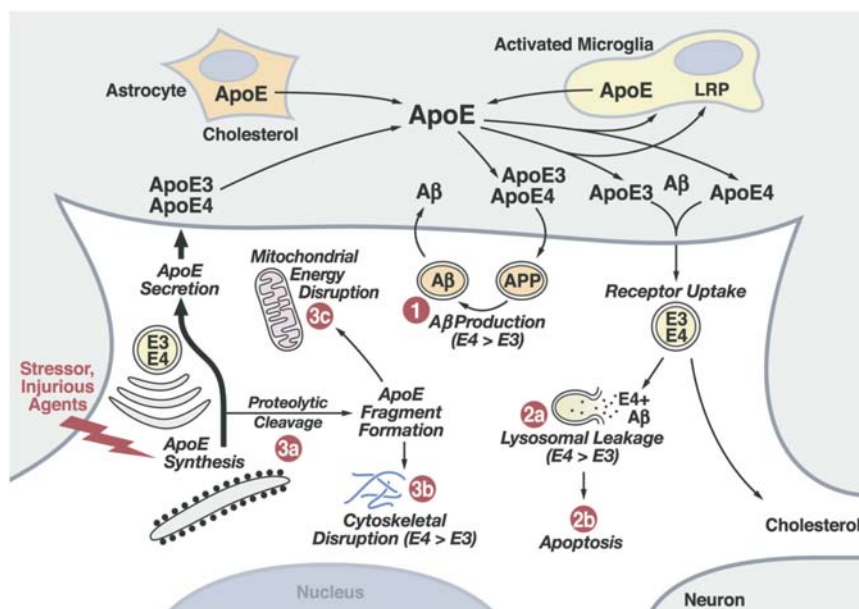
Figure 1.15. Overview of cellular effects induced by full-length and fragmented ApoE4 in neurons. Figure from (Mahley et al. 2006)

1.5 The Role of Autophagy in Alzheimer´s Disease

1.5.1 Biological Function of Autophagy

Autophagy has been recently implicated in various human pathological and physiological conditions like neurodegeneration, immunity, cancer, development, myopathies, etc. Autophagy is essential for removing misfolded proteins and damaged organelles and plays a critical role in maintaining cellular homeostasis (Klionsky 2010). Autophagy is an intracellular protein degradation pathway, in which autophagosome-lysosome and ubiquitin-proteasome pathways are the two major processes for protein clearance in eukaryotic cells. The formation of intraneuronal protein aggregates is a characteristic feature of several human neurodegenerative disorders like AD. One possible approach to treat such diseases may be to enhance degradation of these proteins associated with neurodegeneration.

1.5.2 Involvement of Autophagy in Alzheimer´s Disease

That autophagy plays a role in AD was first described in the 1960s, but the processes and mechanisms involved are almost still unknown. Therefore, it is important to figure out at which sites autophagy may be disrupted to explore possible modulating steps that could have a therapeutic impact on pathology and function in AD. Since autophagy is constitutively active in neurons, autophagic vacuoles (AVs) are very uncommon in healthy brains (Lee et al. 2010). Autophagosomes represent an intermediate step in the autophagy pathway and the amount depends on the rate of formation and clearance controlled by lysosomal degradation. Therefore, constitutive autophagy is essential for both normal protein turnover and for neuron survival.

Mutations in *PS1* and *APP* genes cause the familial forms of AD. PS1, a ubiquitous transmembrane protein and part of the γ-secretase complex, has a critical function in lysosomal and autolysosomal acidification, independent of its γ-secretase roles. It has been shown that in PS1-knockout blastocysts the degradation of autophagic substrates failed due to impaired AV clearance (Lee et al. 2010). Therefore, PS1 is essential for the activation of lysosomal proteases during autophagy to keep the balance between AV induction and clearance. Severe autophagy-related neuropathology is present in all forms of AD and also in AD mouse models carrying APP mutations. In TgCRND8 mice, harboring human APP$_{SwInd}$,

mutant APP over-expression led to autophagic-lysosomal pathology (Yang et al. 2011). However, the underlying mechanism is not well understood. One possible contributor may be the toxic βCTF (or C99), which is generated in the amyloidogenic APP processing pathway (Jiang et al. 2010). It is assumed that it affects the endosomal-lysosomal pathway and is aggravated by the inherited ε4 allele of ApoE (Cataldo et al. 2000, Nixon 2007). In AD, increased endocytosis and enhanced delivery into degradation compartments as well as less efficient lysosomal degradation together with increased oxidative damage (Terman and Brunk 2006, Kurz et al. 2008) and other toxic factors, including Aβ, lead to an impaired autophagy function. Endocytosis and autophagy are highly active in axons and synaptic buttons with high amounts of endosomes and autophagosomes reflecting disturbances in the retrograde organelle trafficking system in highly polarized neurons. This could affect APP processing and has been linked to AD pathogenesis (Overly and Hollenbeck 1996, De Vos et al. 2008, Morfini et al. 2009). At least 95 % of organelles in dystrophic neurites in AD and AD mouse models are AVs, further supporting a cargo-specific defect in axonal transport (Ihara et al. 2012). The impaired autophagic clearance promotes the accumulation of peptides and proteins, like Aβ and tau, which further accelerates the toxic cascade.

1.6 Project Objectives

1.6.1 Project I: Investigations of Pyroglutamate-modified Amyloid Peptides in Familial British and Danish Dementias

Besides Aβ in AD, the post-translational pGlu-modification is also abundant in the case of ABri and ADan peptides in FBD and FDD, respectively. The working hypothesis in this project deals with the question, if such a modification also leads to a drastic increase of toxicity of other amyloidogenic peptides than Aβ. If the pGlu-modification is also involved in the toxic effects of ABri and ADan peptides, it could turn out to be a relevant, general pathological mechanism in neurodegenerative diseases. In scope of this project, the impact of pGlu-modified and non-modified ABri and ADan peptides was investigated in terms of the neuronal integrity *in vitro* as well as *in vivo* with the following inquiries and aims:

I. Does the pGlu-modification of ABri/ADan influence their aggregation propensity?

II. Are pGlu-modified ABri/ADan more toxic compared to their non-modified counterparts?

III. Where are pGlu-modified ABri/ADan peptides distributed in human FBD/FDD brains?

IV. Are pGlu-modified ADan peptides present in the brain of an FDD-mouse model?

V. Development of a new mouse model for FDD

1.6.2 Project II: Aβ triggers Murine ApoE Fragmentation in Transgenic Mouse Models for Alzheimer's Disease

In this project the influence of Aβ peptides on ApoE expression and its proteolytical fragmentation was investigated. There is a mass of studies dealing with the effect of ApoE and its fragments on Aβ deposition and clearance, but it is completely undiscovered if Aβ peptides trigger ApoE fragmentation and the underlying mechanism behind it. Furthermore, it is absolutely unknown if endogenous murine ApoE becomes also proteolytically processed and how Aβ is involved in this pathological process. The working hypothesis is that, in addition, to the well-known effects of ApoE on Aβ levels, an increase in the amount of Aβ peptides in turn influences ApoE by promoting ApoE proteolysis which might imply a vicious

circle leading to neurodegeneration. Therefore, a variety of in vitro and in vivo investigations were performed with several dementia mouse models harboring endogenous murine ApoE as well as a variety of murine and human cell lines with endogenous or elevated ApoE levels in combination with or without increased amounts of intra- and extracellular Aβ peptides. Therefore, the following inquiries and aims were investigated:

I. Does intra- or extracellular Aβ accumulation trigger the ApoE proteolysis?

II. Is murine ApoE proteolytically processed like human ApoE under AD-pathological conditions?

III. Is there an accumulation of ApoE fragments in synapses?

IV. What is the toxic effect of ApoE fragments?

V. Is there a link between axonal degeneration, disrupted autophagy and ApoE processing?

VI. Does the over-expression of human mutant tau influence AD pathology and Aβ-induced proteolysis of murine ApoE in the 5XFAD mouse model?

2 Materials and Methods

2.1 Chemicals and Reagents

3,3'-diaminobenzidine (DAB)	(Sigma-Aldrich)
4',6-diamidino-2-phenylindole (DAPI)	(Sigma-Aldrich)
Agar	(Roth)
Amersham Hybond-ECL Membrane	(GE Healthcare)
Ampicillin	(Roth)
Bacto-Tryptone	(Roth)
Bacto-Yeast	(Roth)
Benzonase	(Merck)
Boric acid (H_3BO_3)	(Sigma)
Bovine serum albumin (BSA)	(Roth)
Cell culture media	(PAN Biotech)
Cell Titer 96®-AQ$_{ueous}$-Non-Radioactive-Cell-Proliferationassay (MTT)	(Promega)
Citric acid	(Roth)
Complete Mini-Protease Inhibitor Tablets	(EASYpack, Roche)
Cytotoxicity Detection KitPLUS (LDH)	(Roche)
Dimethyl sulfoxide (DMSO)	(Roth)
Dimethyl sulfoxide (sterile filtered for cell culture)	(Sigma-Aldrich)
DNA ladder 100 bp	(Bioron)
DNA ladder 1kb, Quick-load	(NEB)
Dulbecco's Phosphate Buffered Salt Solution (DPBS)	(PAN Biotech)
DyNAmo^{TM} Flash SYBR® Green qPCR Kit	(Thermo Fischer Scientific)
Ethanol, 99 %, denatured	(CVH Chemie-Vertrieb)
Ethanol, absolut	(Merck)
Ethidium bromide	(Roth)
Ethylenediaminetetraacetic acid (EDTA)	(Applichem)

32

Fetal Calf Serum (FCS)	(Biochrom)
Formic Acid, 98 %	(Roth)
GeneJET^{TM} Plasmid Miniprep Kit	(Fermentas)
Geneticin (G418)	(Sigma-Aldrich)
Glacial acetic acid	(Applichem)
Glucose	(Sigma)
Glycerol	(Sigma)
Hematoxylin	(Roth)
Histoprime® HistoGreen Chromagen	(Linaris)
Hydrochloric acid (HCl), 37 %	(Roth)
Hydrogen peroxide (H_2O_2)	(Roth)
Hygromycin B	(Invitrogen)
Isopropanol	(Roth)
L-glutamine	(PAN-Biotech)
Lipofectamine 2000®	(Invitrogen)
Luminata Crescendo Western HRP substrate	(Millipore)
Luminol	(Roth)
Magnesium chloride ($MgCL_2$)	(Sigma)
Magnesium sulfate ($MgSO_4$)	(Roth)
Methanol	(AppliChem)
Milk Powder, Blotting Grade	(Roth)
Na_2EDTA	(Roth)
N-acetyl-L-Cysteine (NAC)	(Sigma)
Non-essential amino acid mix (MEM NEAA)	(PAN Biotech)
Nonidet P-40	(Roche)
NZ amine (casein hydrolysate)	(Fluka)
Opti-MEM® Reduced-Serum Medium	(Invitrogen)
Para-coumaric acid	(Roth)
Paraffin	(Roth)
Paraformaldehyde (PFA)	(Roth)
PCR-10 x reaction buffer	(Axon)
PCR-25 mM $MgCl_2$	(Axon)

PCR-dNTPs	(Invitrogen)
PCR-Primer	(Eurofins MWG Operon)
PCR-Taq polymerase	(Axon)
Penicillin/Streptomycin	(PAN Biotech)
peqGold Cycle-Pure Kit	(Peqlab)
Phosphatase Inhibitor Cocktail 3	(Sigma-Aldrich)
Ponceau S	(Roth)
Potassium chloride (KCl)	(Roth)
ProGel Tris-Tricin, 16 %	(Anamed)
Proteinase K	(Peqlab)
QIAquick® Gel Extraction Kit	(Qiagen)
QuickChange® II XL Site-Directed Mutagenesis Kit	(Stratagene)
Rapid DNA Ligation Kit	(Fermentas)
Restriction enzymes and buffers	(NEB)
Roti®-Histokitt	(Roth)
Roti®-Quant universal kit	(Roth)
Sodium chloride (NaCl)	(Roth)
Sodium dodecyl sulfate (SDS)	(Roth)
Sodium hydroxide (NaOH)	(Applichem)
Spectra^{TM} Multicolor Broad Range Protein Ladder	(Fermentas)
Spectra^{TM} Multicolor Low Range Protein Ladder	(Fermentas)
Standard agarose	(Axon)
Sucrose	(Roth)
SulfoLink® Immobilization Kit for Peptides	(Thermo Scientific)
Thioflavin S (Thio-S)	(Sigma)
Thioflavin T (ThT)	(Sigma)
Tricin Running Buffer	(Anamed)
Tris(hydroxymethyl)aminomethane (Tris)	(Roth)
Tris-HCl SDS loading buffer, 2x	(Anamed)
Triton X-100	(Roth)
Trypsin/EDTA	(PAN Biotech)
Trypan Blue	(Sigma-Aldrich)

Tween® 20	(Roth)
VarioGel SDS loading buffer	(Anamed)
VarioGel Tricin, 4-12 %	(Anamed)
VarioGel Tricin running buffer (20 x)	(Anamed)
VECTASTAIN® Elite ABC Vectastain kit	(Vector Laboratories)
X-Ray developer Roentoroll 25	(Tetenal)
X-Ray fixative Superfix 25	(Tetenal)
XRay Screen Film CEA RP Medical, Blue Sensitive	(CEA)
Xylene	(Roth)
β-mercaptoethanol	(Sigma-Aldrich)

2.2 Antibody Generation

New Zealand white rabbits (Covalab, France) were immunized with 1 ml of antigen (pEASNCFAIRHFENK) in complete Freund's adjuvant (CFA) and boosted twice at 3 weeks intervals with 1 ml antigen in incomplete Freund's adjuvant (IFA). Three additional boosts using a shorter peptide (pEASNC) were carried out 3, 5 and 8 weeks later for the generation of AB76-2. Antibodies were purified by peptide affinity chromatography. For the purification of AB77, the peptide fragment pEASNCFAIRHFENK was covalently immobilized to beaded agarose using affinity columns according to manufacturer's instructions (SulfoLink® Immobilization Kit for Peptides). Serum of AB76-2 was first purified using an affinity column, containing the peptide fragment EASNC. The flow-through was subsequently loaded on a second column containing pEASNC immobilized fragments. The resulting eluate was kept as AB76-2. Antibody concentration was determined by photometry at OD280 (Biophotometer, Eppendorf) with a conversion factor of 714.3 according to protein size. The quality of the synthetic peptides was controlled by high-pressure liquid chromatography (HPLC) and mass spectrometry.

2.3 Monomerization of Synthetic Peptides

For monomerization, the pGlu-modified and non-modified peptides CTF23 (pE/EASNCFAIRHFENKFAVETLICS), ABri (pE/EASNCFAIRHFENKFAVETLICSRTVKKNIIEEN) and ADan (pE/EASNCFAIRHFENKFAVETLICFNLFLNSQEKHY, all from Peptide Specialty

Laboratories) were reconstituted in 10 mM NaOH to a final concentration of 1 mg/ml, sonicated for 5 min (Sonorex RK 100H, Bandelin electronic), snap frozen in liquid nitrogen and stored a -80 °C until further use (adapted from (Wirths et al. 2010b)).

2.4 Aggregation Assay

Peptide solutions were prepared on the basis of their molecular mass in physiological buffer (50 mM PBS, 50 mM NaCl, 0.01 % NaN3, pH 7.0) and mixed with 20 µM Thioflavin T (ThT) to a final concentration of 50 µM. 200 µl peptide solution was applied per well in triplicates of a 96-well microplate (Greiner Bio-One) and incubated in a Fluoroskan Ascent FL peltier adapter (Thermo Fisher Scientific) with stirring at 60 rounds per min (rpm) at 37 °C. Fluorescence, reading with excitation at 444 nm and emission at 482 nm, was recorded every 10 min for one week. Data were processed using GraphPad Prism 5 Software and Adobe Illustrator CS6.

2.5 Plasmid Design for the Generation of Stably Transfected Cell Lines and Transgenic Mice

All vectors for stable cell transfections and pronuclear injections were generated via subcloning out of output vectors into the eukaryotic expression vectors pCI-neo and pTSCα2a (Thy1-Promoter), respectively. Output vectors were gene specifically synthesized (Geneart).

2.5.1 Transformation of DH5α E. coli

The amount of output vector as well as all subcloned vectors was amplified using the transformation method into NEB 5-α Competent *Escherichia coli* (DH5α E. coli, NEB). 50 µl bacteria solution was mixed with 100 pg to 1 µg plasmid DNA and kept on ice for 30 min. After heat shock at 42 °C in water bath (Gesellschaft für Labortechnik, GFL) for exactly 30 s, bacteria were incubated on ice for an additional 5 min. Then, 950 µl SOC medium (super optimal broth with catabolite repression (SOC) medium: 20 g Tryptone, 5 g Yeast, 0.5 g NaCl, 2.5 ml 1 M KCl and 970 ml ddH$_2$O, pH 7.0 supplemented with 10 ml 1 M MgCl$_2$ and 20 ml 1 M glucose) were added to the mixture at room temperature (RT) and placed in an orbital shaker (GFL) at 225 rpm for 1.5 h at 37 °C. 100 to 150 µl of bacteria were then spread onto Lysogeny broth (LB)-ampicillin selection agar (15 g agar, 10 g Tryptone, 5 g Yeast, 10 g NaCl,

1 l ddH$_2$O, pH 7.0, 50 µg/ml ampicillin) plates (Greiner Bio-One) and incubated overnight at 37 °C. Single bacteria colonies were then picked and placed into 15 ml tubes (Greiner Bio-One) containing 7 ml LB-ampicillin (10 g Tryptone, 5 g Yeast, 10 g NaCl, 1 l ddH$_2$O, pH 7.0, 50 µg/ml ampicillin). After incubation at 225 rpm at 37 °C, bacteria were either supplemented with same volume of glycerol and frozen at -80 °C or lysed for plasmid purification.

2.5.2 Plasmid Purification

Plasmids were purified using the GeneJET^{TM} Plasmid Miniprep Kit. *E. coli* bacteria were rigorously vortexed, centrifuged at 5000 rpm for 7 min at RT (Megafuge 1.0R, Thermo Fischer Scientific) and further processed according to manufacturer's instructions. After eluting DNA with 30 to 50 µl elution buffer, the purified DNA was measured via photometry at OD260 and plasmids were stored at -20 °C until use.

2.5.3 Mutagenesis

Several mutageneses were performed using the QuickChange® II XL Site-Directed Mutagenesis Kit. Primers were designed using the QuickChange® Primer Design Program (www.genomics.agilent.com), synthesized by Eurofins MWG Operon (Ebersberg, Germany) and diluted to a final concentration of 100 pmol/µl. An overview of the performed mutageneses including the used primers is given in Tab. 2.1 and mutagenesis reagents and set-up are outlined in Tab. 2.2 and 2.3.

After mutagenesis reaction, DNA was digested with 1 µl Dpn I at 37 °C for 1 h. 45 µl XL10-Gold® ultracompetent cells were transfected according to manufacturer´s instruction. After transgene harboring bacteria grown up on LB-ampicillin selection plates, single colonies were picked and introduced into 15 ml tubes containing 7 ml LB-ampicillin medium and incubated overnight at 225 rpm at 37 °C. Afterwards, DNA was purified as described in section 2.5.2 and for sequencing a concentration of 100 ng/µl DNA in a total volume of 15 µl was sent to Eurofins MWG Operon.

Mutagenesis	Primer name (S/AS)	Sequence 5´-3´	Changed amino acid (aa)
ABriPP: ITM2B Stop267R	T969A T969A_AS	GCCGTGGAAACTTTAATTTGTTCTAGAACAGTCAAGAAAAACATTATTG CAATAATGTTTTTCTTGACTGTTCTAGAACAAATTAAAGTTTCCACGGC	aa267: TGA → AGA
ABriPP-244Q: ITM2B E244Q	G900C G900C_AS	TAAAGGTATTCAGAAACGTCAAGCCAGCAATTGTTTCGC GCGAAACAATTGCTGGCTTGACGTTTCTGAATACCTTTA	aa244: GAA → CAA
Thy1-Vector: pTSCα2 removed 2nd Xho I restricton site in cloning region	C329A C329A_AS	CGCGGCCGCATCGATATCGAGGTCC GGACCTCGATATCGATGCGGCCGCG	aa329: CTC → ATC

Table 2.1. Mutations ABriPP and ABriPP-244Q based on the non-mutated BRI2 construct in a pCMV-Sport6 vector. Sequential *in vitro* mutagenesis steps were performed to replace the functional stop codon on position 267 by an arginine (BRI2 → ABriPP) and the glutamate on position 244 by a glutamine (ABriPP-244Q). Thy1-vector mutagenesis was crucial for introducing the ADan1Q-34 construct. (S-Primer sense, AS-Primer antisense)

Reagent	Volume/Mass
10 x Reaction Buffer	5 µl
dsDNA template	50 – 100 ng
QuickSolution	3 µl
Primer sense	125 ng
Primer antisense	125 ng
NTPs	1 µl
PfuUltra HF DNA Polymerase (2.5 U/µl)	1 µl
ddH₂O	X µl to final Volume of 50 µl

Table 2.2. The QuickChange® II XL Site-Directed Mutagenesis Kit was used to mix reaction batch for mutagenesis.

PCR step	Temperature	Duration
1	95 °C	1 min
2	95 °C	50 s
3	60 °C	50 s
4	68 °C	60 min
5	Repetition steps 2 – 4	18 cycles
6	68 °C	7 min
7	4 °C	∞

Table 2.3. PCR protocol used for mutagenesis.

2.5.4   Sequencing

As described before, purified DNA was sequenced by Eurofins MWG Operon, who also synthesized the Primers for sequencing. Mutageneses results were compared with output sequences using the nucleotide basic local alignment search tool (BLASTn, http://blast.ncbi.nlm.nih.gov).

2.5.5   Subcloning into Eukaryotic Expression Vectors

For stable cell transfection and generation of transgenic mice it was necessary to subclone the transgenes out of prokaryotic into eukaryotic expression vectors like pCI-neo and pTSCα2a, respectively. Therefore, using distinct restriction enzymes, sequences of interests were cut off the output vectors (pMA-T and pCMV-Sport6, Tab. 2.4), target vectors (pCI-neo,

pTSCα2a, Tab. 2.4) were linearized and inserts were ligated with these target vectors using the Rapid DNA Ligation Kit (Tab. 2.6). Enzymatic digestion reactions (Tab. 2.5) were incubated for 1 h at 37 °C in a Thermomixer Compact (Eppendorf). Afterwards, 5 µl of the reaction batch containing linearized target vector and total volume of the batch including inserts were mixed with 1 or 3 µl of 10 x agarose gel sample buffer, respectively, and applied on 1 % to 2.5 % agarose gels (agarose boiled in 1 x TAE [TAE 50 x: 242 g Tris, 500 ml ddH$_2$O, 100 ml 0.5 M Na$_2$EDTA and 57.1 ml glacial acetic acid, adjusted to 1 l with ddH$_2$O] or 1 x TBE buffer [10 x TBE: 108 g Tris and 55 g H$_3$BO$_3$, 900 ml ddH$_2$O, 40 ml 0.5 M Na$_2$EDTA] supplemented with 0.33 µg/ml Ethidium bromide). Then, gel was placed in an electrophoresis chamber containing 1 x TAE or TBE buffer, respectively, reaction batches were loaded into gel wells and electrophoresis ran at 130 V using a Powerpack P25 power supply (Biometra) for approximately 30 min. Results were visualized via UV-light-transillumination at 366 nm in a Gel Doc 2000 (Bio-Rad) and analyzed with the Quantity One software program (Bio-Rad).

Inserts were cut out of gels using a scalpel, transferred into a 2 ml reaction tube (Eppendorf) and purified using the QIAquick® Gel Extraction Kit. DNA was purified according to manufacturer's instructions. Eluted inserts were applied one more time on the column membrane and centrifuged again to yield a higher DNA concentration.

The linearized vectors were purified using the peqGold Cycle-Pure Kit according to instruction manual to remove reagents from restriction enzyme digestion. The elution flow-through was also used for a second elution to increase DNA amount.

DNA amounts of insert and linearized vector were determined by photometry at OD260 and for ligation a molar ratio of 1:5 (vector:insert) was chosen. The ligation set-up with the Rapid DNA Ligation Kit is shown in Tab. 2.6. The ligation reaction was performed for 30 min at RT followed by an inactivation step at 65 °C for 10 min in a Thermomixer Compact. Then, 5 µl of the reaction mixture was used for transformation in DH5-α E. coli as described in section 2.5.1 and purified as in 2.5.2.

To verify a successful subcloning, either purified plasmids were further digested with distinct restriction endonucleases (Tab. 2.4) or bacteria colonies were screened in a Polymerase-Chain-Reaction (PCR, see section 2.8) and analyzed using gel electrophoresis as described before.

Insert	Host vector	Excised with	Required enzyme buffer	Target vector	Linearized with	Required enzyme buffer	Verified with	Required enzyme buffer
ABriPP	pCMV-Sport6	Not I / Sal I	NEB 3	pCI-neo	Not I / Sal I	NEB 3	SnaB I	NEB 4
ABriPP-244Q	pCMV-Sport6	Not I / Sal I	NEB 3	pCI-neo	Not I / Sal I	NEB 3	SnaB I	NEB 4
APP$_{751wt}$	pCMV-Sport6	Not I / Sal I	NEB 4	pCI-neo	Not I / Sal I	NEB 4	PCR + Nde I	- NEB 4
BRI2	pCMV-Sport6	Not I / Sal I	NEB 3	pCI-neo	Not I / Sal I	NEB 3	SnaB I	NEB 4
mApoE	pCMV-Sport6	Not I / Sal I	NEB 3	pCI-neo	Not I / Sal I	NEB 3	Bgl II	NEB 3
TRH-ADan1Q-34	pMA-T	Not I / Xho I	NEB 4	pCI-neo	Not I / Xho I	NEB 4	PCR + Pst I	- NEB 3
TRH-ADan1Q-34	pMA-T	Not I / Xho I	NEB 4	pTSCα2a (Thy1)	Not I / Xho I	NEB 4	PCR + Kpn I	- NEB 4

Table 2.4. Several inserts were subcloned into eukaryotic expression vectors with distinct restriction enzymes. Verification of successful subcloning was performed with further enzymatic digestions and PCR.

Reagent	Volume/Mass
10 x NEB Buffer X	2 µl
DNA	up to 1 µg
NEB restriction enzyme X (Y, Z,…)	1 µl
ddH$_2$O	X µl to final Volume of 20 µl

Table 2.5. Reaction batch for DNA digestion with restriction enzymes.

Reagent	Volume/Mass
5 x Rapid Ligation Buffer	4 µl
Linearized vector	100 ng
Insert (molar ratio 1:5)	according to vector amount
T4 DNA Ligase (5 U/µl)	1 µl
ddH$_2$O	X µl to final Volume of 20 µl

Table 2.6. Reaction batch for the ligation of digested inserts and vectors.

2.6 Cell Culture

2.6.1 Cell Lines and General Conditions

2.6.1.1 Cell Lines

Immortalized and pluripotent cell lines that were analyzed in biochemical and cell viability assays were obtained from the *Leibniz Institute DSMZ-German Collection of Microorganisms and Cell Cultures* (DSMZ) and the *American Type Culture Collection* (ATCC) (Tab. 2.7, 2.8).

All stably transfected cell lines (Tab. 2.8) were specifically selected by addition of first 500 µg/ml and later 300 µg/ml antibiotics into cell media. SH-SY5Y cells expressing SPA4CT and the SPA4CTΔcyto were already available (Wirths et al. 2007a).

2.6.1.2 General Conditions

Cells were routinely cultured in 75 cm^2 cell culture flasks (Greiner Bio-One) and kept at 37 °C and 5 % CO_2 in a humidified atmosphere (HERAcell 150 CO_2 Incubator, Thermo Fisher Scientific). Media were exchanged three times a week and cells were split once a week using Trypsin/EDTA. After use cells were frozen in media containing 10 % DMSO at -80 °C. For long term storage cells were kept in liquid nitrogen.

The following media were used for the different cell lines and they were all supplemented with 10 % fetal calf serum (FCS), 100 U/ml Penicillin, 100 µg/ml Streptomycin, 2 mM L-glutamine, and 1 % nonessential amino acids:

Dulbecco's Modified Eagle Medium (DMEM)	Hek293
	HOG
RPMI 1640	Ntera2
Dulbecco's Modified Eagle Medium F12 (DMEM/F12)	SH-SY5Y
	Neuro2a

Cell line	Discription / Source	Reference
Hek293	human embryonic kidney cells / DSMZ: ACC-305	(Graham et al. 1977)
HOG	human oligodendroglioma cell line / kindly provided by J. Thomas-Roig (Göttingen)	(Buntinx et al. 2003)
Ntera2	human testicular embryonal carcinoma cell line / ATCC: CLR-1973	(Fenderson et al. 1987) (Andrews et al. 1984)
SH-SY5Y	human neuroblastoma cell line / DSMZ: ACC-209 ApoE genotype: 3/3	(Biedler et al. 1973) (Jalava et al. 1990) (Ross et al. 1983)
Neuro2a	murine neuroblastoma cell line / DSMZ: ACC-148	(Klebe and Ruddle 1969) (Olmsted et al. 1970)

Table 2.7. List of carcinoma cell lines used in biochemical approaches and cell viability experiments.

Cell line	Transfected with	Vector	Selection with
SH-SY5Y Mock/pCI-neo	blank pCI-neo vector	pCI-neo	G418
SH-SY5Y Mock/pCep4	blank pCep4 vector	pCep4	Hygromycin
SH-SY5Y APP$_{751wt}$	full lenght APP$_{751}$	pCI-neo	G418
SH-SY5Y SPA4CT	SPA4CT (Dyrks et al. 1992, Lichtenthaler et al. 1997)	pCep4	Hygromycin
SH-SY5Y SPA4CTΔcyto	SPA4CT without cytoplasmatic APP domain (Dyrks et al. 1992, Lichtenthaler et al. 1997)	pCep4	Hygromycin
Neuro2a Mock/pCI-neo	blank pCI-neo vector	pCI-neo	G418
Neuro2a Mock/pCep4	blank pCep4 vector	pCep4	Hygromycin
Neuro2a mApoE	murine ApoE sequence	pCI-neo	G418
Neuro2a SPA4CT	SPA4CT	pCep4	Hygromycin
Neuro2a mApoE/SPA4CT	murine ApoE/SPA4CT	pCI-neo/ pCep4	G418/ Hygromycin
Neuro2a SPA4CTΔcyto	SPA4CT without cytoplasmatic APP domain	pCep4	Hygromycin
Neuro2a mApoE/SPA4CTΔcyto	murine ApoE/SPA4CTΔcyto	pCI-neo/ pCep4	G418/Hygromycin
Hek293 Mock/pCI-neo	blank pCI-neo vector	pCI-neo	G418
Hek293 BRI2	full length ITM2B	pCI-neo	G418
Hek293 ABriPP	full length ITM2B with Stop267R (Vidal et al. 1999)	pCI-neo	G418
Hek293 ABriPP-244Q	full length ITM2B with Stop267R and E244Q (Cynis et al. 2006)	pCI-neo	G418
Hek293 ABri1Q-34	TRH-ABri1-34 with E34Q (Cynis et al. 2006)	pCI-neo	G418

Table 2.8. List of several cell lines that were stably transfected for biochemical approaches and cell viability assays.

2.6.2   Stable Transfection

Cells were split using Trypsin/EDTA and transferred into a 6-well plate (Thermo Scientific). They were cultured in complete medium for three days at 37 °C and 5 % CO_2 in a humidified atmosphere. On day of the transfection, medium was exchanged with 2 ml/well antibiotics-free medium and kept for at least 1.5 h in the cell incubator. 4 µg DNA was gently mixed with 250 µl Opti-MEM® Reduced Serum Mix. 10 µl Lipofectamine™ 2000 was applied to 240 µl Opti-MEM® Reduced Serum Mix and incubated for 5 min at RT. Afterwards, both mixtures were combined and further incubated for 20 min at RT. Then, reaction batch was added to the cells and after 6 h medium was replaced again by antibiotics-containing medium. After an incubation time of 24 h in the CO_2 incubator, cells were transferred by splitting with Trypsin/EDTA into 25 cm^2 cell culture flasks (Greiner Bio-One). They were kept there for an additional 24 h before antibiotic selection took place with 500 µg/ml G418 or Hygromycin B to select cells carrying pCI-neo or pCep4 expression vector, respectively. Once the cell line was stably transfected, antibiotic concentration was reduced to 300 µg/ml.

2.6.3   Preparation of Cell Protein Lysates

For protein extraction cell medium was removed and ice-cold DPBS was applied on the cells. Using a cell scraper (Sarstedt AG) the cells were detached, mixed rigorously via pipetting and transferred into a 15 ml tube. After centrifugation at 1100 rpm for 4 min at 4 °C, supernatant was removed and, reliant on the pellet size, 100 to 150 µl lysis buffer (50 mM Tris-HCL [pH 7.5], 150 mM NaCl, 1 % Nonidet P-40, 1 % Triton X-100, 2 mM EDTA, 1 tablet per 10 ml buffer of Complete Mini-Protease Inhibitor) was added for resuspension. Mixture was kept on ice for 1 h with vortexing steps every 10 min, followed by centrifugation at 5000 rpm at 4 °C for 10 min. The supernatant containing extracted proteins was stored at -20 °C until further use. Determination of protein concentrations for Western-blotting was performed as described in section 2.10.3.

2.6.4   Cytotoxicity Assay

Toxicity of pGlu-modified and non-modified ABri/ADan/CTF23 peptides was analyzed using SH-SY5Y neuroblastoma cells. The effect of these peptides on cell viability was assessed by measuring lactate dehydrogenase (LDH) release (Cytotoxicity Detection KitPLUS). For cell

number determination 50 µl cells suspension were mixed with 50 µl Trypan Blue and introduced into a Neubauer-improved counting chamber (Laboroptik). SH-SY5Y cells were plated at a density of 7500 cells/well in 96-well plates in 100 µl fresh medium. After 36 h, medium was exchanged with 200 µl medium including 5 ([pGlu-]ABri/ADan), 50 or 200 µM ([pGlu-]CTF23) freshly prepared and monomerized peptides. After cells were incubated at 37 °C in 5 % CO_2 for 24 h, reagents of the Cytotoxicity Detection KitPLUS were applied to each well corresponding to the directions for use and absorbance values at 490 nm were measured using a µQuant plate reader (BioTek Instruments) combined with the MikroWin 2000 software package (v4.04, Mikrotek). Each assay was performed at least five times. LDH release was calculated with Microsoft Office Excel 2007 (Microsoft) by subtracting the average background absorbance from all experimental absorbance values. The resulting values of cells with peptide application and controls where then normalized to the LDH-high control (lysed cells) and the percentage of LDH-release was calculated. Significance was tested by using Unpaired-t-test and Graphs were generated using GraphPad Prism 5 software. Figures were processed using Adobe Illustrator CS6.

2.6.5   Proliferation Assay

A potential effect of pGlu-modified and non-modified CTF23 peptides on the cell proliferation rate was analyzed on several human cell lines like SH-SY5Y, Hek392, Ntera2 and HOG. These cells were incubated with 5 to 200 µM pGlu-CTF23 or non-modified CTF23. The influence of endogenous generated pGlu-modified ABri on cell viability was studied on Hek293 cells that were stably transfected with genes encoding BRI2, ABriPP, ABriPP-244Q, TRH-ABri1Q-34 and pCI-neo as Mock control. Furthermore, SH-SY5Y neuroblastoma cells stably expressing the SPA4CT construct were treated with 10 µM to 10 mM N-acetyl-L-Cysteine (NAC), an effective antioxidant drug for the reduction of reactive oxygen species (ROS) (Aruoma et al. 1989).

In general, 5000 (Ntera2, HOG) to 7500 (SH-SY5Y, Hek293) cells were transferred per well in a 96-well plate. Cell number was determined as described for the Cytotoxicity assay. After cell growth for 24 h, peptides or NAC, respectively, were applied to the cells and incubated for further 24 h in the CO_2 incubator before assay was performed. Stably transfected Hek293 were directly analyzed after 24 h using the Cell Titer 96®-AQueous-Non-Radioactive-Cell-Proliferation assay. This assay consists of a distinct tetrazolium compound

(3-[4,5-dimethylthiazol-2-yl]-5-[3-carboxymethoxy-phenyl]-2-[4-sulfophenyl]-2H-tetrazolium; MTS) that is converted into formazan by mitochondrial dehydrogenase enzymes in metabolically active cells. The formazan generation results in a color change of the medium that can be measured at 490 nm. Most importantly, concerning the application of NAC, it was crucial to wash the SH-SY5Y$_{SPA4CT}$ cells three times and exchange medium at least 3 h prior the application of proliferation agents, because NAC also promotes a spontaneous conversion of MTS to formazan in the absence of cells (observed in experiments and described in (Iglesias et al. 1999)). For proliferation measurement, 20 µl CellTiter Reagent was added per well and plate was incubated for 2 h at 37 °C and 5 % CO_2. Measurement of absorbance values and data processing were performed as described for the Cytotoxicity assay. Each assay was performed at least five times.

2.7 Laboratory Animals

2.7.1 General Information and Housing Conditions

Mouse lines were maintained in the central animal facility of the University Medicine Göttingen. For phenotyping, mice were kept under constant 12 h/12 h inverted dark/light conditions (light from 20:00 to 08:00 o'clock) and supplied with food and water *ad libitum*. All experiments with laboratory mice were performed in agreement with the German guidelines for animal care and approved by the Landesamt für Verbraucherschutz und Lebensmittelsicherheit (LAVES) Niedersachsen.

2.7.2 Generation of a New Transgenic Mouse Model for Familial Danish Dementia

The development of transgenic mouse models had remarkable impacts on understanding and treating AD and other neurodegenerative disorders. Generation of the Thy1-TRH-ADan1Q-34 construct is described in section 2.5.3 to 2.5.5. For injection, the 7.2 kbp transgene construct was digested with EcoR I and Pvu I to remove most of the prokaryotic DNA and isolated via agarose gel extraction (Fig. 2.1). The DNA was then purified by two centrifugations at 13000 x g at RT for 15 min and the lowermost 20 % were discarded. To achieve a final concentration of 30 ng/µl in a total volume of at least 200 µl, DNA was diluted in 5 mM Tris (pH 7.4) with 0.1 mM EDTA. Via pronuclear injection in C57BL/6J mice, a service

of the Animal Facility at the Max-Planck-Institute for Experimental Medicine Göttingen, transgenic mice were generated by inserting the Thy1-TRH-ADan1Q-34 sequence (Fig. 2.1).
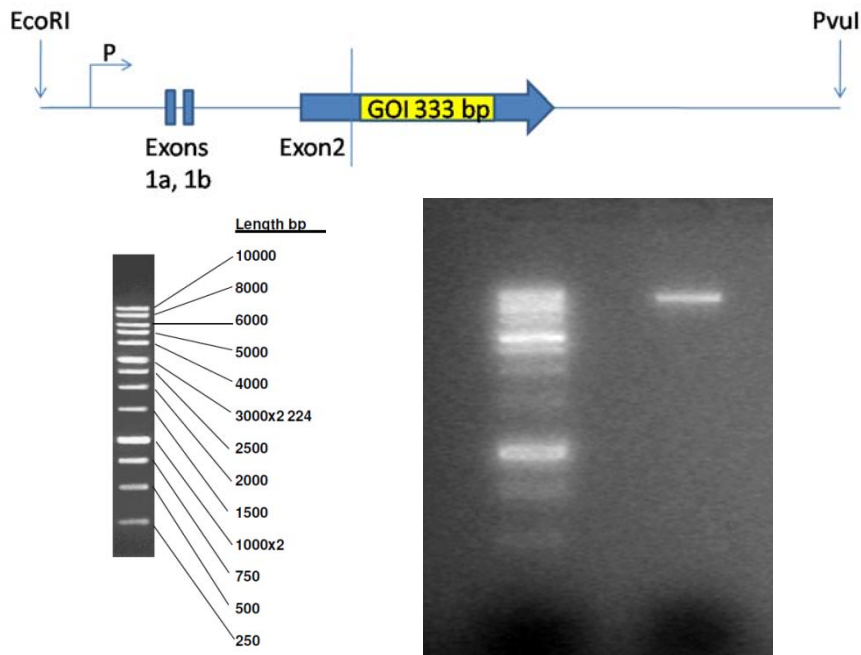
Figure 2.1. The 7.2 kbp transgene used for the generation of TRH-ADan1Q-34 transgenic mice was linearized with EcoR I and Pvu I. The gene of interest (GOI) is positioned in Exon 2 of the Thy1-vector. Insertion of the transgene into C57BL/6J mice was performed via pronuclear injection.

This construct contains glutamine instead of glutamate at position one of the amyloid peptide sequence to rapidly produce high amounts of pGlu-modified ADan. The signal sequence of the thyrotropin-releasing hormone (TRH) was used to achieve the secretion of ADan peptides, whereas the Thy1-promoter should drive a locally controlled expression of the transgene in neurons, especially in pyramidal cells of the hippocampus and cortex (Cynis et al. 2006, Wirths et al. 2009). The injection of the TRH-ADanQ1-34 construct resulted in the generation of 10 founders (OW20-29). Based on results of quantitative real-time polymerase chain reactions (RT-PCR) for measuring gene amounts, so far 3 lines were established (OW20, OW23 and OW24) by subsequently breeding with C57BL/6J mice. For genotyping, as described in section 2.7.4, tail biopsies were taken from generated founders and their offspring with C57BL/6J background that were transgenic for ADanQ1-34.

2.7.3   The ADanPP7 Mouse Model for Familial Danish Dementia

The **ADanPP7** mouse model expresses the Danish mutant form of BRI2 (ADanPP) under the control of the Syrian Hamster prion-protein expression cassette on a C57BL/6 background. This model exhibit age-dependent ADan amyloidosis throughout the brain that is combined with microhemorrhage, neuritic dystrophy and neuroinflammation (Coomaraswamy et al. 2010). Mice at 2, 4, 13 and 20 months of age were used *inter alia* for the characterization of the newly developed antibodies AB77 and AB76-2 detecting pGlu-ADan.

2.7.4   Transgenic Mouse Models for Alzheimer´s Disease

In preparation for this study, several mouse models for AD were used with C57BL/6J background:

The **5XFAD mouse model** (Tg6799) carries five familial mutations under control of the neuron specific Thy1-promoter: three in the human APP gene (APP with the Swedish [KM670/671NL], Florida [I716V] and London [D678N] mutations) and two in the in PS1 gene (M146L and L286V). These mice show early intraneuronal Aβ accumulations and plaque-associated pathology already at 3 months of age, increased anxiety and declined memory performance at 6 months, cortical neuron loss at 12 months and deficits in motor abilities starting at 9 months of age (Oakley et al. 2006, Jawhar et al. 2011b, Jawhar et al. 2012). Animals used in this thesis were 6, 9 and 12 months of age.

The **APP/PS1KI mouse model** was created with two mutations in the human APP with Swedish and London mutations expressed via the Thy1-promoter as well as two mutations in the murine PS1 with M233T and L235P fAD-linked mutations under control of the endogenous mouse PS1 promoter (Casas et al. 2004). This mouse model exhibits robust learning deficits at the age of 6 months (Wirths et al. 2008) and age-dependent axonopathy (Wirths et al. 2007b). Furthermore, these mice show neuron loss in the CA1 cell layer of the hippocampus together with synaptic deficits and hippocampus atrophy that coincide with intraneuronal aggregation of N-terminally modified Aβ variants (Breyhan et al. 2009). In this study, mice were analyzed in an age and genotype depended manner at 2, 6 and 10 months of age. For genotype dependent pathology analyses, mice were used that were single transgenic for APP (hemizygous for APP: APP_{he}) or PS1KI (PS1KI homozygous: $PS1KI_{ho}$) as well

as mice that have mutant APP combined with either hemi- or homozygous expression of mutant PS1 (APP/PS1KI$_{he}$ or APP/PS1KI$_{ho}$).

The **APP/PS1-21 mouse model** harbors human APP with the Swedish mutation as well as mutated PS1 (L166P) also expressed under the control of the murine Thy1-promoter. In these mice cerebral amyloidosis starts at 6 to 8 weeks of age with associated pathologies like dystrophic synaptic boutons, hyperphosphorylated tau-positive neuritic structures and robust gliosis. In addition, local neuron loss in the dentate gyrus and deficits in the spatial reference memory also occur at the age of 8 months (Radde et al. 2006). In the course of this study, mice were analyzed at the age of 2, 5 and 7 months.

The **3xTg triple transgenic mouse model** was generated by inserting human APP with the Swedish mutation and human tau with the P301L mutation driven by Thy1-regulatory elements into homozygous PS1KI (M146V) mouse embryos (Oddo et al. 2003). These mice develop NFTs and age-dependent APP accumulation, but intracellular Aβ initially occurs at the age of 12 months (Winton et al. 2011). In comparison to the previously described mouse models, 3xTg also exhibit obviously less neuritic dystrophy associated with few plaque pathology still at the age of 18 months (Wirths et al. 2012). In this work, mice were analyzed at 16 months of age.

The **PS19 mice** over-express human tau with the P310S mutation under the control of the murine prion protein promoter (Yoshiyama et al. 2007). These mice develop filamentous tau lesions at 6 months of age, whereas the progression of tau pathology correlates with neuron loss as well as hippocampal and entorhinal cortical atrophy by 9 to 12 months of age. Already at 3 months of age, PS19 mice show hippocampal synapse loss as well as impaired synaptic function before the onset of NFT-like tau structures. In the current thesis, PS19 mice were crossed with the 5XFAD mouse model to generate the 5XFAD/PS19 model and female PS19, 5XFAD and triple transgenic 5XFAD/PS19 mice were investigated at 3, 7 and 9 months of age.

2.7.5   Genotyping

Genotyping of the generated ADan-transgenic as well as APP/PS1KI mice was performed using PCR and RT-PCR DNA amplification methods (see section 2.8). For DNA isolation 200 – 500 µl Lysis buffer (100 mM Tris/HCl [pH 8.5], 5 mM EDTA, 0.2 % dodecyl sulfate [SDS] and 200 mM NaCl) supplemented with 10 µl/ml Proteinase K was applied to tail biopsy and incubated at 55 °C for 20 h and 450 rpm in a Thermomixer Compact. Samples were then centrifuged at 17000 rpm and 4 °C for 20 min (Heraeus Biofuge Stratos). Supernatant was transferred into a fresh 1.5 ml reaction tube containing 200 to 500 µl ice-cold isopropanol, respective to Lysis buffer volume, and inverted until precipitate became visible. After centrifugation at 13000 x g at 4 °C for 10 min supernatant was discarded, pellet washed with ice-cold 500 µl ethanol (70 %, absolute) and centrifuged again. Supernatant was removed again and pellet dried at 55 °C for at least 1 h. Dried genomic DNA was then diluted in 30 µl ddH$_2$O and incubated at 55 °C overnight. DNA concentration was determined via photometry at OD260.

2.8   (Quantitative real-time) Polymerase-Chain-Reaction

For genotyping transgenic mice as well as transfected E.coli, both PCR and RT-PCR were performed. The DyNAmo^{TM} Flash SYBR® Green qPCR Kit was used for preparing RT-PCR reaction batches and reaction took place in an Mx3000P cycler (Stratagene), while measurements were recorded with the MxPro Mx3000P software (Stratagene). In the RT-PCR approach, samples were prepared in duplicates for each animal and normalized to the murine house-keeping APP gene to quantify the DNA amount of the ADanQ1-34 transgene. For validating the efficiency of RT-PCR primers, standard curves were created with pooled DNA in serial dilutions (undiluted, 1:10, 1:100 and 1:1000). The set-up and performance steps for both DNA amplification methods are shown in Tab. 2.9, 2.10. Primers (Tab. 2.11) were obtained from Eurofins MWG Operon and diluted to a final concentration of 100 pmol/µl. RT-PCR results were analyzed with the MxPro Mx3000P software and Microsoft Excel. For the PCR screening of transfected E.coli, single colonies were picked from LB-ampicillin selection agar plates and transferred into a 96-well plate containing 200 µl LB-ampicillin medium. After shaking at 225 rpm at 37 °C for 6 h, 2 µl of each colony was used for PCR. As described in section 2.5.5, finished PCR batches were supplemented with 3 µl 10

x agarose gel sample buffer and applied in individual wells of an agarose gel containing 0.33 µg/ml ethidium bromide. After electrophoresis at 130 V, DNA was visualized via UV-light-transillumination and analyzed with the Quantity One software program.

PCR reagent	Volume/Mass	RT-PCR reagent	Volume/Mass
DNA (20 ng/µl) or Bacteria	2 µl	DNA (20 ng/µl)	1 µl
10 x Reaction Buffer BD	2 µl	DyNAmo™ Flash master mix	10 µl
dNTP mix (2 mM)	2 µl	Rox dye	0.2 µl
$MgCl_2$ (25 mM)	3.2 µl	Primer sense (10 pmol/µl)	1.5 µl
Primer sense (10 pmol/µl)	0.5 µl	Primer antisense (10 pmol/µl)	1.5 µl
Primer antisense (10 pmol/µl)	0.5 µl	ddH_2O	5.8 µl
ddH_2O	9.6 µl		
Taq-Polymerase (5 U/µl)	0.2 µl		

Table 2.9. Reagents used for PCR and RT-PCR genotyping.

PCR step	Temperature	Duration	RT-PCR step	Temperature	Duration
1	94 °C	3 min	1	95 °C	10 min
2	94 °C	3 min	2	95 °C	15 s
3	58 °C	1 min	3	64 °C	20 s
4	72 °C	1 min	4	72 °C	30 s
5	Repetition steps 2 – 4	35 cycles	5	Repetition steps 2 – 4	40 cycles
6	72 °C	5 min	6	55 °C	30 s
7	4 °C	∞	7	4 °C	∞

Table 2.10. PCR and RT-PCR protocol used for mouse genotyping.

Object	PCR/ RT-PCR	Primer name (S/AS)	Sequence 5´-3´	Product size	Agarose gel [%]
Genotyping TRH-ADanQ1-34 mice (transgene)	RT-PCR	RT-OW20-b_for RT-OW20-b_rev	AGAAAGGACCTGCAGAGAGTGC TTCCACGGCGAACTTGTTCTCG	118 bp	-
Genotyping TRH-ADanQ1-34 mice (house keeping gene)	RT-PCR	APP_int for APP_int rev	TCTTGTCTTTCTCGCCACTGGC GCAGTCAGAAGTTCCTAGG	250 bp	-
Genotyping TRH-ADanQ1-34 mice	PCR	Thy1_for ADan_rev	TGATCTTCGTGCTGACCGGC GTTCAGGAACAGGTTGAAGC	278 bp	2 %
Genotyping APP/PS1KI mice	PCR	hAPP_for hAPP_rev	GTAGCAGAGGAAGAAGTG CATGACCTGGGACATTCTC	505 bp	1 %
Screening for transfected E.coli (APP751wt/pCI-neo)	PCR	hAPP_for hAPP_rev	GTAGCAGAGGAAGAAGTG CATGACCTGGGACATTCTC	505 bp	1 %
Screening for transfected E.coli (TRH-ADan1Q-34 in pCI-neo and Thy1)	PCR	Thy1_for ADan_rev	TGATCTTCGTGCTGACCGGC GTTCAGGAACAGGTTGAAGC	278 bp	2 %

Table 2.11. Primers used for genotyping via PCR and RT-PCR approaches as well as agarose gels applied for DNA visualization. (S-Primer sense, AS-Primer antisense)

2.9   Behavioral Analyses

Behavior experiments were performed with the newly generated mouse lines OW20 (n = 5), OW23 (n = 3) and OW24 (n = 4) harboring the transgene ADan1Q-34. Mice were tested at the age of 6 months and data were compared to age-matched wild-type C57BL/6J controls (n = 5). Several paradigms were used to analyze motor and coordination ability, which can be tested by balance beam and string suspension task, changes in anxiety behavior, measurable by the elevated plus maze, and memory impairment, which is evaluated by performing cross maze and Morris water maze.

2.9.1   Balance Beam

For the detection of possible disturbances of balance and general motor deficits, the balance beam task was performed (Arendash et al. 2001). Mice were positioned in the middle of a 50 cm long and 1 cm wide wooden bar, which was 44 cm elevated and affixed above a padded surface. At both ends of the bar, two 14 x 10 cm wooden escape platforms were installed. Each test was performed three times for a duration of 60 s. The time, in which mice stayed on the beam, was measured and in case of reaching the platform a time of 60 s was given. Data were processed using GraphPad Prism 5 software and statistical analyses were carried out using the Unpaired-t-test.

2.9.2   String Suspension

The string suspension test is a method to determine a mouse´s agility and fitness. A 3 mm thick rope was anchored to the balance beam apparatus in 35 cm height. Mice were attached in the middle of this rope only by their fore-paws. For data evaluation a score system of 0 to 5 was used during the 60 s test duration: 0 = unable to stay on rope; 1 = hanging on rope with one pair paws; 2 = like 1, but with attempt to climb; 3 = sitting on rope, keep in balance; 4 = rope is surrounded by all paws and tail together with a laterally movement of the mouse; 5 = escape (Jawhar et al. 2012). Data processing and statistics were performed as described for the balance beam task.

2.9.3   Elevated Plus Maze

In order to assess changes in avoidance behavior, the elevated plus maze was performed (Lister 1987). The apparatus consisted of a 75 cm elevated plus-shaped construction with two 15 cm long and 5 cm wide open and enclosed arms with 15 cm high walls. The mouse was positioned in the 25 cm^2 central region and was allowed to explore for 5 min. Via the ANY-maze^{TM} video tracking system, the total distance travelled and the time spent in open arms compared to the time in closed arms were measured and calculated. Further data processing occurred as previously described.

2.9.4   Cross Maze

The cross maze is one method *inter alia* to analyze the performance of working memory in terms of spontaneous alternations (Jawhar et al. 2012). The experimental set-up was assembled out of four 90° angled arms (30 cm length x 8 cm width x 15 cm height) surrounding a central region (8 x 8 cm). Animals were always placed in the same arm as starting position and were allowed to explore for 10 min. The total distance travelled and alternations were recorded by the ANY-maze^{TM} video tracking system. The number of alternations possible was calculated as the total number of recorded arm entries minus three. The alternation percentage was calculated as the percentage of actual alternations to the possible number of arm entries. Data were analyzed using Microsoft Excel and GraphPad Prism Software. For statistics, the Unpaired-t-test was used.

2.9.5   Morris Water Maze

Using the Morris water maze, motor skills, learning ability and access on the spatial reference memory were analyzed. Mice were confronted with the task to find a hidden platform (diameter 10 cm) in a round basin (diameter 110 cm) filled with opaque water (modified after (Morris 1984, Vorhees and Williams 2006)). The pool was divided into four equally spaced quadrants. First of all, in the cued training (3 days), animals were conditioned to the existence of a visible platform (cued with a flag), whereas position of the platform was altered in all four trials. Next stage, in the acquisition training, platform was hidden and positioned during all four trials on five test days at the same location within the target quadrant. Cues were placed between the quadrants for orientation and start positions were

varied. In the last passage, the probe trial, the platform was removed. Each test trial lasted 60 s. The ANY-maze™ video tracking system was used to measure escape latency, total distance travelled and swimming speed. In probe trial, additionally, percentages of time in target, left, right and opposite quadrant were recorded. Data analyses were performed with Microsoft Excel and GraphPad Prism. The Unpaired-t-test and One-Way-Anova were used to find statistically significant differences between ADan1Q-34 transgenic mice and wild-type C57BL/6J.

2.10 Preparation of Human and Mouse Tissue for Biochemistry

2.10.1 Extraction of Soluble and Insoluble Fractions

For mouse brain and spinal cord extraction, animals were sacrificed by CO_2 narcosis followed by cervical dislocation and decapitation. Brain hemisphere and spinal cord were directly frozen on dry ice and kept at -80 °C until further use. Murine and human tissues were homogenized with 10 strokes of a glas-teflon homogenizer (800 rpm, CAT) in 700 µl Lysis buffer 1 (120 mM NaCl, 50 mM Tris, 1 tablet Complete Mini-Protease Inhibitor and 100 µl Phosphatase Inhibitor Cocktail 3, dissolved in 10 ml ddH_2O, pH 8) per 100 mg tissue. After centrifugation at 17000 x g and 4 °C for 20 min, supernatant was stored as soluble fraction at -80 °C until use. Pellet was resuspended via sonication (Branson Sonifier 150, G. Heinemann, Ultraschall- und Labortechnik) in either 800 µl (brain hemisphere) or 200 µl (spinal cord) 2 % SDS (dissolved in 10 ml ddH_2O, supplemented with 1 tablet Complete Mini-Protease Inhibitor and 100 µl Phosphatase Inhibitor Cocktail 3), 1 µl Benzonase was added and incubated for 5 min at RT. After centrifugation at 17000 x g and 4 °C for 20 min, supernatant was saved as insoluble fraction at -80 °C until further use.

2.10.2 Extraction of Crude Synaptosomal Fractions

For the preparation of crude synaptosomal fractions, mouse brains were extracted as described before. Brains were homogenized at 800 rpm in 1 ml Lysis buffer (0.32 M sucrose, 5 mM Hepes and 10 ml ddH_2O supplemented with 1 tablet Complete Mini-Protease Inhibitor and 100 µl Phosphatase Inhibitor Cocktail 3, pH 7.5) per 100 mg tissue. After centrifugation at 1000 x g at 4 °C for 10 min, supernatant was transferred into a new 2 ml reaction tube and centrifuged again at 12000 x g at 4 °C for 20 min. Supernatant containing mainly microsomes

and soluble enzymes was immediately frozen on dry ice and pellet containing crude synaptosomes was resuspended in 500 µl 0.01 M PBS and stored at -80 °C until further use.

2.10.3 Determination of Protein Concentrations

For Western-blotting, protein concentrations of lysates were determined using the Roti®-Quant universal kit. Therefore, 50 µl of 1:10 dilutions of samples (lysate:H_2O) as well as albumin dilutions (2, 1.5, 1.0, 0.75, 0.5, 0.25, 0.125 mg/ml and H_2O) for the generation of a standard curve were applied in triplicates into a 96-well plate. A mixture of Reagent 1 and Reagent 2 was added in a ratio of 15:1, respectively, in a total volume of 100 µl to each well. After incubation at 37 °C for 30 min in darkness, concentrations were measured at 490 nm using a µQuant plate reader combined with the MikroWin 2000 software package.

2.11 Immunoblot Analyses

2.11.1 Dot-blot Analyses

Prior to experiments, pGlu-modified and non-modified ABri and Aβ (Aβ$_{1-42}$ and Aβ$_{pGlu3-42}$) peptides were dissolved to 1 mg/ml in ddH$_2$O. Peptide amounts of 20, 100 and 250 ng were spotted on a 0.45 µm nitrocellulose membrane (GE Healthcare) and detected by polyclonal antisera AB77 and AB76-2 (Tab. 2.12). Before the primary antibodies were applied overnight at 4 °C, membranes were blocked in 10 % skim milk/TBST (0.1 M Tris, 1.5 M NaCl, 0.5 % Tween 20, pH 8.0) for 1 h at RT. After rinsing with TBST for two times 10 min, membranes were incubated with secondary anti-rabbit IgG-HRP (Tab. 2.13) in TBST for 2 h at RT with gently shaking. After additional washes with TBST for two times 10 min, blots were developed using enhanced chemiluminescence (5 ml Solution A [50 mg Luminol, 200 ml 0.1 Tris-HCl, pH 8.6], 500 µl Solution B [22 mg para-coumaric acid, 20 ml DMSO] and 1.5 µl 30 % H_2O_2) and then imaged using standard emulsion films (CEA).

2.11.2 Western-blot Analyses (classical and SNAP i.d.®)

For each Western-blot, 20 to 250 ng peptides or 20 to 50 µg protein lysates (brain or spinal cord) were mixed 1:1 with Vario Gel SDS loading buffer in 0.5 ml reaction tubes and denatured up to 10 min at 95 °C (Uno-Thermoblock, Biometra). Samples were loaded on individual lanes of a 4–12 % VarioGel or 16 % ProGel set in an X-Cell II™ SureLock chamber

(Invitrogen), filled with 500 ml appropriate running buffer. After electrophoresis, starting with 60 V then 120 V, samples were transferred to nitrocellulose membranes at 25 V for at least 40 min per membrane using a semi-dry transfer protocol (Trans- Blot® SD Semi-Dry Transfer cell, Bio-Rad). Membranes were then incubated in TBST for two times 10 min at RT and boiled in 0.01 M PBS for 5 min, which allows an improved access to the antigen. Membranes were then blocked in 10 % nonfat dry milk/TBST for 1 h at RT while gently mixing, before primary antibodies were applied overnight at 4 °C (Tab. 2.12). Membranes were then washed in TBST two times for 10 min. Secondary HRP-conjugated antibodies (shown in Tab. 2.13) were applied for 2 h at RT. Afterwards, membranes were rinsed again in TBST two times for 10 min. The blots were developed using enhanced chemiluminescence and imaged using standard emulsion film. For signal visualization, either self-made solution (see Dot-blot protocol) or commercial Luminata Crescendo Western HRP substrate (Millipore) was used.

Using the SNAP i.d.® System (Millipore) incubation times of blocking, primary and secondary antibody administration could be clearly decreased. Protocol is modified by drawing the blocking solution (0.2 % nonfat dry milk/TBST) immediately through the membrane, using a vacuum pump, followed by primary antibody incubation for at least 10 min at RT. After washing three times with TBST, membranes were incubated with the secondary antibody for 10 min at RT. Again, membranes were washed three times with TBST and developed as described before.

2.11.3 Quantification of Protein Levels

Protein levels were determined via ImageJ software (1.46r, National Institutes of Health, USA) by measuring band intensity in densitometric analyses and normalized to β-Actin or CoxIV levels using Microsoft Excel. Statistical analyses were performed with GraphPad Prism using Unpaired-t-test and One-Way-Anova followed by Bonferroni's Multiple Comparison Test calculations. Figures were processed using Adobe Photoshop and Illustrator CS6.

2.12 Preparation of Human and Mouse Tissue for Immuno-histochemistry

For preparation of mouse brains, mice were sacrificed using CO_2 followed by cervical translocation and decapitation. Brains were fixed in 4 % PFA in 0.01 M PBS for at least 3 days, dehydrated and immersed in paraffin (TP1020 Automatic Tissue Processor, Leica). Tissues were then embedded in paraffin blocks using an EG1140 H Embedding Station (Leica). For immunohistochemistry, 2 to 4 µm sagittal sections were produced by cutting paraffin blocks using a HM 335E microtome (Microm) and transferring tissue sections onto Superfrost® slides (Thermo Fischer Scientific) in a 50 °C hot ddH_2O bath (Medax). Slides were dried at 37 °C for at least overnight before they were used for immunohistochemistry.

2.13 Immunohistochemistry

2.13.1 Diaminobenzidine (DAB) Histochemistry

Immunohistochemistry was performed on 2 to 4 µm sagittal paraffin sections from wild-type and transgenic mice. In brief, sections were deparaffinized in xylene (2 x 5 min) and rehydrated in a series of ethanol (100 % for 10 min; 95 %, 70 % each for 5 min; ddH_2O for 1 min). After treatment with 0.3 % H_2O_2 in 0.01 M PBS to block endogenous peroxidases, antigen retrieval was achieved by boiling sections in 0.01 M citrate buffer (pH 6.0), followed by 3 min incubation in 88 % formic acid. Slides were washed in between with 0.1 % Triton X-100 in 0.01 M PBS for 15 min. Non-specific binding sites were blocked by treatment with 4 % skim milk and 10 % FCS in 0.01 M PBS for 1 h at RT, prior to the addition of the primary antibodies. Primary antibodies (see Tab. 2.12) were incubated overnight in a humid chamber at RT, followed by washing with 0.1 % Triton X-100 in 0.01 M PBS and incubation with biotinylated secondary antibodies (shown in Tab. 2.13) at 37 °C for 1 h. Staining was visualized using the ABC method with the Vectastain kit and diaminobenzidine (DAB) developing solution (100 µl of 25 mg/ml DAB in 50 mM Tris/HCl [pH 7.5]; 5 ml 50 mM Tris/HCL; 2.5 µl H_2O_2) with DAB as chromogen providing a reddish brown color. ABC-reaction batch (Solution A [1:10], Solution B [1:10], 10 % FCS in 0.01 M PBS) was incubated on slides for 1.5 h at 37 °C and sections were washed 15 min in 0.01 M PBS before visualization. Counterstaining was carried out with hematoxylin for 40 s, followed by washing in running

tap water for 5 min. Afterwards, slides were dehydrated in series of ethanol (70 %, 95 % for each 5 min; 100 % for 10 min) and xylene (2 x 5 min) and, then, finished with Roti®-Histokitt mounting medium (Roth) and a cover slip. Images were captured using an Olympus BX-51 microscope equipped with an Olympus DP-50 camera and figures generated with Adobe Photoshop and Illustrator CS6.

To further characterize the distribution and aggregation propensies of pGlu-modified ADan peptides, we compared Thioflavin-S (Thio-S) staining with the distribution of non-modified and pGlu-modified peptides. Therefore, three equally 2 µm spaced apart sections were taken from ADanPP7-transgenic mice at different months of age, mounted on slides and stained with 1 % Thio-S/4',6-diamidino-2-phenylindole (DAPI) and either AB76-2 or AB77.

2.13.2 Quantification of Immunopositive Structures

APP_{he} (n = 6), $APP/PS1KI_{he}$ (n = 6) and $APP/PS1KI_{ho}$ mice (n = 7) at 10 months of age were stained using DAB method with anti-pT668, an antibody detecting phosphorylated APP in dystrophic neurites. Serial images of 20 x magnification of the cortex were captured using an Olympus BX-51 microscope equipped with an Olympus DP-50 camera. pT668-positive structures were quantified using ImageJ software by binarizing the pictures to 8-bit black and white images and a fixed intensity threshold was applied defining the DAB staining. Measurements were performed for a percentaged area covered by DAB staining (Breyhan et al. 2009). For statistical analyses, means of 3 to 6 sections per animal were compared between genotypes. Significances were calculated with One-Way-Anova together with Bonferroni's Multiple Comparison Test using GraphPad Prism software.

Accordingly, quantification of Aβ plaque load (using antiserum 24311 without hematoxylin counterstaining), GFAP staining, tau pathology (using AT8 and MC1 antibodies) and synaptic markers (using synapsin-1, synaptobrevin and synaptoporin antibodies) was evaluated in the hippocampus and/or cortex and thalamus (Bregma 1.08-1.32) of 3- and 9-month-old female PS19, 5XFAD and 5XFAD/PS19 mice (n = 3). Quantification of extracellular Aβ load was performed by capturing serial images of 40 x magnification (hippocampus) using 4 sections per animal, which were 30 µm apart. Accordingly, for GFAP staining quantification, images of 40 x (hippocampus) and 200 x (cortex and thalamus) were captured and the astrocyte-covered areas were analyzed as described before. AT8 and MC1 were

used to quantify phospho-tau pathology in the CA1 and CA3 region of the hippocampus (400 x magnification) as well as the cortex (100 x magnification). Antibodies against synapsin-1, synaptobrevin and synaptoporin were used to quantify mossy fiber density in the CA3 region of the hippocampus (400 x magnifications). Significances were calculated using One-Way-Anova together with Bonferroni's Multiple Comparison Test or with Unpaired-t-test performed by GraphPad Prism software.

Assessment of neuronal loss in the CA1 region of the hippocampus of 3- and 9-month-old 5XFAD, PS19 and 5XFAD/PS19 mice (n = 3 for each time point and genotype) was carried out on sagittal brain sections (Bregma 1.08-1.32) that were stained with hematoxylin. Images of the CA1 layer were captured at 400 x magnifications. Neuronal nuclei were identified according to their size and characteristic appearance clearly differing from glial cells. The number of CA1 neurons in a defined area per section (n = 3 per animal) was counted using the cell counting tool implemented in the ImageJ software package. Significant differences were evaluated with One-Way-Anova combined with Bonferroni's Multiple Comparison Test using GraphPad Prism.

2.13.3 Combined Diaminobenzidine/HistoGreen Histochemistry

DAB staining was also combined with HistoGreen to sequentially stain with two different antibodies. DAB staining was performed first and as described before in section 2.13.1. After DAB visualization, sections were blocked again in 0.3 % H_2O_2 in 0.01 M PBS for 30 min at RT followed by blocking with 4 % non-fat dry milk and 10 % FCS in 0.01 M PBS. Primary and secondary antibody (Tab. 2.12, 2.13) as well as ABC incubation was performed as described above. For visualization of the second antibody reaction the Histoprime® HistoGreen Chromagen Kit was prepared according to the protocol of the supplier. For development, one drop was used per section. Counterstaining, washing and covering were performed as described above. Dehydration reagents were similar to single DAB staining, but incubation steps were minimized to maintain HistoGreen staining (70 % and 95 % ethanol for each 30 s; 100 % ethanol and xylene each for 2 x 30 s). Figures of DAB and/or HistoGreen staining were generated using Images an Olympus BX-51 microscope equipped with an Olympus DP-50 camera and further processed with Adobe Photoshop and Illustrator CS6.

2.13.4 Immunofluorescent Staining

For immunofluorescent stainings, paraffin embedded tissue was deparaffinized and rehydrated as described in section 2.13.1. Antigen retrieval was carried out by boiling in 10 mM citrate buffer (pH 6.0) for 10 min followed by 15 min washing in 0.1 % Triton-X in 0.01 M PBS. For the detection of intracellular peptides, slides were incubated in 88 % formic acid for 3 min and washed in 0.01 M PBS for 5 min. For LC3 staining, slides were further permeabilized by incubation in methanol at -20 °C for 10 min. Unspecific binding sites were blocked with 4 % skim milk and 10 % FCS in 0.01 M PBS for 1 h at RT in a humid chamber. Primary antibodies (see Tab. 2.12) were diluted in 10 % FCS in 0.01 M PBS and incubated overnight at RT. Before secondary antibodies conjugated with either Alexa Fluor® or DyLight® Fluor (shown in Tab. 2.13) were applied for at least 1.5 h at 37 °C, slides were washed with 0.1 % Triton-X in 0.01 M PBS three times for 5 min. Then, slides were washed again three times in 0.01 M PBS to reduce fluorescent background and counterstained with DAPI for 1 min. After washing twice with ddH$_2$O for 1 min, sections were covered in water based medium (Dako cytomation). Images were captured using an Olympus BX-51 microscope equipped with an Olympus DP-50 camera. Figures were processed using Adobe Photoshop and Illustrator CS6.

2.14 Antibodies

2.14.1   Primary Antibodies

Antiserum	Host	Source	Isotype	Dilution: IHC / IF	Dilution: WB / DB	Immunogen
24311	rabbit	AG Bayer	polyclonal	1:500	-	pan-Aβ
Ab 5282	rabbit	generous gift of J. Ghiso	polyclonal	1:3000	1:10000	ADan$_{22-34}$
AB76-2	rabbit	-	polyclonal	1:20-1:50	1:50	pGlu-ADan$_{1-5}$
AB77	rabbit	-	polyclonal	1:50-1:500	1:500	pGlu-ADan$_{1-14}$
anti-APP	rabbit	Synaptic Systems	polyclonal	1:500	-	aa681-695 of C-terminal human APP
anti-ApoE (WU-E4)	mouse	Santa Cruz	monoclonal	-	1:200	human ApoE
anti-ApoE (C-term)	goat	Sigma Aldrich	polyclonal	-	1:500	ApoE$_{289-301}$
anti-ApoE (M20)	goat	Santa Cruz	polyclonal	1:100	1:100	C-terminus of murine ApoE
AT8	mouse	Thermo Scientific	monoclonal	1:500	-	tau$_{pS202/T205}$
anti-GFAP	rabbit	Dako	polyclonal	1:3000	1:500	cow GFAP
anti-GFAP	rabbit	Synaptic Systems	polyclonal	1:2000	1:4000	human GFAP
anti-human Cathepsin D	rabbit	Dako	polyclonal	1:250	-	Cathepsin D
anti-Iba1	rabbit	Synaptic Systems	polyclonal	1:300	-	rat Iba1$_{134-147}$
anti-ITM2B	chicken	Sigma Aldrich	polyclonal	-	1:500	human ITM2B$_{1-60}$
anti-pT668	rabbit	Cell signaling	polyclonal	1:500	-	phosphorylated APP$_{668T}$
anti-Synaptophysin	mouse	Dako	monoclonal	1:500	1:10000	C-terminal cytoplasmic tail of Synaptophysin
anti-β-Actin	mouse	Sigma-Aldrich	monoclonal	-	1:5000	β-cytoplasmic actin N-terminal peptide
anti-β3-tubulin	rabbit	Millipore	polyclonal	1:1000	-	human β3-tubulin
CoxIV	rabbit	Cell Signaling	monoclonal	-	1:500	human CoxIV$_{29K}$
G2-10	mouse	The Genetics Company	monoclonal	1:250	-	Aβ_{x-40}
CP13	mouse	generous gift of S. Weggen	monoclonal	-	1:500	tau$_{pS202}$
IC16	mouse	generous gift of S. Weggen	monoclonal	1:2000	1:2000	Aβ_{1-16}
MAP2	mouse	Sigma Aldrich	monoclonal	1:500	-	bovine MAP2
MAP-LC3β (N-20)	goat	Santa Cruz	polyclonal	1:100	1:250	N-terminus of human MAP-LC3β
MC1	mouse	generous gift of P. Davies	monoclonal	1:500	1:500	tau$_{312-322}$, conformation-specific
NT78	mouse	AG Bayer	monoclonal	1:1000	-	Aβ
PSD95	rabbit	Cell Signaling	polyclonal	-	1:500	human PSD95
Synapsin-1	mouse	Synaptic Systems	monoclonal	1:1000	-	rat synapsin 1
Synaptobrevin	rabbit	Synaptic Systems	polyclonal	1:500	-	rat cellubrevin$_{1-81}$
Synaptoporin	rabbit	Synaptic Systems	polyclonal	1:500	-	Synthetic peptide EFGQQPSGPTSFNN
W0-2	mouse	The Genetics Company	monoclonal	-	1:5000	Aβ_{5-8}

Table 2.12. Primary antibodies used for immunohistochemical (IHC) and immunofluorescence staining (IF) as well as Western- and Dot-blot experiments (WB and DB, respectively).

2.14.2 Secondary Antibodies

Antiserum	Host	Source	Conjugate	Dilution
anti-chicken	rabbit	Promega	HRP	1:1000
anti-goat	rabbit	Dako	biotin	1:200
anti-goat	rabbit	Dako	HRP	1:2000
anti-goat	donkey	Invitrogen	Alexa488	1:500
anti-goat	donkey	Invitrogen	Alexa594	1:500
anti-mouse	rabbit	Dako	biotin	1:200
anti-mouse	goat	Dianova	HRP	1:4000
anti-mouse	donkey	Invitrogen	Alexa488	1:500
anti-rabbit	swine	Dako	biotin	1:200
anti-rabbit	swine	Dianova	HRP	1:3000
anti-rabbit	goat	Thermo Fischer Scientic	DyLight488	1:500
anti-rabbit	donkey	Invitrogen	Alexa568	1:500

Table 2.13. Polyclonal secondary antibodies used for immunohistochemistry (biotinylated), immuno-fluorescence (Alexa Fluor® or DyLight® Fluor conjugated) and Western-/Dot-Blotting (horseradish-peroxidase [HRP]-conjugated).

3 Results

3.1 Project I: Investigations of Pyroglutamate-modified Amyloid Peptides in Familial British and Danish Dementias[1]

3.1.1 Aggregation Kinetics of N-terminally modified ABri, ADan and CTF23 Peptides

The aggregation of monomeric N-terminally modified and non-modified ABri, ADan and CTF23 peptides (each 50 µM) was investigated using a Thioflavin-T (ThT) assay under physiological conditions at pH 7.0 and 37 °C (Fig. 3.1).

While ABri exhibited an aggregation profile with a prolonged lag phase prior the formation of higher aggregates, pGlu-ABri peptides showed a much more rapid generation of intermediate oligomeric assemblies and strongly enhanced fibril formation (Fig. 3.1a). At the same concentrations, ADan and pGlu-ADan peptides showed an immediately rapid formation of fibrils, which were indistinguishable from each other, without a lag phase (Fig. 3.1b) indicating a drastic elevated aggregation propensity compared to pGlu-modified and non-modified ABri peptides. Interestingly, under the same conditions non-modified CTF23 showed almost no aggregating behavior, whereas its pGlu-modified counterpart started to aggregate early and formed higher aggregation assemblies (Fig. 3.1c), although highest aggregation peaks were much lower and occurred later than these observed for pGlu-modified and non-modified ABri and ADan peptides.

---

[1] Parts of this project have been published in **Saul, A.**, Lashley, T., Revesz, T., Holton, J., Ghiso, J. A., Coomaraswamy, J. & Wirths, O. 2013. Abundant pyroglutamate-modified ABri and ADan peptides in extracellular and vascular amyloid deposits in familial British and Danish dementias. *Neurobiol Aging*, 34, 1416-25.
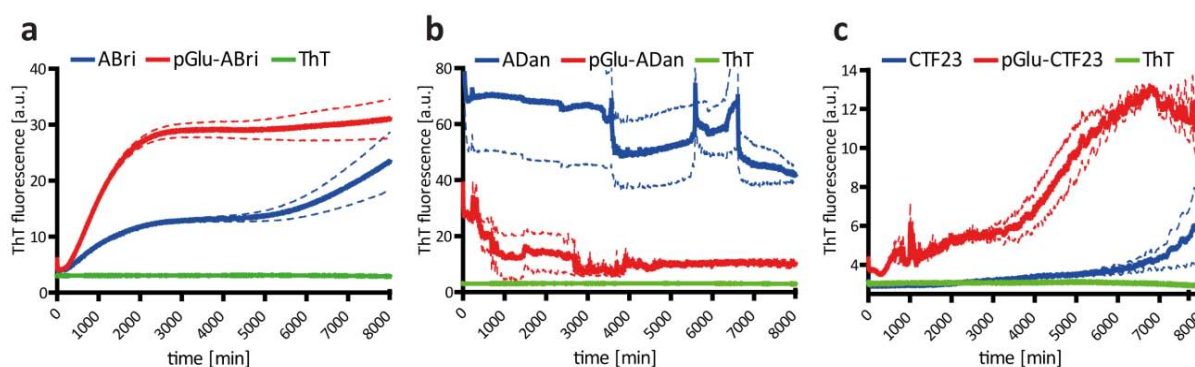
Figure 3.1. Aggregation kinetics monitored via Thioflavin-T (ThT) assays of 50 µM pGlu-modified and non-modified ABri (a), ADan (b) and CTF23 peptides (c). The pGlu-modification of ABri (a) and CTF23 (c) led to drastically increased aggregation propensity, whereas initial aggregation state of pGlu-modified and non-modified ADan (b) was that high that no differences could be observed. Standard errors of the mean (SEM) are illustrated as dotted lines for each peptide. Each assay was measured in triplicates.

3.1.2   Increased Cytotoxicity of pGlu-modified ABri and ADan Peptides

Human SH-SY5Y neuroblastoma cells were exposed to synthetic non-modified and pGlu-modified ABri and ADan peptides to assess if the pGlu-modification provides an increased toxicity to ABri and ADan peptides (Fig. 3.2a, b). The application of 5 µM non-modified ABri or ADan peptides had no impact on the cell viability as measured by LDH release, whereas the incubation with either 5 µM pGlu-modified ABri or ADan peptides resulted in a significantly increased toxicity compared to untreated control cells ($p < 0.01$ for pGlu-ABri and $p < 0.05$ for pGlu-ADan). Furthermore, Hek293 human embryonic kidney cells stably expressing ABri1Q-34, showed a significantly decreased proliferation rate compared to Mock controls or cells stably transfected with wild-type BRI2 or ABriPP precursors ($p < 0.001$) as measured by MTT to formazan conversion (Fig. 3.2c).
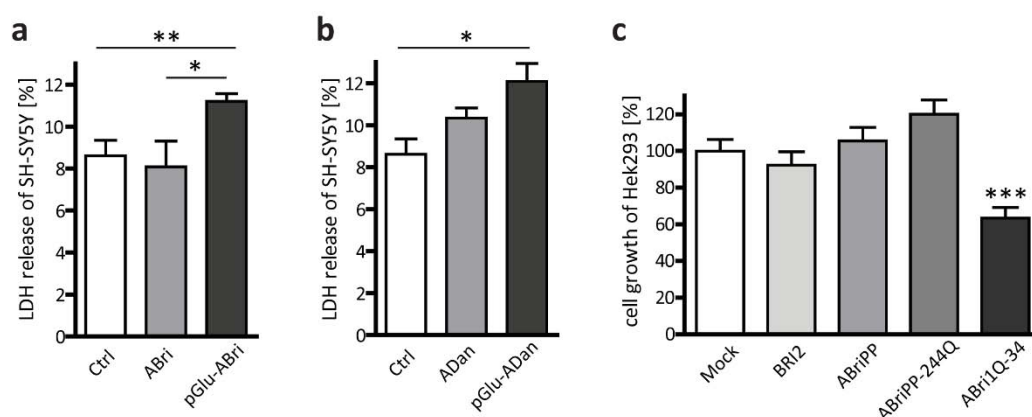
Figure 3.2. Application of 5 µM ABri (a) and ADan peptides (b) starting with a pGlu-modification impaired cell viability of SH-SY5Y cells as indicated by LDH-release. (c) Stable expression of ABri1Q-34 decreased the cell proliferation rate of Hek293 cells as measured by MTT-assay. Each assay was performed at least five times. All error bars represent SEM. (Ctrl: control; $p < 0.05^*$, $p < 0.01^{**}$, $p < 0.001^{***}$)

3.1.3 Enhanced Cell Viability by CTF23 Peptides

So far, almost nothing is known about the function of the CTF23 peptide, which is released after furin processing of BRI2 wild-type protein. Therefore, cell viability assays were performed using different cell lines. The application of 200 µM non-modified and pGlu-modified CTF23 on SH-SY5Y cells led not only to a significantly decreased LDH-release ($p < 0.001$), but also to elevated cell proliferation rate up to 100 % compared to controls measured by MTT-assay ($p < 0.001$) suggesting a trophic effect of CTF23 (Fig. 3.3a, b). Noteworthy, the positive impact on SH-SY5Y viability was stronger for non-modified CTF23, since already 50 µM of this peptide applied to the cells increased the proliferation rate significantly up to 40 % ($p < 0.05$, Fig. 3.3b). The same holds true for the application of 25 µM CTF23 to Hek293 cells ($p < 0.01$), whereas pGlu-CTF23 had no influence on proliferation at this concentration (Fig. 3.3c). Likewise, supplementation of CTF23 to human Ntera2 teratocarcinoma cells had the same effect on proliferation in a dose-dependent manner with 40 to 60 % increased cell growth ($p < 0.001$, Fig. 3.3d), whereas only a higher concentration of 200 µM pGlu-CTF23 elevated cell growth significantly to 30 % compared to controls ($p < 0.01$). Interestingly, CTF23 had not the same effects in HOG human oligodendroglioma cells (Fig. 3.3e).
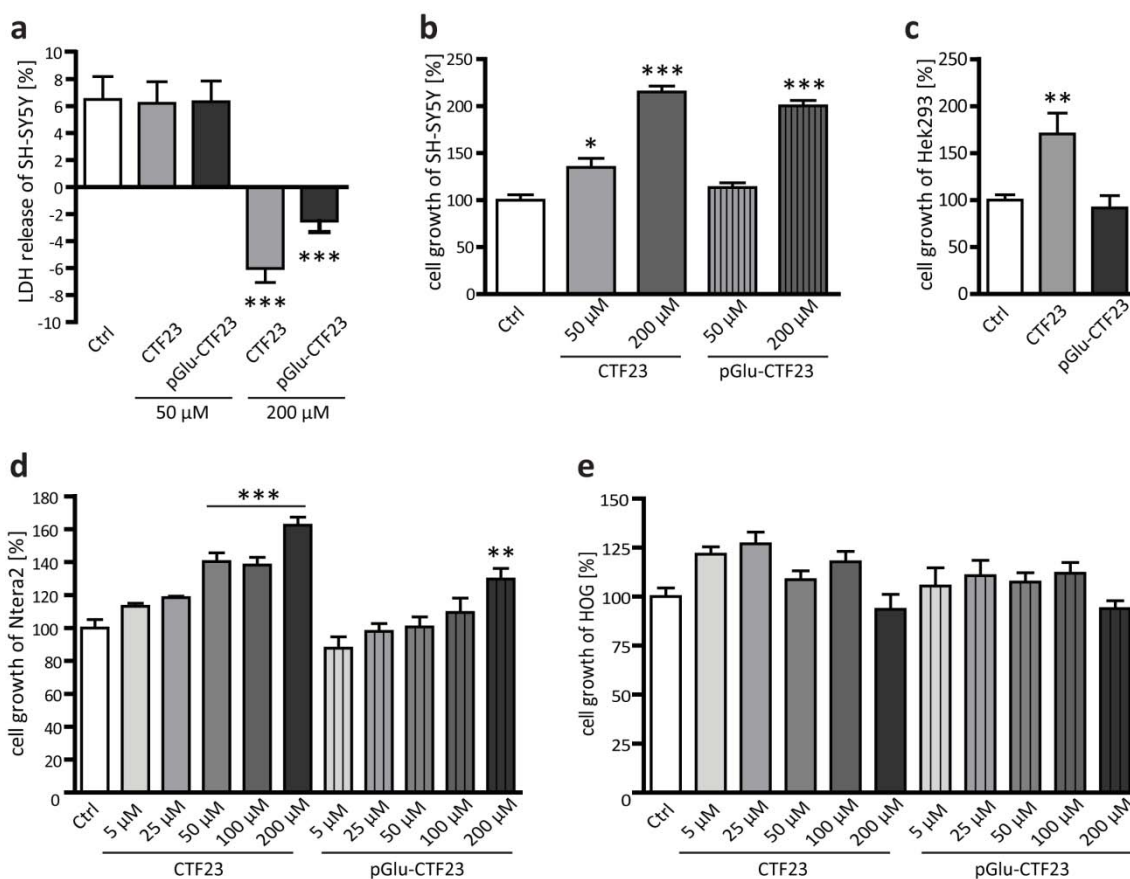
Figure 3.3. Application of pGlu-modified and non-modified CTF23 led to increased cell viability in SH-SY5Y (a, b), Hek293 (25 µM, c) and Ntera2 (d) cells as measured by LDH-release (a) and MTT-assay (b-e), whereas non-modified CTF23 had a stronger impact than its pGlu-modified counterpart. HOG cells did not react to peptides (e). Each assay was performed at least five times. All error bars represent SEM. (Ctrl: control; p < 0.05*, p < 0.01**, p < 0.001***)

3.1.4   Characterization of N-terminal ABri/ADan Antibodies

Using dot-blot analysis with synthetic pGlu-modified and non-modified ABri peptides, as well as pGlu-modified and non-modified Aβ peptides in different amounts (20, 100 and 250 ng), the sensitivity and specificity of the novel N-terminal specific ABri/ADan antisera were determined (Fig. 3.4a). Whereas AB76-2 revealed a clear preference for pGlu-modified peptides, AB77 detected pGlu-modified and non-modified ABri peptides with comparable sensitivity and showed only a minor preference for pGlu-modified ABri peptides. No signal of both antibodies was observed using $Aβ_{1-42}$ or pGlu-modified $Aβ_{3-42}$ peptides, excluding a cross-reactivity against other pGlu-modified peptides (Fig. 3.4a). These findings were confirmed by Western-blot analysis using pGlu-modified and non-modified ABri, ADan and CTF23. Like in the dot-blot approach, AB76-2 revealed only a minor cross-reactivity with non-

modified ABri peptides at higher peptide quantities (250 ng) and a clear preference for pGlu-modified ABri, ADan and CTF23 peptides, detecting also higher molecular weight species like pGlu-ABri and pGlu-CTF23 dimers as well as dimers and low-molecular weight oligomers of pGlu-ADan (Fig. 3.4b). However, AB77 detected both pGlu-modified and non-modified ADan and CTF23 peptides in equal amounts, and showed a higher sensitivity for pGlu-modified ABri peptides compared to its non-modified counterpart confirming the results of the dot-blot assay (Fig. 3.4b).
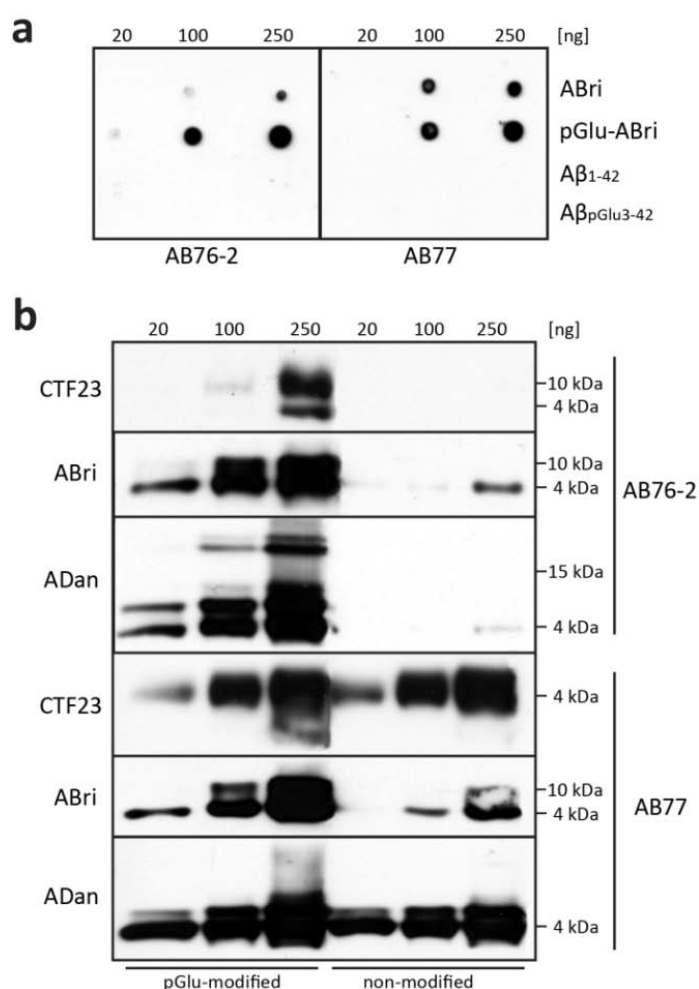
Figure 3.4. Dot-blot (a) and Western-blot analyses (b) of N-terminal ABri/ADan antibodies. (a) AB76-2 revealed a clear preference for pGlu-modified ABri peptides, whereas AB77 showed no preference for ABri or pGlu-ABri peptides. (b) Western-blot analysis confirmed the dot-blot result with AB76-2 showing only a minor cross-reactivity with non-modified ABri or ADan peptides at higher peptide quantities (250 ng) and a clear preference for pGlu-modified ABri, ADan and CTF23 peptides.

To assess whether AB77 shows the same behavior in immunohistochemical stainings, immunoadsorption experiments were performed with synthetic non-modified and pGlu-modified ADan peptides in a 13-month-old ADanPP7 mouse, representing a transgenic mouse model for familial Danish dementia (FDD) (Coomaraswamy et al. 2010). Full-length non-modified and pGlu-modified synthetic ADan peptides were incubated with AB77 (5 µg of peptide per 20 µl of antibody) overnight at 4 °C with continuous agitation, followed by centrifugation at 14.000 x g for 5 min as described previously (Lashley et al. 2008).

Application of the pre-incubated antibodies revealed that the prominent parenchymal staining pattern of AB77 is mainly due to a detection of pGlu-modified ADan peptides, as the signal was strongly reduced when pGlu-modified ADan peptides were used for pre-incubation (Fig. 3.5c). In contrast, pre-incubation with non-modified ADan peptides had a much weaker effect on signal reduction (Fig. 3.5b). Additionally, these results suggest that most of the extracellular deposits in the ADanPP7 mouse model mainly contain pGlu-modified ADan peptides.
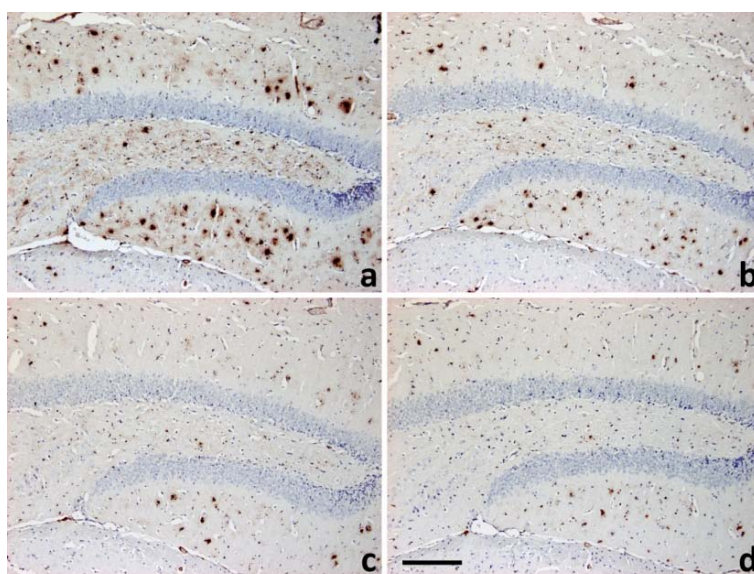
Figure 3.5. Immunoadsorption using non-modified and pGlu-modified ADan peptides. Staining of a ADanPP7 mouse hippocampus at 13 months of age using AB77 with either (a) no blocking peptide, (b) 5 µg non-modified ADan, (c) 5 µg pGlu-modified ADan or (d) both peptides. Most of the AB77 immunoreactivity was blocked after pGlu-ADan pre-incubation, suggesting that AB77 preferentially detects pGlu-modified ADan peptides in this model. Scale bar: 200 µm

3.1.5 Immunohistochemical Analyses of pGlu-modified ABri and ADan Peptides in Familial British and Danish Dementia Brains

In order to characterize the staining pattern of the novel generated antibodies, formalin-fixed and paraffin embedded cortical and cerebellar tissue from patients with FBD and FDD have been used. Histochemical stainings of tissue from patients with FBD and FDD were performed by collaborators T. Revesz and T. Lashley UCL, London (Saul et al. 2013). Double fluorescent immunohistochemistry was also carried out to investigate the co-localization of N-terminal pGlu-antibodies (AB77 [1:50] and AB76-2 [1:20]) with C-terminal ABri (Ab338, (Holton et al. 2001)) and C-terminal ADan antibodies (Ab5282, (Holton et al. 2002)).

In the cerebellum of an FBD patient, extracellular parenchymal deposits were abundantly recognized by AB77 (Fig. 3.6a) and AB76-2 (Fig. 3.6b). Furthermore, prominent

vascular AB77 (Fig. 3.6c, e) and AB76-2 (Fig. 3.6d, f) staining was detected in the dentate gyrus (Fig. 3.6c, d) and the CA4 region of the hippocampus (Fig. 3.6e, f) from an FDD patient.
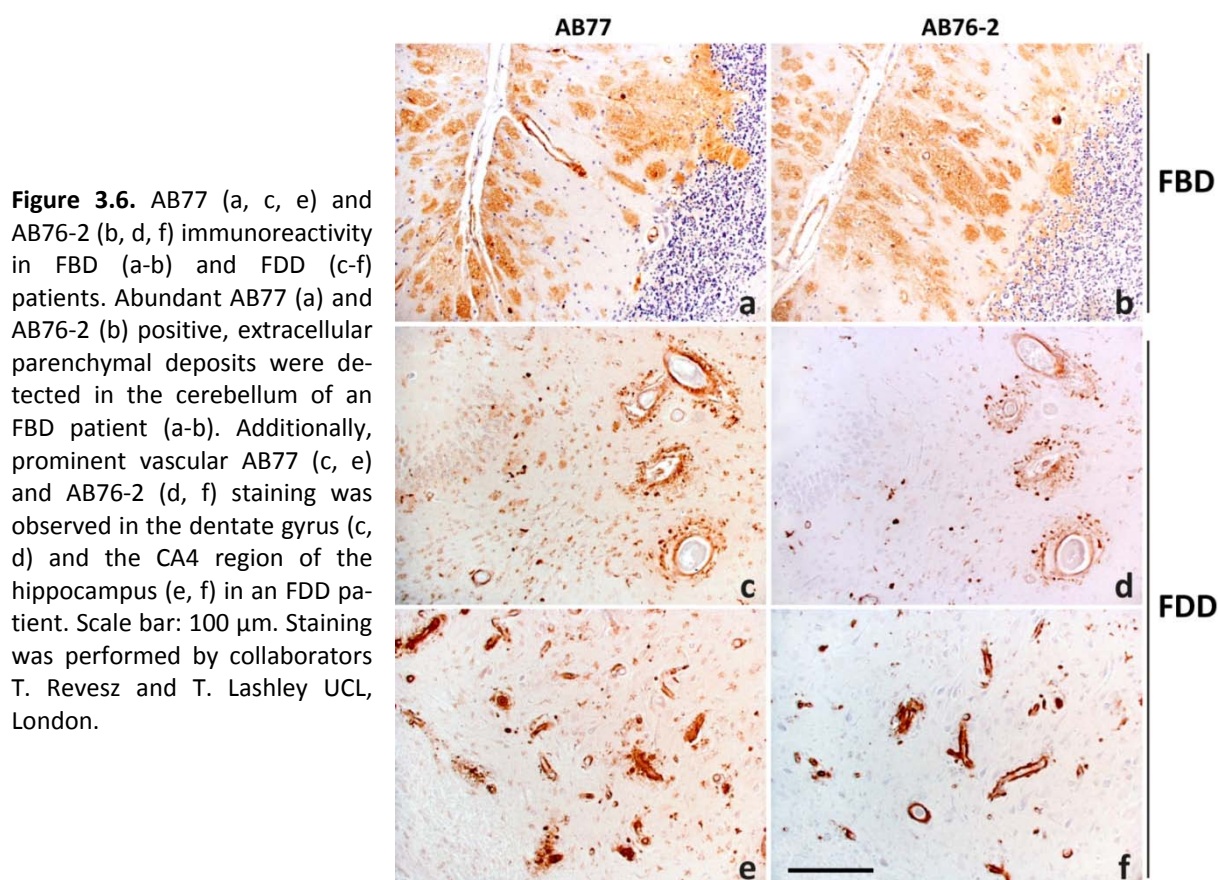
Figure 3.6. AB77 (a, c, e) and AB76-2 (b, d, f) immunoreactivity in FBD (a-b) and FDD (c-f) patients. Abundant AB77 (a) and AB76-2 (b) positive, extracellular parenchymal deposits were detected in the cerebellum of an FBD patient (a-b). Additionally, prominent vascular AB77 (c, e) and AB76-2 (d, f) staining was observed in the dentate gyrus (c, d) and the CA4 region of the hippocampus (e, f) in an FDD patient. Scale bar: 100 µm. Staining was performed by collaborators T. Revesz and T. Lashley UCL, London.

To verify to what extent parenchymal and vascular deposits in FBD and FDD patients consist of pGlu-modified and aggregated amyloid peptides, AB77 and AB76-2 were combined with C-terminal ABri (Ab338, Fig. 3.7a-f) and ADan antibodies (Ab5282, Fig. 3.8a-f) as well as Thioflavin-S (Thio-S), respectively (Fig. 3.7g-l and Fig. 3.8g-i). Abundant ABri-positive parenchymal deposits were stained in the hippocampus of an FBD patient using Ab338 (Fig. 3.7b), whereas most of these deposits were also AB77 immunopositive (Fig. 3.7a) apart from the plaque periphery (Fig. 3.7a-c). A similar staining pattern was observed when AB76-2 (Fig. 3.7d) was combined with Ab338 (Fig. 3.7e) suggesting that the majority of deposited amyloid peptides in this FBD patient is pGlu-modified ABri. In addition, AB76-2 detected parenchymal plaques and deposits within the blood vessels, but no perivascular deposits (Fig. 3.7d-f) revealing that this perivascular structures contain only non-modified ABri peptides. The combination of AB77 (Fig. 3.7g) with Thio-S (Fig. 3.7h) exhibited a similar staining pattern,

whereas AB76-2 (Fig. 3.7j) immunostaining completely co-localized with Thio-S (Fig. 3.7j-l) indicating that AB76-2 stained exclusively highly aggregated material.
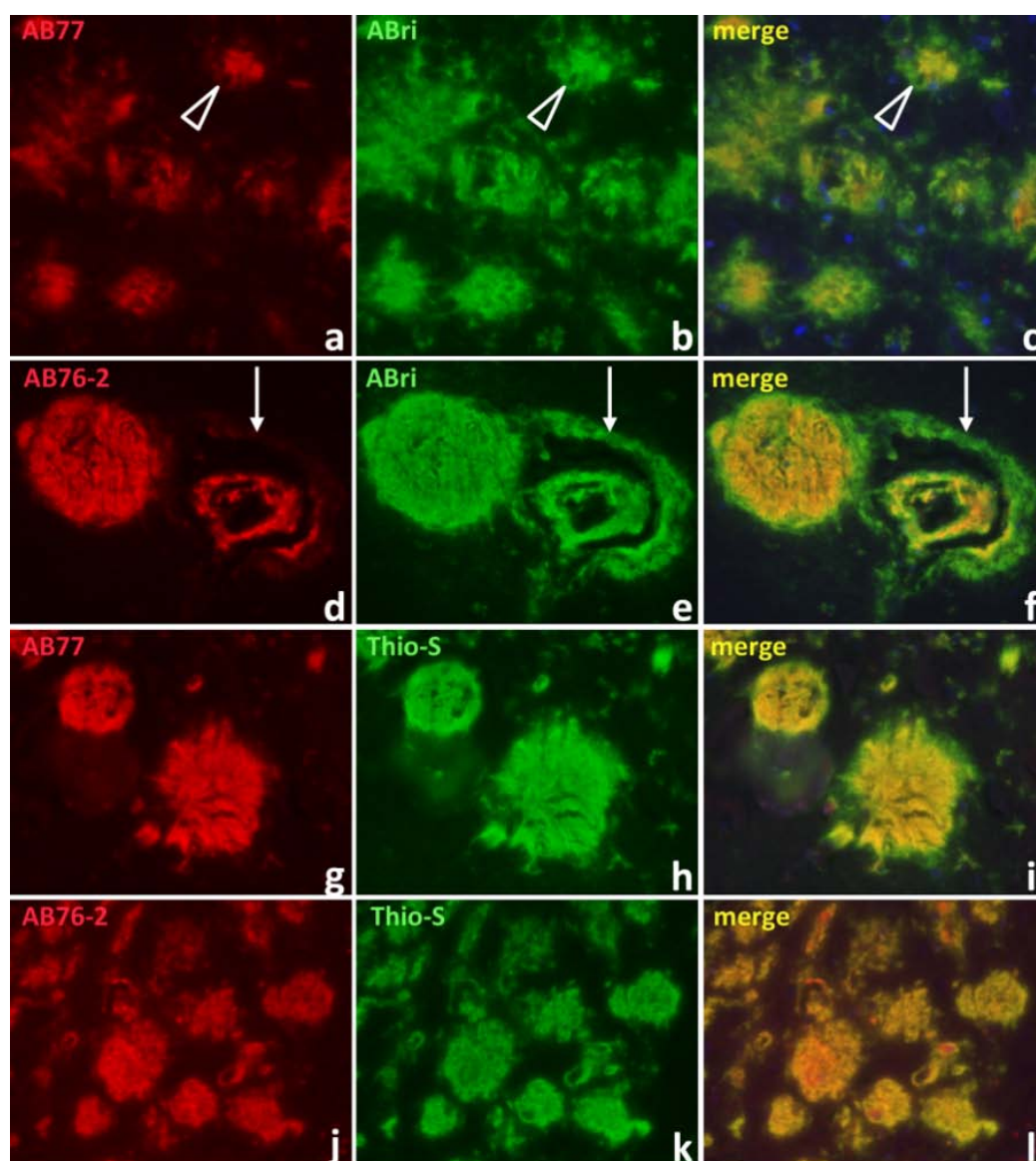
Figure 3.7. Immunofluorescent stainings of a brain from an FBD patient combining AB77 (a, g) or AB76-2 (d, j) with Ab338, a C-terminal ABri antibody (b, e) or Thio-S (h, k), respectively. (b) Abundant ABri-positive parenchymal deposits were detected in the hippocampus of an FBD patient. Most of these deposits were also stained with AB77 (a) apart from the plaque periphery (c, arrowhead). Likewise, AB76-2 (d) detected parenchymal plaques and Ab388-positive (e) structures within the blood vessels, whereas the perivascular deposits remained unstained (f, arrow). Similar staining was observed with AB77 (g) when combined with Thio-S (h, i), whereas a complete co-localization was detected using AB76-2 (j-l). Original magnification: 200 x. Staining was performed by collaborators T. Revesz and T. Lashley UCL, London.

Prominent vascular staining was detected in the cerebellum of an FDD patient using AB77 (Fig. 3.8a), which co-localized with a C-terminal ADan antibody (Ab5282, Fig. 3.8b). A comparable staining pattern was detected using AB76-2, however, only partial co-

localization between AB76-2 and the C-terminal ADan antibody could be observed (Fig. 3.8d-f). Combining AB76-2 with Thio-S revealed a complete overlap (Fig. 3.8g-i) indicating that most of the vascular AB76-2 staining might be due to a detection of aggregated, pGlu-modified ADan peptides.
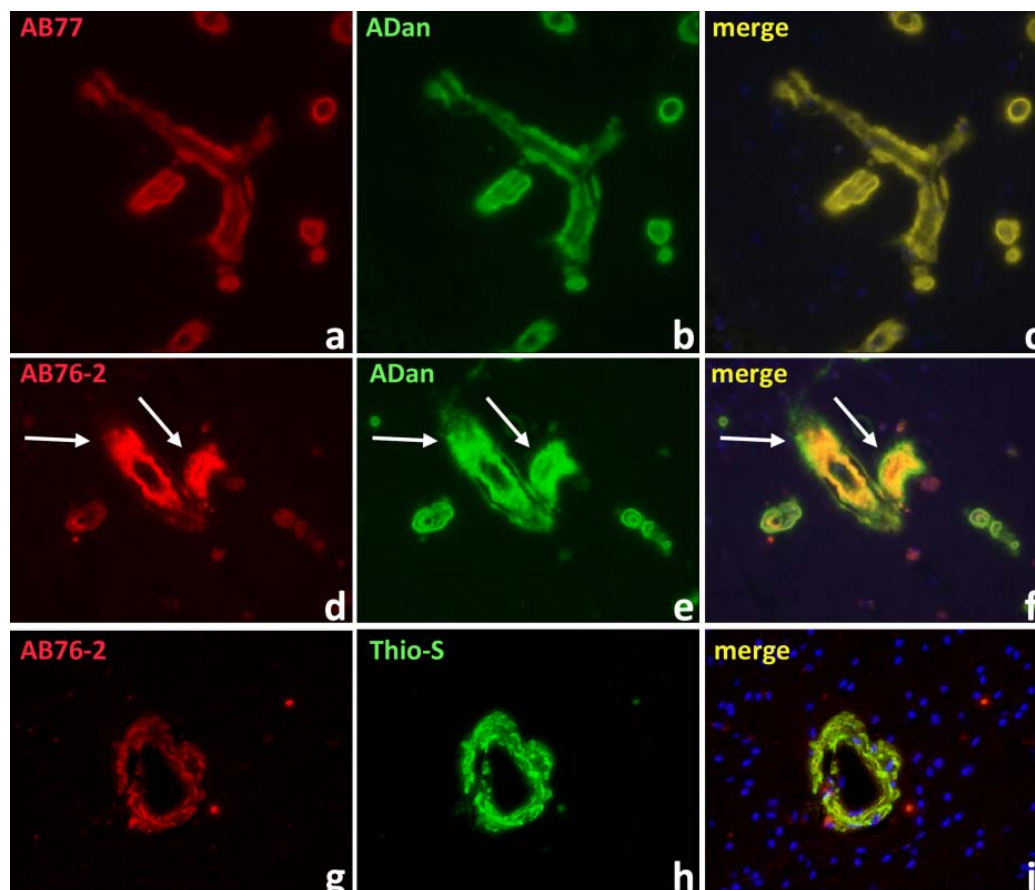
Figure 3.8. Double immunofluorescent staining of brain tissue from a patient suffering from FDD using AB77 (a) or AB76-2 (d) in combination with Ab5282, an ADan C-terminal antibody (b, e) or AB76-2 (g) combined with Thio-S (h). Like in FBD, a comparable staining pattern was detected with both AB76-2 and AB77 when combined with the ADan C-terminal antibody. Whereas AB77 completely co-localized with Ab5282 (a-c), AB76-2 showed only a partial co-localization especially in the vessel periphery (d-f, arrows). Notably, AB76-2 and Thio-S showed a complete overlap (g-i). Original magnification: 400 x. Staining was performed by collaborators T. Revesz and T. Lashley UCL, London.

3.1.6 Pyroglutamate-modified ADan Peptides in an Established Mouse Model for Familial Danish Dementia

In order to corroborate the observations in brains of patients suffering from FBD and FDD, formalin-fixed and paraffin-embedded brain tissue from transgenic ADanPP7 mice expressing the Danish mutant form of BRI2 (Coomaraswamy et al. 2010) were analyzed at the age of 2, 4, 13 and 20 months. Already at 2 months of age, an initial AB77-

immunoreactivity was detected in the stratum lacunosum moleculare (Fig. 3.9e), which strongly spreads over the entire hippocampus at later stages (Fig. 3.9a-h) confirming previous observations with a C-terminal ADan-specific antibody (Coomaraswamy et al. 2010). Further prominent parenchymal immunoreactivity with abundant plaque and vascular staining was found in aged animals (Fig. 3.9a-d). AB76-2 staining (Fig. 3.9i-p) corroborates this observation as it demonstrates single extracellular deposits in the hippocampus and frontal cortex of ADanPP7 mice already at the age of 2 months with increasing amounts of immunoreactive vessels and extracellular amyloid plaques and in aged animals.
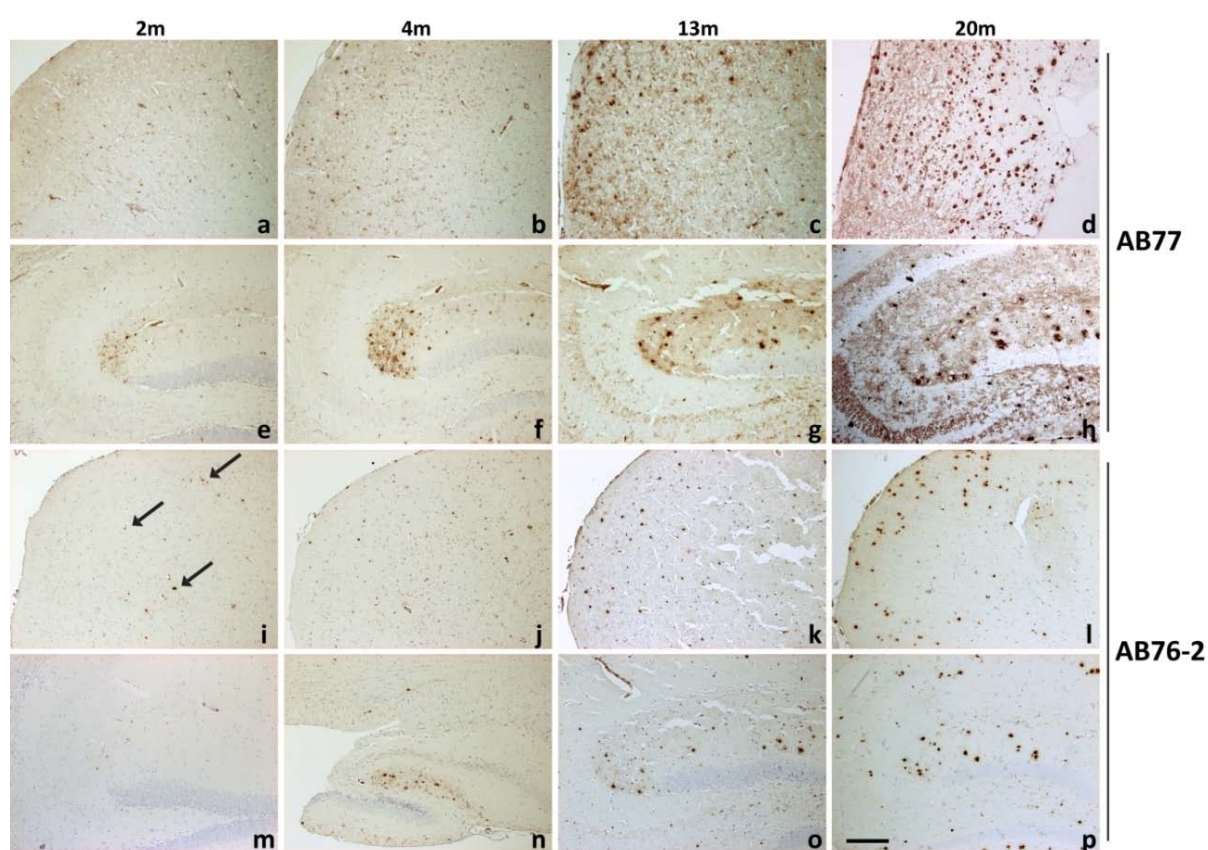
Figure 3.9. Immunostaining of brains from ADanPP7 mice using AB77 (a-h) and AB76-2 (i-p) revealed an age-dependent accumulation of ADan/pGlu-ADan deposits. ADan/pGlu-ADan immunoreactivity was detected in the frontal cortex (a, i, arrows) and hippocampus (e, m) already at 2 months of age showing a strong increase at 4 (b, f, j, n), 13 (c, g, k, o) and 20 months of age (d, h, l, p). Scale bar: 200 μm

Furthermore, AB77-positive extracellular parenchymal deposits were detected in the cerebellum of a 13-month-old ADanPP7 mouse (Fig. 3.10a) reflecting the same staining pattern as for the C-terminal ADan antibody (Fig. 3.10b).
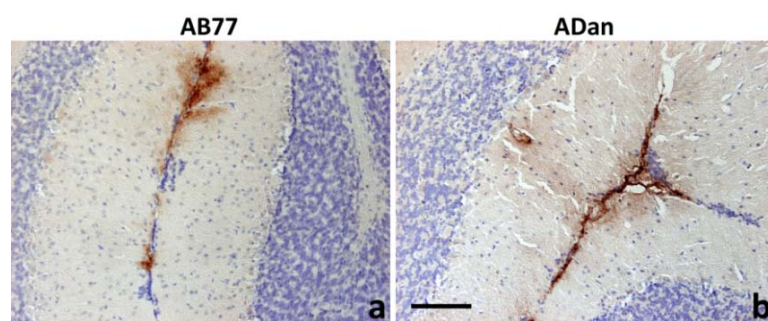
Figure 3.10. Parenchymal AB77-positive deposits (a) in the cerebellum of a 13-month-old ADanPP7 mouse were consistent with the staining pattern of the C-terminal ADan antibody (Ab5282, b). Scale bar: 100 μm

Western-blot analysis using SDS-soluble fractions from ADanPP7 mouse brains revealed a faint AB77-positive band at 2 months of age, with strongly enhanced signal intensity at 4 and 13 months of age (Fig. 3.11a). A clear signal was observed at 4 months of age using AB76-2 that was drastically increased in a 13-month-old ADanPP7 mouse suggesting that pGlu-modified ADan peptides already exist in these mice at a very young age. Western-blot analysis using an antibody against ITM2B revealed the expected band at approximately 45 kDa without indication of cross-reactivity of AB77 and AB76-2 with the parental ITM2B full-length protein (Fig. 3.11b).
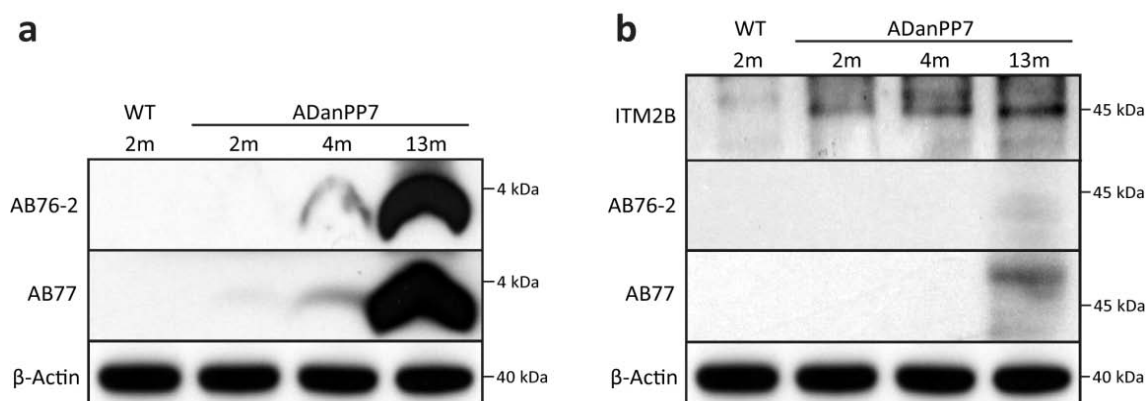
Figure 3.11. (a) Western-blot analysis of SDS-soluble brain fractions from ADanPP7 mice revealed a faint signal already at 2 months of age using AB77, with strongly increased signal intensity at 4 and 13 months of age. A clear Ab76-2 signal was detected at 4 months of age, which was strongly enhanced at 13 months of age. (b) No cross-reactivity of AB77 or AB76-2 was observed with the precursor protein BRI2 (ITM2B), which migrates at approximately 45 kDa. (WT: wild-type)

Stainings of serial sections of the hippocampus from a 13-month-old ADanPP7 mouse using AB77 (Fig. 3.12a), anti-ITM2B (Fig. 3.12b) and Thio-S/DAPI (Fig. 3.12c) revealed that compact and diffuse AB77- and Thio-S-positive plaques were surrounded by ITM2B-positive material suggesting an accumulation in axonal swellings, whereas less ITM2B-immunoractivity around AB76-2- and Thio-S-positive deposits could be detected (Fig.3.12d-f).
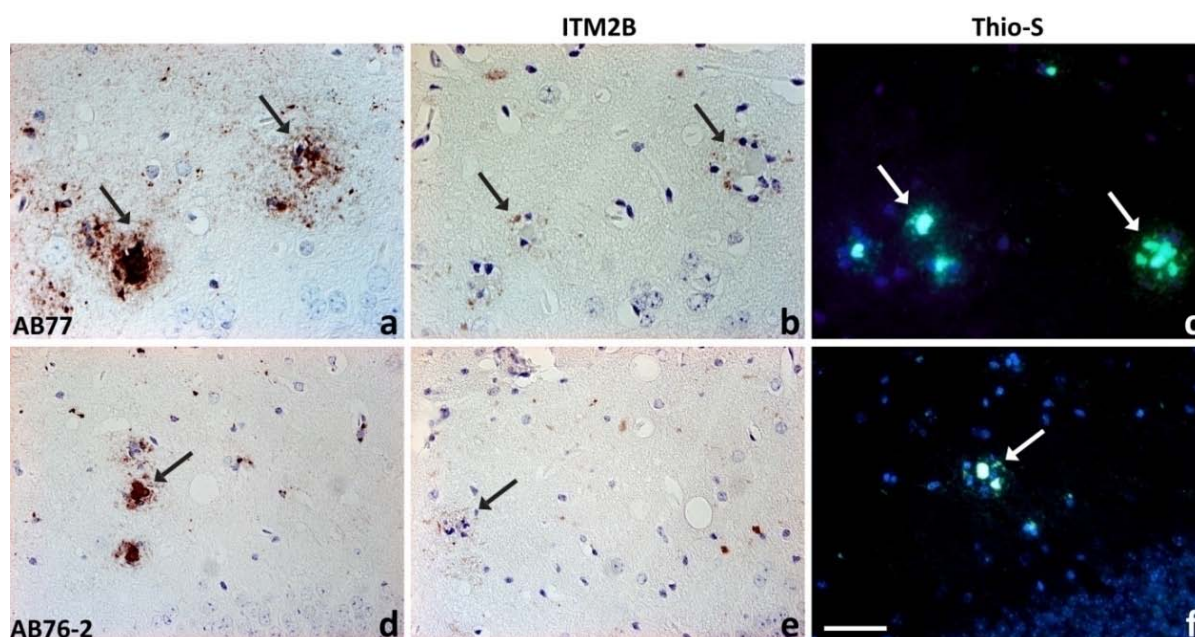
Figure 3.12. ITM2B-immunoreactive material was detected surrounding AB77- and Thio-S-positive deposits in an ADanPP7 mouse (a-c, arrows). The same holds true for AB76-2-positive structures, but to a much lesser extent (d-e, arrow). Scale bar: (a-c) 33 µm, (d-f) 50 µm

Further stainings of serial sections from this mouse showed that most of the larger blood vessels contained both non-modified and pGlu-modified ADan peptides as they were detected by either AB77 or AB76-2 and were in addition Thio-S-positive (Fig. 3.13a-f), which holds also true for the majority of extracellular deposits. Almost all of the deposits that were AB76-2-positive (Fig. 3.13h) were also stained by Thio-S (Fig. 3.13i). Some deposits were only labeled with AB77, but lacking AB76-2 or Thio-S staining (Fig. 3.13g) suggesting a sequential maturation of amyloid plaques in this mouse model.
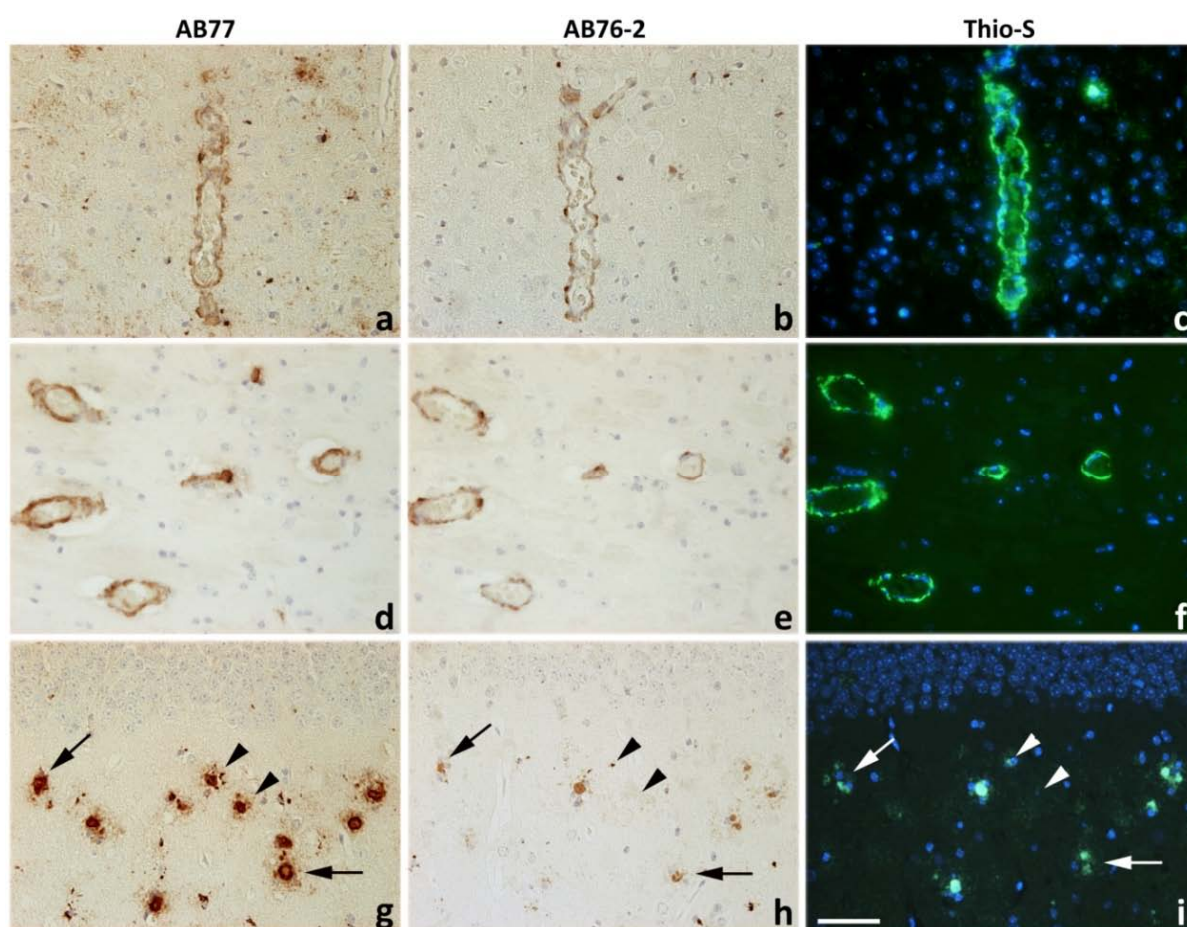
Figure 3.13. Most of the larger blood vessels in brains of ADanPP7 mice were recognized by AB77 (a, d), AB76-2 (b, e) and Thio-S (c, f). Almost all deposits detected by AB76-2 (h) were also stained with Thio-S (i, arrows). However, some deposits were only labeled with AB77 (g) and revealed neither AB76-2 (h) nor Thio-S staining (i, arrowheads). Scale bar: 50 µm

Mossy fibers of the hippocampal CA3-region were prominently stained using AB77 antibody in aged ADanPP7 mice (Fig. 3.9h). Double immunofluorescent stainings using the dendritic marker MAP2 in combination with AB77 revealed only a marginal presence of ADan peptides in dendritic processes near the hippocampal CA3 perikarya (Fig. 3.14a-c). However, combined double labeling using AB77 and the synaptic marker synaptophysin showed that ADan-positive structures accumulate in the stratum lucidum of the hippocampal mossy fiber pathway (Fig. 3.14d-f), indicating the abundant presence of ADan/pGlu-ADan peptides in pre-synaptic terminals. Furthermore, double immunofluorescence staining using antibodies AB77 and GFAP, which is a marker for activated astrocytes, revealed an association of non-modified and pGlu-modified ADan peptides with gliosis in the cortex of aged ADanPP7 mice (Fig. 3.14g-i).
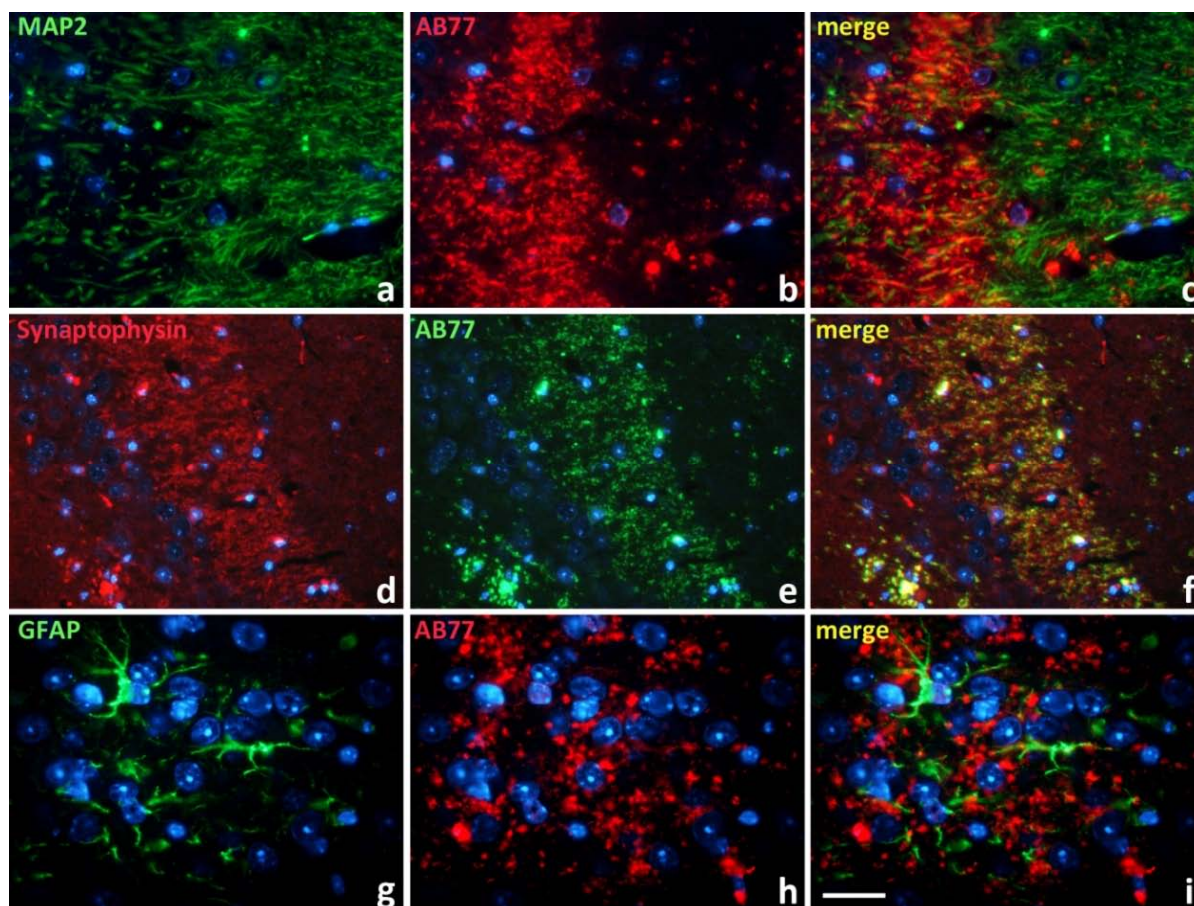
Figure 3.14. Immunofluorescence stainings using MAP2 (a) and AB77 (b) of a 13-month-old ADanPP7 mouse revealed only a minor co-localization in dendritic processes (c). Synaptophysin (d) broadly co-localized with AB77-positive material (e) in the hippocampal stratum lucidum (f) revealing the presence of ADan/pGlu-ADan peptides in pre-synaptic terminals. AB77-positive material (g, i) was closely localized to GFAP signal in the cortex (h, i) suggesting that astrocytes were attracted by non-modified and/or pGlu-ADan aggregates. Scale bar: (a-c) 33 µm, (d-f) 50 µm, (g-i) 20 µm

3.1.7   Distribution of CTF23 in Human Alzheimer´s Disease and Alzheimer´s Disease Mouse Models

So far, nothing is known about the distribution of CTF23 peptides in the brain. Therefore, immunohistochemical stainings were performed using AB77 in AD mouse models like APP/PS1KI and 5XFAD as well as human AD patients and non-demented controls. Since these human and murine control and AD brains carry only non-mutant BRI2, AB77 signals must result from antibody binding to CTF23 peptides. In a 10-month-old APP/PS1KI mouse abundant plaque-shaped structures were stained with AB77 in the hippocampus and cortex (Fig. 3.15a). In higher magnification it gets clear that only the periphery of plaques, which were surrounded by astrocytes and dystrophic neuritic swellings, contains AB77-positive

structures (Fig. 3.15b) suggesting an accumulation of CTF23 in axonal compartments under pathological conditions. This could be further confirmed in a 3-month-old 5XFAD mouse, in which CTF23 was detected intracellularly and putatively at the axon hillock that was also associated with surrounding astrocytes (Fig. 3.15c). Under normal conditions in a non-demented human brain (Fig. 3.15e) as well as in a 10-month-old wild-type mouse (Fig. 3.15d), CTF23-positive structures were only labeled intracellularly in somata and axonal processes. However, CTF23 was detected in vessel walls (not shown), focal accumulations and putatively in dystrophic neurites of an AD brain (Fig. 3.15f).
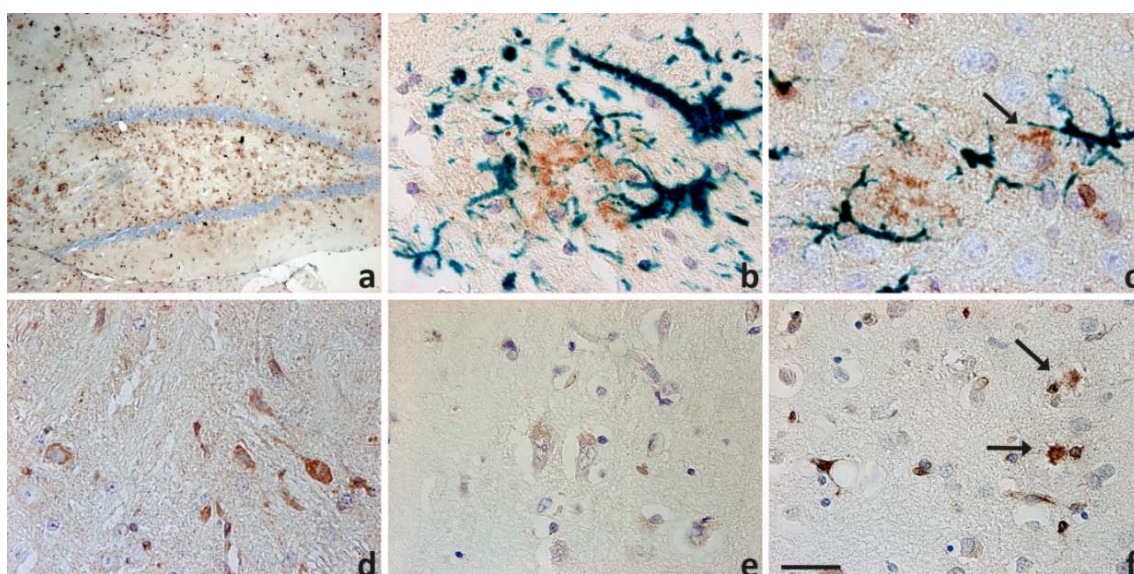
Figure 3.15. AB77-positive structures (DAB-brown) were found in the plaque periphery and dystrophic neurites that were surrounded by astrocytes (GFAP-HistoGreen) in a 10-month-old APP/PS1KI mouse (a, b). The same holds true for a 3-month-old 5XFAD mouse (c), in which AB77- (DAB-brown, GFAP-HistoGreen) positive material also accumulated in the axon hillock (arrow). In a 10-month-old wild-type mouse (d) and in a non-demented human control (e) AB77-staining only occurred intracellularly, whereas focal deposits (arrows) were AB77 immunoreactive in an AD patient (f). Scale bar: (a) 200 µm, (b-c) 20 µm, (d-f) 33 µm

To further confirm these observations, double immunofluorescent stainings were performed in an APP/PS1KI mouse at 10 months of age as well as in a human AD brain using AB77 and NT78 detecting Aβ (Fig. 3.16). In human AD, intracellular Aβ deposits as well as some extracellular plaques also contained CTF23 represented as AB77-positive structures (Fig. 3.16a-c). This finding was corroborated in an APP/PS1KI mouse, in which AB77 and NT78 signals were co-localized in extracellular plaques as well as in intracellular deposits (Fig. 3.16d-f) suggesting an interaction between CTF23 and Aβ peptides.
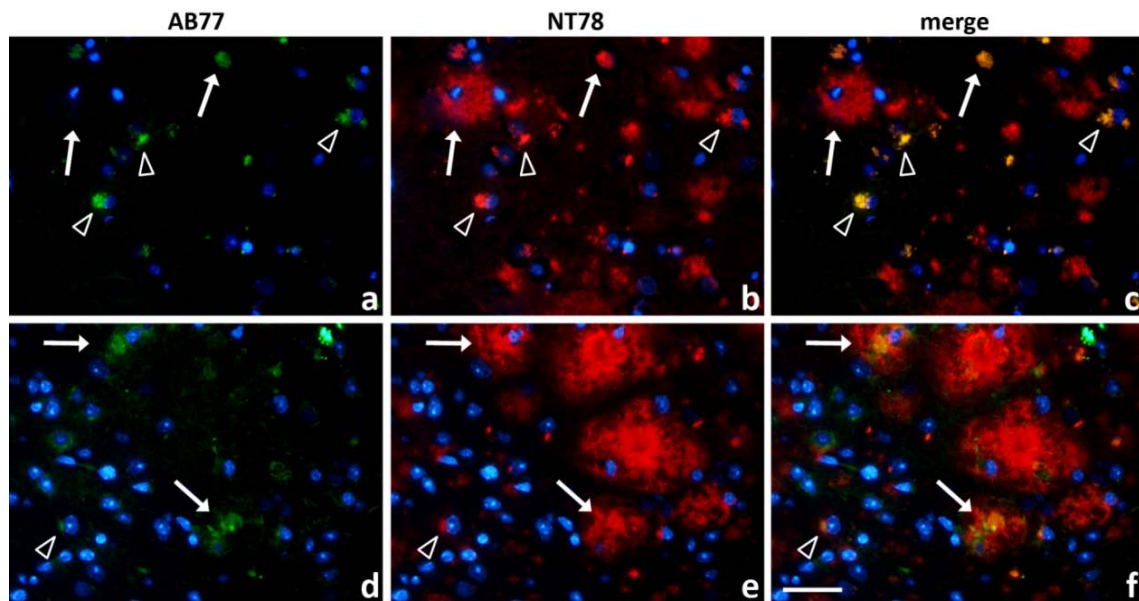
Figure 3.16. Double immunofluorescent stainings using AB77 (a, d) and NT78 (b, e) revealed a co-localization of CTF23 peptides in intra- (arrowheads) and in some extracellular Aβ deposits (arrows) in a human AD brain (a-c) as well as in the APP/PS1KI mouse model (d-f). Scale bar: 33 μm

3.1.8 Generation and Initial Characterization of a Novel Mouse Model for Familial Danish Dementia

In the course of this thesis, a novel mouse model for FDD was developed that expresses high levels of ADan peptides in consideration of the pGlu-modification aspect. This model exclusively expresses the ADan sequence beginning with a glutamine instead of a glutamate at position one combined with the signal peptide sequence of the thyrotropin-releasing-hormone (TRH-ADan1Q-34), ensuring secretion through the secretory pathway, under the control of the neuron-specific Thy1-promoter as described previously (Wirths et al. 2009, Alexandru et al. 2011) (Fig. 3.17). Transgenic mice expressing ADan1Q-34 were generated via pronuclear injection on a C57Bl/6 background using Thy1-expression cassette, in which the ADanQ1-34 sequence was inserted (Fig. 3.17). The injection resulted in the generation of ten transgenic founder animals (OW20-29), which were analyzed for the presence and quantity of the transgene via RT-PCR (Fig. 3.18). Founders OW20, OW23 and OW24, which harbored highest transgene quantities, were bred with wild-type C57Bl/6 mice to establish transgenic mouse lines that carry a stable genomic integration and germ line heredity transmission of the transgene.
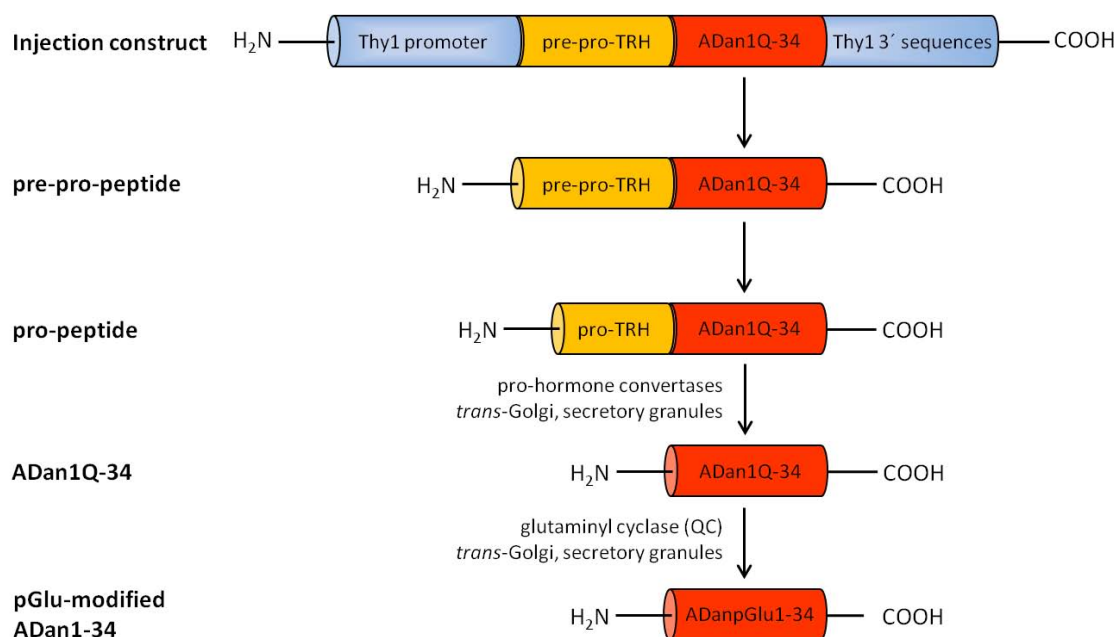
Figure 3.17. Injection construct for the generation of ADan1Q-34 mice. The Thy1-promoter sequence drives neuronal expression in the mouse brain and the fused pre-pro-TRH enables entry of the product into the secretory pathway, where it is released by pro-hormone convertases. In the *trans*-Golgi network product is available for pGlu-modification catalyzed by QC. Figure generated after (Alexandru et al. 2011)
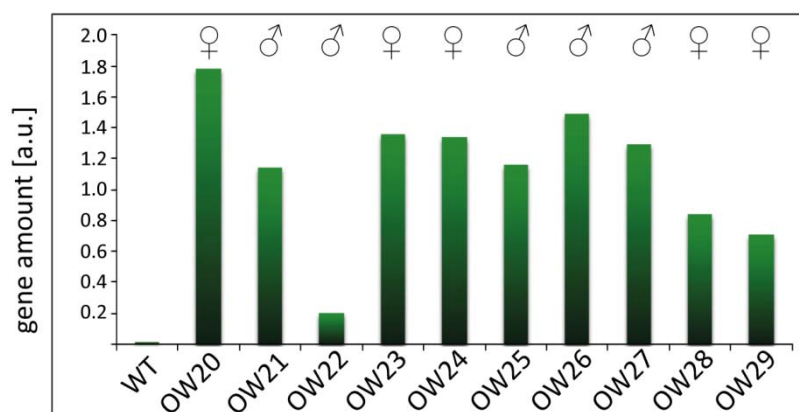
Figure 3.18. Gene amounts of 2-month-old transgenic ADan1Q-34 founder mice measured by RT-PCR using tail biopsies. Highest transgene levels were detected in line OW20. For further investigations, lines OW20, OW23 and OW24 were chosen. (WT: wild-type)

78

3.1.8.1   ADan Expression in ADan1Q-34 Transgenic Mice

Western-blot assay using a C-terminal ADan antibody (Ab5282) revealed quantitative ADan1Q-34 peptide amounts from brain lysates of several 6 to 8-month-old founders as well as the first offspring of founder OW20 at the age of 6 months (Fig. 3.19a). Founder animals OW20, OW23, OW24 and OW26 harbored highest levels of ADan peptides, whereas a pattern of higher oligomeric assemblies could be also detected that is quite similar to that observed for synthetic ADan peptide (Fig. 3.19a, last lane). In addition, analysis of 6-month-old offspring of OW20 (OW20-6 and OW20-8) showed that the transgene was successfully integrated into germ line and stably inherited. Immunohistochemical staining using the same antibody Ab5282 was performed for the characterization of the expression pattern of ADan peptides in cells of different brain regions of the transgenic lines OW20, OW23 and OW24. Abundant ADan-positive structures were observed in all lines to a greater or lesser extent in several layers of the cortex, hippocampus (Fig. 3.19b-d) and brain stem (Tab. 3.1). Particularly, lines OW20, OW23 and OW24 showed strongest intracellular ADan immunoreactivity in CA1 hippocampal neurons (Fig. 3.19f-h) and mossy fibers as well as in layer IV and V of the cortex. Furthermore, transgenic mice from OW20 and OW23 lines harbored strong ADan expression in Purkinje cells of the cerebellum (Fig. 3.19j-k). Even offspring at the young age of 1 month showed this strong expression pattern that was indistinguishable from that observed in founder mice (not shown). ADan expression was restricted to intracellular compartments, whereby no plaque pathology or amyloid angiopathy could be observed in the investigated mice, with 6 months of age being the latest time point that was analyzed.
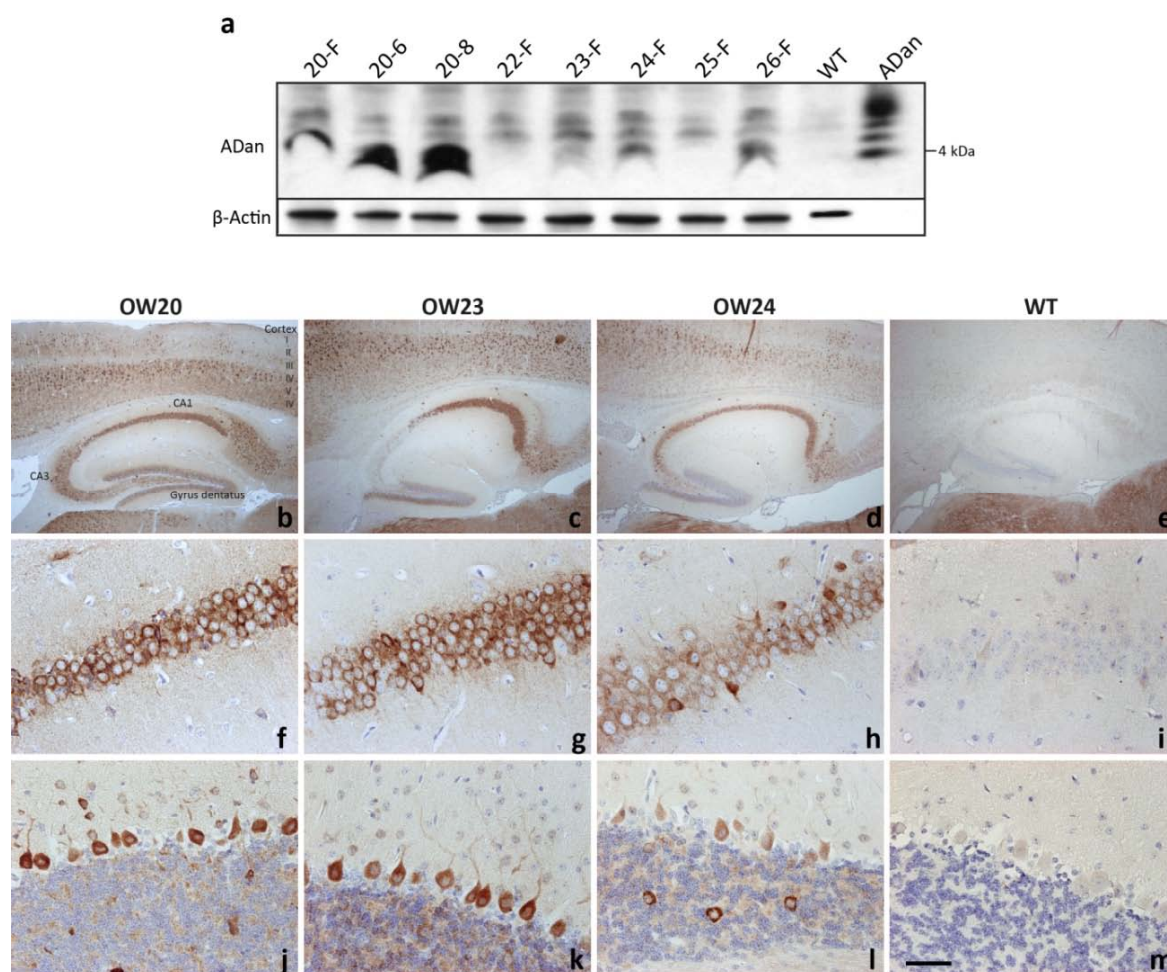
Figure 3.19. Western-blot (a) and immunohistochemistry (b-m) on brains of the novel generated ADan1Q-34 transgenic mice using Ab5282. (a) Founders (F) OW20 (and offspring: OW20-6/8), OW23, OW24 and OW26 showed strongest ADan immunoreactivity with a higher oligomerization profile comparable to synthetic ADan peptide. In lines OW20, OW23 and OW24 abundant ADan immunoreactivity was observed in multiple cortical layers and hippocampus (b-d) especially in CA1 cells (f-h). ADan peptides were also identified in single Purkinje cells (OW20, 23, 24) and granula cells (OW24) of the cerebellum (j-l). (WT: wild-type, e, i, m). Scale bar: (b-e) 500 µm, (f-m) 50 µm

	OW20	OW23	OW24
CA1	+++	+++	++
CA3	+	-	+
Gyrus dentatus	+	+	-
Cortex (layer)	II+, IV-V++	II, IV-V+	IV-V+
Cerebellum (cell type)	Purkinje+ Granula(+)	Purkinje++	Purkinje (+) Granula(+)
Brain stem	++	+	++
Olfactory bulb	+	-	+

Table 3.1. Overview of ADan1Q-34 expression pattern in different brain regions of the novel generated mouse lines OW20, OW23 and OW24. (– negative, (+) weak expression/scattered neurons, + to +++ single to abundant ADan immunopositive neurons)

80

3.1.8.2   Inflammation in ADan1Q-34 Transgenic Mice

Inflammation represented by astro- and microgliosis is associated with Aβ and ADan accumulations in AD and FDD, respectively. Therefore, immunohistochemical stainings were performed on brain sections of the novel generated transgenic mouse lines OW20, OW23 and OW24 at the age of 6 months using markers for activated astrocytes (GFAP) and microglia/macrophages (Iba1) (Fig. 3.20 and 3.21, respectively). Although plaque pathology was absent, activated astrocytes and to a lesser extent reactive microglia could be observed throughout the hippocampus in comparison to a wild-type animal at 10 months of age. Additionally, enriched immunoreactive astrocytic processes from Bergmann glia were detected in transgenic mice that extend into the molecular layer of the cerebellum (Fig. 3.20i-l).
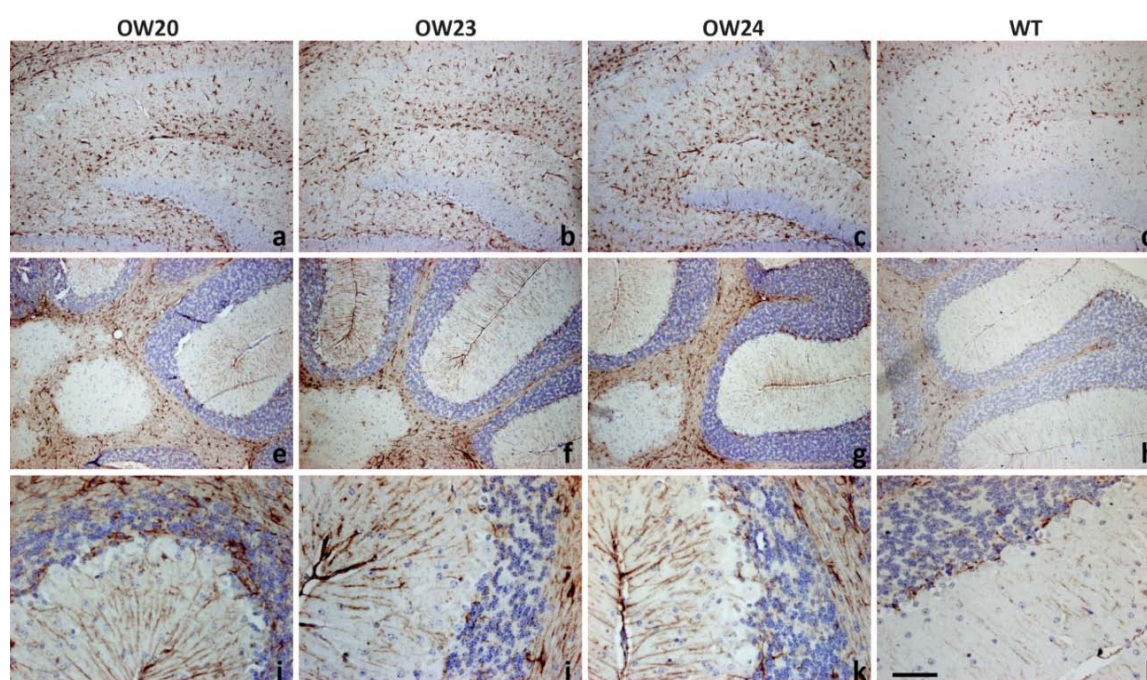
Figure 3.20. Increased amounts of reactive astrocytes were detected using anti-GFAP in the hippocampus (a-d) and the cerebellum (e-h) including Bergmann glia (i-l) of 6-month-old ADan1Q-34 transgenic mice. (WT: wild-type). Scale bar: (a-h) 200 µm, (i-l) 50 µm
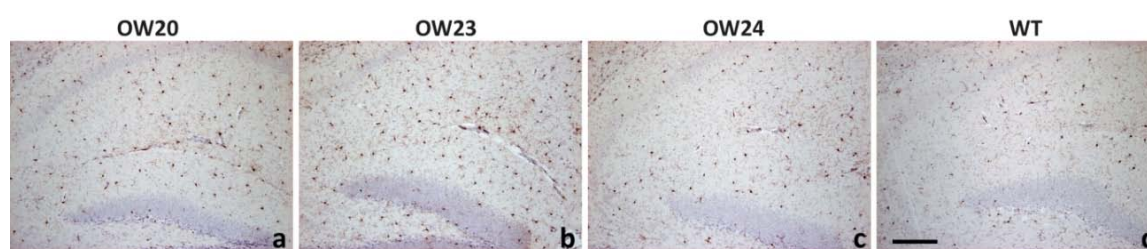
Figure 3.21. Immunohistochemistry with IBA1 antibody also revealed increased amounts of reactive microglia in the hippocampus of 6-month-old ADan1Q-34 transgenic mice (a-c) in comparison to a 10-month-old wild-type mouse (WT, d). Scale bar: 200 µm

3.1.8.3   Behavioral Changes of ADan1Q-34 Transgenic Mice

Lines OW20 (n = 5), OW23 (n = 3) and OW24 (n = 4) were tested at 6 months of age in different paradigms to assess behavioral impairments due to the transgene expression in comparison to age-matched wild-type animals (n = 6).

To analyze motor and coordination abilities, balance beam (Fig. 3.22a-b) and string suspension task (Fig. 3.22c-d) were performed. At 6 months of age, no difference compared to controls in task performance could be observed suggesting no impairment in balance and general motor deficits as measured by balance beam test or reduced agility and fitness assessed by string suspension.
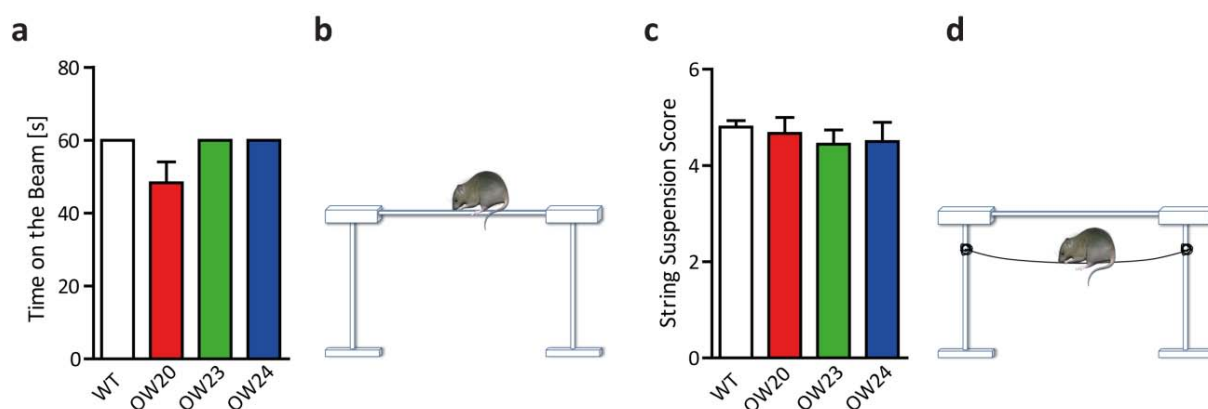
Figure 3.22. No changes in general health or motor ability were detected using balance beam (a-b) and string suspension tasks (c-d) in neither OW20 (n = 5), OW23 (n = 3) nor OW24 (n = 4) compared to wild-type animals (WT, n = 6) at 6 months of age. All error bars represent SEM.

Changes in anxiety behavior were investigated using the elevated plus maze paradigm (Fig. 3.23c), in which OW23 mice showed an increased anxiety behavior compared to controls by spending significantly less time in the open arms of the apparatus ($p < 0.05$, Fig. 3.23a). Moreover, a tendency towards a reduced exploratory behavior was observed for these mice as measured by the total distance travelled, which became significant for OW24 animals ($p < 0.05$, Fig. 3.23b).

The cross maze was used to analyze the performance of working memory in terms of spontaneous alternations. In this test, transgenic mice from lines OW23 and OW24 did significantly less alternations compared to wild-type mice ($p < 0.01$ and $p < 0.001$, respectively, Fig. 3.24a). Furthermore, even in this task OW24 mice showed a significant

decrease (p < 0.05) and OW23 mice a trend towards a reduction in overall activity and exploration behavior (Fig. 3.24b) confirming the previously described behavior data.
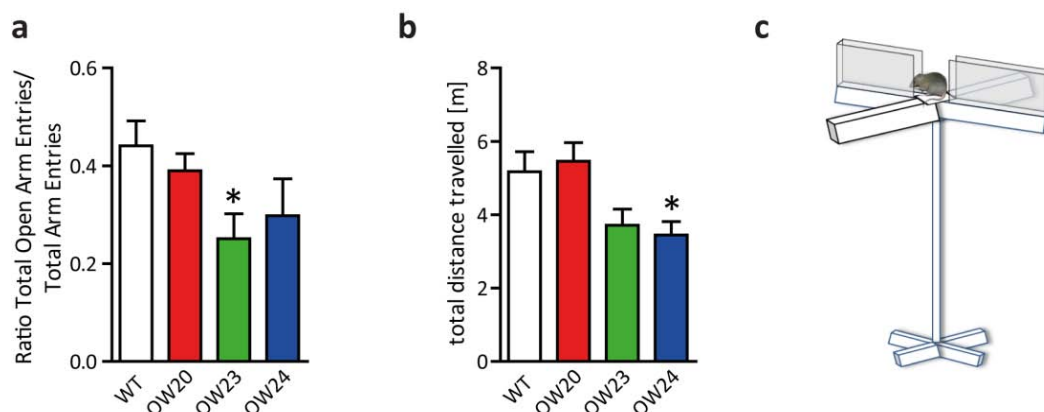
Figure 3.23. The elevated plus maze test (c) revealed a significantly increased anxiety of OW23 mice (a) and a reduced exploratory behavior of OW24 animals (b). All error bars represent SEM. (wild-type [WT]: n = 6, OW20: n = 5, OW23: n = 3, OW24: n = 4; p < 0.05*)
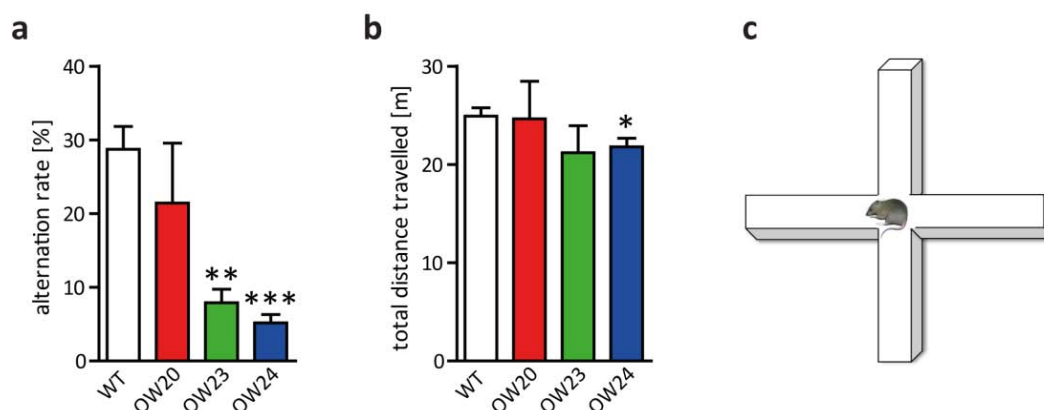
Figure 3.24. OW23 and OW24 mice did significantly less alternations in the cross maze experiment (a, c). Additionally, OW24 mice exploited the apparatus significantly fewer than wild-type controls. All error bars represent SEM. (wild-type [WT]: n = 6, OW20: n = 5, OW23: n = 3, OW24: n = 4; p < 0.05*, p < 0.01**, p < 0.001***)

For further analysis of motor skills, learning abilities and integrity of the spatial reference memory the Morris water maze task was performed (Fig. 3.25c). ADan1Q-34 transgenic mice were able to find the escape platform in the same time as wild-type animals in the cued (Fig. 3.25a) and the acquisition training (Fig. 3.25b) suggesting no learning impairment. However, in the probe trail, in which the platform was removed, OW23 mice had problems to

distinguish target from left quadrant (Fig. 3.25d) indicating an initial impairment of the recall ability of the spatial reference memory at 6 months of age. In line with the balance beam and string suspension task, no motor dysfunction could be observed, since swimming speed did not differ between transgenic and control mice (Fig. 3.25e).
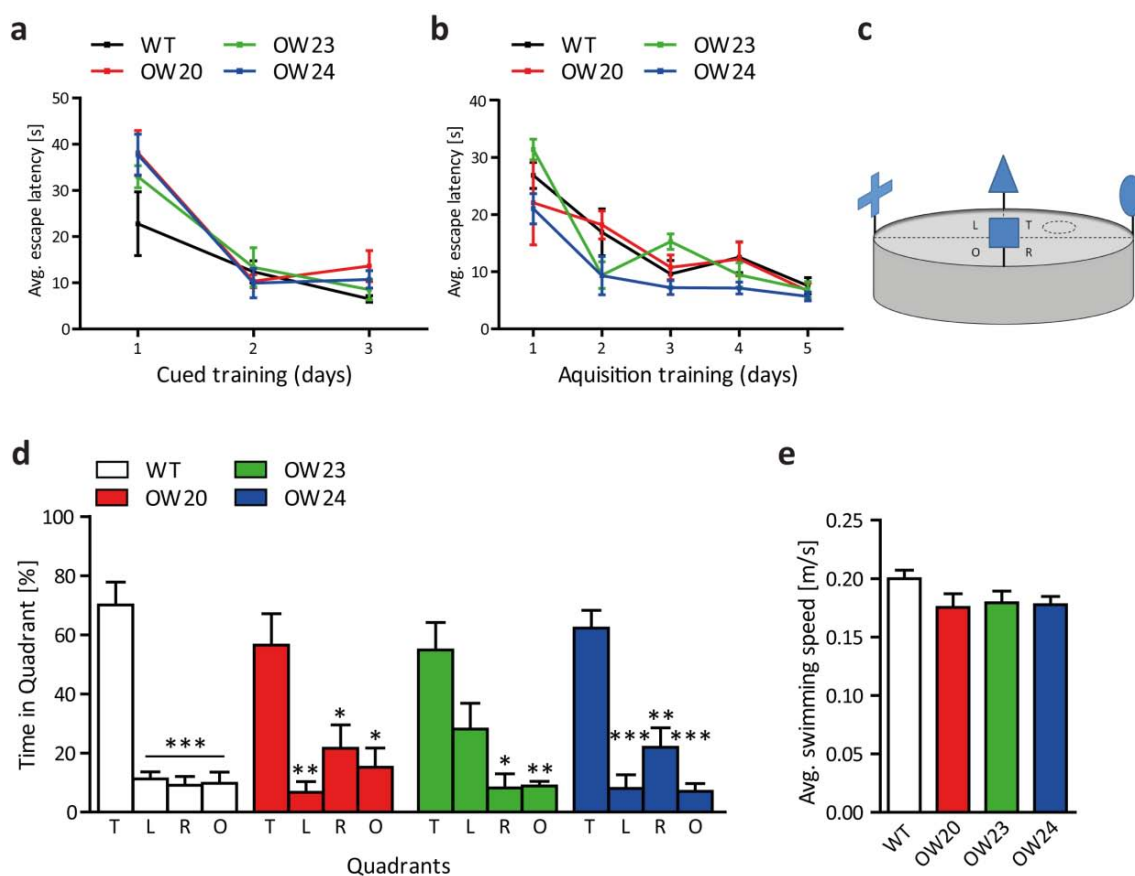
Figure 3.25. No disability in learning of 6-month-old OW20 (n = 5), OW23 (n = 3) and OW24 (n = 4) mice were measured in comparison to wild-type animals (WT, n = 6) during cued (a) and acquisition training (b) in the Morris water maze experiment (c). The Probe trail revealed starting impairment in spatial reference memory recall in OW23 mice (d). Again, no decrease in motor function of ADan1Q-34 mice was monitored according to absent changes in swimming speed (e). All error bars represent SEM. (T-target, L-left, R-right and O-opposite quadrant; p < 0.05*, p < 0.01**, p < 0.001***)

3.2 Project II: Aβ triggers Murine ApoE Fragmentation in Transgenic Mouse Models for Alzheimer's Disease

3.2.1 Intracellular Aβ triggers ApoE Fragmentation in Human Tissue

Brain lysates of human control brains (n = 3) and sporadic AD cases (sAD, n = 3) as well as one familial AD brain (fAD) with the African APP-Mutation (I716F in APP or I45F in Aβ) were used in Western-blot assay with antibodies against full-length (antibody WU-E4) and C-terminal ApoE (anti-ApoE C-term) (Fig. 3.26a). Using WU-E4 antibody, N-terminal ApoE fragments were detected with a size of approximately 29 and 20 to 25 kDa. Furthermore, using a C-terminal specific ApoE antibody 10 to 15 kDa C-terminal fragments could be identified. Most of the ApoE fragments occurred in the familial AD case in different brain regions like frontal and occipital lobe, whereas they were almost absent in the control brains. Also C-terminal fragments were most prominent in the familial AD brain, in which the African APP mutation leads to a strongly increased 42/40 ratio and high amounts of intraneuronal Aβ (Lichtenthaler et al. 1999b). ApoE proteolysis is linked to Aβ burden, since total ApoE with a size of 34 kDa remained unaltered, but N-terminal and C-terminal ApoE fragments were significantly increased in sAD ($p < 0.05$ and $p < 0.01$, respectively), in which also Aβ levels were strongly elevated, compared to non-demented controls ($p < 0.01$, Fig. 3.26b).
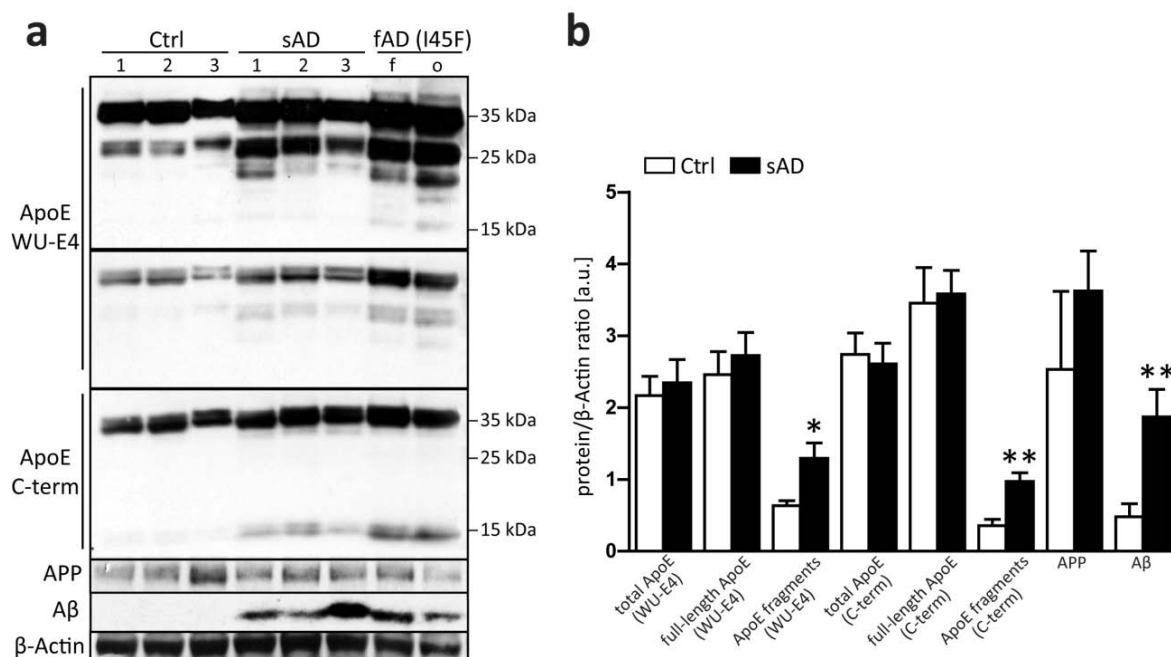
Figure 3.26. Western-blot analysis revealed approximately 29 and 20 to 25 kDa N-terminal ApoE fragments using WU-E4 as well as 10-15 kDa C-terminal fragments using an ApoE C-terminal antibody (C-term) (a). In the African familial AD (fAD) case (I716F) highest amounts of fragmented ApoE were observed in different brain regions (f-frontal lobe, o-occipital lobe). (b) Quantification revealed significantly increased Aβ as well as N-terminal and C-terminal ApoE fragments in sporadic AD (sAD, n = 3) compared to non-demented controls (Ctrl, n = 3). All error bars represent SEM. ($p < 0.05$*, $p < 0.01$**)

To examine if extracellular Aβ might influence the generation of ApoE fragments, 5, 10 and 25 μM of synthetic $Aβ_{1-42}$ were applied on human Ntera2 teratocarcinoma cells that harbor high endogenous levels of human ApoE for 24 h (n = 5 for each condition). Using WU-E4 antibody in Western-blot assay the exogenous treatment resulted in significantly increased overall ApoE levels compared to control cells ($p < 0.01$), without evidence for ApoE fragmentation (Fig. 3.27a-b). Additionally, increased levels of intracellular Aβ could be observed ($p < 0.05$ for 10 μM and $p < 0.01$ for 25 μM Aβ), suggesting that Aβ was taken up by the cells from the medium and induced ApoE production. In order to assess if intracellular Aβ triggers ApoE fragmentation, human SH-SY5Y neuroblastoma cells were stable transfected with different APP constructs like APP_{751wt} and SPA4CTΔcyto. The SPA4CTΔcyto construct lead to a high production of intracellular Aβ (Dyrks et al. 1992, Lichtenthaler et al. 1997, Fossgreen et al. 1998). These cells showed elevated full-length ApoE levels in Western-blots as well, but in addition there was a strong increase of ApoE fragments with highest levels in $SH-SY5Y_{SPA4CTΔcyto}$ compared to Mock control (Fig. 3.27c). This leads to the

assumption that intracellular Aβ accumulation has a different effect on ApoE than exogenous application of Aβ peptides. The pattern of ApoE fragments resembles the pattern in human AD cases (compare with Fig. 3.26a, second row).
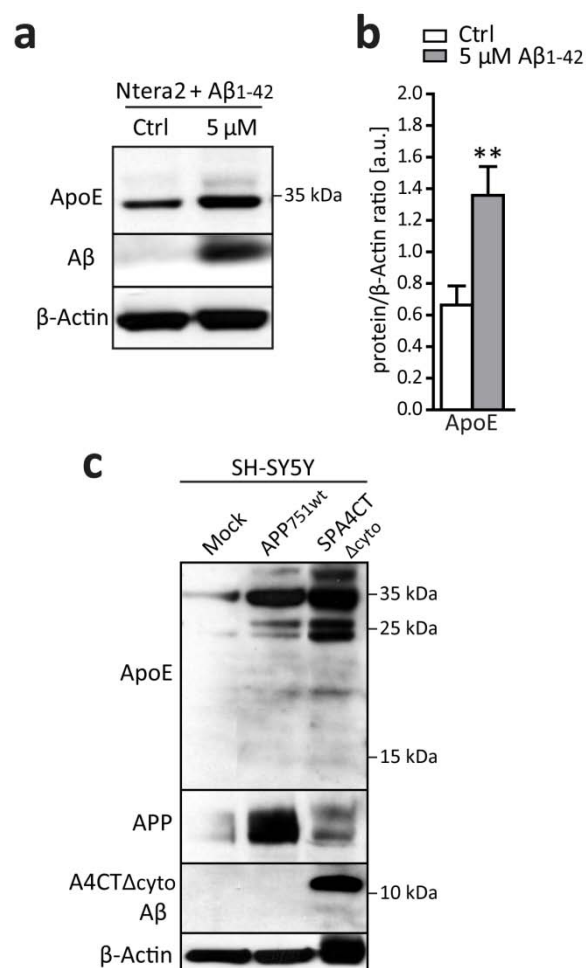
Figure 3.27. (a, b) Application of different Aβ$_{1-42}$ concentrations (n = 5) on cultured human Ntera2 cells led to enhanced expression of full-length ApoE, but fragmentation was absent. (c) Human SH-SY5Y stably expressing APP$_{751wt}$ (wild-type) or SPA4CTΔcyto harbored elevated total ApoE levels and increased fragmentation with highest amounts in SPA4CTΔcyto transfected cells. All error bars represent SEM. (Ctrl: control; $p < 0.05$*, $p < 0.01$**)

3.2.2 Murine ApoE accumulates and becomes fragmented under Amyloid Burden

The assumption that fragmentation is associated with intracellular Aβ raises the question whether this is also the case for AD mouse models carrying high levels of intracellular Aβ in cortex and hippocampus. To answer this question, Western-Blot analyses were performed with several appropriate mouse models: 5XFAD (APP$_{SwFlLon}$, PS1$_{M146L,L286V}$), APP/PS1KI (hAPP$_{SwLon}$, mPS1$_{M233T,L235P}$) and APP/PS1-21 (APP$_{Sw}$, PS1$_{L166P}$). Western-blot analyses using an antibody M-20 against murine ApoE (mApoE) revealed that increased ApoE fragmentation as well as enhanced ApoE expression could be detected in the different AD mouse models compared to wild-type mice.

Regarding the APP/PS1KI mouse model, using M-20 antibody in Western-blotting of soluble (TBS) and insoluble (SDS) brain fractions of 10-month-old APP$_{he}$ and PS1KI$_{ho}$ single transgenic mice showed increased expression of full-length ApoE compared to aged-matched wild-type control, but ApoE fragments were absent in PS1KI$_{ho}$ and only slightly present in APP$_{he}$ (Fig. 3.28a). However, APP/PSKI hemizygous and homozygous double transgenic mice (APP$_{he}$/PS1KI$_{he}$ and APP$_{he}$/PS1KI$_{ho}$, respectively) harbored highest amounts of full-length ApoE and, additionally, the endogenous mApoE became strongly processed into 10 to 15, 25 and 29 kDa fragments with highest levels in APP/PS1KI$_{ho}$ especially in the insoluble fraction (Fig. 3.28a). However, there was no big difference between APP levels of APP$_{he}$ single and APP/PS1KI mice, but the amounts of Aβ as well as C99 were drastically elevated in the double transgenic animals. In hippocampus lysates of 2-month-old APP/PS1KI$_{ho}$ mice, a time point where intracellular Aβ and almost no plaque pathology is present in these animals (Wirths and Bayer 2010), initial ApoE fragmentation showing especially 10 to 15 and 25 kDa fragments was observed in contrast to wild-type and PS1KI$_{ho}$ mice (p < 0.05), whereas full-length ApoE levels did not change significantly between genotypes (n = 3 for each genotype; Fig. 3.28b-c). Furthermore, antibody IC16 detects Aβ peptides at this young age (p < 0.001) as well as strongly elevated C99 levels in APP/PS1KI$_{ho}$ mice (p < 0.001) already in comparable amounts as in 10-month-old mice (Fig. 3.28a-b).
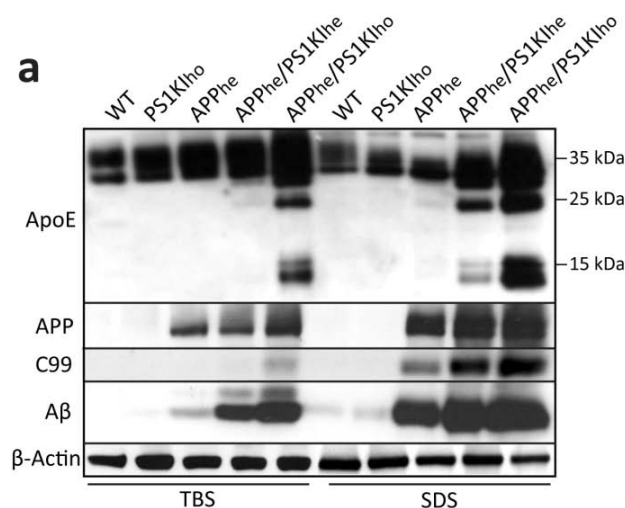
Figure 3.28. (a) Western-blot analyses using M-20 antibody of brains from 10-month-old APP/PS1KI mice revealed that murine ApoE (mApoE) becomes fragmented with fragment sizes of 10 to 15, 25 and 29 kDa that increased also like Aβ and C99 (IC16) in a genotype and gene-dose dependent manner. Western-blot assay (b) and appropriate quantification (c, n = 3) of hippocampi from 2-month-old APP/PS1KI$_{ho}$ already revealed ApoE fragmentation (M-20) and high expression of C99 (IC16) compared to wild-type or PS1KI$_{ho}$. All error bars represent SEM. (TBS: soluble fraction, SDS: insoluble fraction, WT: wild-type; p < 0.05*, p < 0.001***)
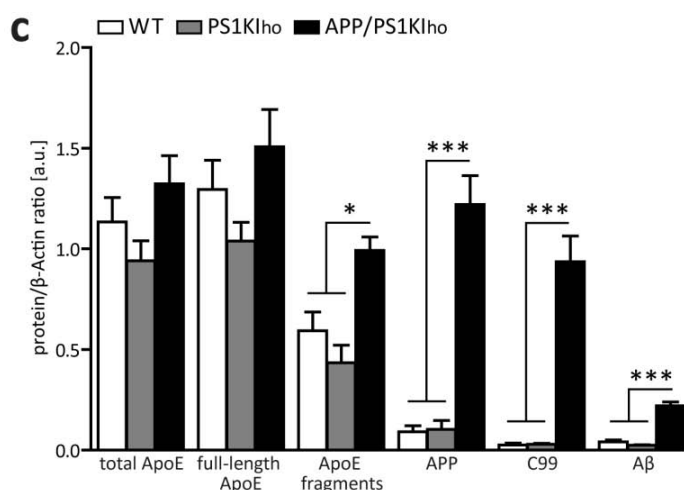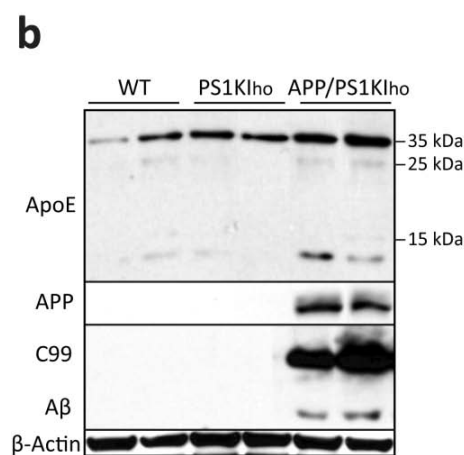
Furthermore, double immunofluorescent staining using the ApoE antibody M-20 and 24311, an antibody detecting pan-Aβ, revealed that ApoE and putatively its fragments is localized in almost all extracellular Aβ deposits and in Aβ containing neuritic swellings in the hippocampus of a 10-month-old APP/PS1KI$_{ho}$ mouse (Fig. 3.29a-c). ApoE-immunofluorescent structures with a granule-like morphology were also found intraneuronally co-localizing with Aβ in cortical tissue of this mouse model (Fig. 3.29d-f). The same holds true for a 9-month-old 5XFAD female using M-20 and anti-APP antibodies, whereby ApoE seemed to be accumulated in axon hillocks of cortical neurons (Fig. 3.29g-i).
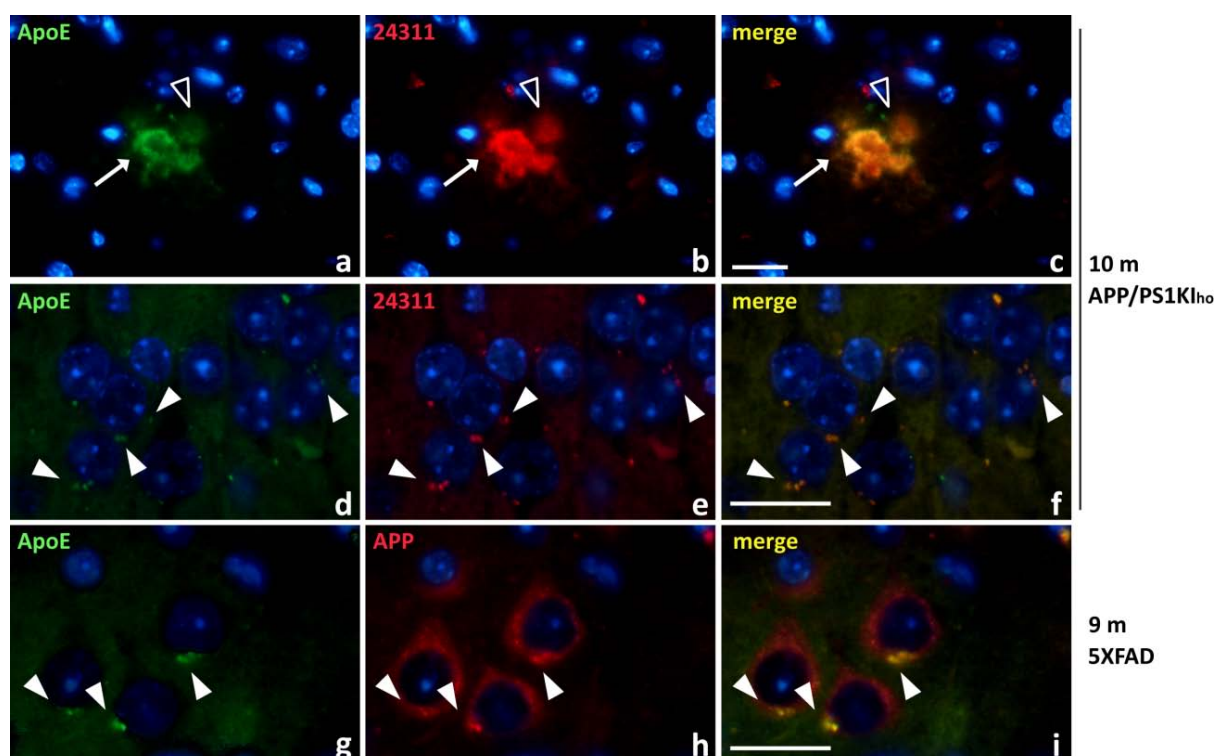
Figure 3.29. (a-f) Double immunofluorescent staining of a 10-month-old APP/PS1KI$_{ho}$ mouse using M-20 (a, d) and 24311 antibodies (b, e) revealed the presence of mApoE in Aβ plaques (arrow) and in plaque-associated dystrophic neurites (black arrowhead) in the hippocampus (a-c). Additionally, ApoE has been detected intracellularly together with Aβ deposits (white arrowheads) in cortical neurons (d-f). (g-i) Immunostaining of a 9-month-old 5XFAD mouse using M-20 (g) and anti-APP antibodies (h) showed the same results with granule-shaped ApoE structures in axon hillocks of cortical neurons expressing APP (white arrowheads). Scale bar: 20 µm

To confirm the observations in the APP/PS1KI mouse model, soluble (TBS) and insoluble (SDS) brain as well as spinal cord lysates of 6-, 9- and 12-month-old 5XFAD (Fig. 3.30), in addition to brain lysates of 2-, 5- and 7-month-old APP/PS1-21 (Fig. 3.31) were investigated via Western-blotting using M-20 and IC16 antibodies.

In 5XFAD mice, an age-dependent accumulation of ApoE fragments was seen together with elevated full-length ApoE levels compared to wild-type control mice with 12-month-old animals showing highest levels of ApoE fragments in the insoluble brain fraction ($p < 0.001$, n = 3 for each genotype, Fig. 3.30). Interestingly, significantly increased amounts of full-length ApoE and fragments ($p < 0.05$) could be already observed at 6 months of age in the SDS fraction, resembling the same pattern with fragment sizes of approximately 10 to 15, 25 and 29 kDa as observed in the APP/PS1KI mouse model (Fig. 3.28a). The occurrence of ApoE fragments in 6-month-old 5XFAD mice suggests that ApoE fragmentation is an early event that coincides with increasing insoluble Aβ and C99 levels (Fig. 3.30a), with the onset

of plaque pathology and behavior deficits in these mice (Jawhar et al. 2012). However, no ApoE fragments were detected in spinal cord tissue of 6- and 12-month-old 5XFAD (Fig. 3.30a).
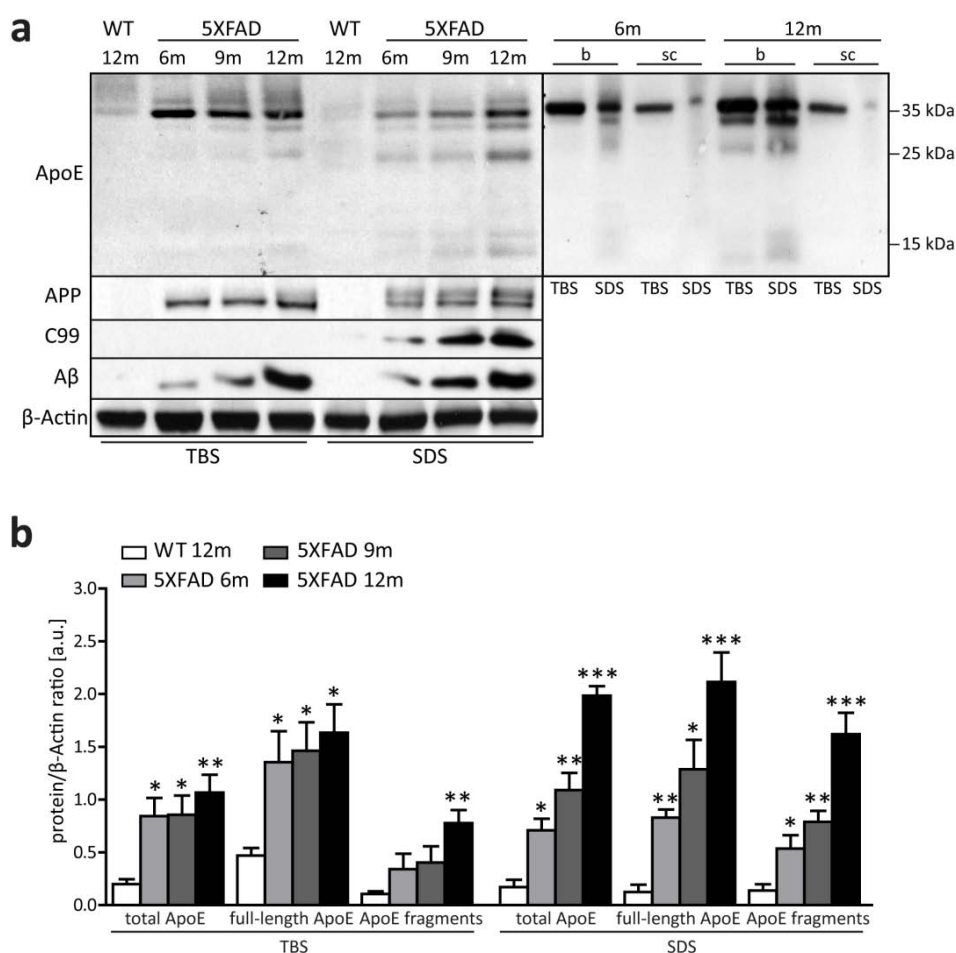
Figure 3.30. Western-blot analysis of soluble (TBS) and insoluble (SDS) lysates of 6-, 9- and 12-month-old 5XFAD mice using M-20 and IC16 antibodies. (a) Coinciding with Aβ and C99 amounts, an age-dependent accumulation of full-length ApoE and fragments occurred in brains of 5XFAD mice that were absent in spinal cord and in the brain of a 12-month-old wild-type (WT) control. (b) Quantification of Western-blot data (n = 3) revealed significantly increased levels of ApoE fragments in SDS brain fractions of 5XFAD already at the age of 6 months. All error bars represent SEM. (b: brain, sc: spinal cord; $p < 0.05*$, $p < 0.01**$, $p < 0.001***$)

Western-blot analyses of soluble and insoluble brain lysates of 2- and 10-month-old wildtype as well as 2-, 5- and 7-month-old PS1APP-21 mice using M-20 and IC16 antibody (n = 3 for each genotype, Fig 3.31) corroborated the previous findings, in which most of the 10 to 15, 25 and 29 kDa ApoE fragments were detected in the insoluble fraction in an age-dependent manner that were also associated with high amounts of insoluble Aβ peptides.
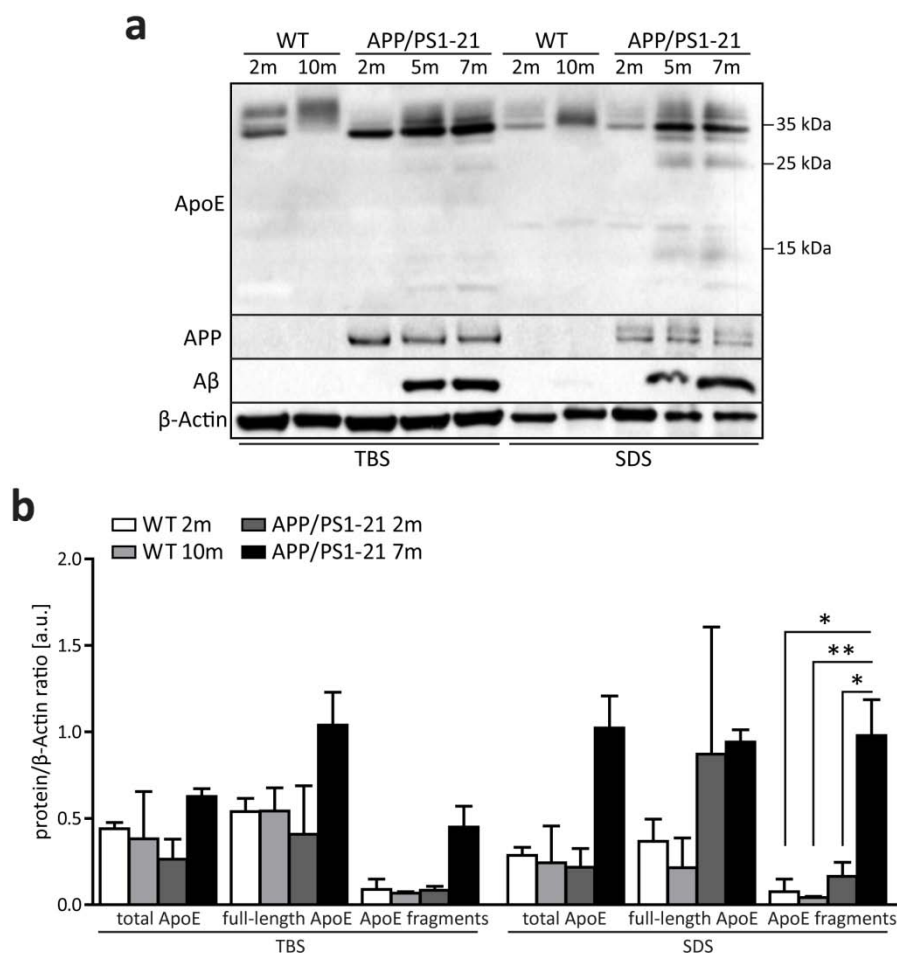
Figure 3.31. Western-blot analysis of soluble (TBS) and insoluble (SDS) brain lysates of 2-, 5- and 7-month-old APP/PS1-21 mice using M-20 and IC16 antibodies. Age-dependent accumulation of full-length ApoE and fragments were detected in brains of APP/PS1-21 mice that were absent in brains of 2- and 10-month-old wild-type (WT) controls (a). Quantification of Western-blot data (n = 3) revealed significantly increased levels of ApoE fragments in insoluble fractions (SDS) of APP/PS1-21 brains already at the age of 7 months (b). All error bars represent SEM. ($p < 0.05^*$, $p < 0.01^{**}$)

A further proof of concept was to analyze if intracellular Aβ triggers mApoE fragmentation *in vitro* as well. Therefore, murine Neuro2a neuroblastoma cells were employed, which carried either high/over-expressed (stably transfected with mApoE) or low, endogenous levels of mApoE, which have been stably transfected with SPA4CT or SPA4CTΔcyto (corresponding to C99 or C99 without cytoplasmic domain, respectively) to ensure a high production of intracellular Aβ levels. Western-blot assays using antibodies detecting mApoE (M-20) and SPA4CT or SPA4CTΔcyto (W0-2) revealed the presence of detectable 10 to 15 and 25 kDa ApoE fragments in mApoE/SPA4CT and mApoE/SPA4CTΔcyto double transgenic Neuro2a cells ($p < 0.001$), whereas no fragmentation could be observed in cells only over-expressing mApoE (n = 3 for each cell line, Fig. 3.32). Furthermore, total ApoE levels were significantly elevated in mApoE/SPA4CT cells compared to mApoE single transgenic Neuro2a ($p < 0.05$).

Notably, in mApoE/SPA4CT and mApoE/SPA4CTΔcyto a tendency towards increased C99 and A4CTΔcyto production was observed, respectively, compared to their single transgenic counterparts expressing endogenous mApoE. Almost no ApoE could be detected in murine neuroblastoma carrying endogenous ApoE.

Figure 3.32. Neuro2a cells overexpressing mApoE and SPA4CT or SPA4CTΔcyto showed ApoE fragmentation with approximately 10 to 15 and 25 kDa fragments using Western-blot assay with M-20 and W0-2 antibodies (a). Almost no mApoE signal could be detected in cells harboring endogenous mApoE. (b) Quantification (n = 3) revealed significant differences between ApoE fragment levels of mApoE single transgenic Neuro2a and mApoE/ SPA4CT or SPA4CTΔcyto cells. All error bars represent SEM. ($p < 0.05$*, $p < 0.001$***)

That amyloid burden in the brain can induce proteolytical processing of mApoE could be further confirmed in biochemical approaches using a non-AD mouse model (ADanPP7), which expresses no Aβ, and the triple transgenic mouse model 3xTg mouse model (mutant APP, PS1 and tau) harboring quite few intracellular Aβ and plaque associated axonal swellings. Western-blot assay of brains from 2-, 4- and 13-month-old ADanPP7 mice (Fig. 3.33a), which develop ADan plaque pathology combined with neuritic dystrophy (see results from project I and (Coomaraswamy et al. 2010)), also revealed the presence of 10 to 15, 25 and 29 kDa mApoE fragments detected with M-20 antibody that coincide with the amount of detectable pGlu-modified and non-modified ADan peptides (using AB76-2 and AB77), whereas full-length ApoE amounts were increased as well compared to wild-type control.

Interestingly, Western-blot analyses of 16-month-old 3xTg mice showed no indication for ApoE fragmentation (Fig. 3.33b).

Figure 3.33. (a) Western-blot analysis of ADanPP7 revealed elevated full-length mApoE (M-20) and ApoE fragmentation starting at 2 to 4 months of age simultaneously to the increase of ADan peptide amounts (AB76-2, AB77). (b) No mApoE fragments (M-20) were observed in 16-month-old 3xTg mice that also coincide with very low Aβ levels (W0-2). (WT: wild-type)
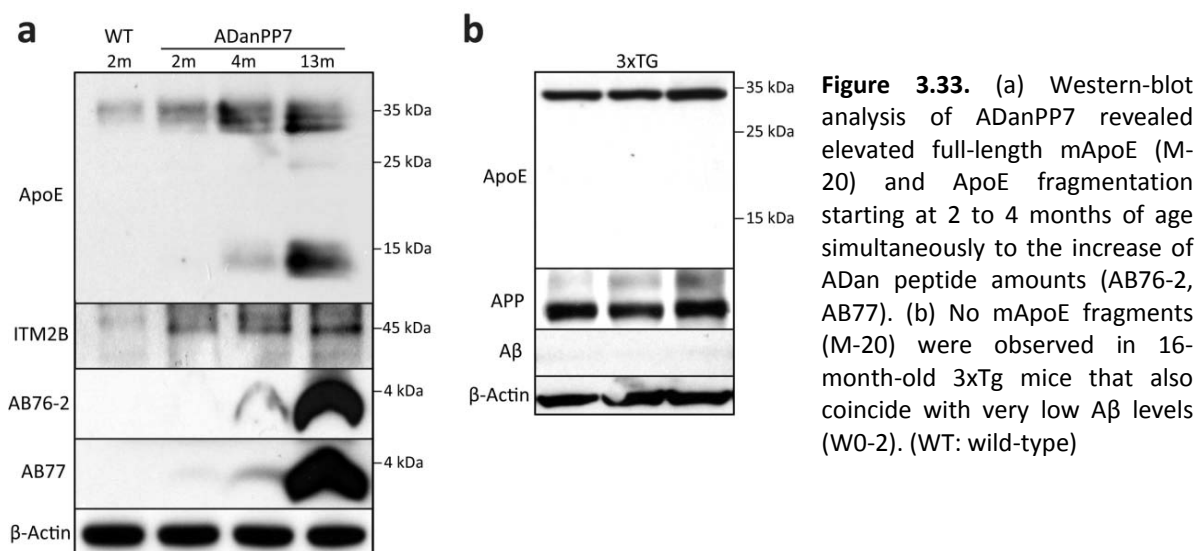
3.2.3 ApoE Fragments accumulate in Synapses

To investigate the possible toxic site of action of fragmented mApoE, crude synaptosomal fractions of 9-month-old wild-type and 5XFAD mouse brains (each n = 3) were analyzed by Western-blotting. As expected and as a proof for protocol efficiency, enriched amounts of PSD95 and CoxIV, which are markers for postsynaptic structures and mitochondria, respectively, were detected in crude synaptosomal fractions P2 rather than in microsomal S2 fractions of wild-type and 5XFAD brains (Fig. 3.34). Notably, wild-type mice showed only barely detectable mApoE in P2 using antibody M-20, but considerable amounts in the S2, whereas in 5XFAD most mApoE was detected in P2 fractions (p < 0.01). Interestingly, using IC16 antibody, high amounts of APP (p < 0.001), C99 and Aβ (both p < 0.01) were detected in P2 fractions that were significantly increased compared to age-matched controls. These Western-blot experiments furthermore suggested that highest amounts of Aβ peptides correlate well with increased mApoE fragments in synaptosomal fractions of 5XFAD mice, since total and full-length mApoE (both p < 0.01) as well as mApoE fragments (p < 0.001) were strongly elevated in P2 fractions of 5XFAD compared to controls.
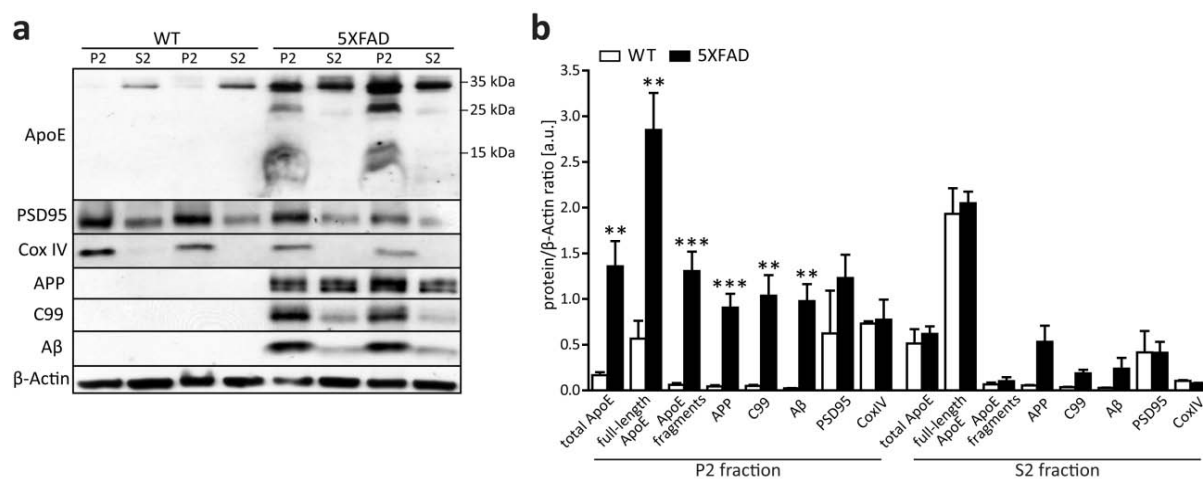
Figure 3.34. Western-blot analysis using crude synaptosomal fractions (P2) marked full-length mApoE levels (antibody M-20) were detected in 5XFAD mice, whereas wild-type mice (WT) showed only barely detectable mApoE in P2, but considerable amounts in the microsomal (S2) fraction. As expected, the P2 fraction contained enriched synaptosomes, as shown by increased levels of the post-synaptic density protein 95 (PSD95), as well as strong enrichment in mitochondria, as shown by the mitochondrial marker protein CoxIV (a). Interestingly, total, full-length and fragmented mApoE as well as C99 and Aβ levels (antibody IC16) were strongly enriched in synaptosomal fractions (n = 3, b). All error bars represent SEM. (n = 3 for each genotype; $p < 0.01$**, $p < 0.001$***)

To corroborate this finding, brain samples from 6-month-old wild-type, PS1KI$_{ho}$, APP$_{he}$ (each n = 3) and APP/PS1KI$_{ho}$ (n = 7) mice were extracted using the same protocol and the P2 and S2 fractions were analyzed by Western-blot (Fig. 3.35a). In good agreement with the 5XFAD data, P2 fractions of APP/PS1KI$_{ho}$ mice contained highest total ApoE levels (antibody M-20) consisting of full-length ApoE and its fragments in contrast to wild-type and APP$_{he}$ mice that harbored most ApoE in the S2 fraction. Furthermore, PSD95 and CoxIV levels were also enriched in the P2 fraction confirming protocol efficiency. Like in 5XFAD, occurrence of ApoE fragments correlated with enhanced Aβ and C99 amounts (antibody IC16) in the P2 crude synaptosomal fraction of APP/PS1KI$_{ho}$ brains. As expected, APP/PS1KI$_{ho}$ mice showed significantly increased total and full-length ApoE as well as fragmented ApoE levels (all $p < 0.05$ and $p < 0.01$, respectively) compared to the three other genotypes accompanied by significantly elevated levels of Aβ and C99 (n = 3, Fig. 3.35b). The same holds true for Western-blot analyses of P2 fractions from 10-month-old wild-type, PS1KI$_{ho}$, APP$_{he}$ and APP/PS1KI$_{ho}$ mice (each n = 3), where an age-dependent effect with enhanced accumulations of ApoE fragments and Aβ was observed (Fig. 3.36). Interestingly, C99 levels did not differ in APP/PS1KI$_{ho}$ mice at 6 and 10 months of age, whereas Aβ amounts doubled which correlates with doubled quantities of ApoE fragments (Fig. 3.35c and Fig. 3.36b).
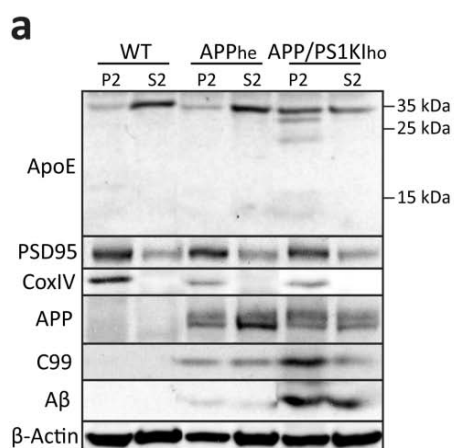
Figure 3.35. (a) P2 synaptosomal fractions of 6-month-old wild-type (WT), APPhe and APP/PS1KIho contained enriched amounts of PSD95 and CoxIV. Whereas wild-type and APPhe mice had most mApoE (antibody M-20) in S2 microsomal fraction, APP/PS1KIho mice showed elevated full-length ApoE and fragments in the P2 fraction. (b) Quantification of P2 fractions revealed significant increased levels of total and full-length mApoE as well as its fragments, C99 and Aβ (antibody IC16) in APP/PS1KIho (n = 7) compared to the other genotypes (each n = 3). All error bars represent SEM. (p < 0.05*, p < 0.01**, p < 0.001***)
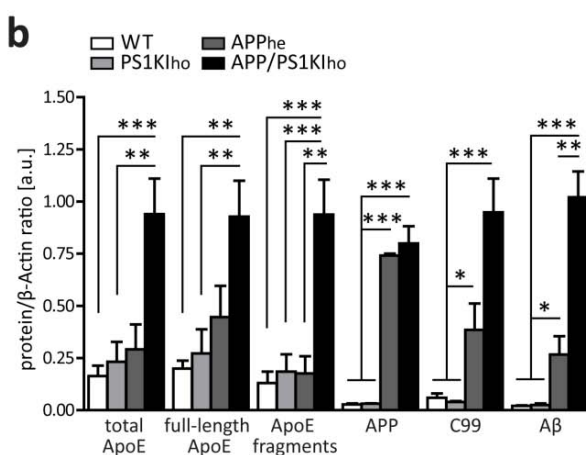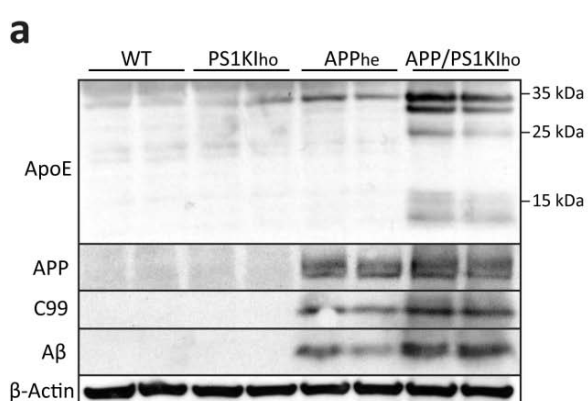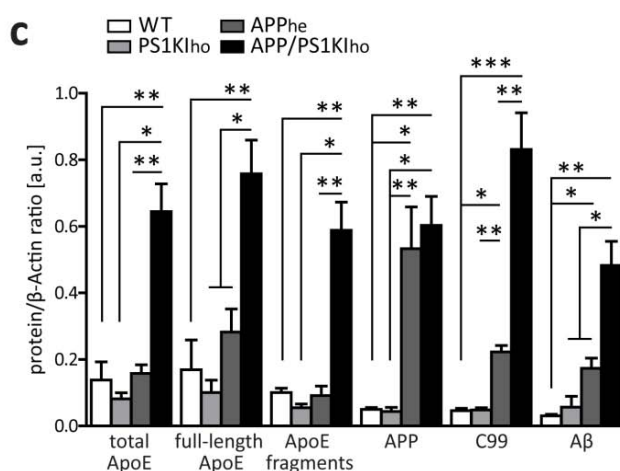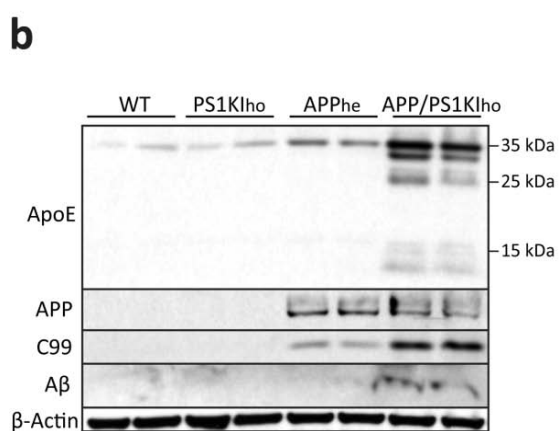
Figure 3.36. (a) P2 synaptosomal fractions of 10-month-old APP/PS1KIho revealed further accumulation of mApoE fragments (antibody M-20) that were lacking in wild-type and APPhe. (b) Quantification of P2 immunoblots showed that Aβ (antibody IC16) and ApoE fragment aggregation extended in APP/PS1KIho at 10 months of age. All error bars represent SEM. (n = 3; p < 0.05*, p < 0.01**, p < 0.001***)

96

3.2.4   ApoE Fragments and Oxidative Stress

Western-blot analyses in the 5XFAD and APP/PS1KI mouse model revealed an accumulation of mApoE fragments together with Aβ peptides in synaptosomal fractions, where by using CoxIV antibody a major portion of mitochondria could be detected. It is assumed that ApoE fragmentation is linked to a disrupted mitochondrial metabolism leading to oxidative stress that is reflected in the production of reactive oxygen species (ROS) (Mahley et al. 2006). To examine whether cell lines carrying high amounts of intracellular Aβ as well as ApoE fragments are also seriously affected by oxidative stress, cell viability assays with SH-SY5Y cells expressing the SPA4CT construct (Lichtenthaler et al. 1997) were performed. These cells were treated with multiple concentrations of N-acetyl-L-Cysteine (NAC, n = 5-10; Fig. 3.37), an effective anti-oxidant drug for the reduction of reactive oxygen species (ROS) (Aruoma et al. 1989). The application of NAC led to a restored cell proliferation as measured by MTT to formazan conversion after 24 h in a dose-dependent manner with significantly increased cell growth rates of SH-SY5Y$_{SPA4CT}$ cells that were incubated with 1 and 10 mM NAC (p < 0.001, Fig. 3.37a). To investigate if the production of ROS is a down- or upstream process of Aβ linked ApoE fragmentation, immunoblotting was performed with SH-SY5Y$_{SPA4CT}$ cells with or without NAC application using W0-2 and WU-E4 antibodies (Fig. 3.37b). This experiment revealed no changes in APP and C99 levels as well as full-length ApoE amounts, whereas 1 mM drug application resulted in significantly reduced ApoE fragments (p < 0.05, Fig. 3.37c) suggesting that reduced oxidative stress by NAC application led to diminished ApoE fragmentation and improved cell viability *in vitro*.
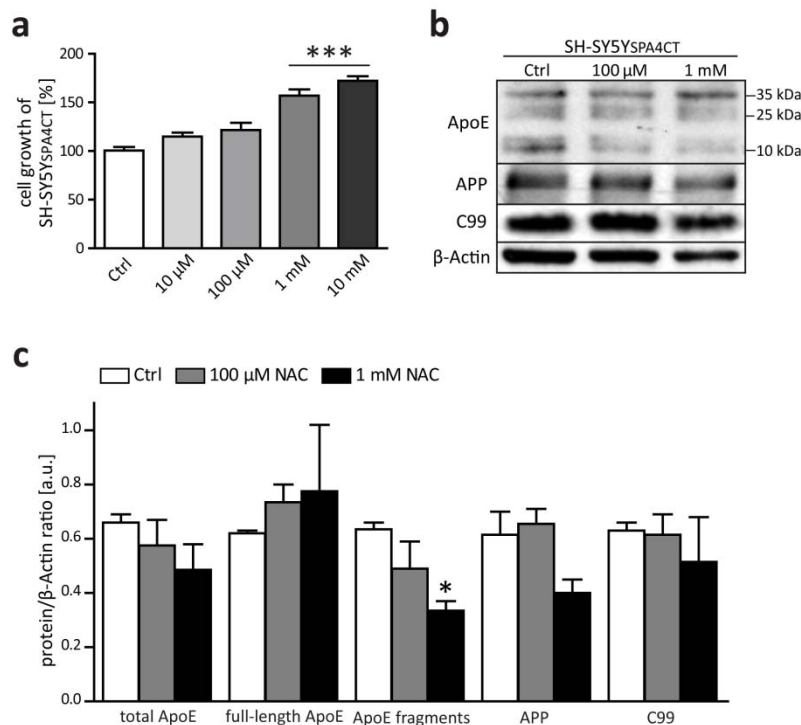
Figure 3.37. (a) The application of NAC on SH-SY5Y$_{SPA4CT}$ led to increased cell proliferation rates as measured by MTT assay that became significant in higher doses (1 and 10 mM NAC). (b) Western-blot analysis of these cells and (c) quantification revealed significantly decreased ApoE fragmentation (antibody WU-E4) in cells treated with 1 mM NAC, whereas full-length ApoE as well as APP and C99 levels (antibody W0-2) remained unchanged. All error bars represent SEM. (n = 5-10; Ctrl: control; $p < 0.05^*$, $p < 0.001^{***}$)

3.2.5 ApoE Fragmentation correlates with Axonopathy and Disturbed Autophagy in the APP/PS1KI Mouse Model

The APP/PS1KI mouse model harbors a severe axonopathy phenotype reflecting very well the AD pathology in humans (Wirths et al. 2007b). Therefore, this model is highly suitable to study if the swollen axons that occur in these mice contain accumulated autophagic vacuoles (AVs) as it has been shown in AD patients (Nixon and Yang 2011) and if this also correlates with ApoE fragments and synaptic loss. Immunohistochemical stainings of brains from 10-month-old APP$_{he}$, APP/PS1KI$_{he}$ and APP/PS1KI$_{ho}$ were performed using an antibody detecting phosphorylated APP in dystrophic neurites (antibody pT668, n = 6-7 for each genotype using means of 3 sections per animal). This staining revealed that a limited number of swollen axons was present in the cortex of APP$_{he}$ mice (Fig. 3.38a), whereas the amount of dystrophic neurites increased significantly with each copy of mutant PS1 in APP/PS1KI$_{he}$ (Fig. 3.38b, d), leading to highest levels in the APP/PS1KI$_{ho}$ mice (Fig. 3.38c), which differed also significantly from the amounts of APP/PS1K$_{he}$ animals (each $p < 0.001$, Fig. 3.38d).
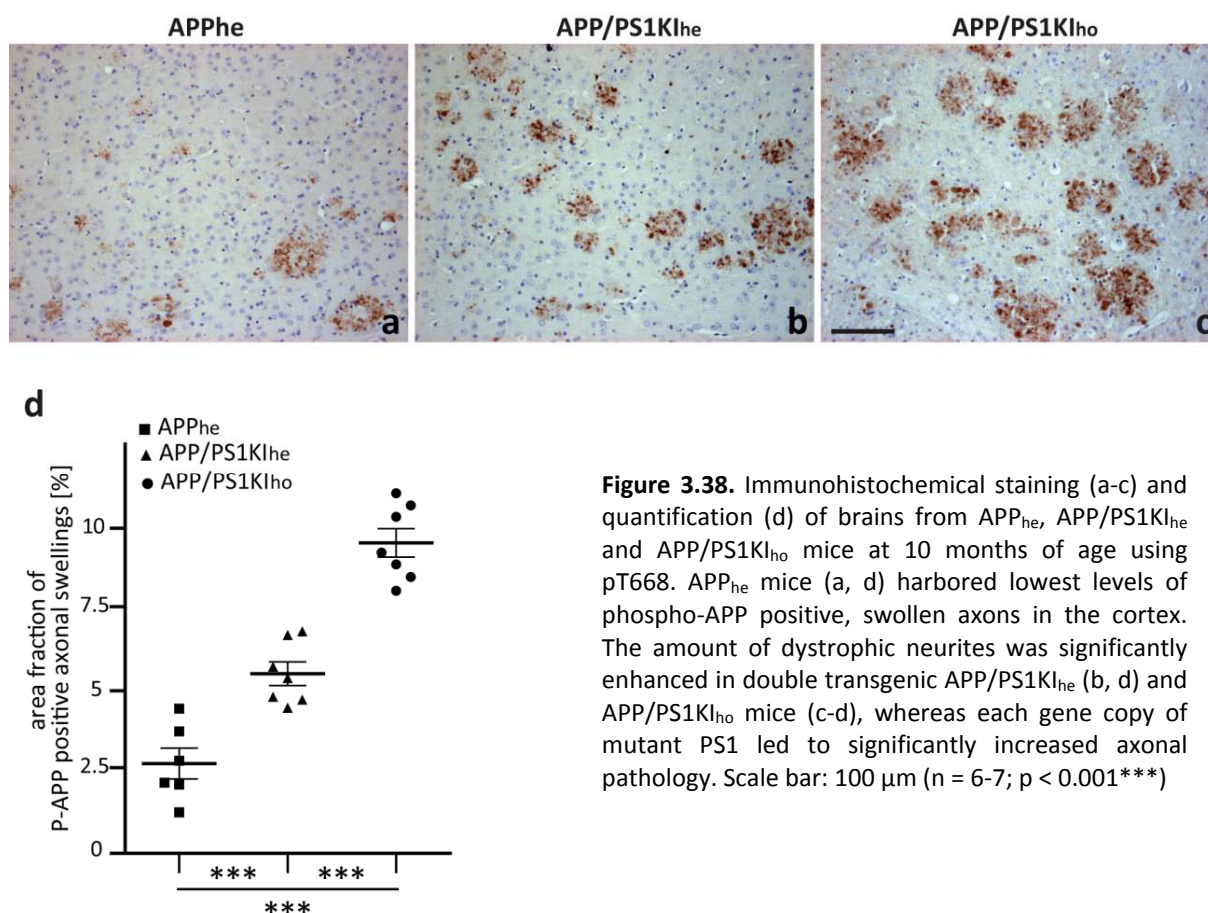
Figure 3.38. Immunohistochemical staining (a-c) and quantification (d) of brains from APP$_{he}$, APP/PS1KI$_{he}$ and APP/PS1KI$_{ho}$ mice at 10 months of age using pT668. APP$_{he}$ mice (a, d) harbored lowest levels of phospho-APP positive, swollen axons in the cortex. The amount of dystrophic neurites was significantly enhanced in double transgenic APP/PS1KI$_{he}$ (b, d) and APP/PS1KI$_{ho}$ mice (c-d), whereas each gene copy of mutant PS1 led to significantly increased axonal pathology. Scale bar: 100 µm (n = 6-7; p < 0.001***)

In order to examine if the axonopathy phenotype of these mice correlates with synaptic loss and mitochondrial reduction, Western-blot analyses were performed of hippocampus lysates of 2-month-old wild-type, PS1KI$_{ho}$ and APP/PS1KI$_{ho}$ animals (each n = 3, Fig. 3.39) as well as synaptosomal fractions of wild-type, PS1KI$_{ho}$, APP$_{he}$ and APP/PS1KI$_{ho}$ mice at 6 (each n = 3, Fig. 3.40) and 10 months of age (each n = 3, Fig. 3.41) using antibodies against PSD95 and CoxIV. Interestingly, PSD95 levels were significantly elevated in hippocampi of 2-month-old APP/PS1KI$_{ho}$ mice compared to wild-type controls (p < 0.01) and PS1KI$_{ho}$ animals (p < 0.05, Fig. 3.39) suggesting that the double transgenic mice had most synaptic compartments at this age. However, these highest amounts of synaptic structures drastically decreased in an age-dependent manner, in which PSD95 signals in APP/PS1KI$_{ho}$ were not indistinguishable anymore from that observed in wild-type, PS1KI$_{ho}$ and APP$_{he}$ at 6 months of age (Fig. 3.40) to the point of an almost complete loss of post-synaptic proteins (wild-type: p < 0.01 and PS1KI$_{ho}$: p < 0.001) at 10 months of age (Fig. 3.41). At any investigated time point, no differences in CoxIV levels were observed in APP/PS1KI$_{ho}$ mice compared to the three other genotypes (Fig. 3.39-3.41).
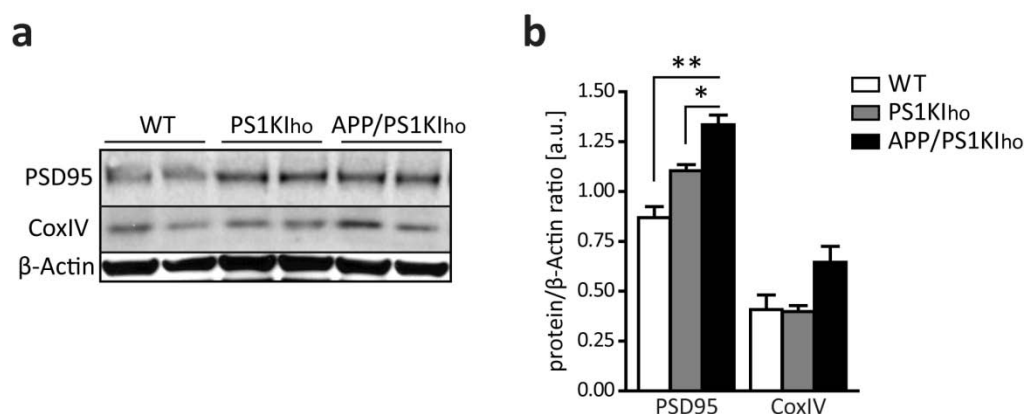
Figure 3.39. (a) Western-blot analysis and quantification (b) of hippocampus lysates of 2-month-old wild-type, PS1KI$_{ho}$ and APP/PS1KI$_{ho}$ using PSD95 and CoxIV antibodies revealed no changes in mitochondrial numbers (CoxIV), but drastically elevated amounts of post-synaptic proteins (PSD95) in APP/PS1KI$_{ho}$. All error bars represent SEM. (n = 3; p < 0.05*, p < 0.01**)

In the P2 crude synaptosomal fractions of APP/PS1KI$_{ho}$ highest amounts of mApoE fragments were detected compared to wild-type, PS1KI$_{ho}$ and APP$_{he}$ mice (see section 3.23). Notably, in this fraction, which contained highest amounts of CoxIV and PSD95, abnormally increased levels of the autophagy substrate LC3-II were detected in APP/PS1KI$_{ho}$ animals using LC3β antibody (Fig 3.40a). This leads to the assumption that autophagosomes accumulate in APP/PS1KI$_{ho}$ mice, especially in synapses, since LC3-II levels were significantly elevated (n = 7 for 6-month-old and n = 3 for 10-month-old mice; p < 0.001) in synaptosomal fractions of these mice compared to wild-type, PS1KI$_{ho}$ and APP$_{he}$ mice at 6 (each n = 3, Fig. 3.40) and 10 months of age (each n = 3, Fig. 3.41).
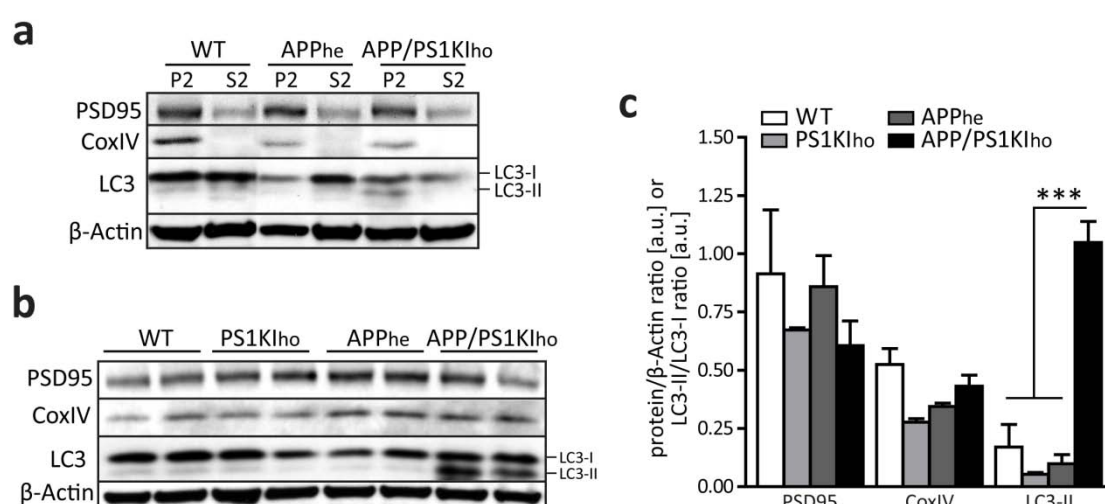
Figure 3.40. (a) P2 fractions of 6-month-old wild-type (WT), APP$_{he}$ and APP/PS1KI$_{ho}$ with elevated PSD95 and CoxIV levels also contained elevated LC3-II (antibody MAP-LC3β) levels in APP/PS1KI$_{ho}$. (b) Immunoblotting and (c) quantification of P2 fractions from wild-type, PS1KI$_{ho}$, APP$_{he}$ (each n = 3) and APP/PS1KI$_{ho}$ (n = 7) revealed significant increased levels of LC3-II in double transgenic mice compared to the other genotypes. No differences regarding PSD95 or CoxIV signals were observed. All error bars represent SEM. (P2: synaptosomal fraction, S2: microsomal fraction; p < 0.001***)
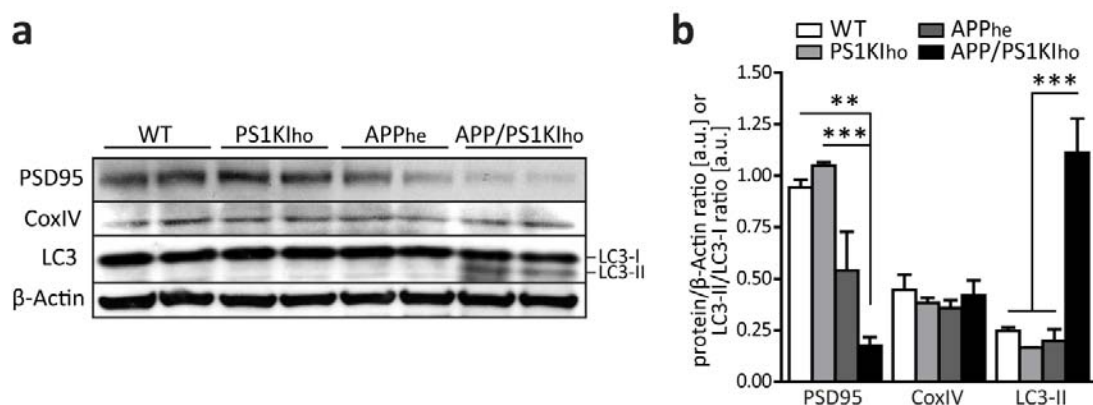
Figure 3.41. (a) Western-blots and quantification (b) of crude synaptosomal fractions (P2) of 10-month-old wild-type (WT), PS1KI$_{ho}$, APP$_{he}$ and APP/PS1KI$_{ho}$ using PSD95, CoxIV and LC3β antibodies revealed no changes in mitochondrial numbers (CoxIV), but drastically decreased amounts of post-synaptic proteins (PSD95) and a strongly increased LC3-II/LC3-I ratio in APP/PS1KI$_{ho}$ mice. All error bars represent SEM. (n = 3; p < 0.01**, p < 0.001***)

In addition, double fluorescent immunostainings using LC3β/G210 (Fig. 3.42d-f, j-l) and anti-human Cathepsin D/IC16 antibodies (Fig. 3.42a-c, g-i) revealed the co-localization of LC3 with intracellular APP and Aβ (Fig. 3.42j-l), as well as the co-occurence of Cathepsin D, which is a crucial component in lysosomal maturation, with intracellular Aβ accumulations (Fig. 3.42g-i) of CA1 hippocampal neurons in a 10-month-old APP/PS1KI$_{ho}$ mouse. Almost no LC3 (Fig. 3.42d-f) and Cathepsin D (Fig. 3.42a-c) were detected in CA1 cells of an APP/PS1KI$_{ho}$ mouse at 2 months of age, whereas Cathepsin D-positive intraneuronal vesicles were equally distributed and morphologically small and uniform (Fig. 3.42a). In contrast, in the 10-month-old APP/PS1KI$_{ho}$ mouse signals of LC3 and Cathepsin D were strongly enhanced and vesicles´ morphology altered into clotted, accumulated structures (Fig. 3.42j and Fig. 3.42g, respectively). Both, Western-blot analyses and immunostaining suggest an impaired autophagy especially in neurites of APP/PS1KI$_{ho}$ mice that is manifested as accumulated lysosomes and autophagosomes.
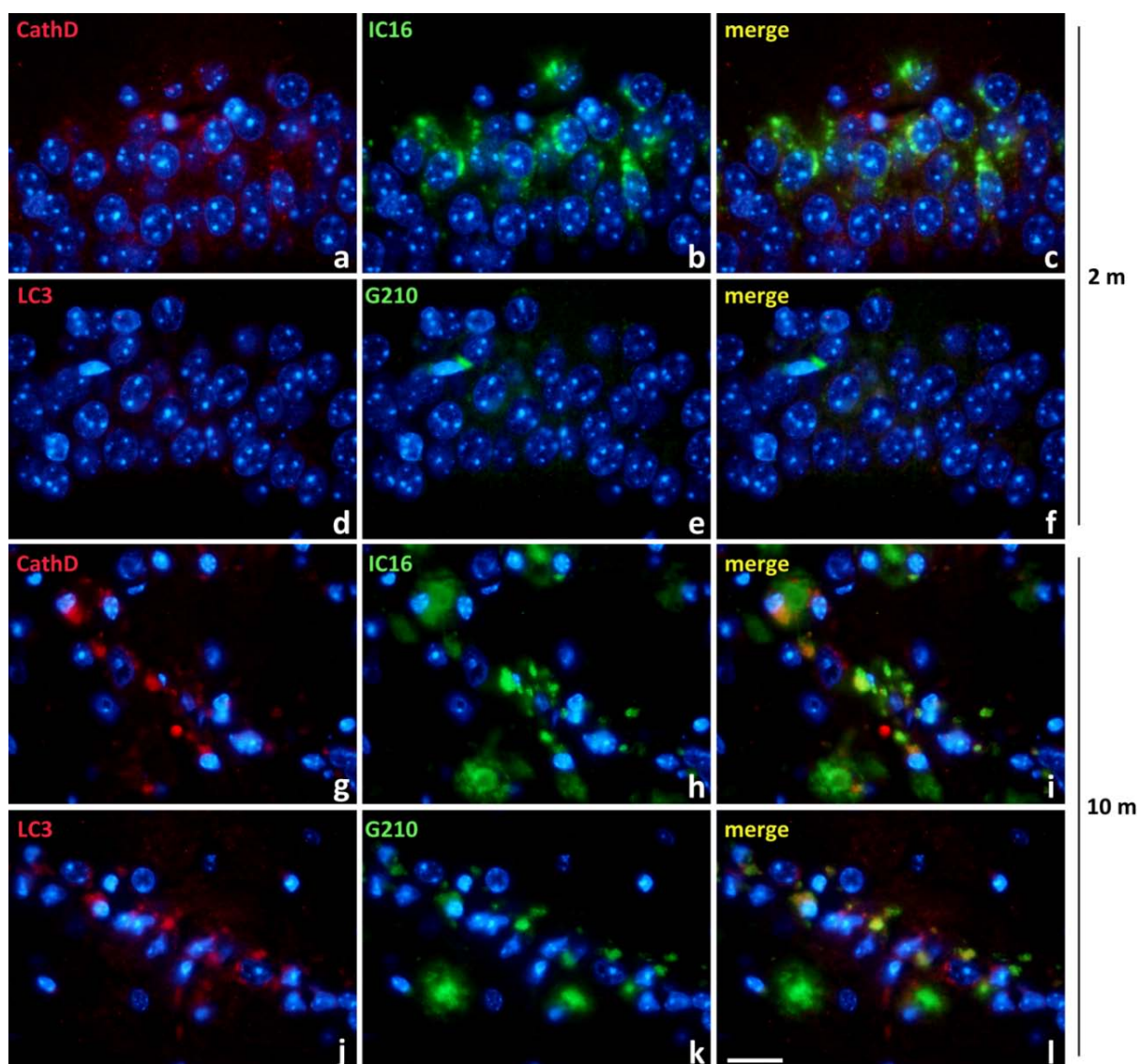
Figure 3.42. Double fluorescent immunostainings of CA1 hippocampal neurons from APP/PS1KI$_{ho}$ mice at 2 (a-f) and 10 months of age (g-l) using antibody combinations anti-human Cathepsin D/IC16 (a-c, g-i) and LC3β/G210 (d-f, j-l). In a 2-month-old mouse Cathepsin D (CathD) vesicles (a) were small shaped and equally distributed that partially co-localized with intraneuronal APP/Aβ (b-c). At the same age, LC3 positive structures (d) were sparsely present in CA1 neurons that also partially contained Aβ peptides (e-f). In contrast, in 10-month-old APP/PS1KI$_{ho}$ CathD- (g) and LC3- (j) vesicles clearly appeared as clotted, accumulated intraneuronal structures that also contained APP/Aβ (h, i) and Aβ (k, l), respectively. Scale bar: 20 μm

3.2.6   AD Pathology and Murine ApoE Proteolysis in 5XFAD Mice over-expressing Human Mutant Tau

In order to examine if proteolyzed mApoE, which showed the same fragmentation pattern as in human AD brains, and hyperphosphorylated tau in concert with Aβ interact in a pathological manner, a novel 5XFAD/PS19 triple transgenic mouse model was generated by crossing PS19 mice over-expressing human mutant tau harboring the P301S mutation with the 5XFAD model co-expressing human mutant APP (APP$_{695}$ with the Swedish, Florida and London mutations) as well as human mutant PS1 (PS1$_{M146L,L286V}$).

3.2.6.1   Co-Expression of Tau and Aβ accelerates Tau but not Aβ Pathology

To investigate if tau expression influences amyloid pathology, sagittal brain sections (Bregma 1.08 – 1.32, n = 3 for each genotype using means of 4 sections per animal) of 3- and 9-month-old 5XFAD and 5XFAD/PS19 mice were stained with 24311 antibody detecting a variety of different Aβ peptide isoforms (Fig. 3.43). Quantification of the plaque load revealed a tendency towards a reduced plaque pathology in the hippocampus of 3- (Fig. 3.43a, b, e) and 9-month-old 5XFAD/PS19 mice (Fig.3.43c-e) compared to their 5XFAD littermates, which did not reach statistical significance (p > 0.05).
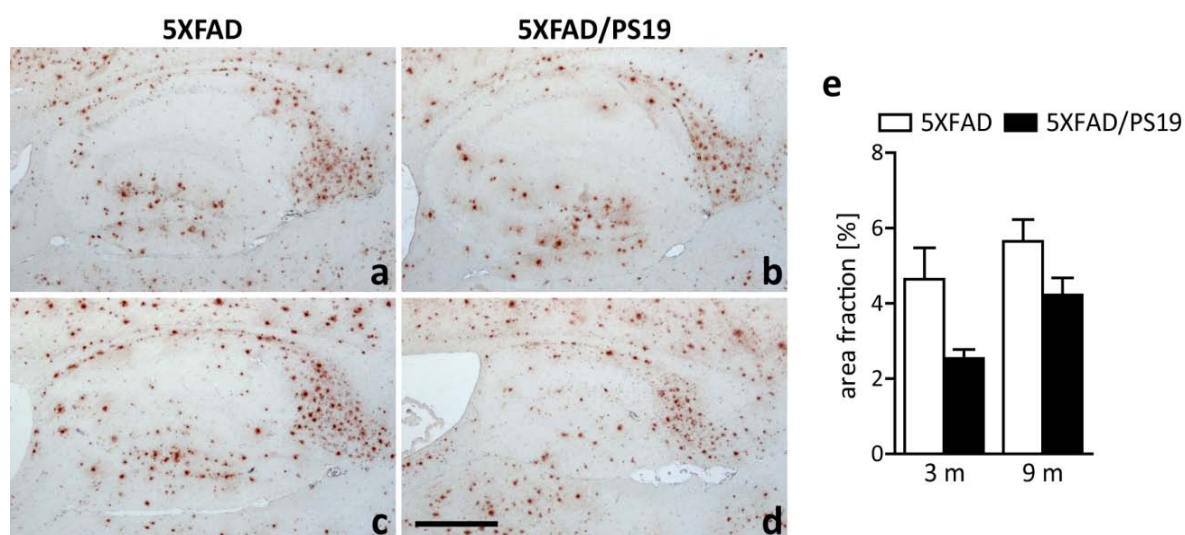
Figure 3.43. Immunostaining and plaque load quantification in the hippocampus of 3- (a-b, e) and 9-month-old (c-e) 5XFAD and 5XFAD/PS19 mice using the Aβ-detecting antibody 24311. There were no significant changes (p > 0.05, each n = 3) in amyloid load comparing 5XFAD and 5XFAD/PS19 mice at 3 and 9 months of age. All error bars represent SEM. Scale bar: 200 µm

To assess if Aβ, which is highly produced in the 5XFAD mouse model by over-expression of mutant APP and PS1, influences pathological tau aggregation in a downstream event in PS19 mice, immunohistochemical analyses were performed on brains of 3- and 9-month-old PS19 and 5XFAD/PS19 animals (each n = 3) using AT8 antibody (Fig. 3.44) recognizing phosphorylated tau epitopes (pS202/T205) and the tau conformation-specific antibody MC-1 detecting PHF-like structures. AT8-immunohistochemistry revealed that some neurons and their processes including both dendrites and axons in the hippocampal CA1 region of 3-month-old 5XFAD/PS19 mice contain high amounts of phosphorylated tau (Fig. 3.44f), whereas PS19 littermates were negative at this age (Fig. 3.44e), resulting in a significantly enhanced overall immunoreactivity in this brain region (p < 0.05, Fig. 3.44q). Interestingly, the initial faint AT8-immunostaining of the mossy fibers in the hippocampal CA3 region of both 3-month-old PS19 (Fig. 3.44a) and 5XFAD/PS19 mice (Fig. 3.44b) was more prominent in aged PS19 animals (Fig. 3.44c), but disappeared almost completely in 5XFAD/PS19 littermates at 9 months of age (Fig. 3.44d). In young 5XFAD/PS19 mice, single cortical neurons were detected by AT8-staining (Fig. 3.44n), whereas in comparison with aged-matched single transgenic PS19 mice no significant differences were observed in total immunoreactivity in this brain region (p > 0.05; Fig. 3.44m, q). However, abundant AT8-immunostaining was detected in hippocampal CA1 (Fig. 3.44h) and CA3 perikarya (Fig. 3.44l) as well as in cortical neurons (Fig. 3.44p) in aged 9-month-old 5XFAD/PS19 mice. Although AT8-positive neuronal processes disappeared in older 5XFAD/PS19 animals (Fig. 3.44f, h), immunoreactivity was significantly enhanced compared to PS19 littermates in the investigated brain regions (CA1: p < 0.001, CA3: p < 0.01, cortex: p < 0.001; Fig. 3.44g, k, o, q, respectively).

Similar results were obtained using the conformation-specific MC1 antibody detecting PHF-like aggregates (not shown). Interestingly, only cortical neurons in 9-month-old 5XFAD/PS19 animals showed MC1-immunoreactivity that was absent in age-matched single transgenic PS19 mice.
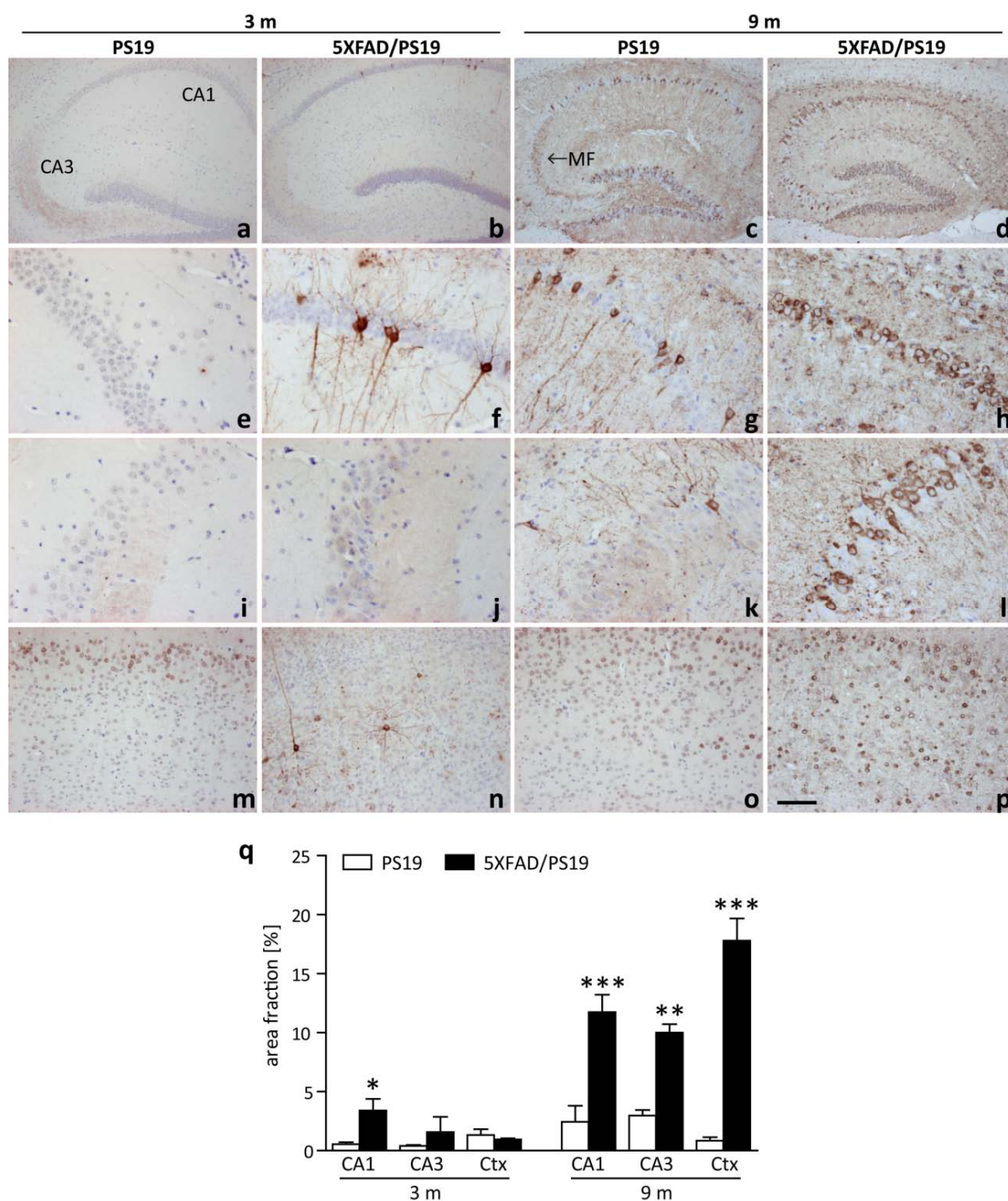
Figure 3.44. 5XFAD/PS19 mice harbored significantly enhanced tau phosphorylation (q, each genotype n = 3) in the entire hippocampus (a-l) and cortical regions (m-p) compared to age-matched PS19 mice using AT8-immunostaining. Single AT8-positive neurons were detected in CA1 (f) and cortical neurons (n) of 3-month-old 5XFAD/PS19, whereas PS19 littermates were consistently negative (e, m, respectively). At 9 months of age, 5XFAD/PS19 mice showed significantly more AT8-immunoreactivity in CA1 (h) and CA3 (l) hippocampal as well as cortical neurons (p) than age-matched PS19 animals (g, k, o, respectively). SEM is given as error bars. Scale bar: (a-d) 200 µm, (e-l) 50 µm, (m-p) 100 µm (Ctx: cortex, MF: mossy fibers; p < 0.05*, p < 0.01**, p < 0.001***)

3.2.6.2 Loss of Dendrites, Synapses and Neurons in the Hippocampus of 5XFAD/PS19 Mice

To investigate if the enhanced tau pathology observed in 5XFAD/PS19 mice leads to a loss of neuronal integrity by inducing dendritic and synaptic diminishment, stainings were performed on hippocampi of 5XFAD, PS19 and 5XFAD/PS19 mice (Bregma 1.08 – 1.32, n = 3 for each genotype using means of 4 sections per animal) using an antibody against β3-tubulin (Fig. 3.45a-f) as well as several synaptic markers like synapsin-1 (Fig. 3.45g-l), synaptobrevin and synaptoporin (both not shown). Immunostaining using β3-tubulin antibody revealed a drastic reduction of apical dendrites in the hippocampal stratum radiatum, which mainly contains apical dendrites, in 5XFAD/PS19 mice at 9 months of age (Fig. 3.45c, f) compared to their age-matched PS19 (Fig. 3.45a, d) and 5XFAD littermates (Fig. 3.45b, e). The mossy fiber tract forms the major input from the gyrus dentatus to CA3 pyramidal cells. Synapsin-1-immunostaining revealed an aggregated appearance of synapses and a drastic loss of synaptic integrity of the mossy fibers in the stratum lucidum of hippocampal CA3 neurons in 9-month-old PS19 mice (Fig. 3.45g, j) compared to age-matched 5XFAD animals (p < 0.05; Fig. 3.45h, k, p). This pattern was further exacerbated in triple transgenic 5XFAD/PS19 mice (significances relating to 5XFAD: p < 0.01 and PS19: p < 0.05; Fig. 3.45i, l, p). These findings were confirmed by immunostainings using antibodies against synaptobrevin and synaptoporin (not shown), which quantitatively resulted in the same observations.

Furthermore, macroscopic analysis of hippocampi from 5XFAD/PS19 animals revealed a marked atrophy compared to age-matched PS19 and 5XFAD littermates at 9 months of age (e.g. Fig. 3.45a-c and g-l, respectively). Due to this observation and together with the drastic loss of neuronal processes in aged triple transgenic 5XFAD/PS19 mice, a potential loss of neurons was examined by quantification of hematoxylin-stained neuronal nuclei in a defined area of the hippocampal CA1 region in 3- and 9-month-old 5XFAD, PS19 and 5XFAD/PS19 mice (Bregma 1.08 – 1.32, n = 3 for each genotype using means of 4 sections per animal; Fig. 3.45m-o, q). It has been previously reported that 5XFAD mice have harbor neuron loss in the cortex, but not in the hippocampal CA1 region at 12 months of age (Jawhar et al. 2012). Compared to this model, PS19 mice showed a tendency towards less CA1 neurons with approximately 17 % at the age of 9 months (p = 0.055, Fig. 3.45m-n, q, respectively). In contrast, 9-month-old triple transgenic 5XFAD/PS19 mice (Fig. 3.45o, q) only

harbored a fractional amount of CA1 neurons compared to PS19 and 5XFAD littermates that reached high statistical significances (both p < 0.001).
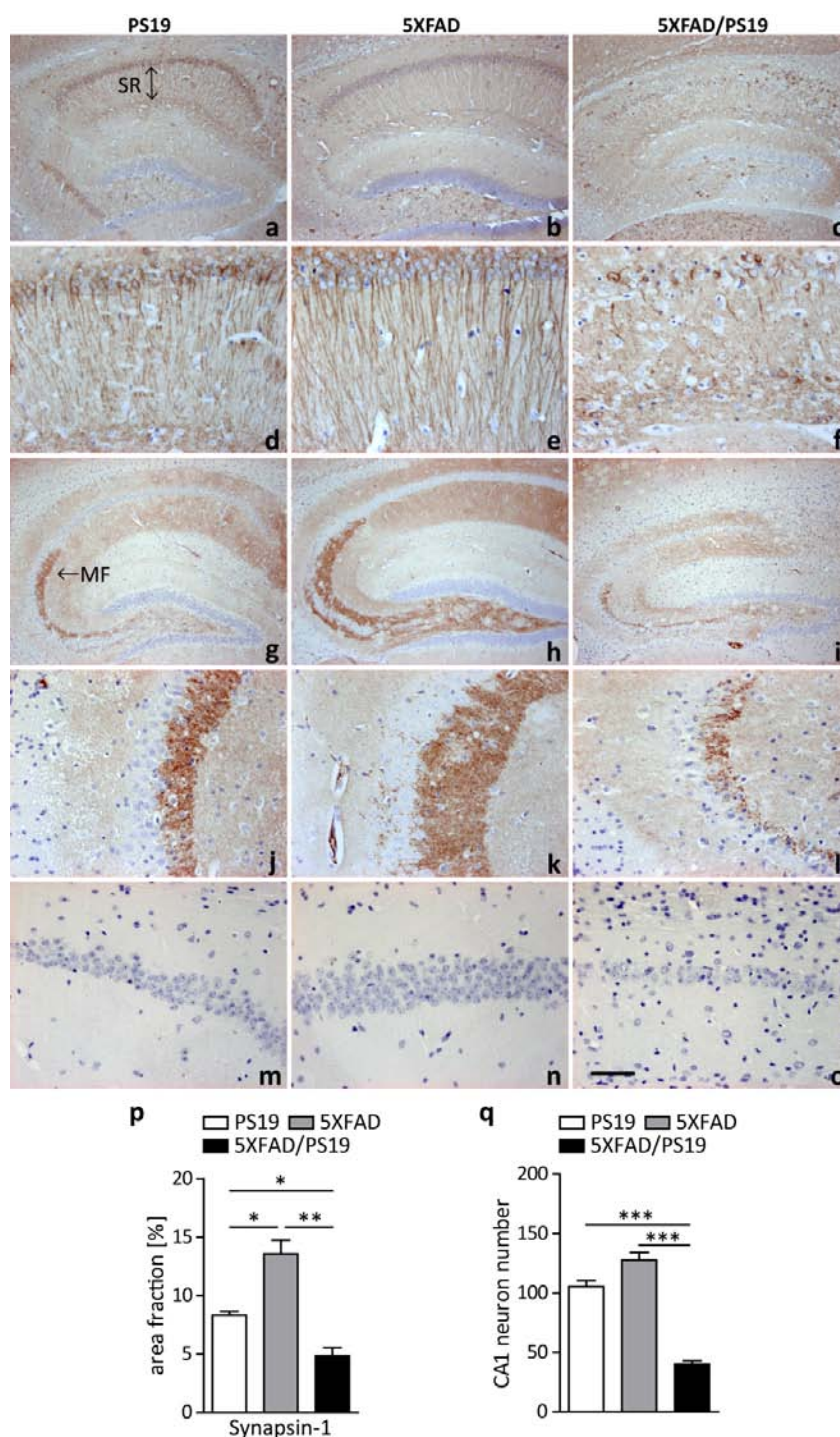
Figure 3.45. (a-f) Immunostaining using anti-β3-tubulin showed no disintegration of apical dendrites of hippocampal CA1 neurons in the stratum radiatum (SR) of 9-month-old PS19 (a, d) and 5XFAD mice (b, e), whereas these neuronal processes were highly affected in aged-matched 5XFAD/PS19 animals (c, f). (g-l) Synapsin-1 staining revealed a significant loss and a pathological aggregation pattern of mossy fibers (MF) in the stratum lucidum of hippocampal CA3 neurons in 9-month-old PS19 (g, j, p) compared to aged-matched 5XFAD mice (h, k, p), which was significantly aggravated in 5XFAD/PS19 animals (i, l, p). (m-o, q) Quantification of hematoxylin-stained CA1 neurons demonstrated a significant diminishment in 5XFAD/PS19 mice at 9 months of age (o, q) compared to PS19 (m, q) and 5XFAD littermates (n, q), whereas PS19 mice also showed a tendency towards CA1 neuron loss. All error bars show SEM. Scale bar (a-c, g-i) 200 μm, (d-f, j-o) 50 μm (p < 0.05*, p < 0.01**, p < 0.001***)

3.2.6.3 Increased Astrocytosis in Aged 5XFAD/PS19 Mice

So far, it could be shown that co-expression of Aβ in PS19 mice results in aggravation of tau pathology, disintegration of neuronal processes, neuron loss and hippocampal atrophy, which are major hallmarks of AD. In order to examine if 5XFAD/PS19 mice also show chronic inflammation, immunostaining was performed on 3- and 9-month-old PS19, 5XFAD and 5XFAD/PS19 mice using an antibody against GFAP labeling activated astrocytes (Bregma 1.08 – 1.32, n = 3 for each genotype at both time-points using means of 4 sections per animal; Fig. 3.46). At 3 months of age no differences (p > 0.05) regarding astrocytosis were detected in hippocampi of PS19 (Fig. 3.46a, d), 5XFAD (Fig. 3.46b, d) and 5XFAD/PS19 mice (Fig. 3.46c, d). However, significantly increased GFAP-covered areas were observed at this young age in cortices of 5XFAD/PS19 mice compared to the other genotypes (significances: PS19 – 5XFAD/PS19 p < 0.01 and 5XFAD – 5XFAD/PS19 p < 0.05; Fig. 3.46d) as well as increased GFAP-staining in thalami of 5XFAD/PS19 mice compared to PS19 littermates (PS19 – 5XFAD/PS19 p < 0.01; Fig. 3.46d). The amount of activated astrocytes was strongly elevated in 5XFAD/PS19 mice at 9 months of age (Fig. 3.46g, h), in which GFAP-immunoreactivity was strongly enhanced in the hippocampus (significances relating to PS19: p < 0.001 and 5XFAD: p < 0.01), cortex (significances relating to PS19: p < 0.001 and 5XFAD: p < 0.01) and thalamus (significances relating to PS19: p < 0.001 and 5XFAD: p < 0.05) compared to age-matched PS19 (Fig. 3.46e, h) and 5XFAD mice (Fig. 3.46f, h). Notably, 5XFAD mice also showed significantly increased GFAP-immunostaining in the cortex and thalamus compared to PS19 littermates (p < 0.001 and p < 0.05, respectively; Fig. 3.46h), whereas no differences were observed in the hippocampus.
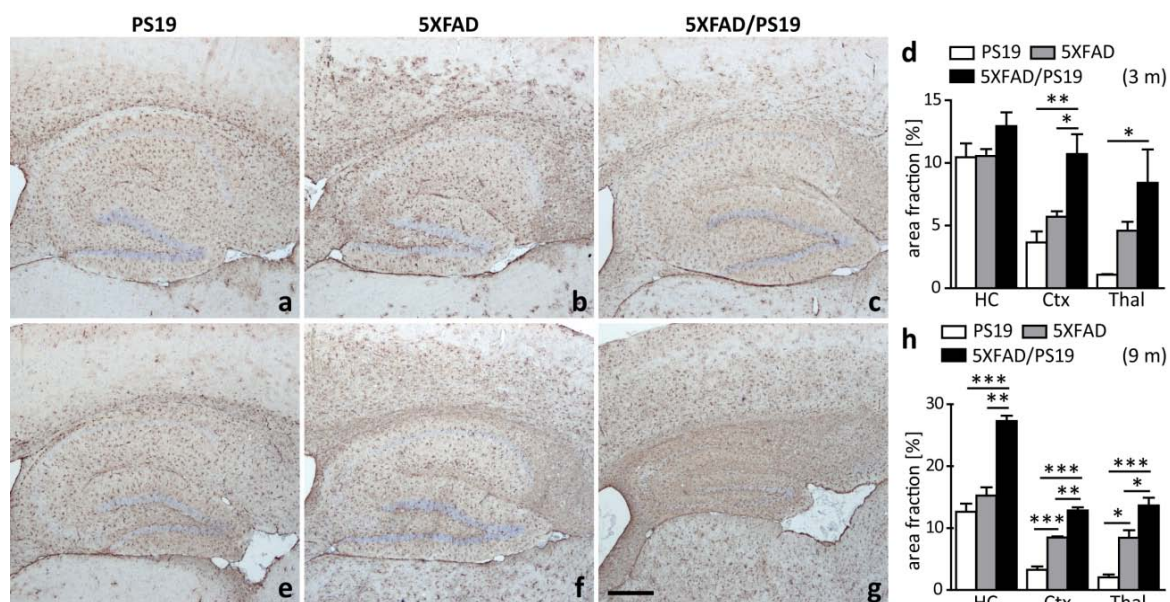
Figure 3.46. Immunohistochemistry of 3- and 9-month-old PS19, 5XFAD and 5XFAD/PS19 mice using a GFAP antibody labeling activated astrocytes. (a-d) All three genotypes did not differ in GFAP-immunoreactivity of the hippocampus (HC) at 3 months of age, whereas 5XFAD/PS19 mice harbored a significantly elevated inflammatory response in the cortex (Ctx) and thalamus (Thal) compared to PS19 and 5XFAD littermates. (e-h) 9-month-old 5XFAD/PS19 showed significantly increased GFAP-staining in all analyzed brain regions compared to age-matched PS19 and 5XFAD mice. All error bars represent SEM. Scale bar: 500 µm (p < 0.05*, p < 0.01**, p < 0.001***)

3.2.6.4 Biochemical Analyses of ApoE Fragmentation and Tau/Aβ Pathology in PS19, 5XFAD and 5XFAD/PS19 Mice

Western-blot analyses of whole brain lysates (n = 3 for each genotype and age) using antibodies against phosphorylated and aggregated tau like CP13 and MC-1 as well as IC16 antibody detecting APP and its proteolytic metabolites confirmed the immunohistochemical findings (Fig. 3.47a-b). No differences were observed regarding APP, C99 and Aβ levels using IC16 antibody in 5XFAD and 5XFAD/PS19 mice at 3 (not shown) and 9 months of age (Fig. 3.47a, d). CP13- and MC1-levels were also not altered in young PS19 and 5XFAD/PS19 mice (not shown). However, at 9 months of age triple transgenic 5XFAD/PS19 animals showed more than threefold elevated amounts of phosphorylated tau using both CP13 and MC1 antibodies compared to their single transgenic PS19 counterparts (both p < 0.01, Fig. 3.47b, d).

As described in section 3.2.2, 5XFAD mice harbor an age-dependent accumulation of approximately 10 to 15, 25 and 29 kDa ApoE fragments with simultaneously increased full-length ApoE levels at 34 kDa that was already seen in 6-month-old animals. In order to examine if the fragmentation of mApoE linked to Aβ pathology is an upstream or

downstream event regarding tau pathology, Western-blot analysis was performed on female PS19, 5XFAD and 5XFAD/PS19 mice at 7 months of age (n = 3 for each genotype) using M-20 antibody detecting mApoE (Fig. 3.47c-d). In this approach, PS19 mice expressing human mutant tau showed no evidence for ApoE fragmentation, since only a faint full-length ApoE band at 34 kDa was detected. In contrast, levels of total endogenous mApoE were strongly increased in both 5XFAD (p < 0.05) and 5XFAD/PS19 mice (p < 0.01) compared to PS19 littermates with a drastic fragmentation pattern that was indistinguishable between 5XFAD mice harboring endogenous tau and 5XFAD mice over-expressing human mutant tau (p > 0.05).
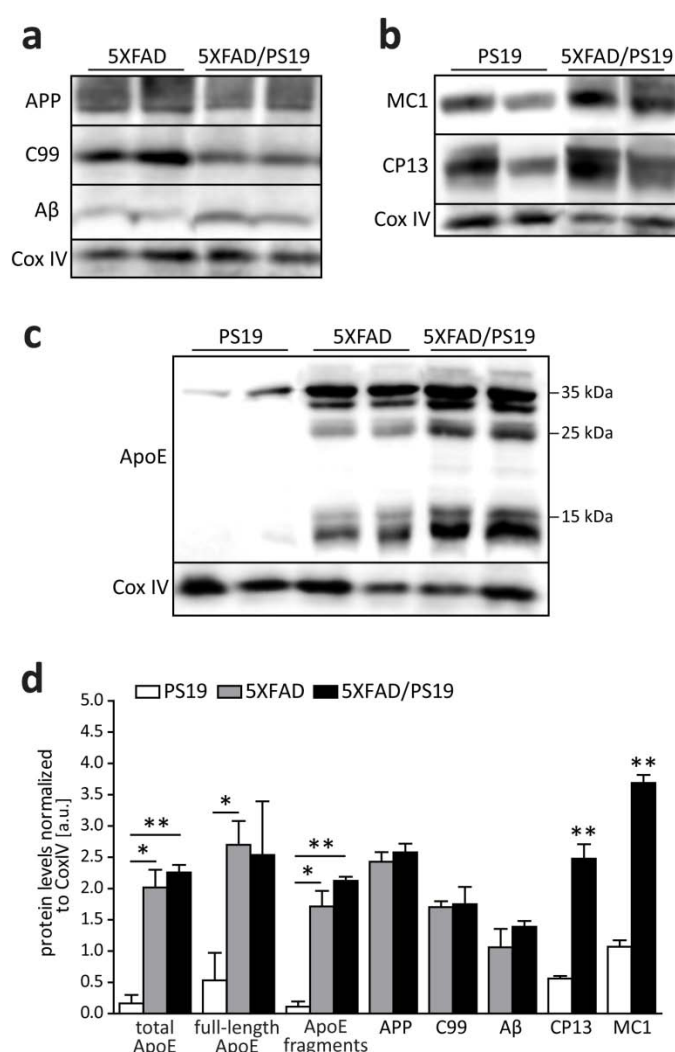
Figure 3.47. (a) Western-blot analysis using IC16 antibody revealed no alterations in APP, C99 or Aβ levels in brains of 9-month-old 5XFAD/PS19 compared to aged-matched 5XFAD littermates. (b) Both, CP13- and MC1-immunoreactivity were significantly enhanced in 5XFAD/PS19 compared to PS19 mice at 9 months of age. (c) Immunoblot using M-20 antibody detecting endogenous mApoE showed drastically enhanced total and full-length ApoE levels in 5XFAD and 5XFAD/PS19 compared to PS19 mice at 7 months of age. Whereas PS19 data did not provide any indication for ApoE processing, high amounts of fragmentized ApoE at 10-15, 25 and 29 kDa were present in 5XFAD and 5XFAD/PS19 mice that were indistinguishable from each other. (d) Quantification of relative protein amounts normalized to CoxIV-levels. All error bars show SEM. (p < 0.05*, p < 0.01**)

4 Discussion

4.1 Project I: Investigations of Pyroglutamate-modified Amyloid Peptides in Familial British and Danish Dementias

FBD and FDD show striking neuropathological similarities to AD: I. highly aggregated amyloid deposits in parenchyma; II. cerebral amyloid angiopathy; III. hyperphosphorylated tau deposits with the formation of neurofibrillary tangles; and IV. amyloid associated neuroinflammation reflected as astro- and microgliosis. In AD, the post-translational pGlu-modification of Aβ plays an important role in plaque deposition, since pGlu-Aβ is considered as one of the most toxic forms especially due to its high aggregation propensity and represents a main portion of amyloid deposits (Harigaya et al. 2000, Russo et al. 2002). It has been found that a major part of ABri and ADan peptides deposited in brains of patients with FBD and FDD, respectively, are also equipped with a post-translational pGlu-modification (Ghiso et al. 2006). Due to these similar pathological lesions, there is support for a unifying pathological mechanism, in which accumulation of amyloidogenic peptides trigger a complex pathological cascade leading to neurodegeneration. Therefore, the primary objective of the present project was to generate novel antibodies detecting pGlu-ABri/ADan to characterize their presence and distribution pattern in brains of FBD/FDD patients as well as in an established transgenic mouse model for FDD. So far, the effect of pGlu-modified ADan peptides has been not considered in FDD transgenic mice. Therefore, a novel mouse model was generated and initially characterized that exclusively expresses ADan1Q-34.

4.1.1 Abundant pGlu-modified ABri and ADan Peptides in Human Familial British and Danish Dementia Brains

In course of this thesis, two novel N-terminal specific antibodies (AB76-2 and AB77) were generated that detect pGlu-modified CTF23, ABri and ADan peptides, underlying the furin-mediated cleavage of wild-type or mutant BRI2, respectively. Thereby, AB76-2 showed a

strong specificity for pGlu-modified species as estimated by dot- and Western-blotting (Fig. 3.4). Using these antibodies, it could be shown that a large number of extracellular amyloid deposits and blood vessels in FBD and FDD brains exhibits substantial amounts of pGlu-modified ABri and ADan peptides, respectively (Fig. 3.6). That pGlu-modified ABri and ADan peptides are present in patients with FBD and FDD, respectively, has been previously demonstrated in brain tissue and vessels using mass spectrometry (Tomidokoro et al. 2005, Ghiso et al. 2006). These analyses revealed that approximately 60 % of the peptides carry the pGlu-modification (Ghiso et al. 2006). Furthermore, it has been shown that pGlu-ABri peptides are deposited in systemic organs like pancreas, skeletal muscle or uterus in patients suffering from FBD providing this peptide species as an interesting diagnostic tool (Tomidokoro et al. 2010).

In mammals, N-terminally located pGlu-residues are widespread in a variety of neuronal secretory peptides and hormones, including thyrotropin- and gonadotropin-releasing hormones, gastrin as well as neurotransmitters like neurotensin (Sykes et al. 1999). Unmasking of glutaminyl residues is usually achieved by pro-hormone convertase mediated endoproteolytic processing (Steiner 1998). The conversion of an L-glutaminyl-peptide into an N-terminal 5-oxoprolyl-peptide and NH_3 is catalyzed by the enzyme glutaminyl cyclase (QC) (Busby et al. 1987) and causes the bioactive structure of hormones as well as enhances their stability towards N-terminal proteolysis (Fischer and Spiess 1987). Thereby, QC mediated pGlu-conversion predominantly takes place in the acidic milieu of secretory compartments like the Golgi apparatus (Cynis et al. 2008). In AD, the formation of pGlu-Aβ is a well-known post-translational modification (Jawhar et al. 2011a) with $Aβ_{pGlu3-42}$ representing a dominant fraction of Aβ peptides in senile plaques from AD patients (Saido et al. 1995, Tabaton and Piccini 2005). It has been recently shown that 5XFAD mice over-expressing human QC harbored enhanced pGlu-Aβ amounts, which further aggravated their behavioral deficits, whereas a knock-out of QC rescued the behavioral phenotype in these mice (Jawhar et al. 2011b). Furthermore, oral application of the QC inhibitor PBD150 led to reduced pGlu-Aβ levels in Tg2576 and TASD-41 transgenic mouse models for AD expressing APP_{Sw} and APP_{SwLon}, respectively, as well as in the fruit fly *Drosophila melanogaster* harboring neuron-specific $Aβ_{3Q-42}$ expression (Schilling et al. 2008).

All of these studies indicate an enhanced pathological role of pGlu-modified Aβ in AD and together with the abundant presence of pGlu-modified ABri and ADan deposits detected

with AB76-2 and AB77 antibodies in brains of patients with FBD and FDD, respectively, support that pGlu-modified amyloidogenic peptides may reflect a general pathological feature in neurodegenerative diseases.

4.1.2 Post-translational pGlu-modification of ABri/ADan Peptides is putatively involved in Amyloid Seeding and Plaque Maturation in FBD/FDD

It is currently discussed if Aβ, especially Aβ$_{42}$, possibly harbors "prion"-like characteristics that accelerate amyloid formation in AD brains. Several studies support this hypothesis, since synthetic peptides and brain extracts from human AD brains as well as aged AD mouse models were able to induce Aβ-mediated plaque deposition, even in mice that normally develop no plaque pathology (Meyer-Luehmann et al. 2006, Morales et al. 2011, Watts et al. 2011). Interestingly, pGlu-modified Aβ species were highly capable in transmission of their toxicity to non-modified Aβ$_{1-42}$, since just about 5 % of Aβ$_{pGlu3-42}$ mixed with Aβ$_{1-42}$ led to a 50 % reduced number of mouse neuronal cells *in vitro* (Nussbaum et al. 2012). Immunostaining of ADanPP7 brain tissue using AB76-2 and AB77 revealed an age-dependent spreading of pGlu-modified and non-modified ADan deposits, starting in the hippocampal stratum lacunosum moleculare and the frontal cortex already at 2 months of age, that was strongly increased involving the entire brain in older animals (Fig. 3.9). Therefore, it can be hypothesized that even pGlu-modified non-Aβ amyloids, like ADan, may also have this "prion"-like spreading feature that would further reflect a striking similarity between FDD and AD.

Vascular and parenchymal pGlu-modified ADan and ABri deposits were largely co-localized with Thio-S staining in brains of ADanPP7 mice as well as FDD and FBD patients, respectively, suggesting a highly aggregated status of these peptides (Fig. 3.7, 3.8 and 3.13, respectively). Interestingly, some deposits were only labeled with AB77 and lacked both AB76-2 and Thio-S staining in ADanPP7 mice (Fig. 3.13). Moreover, highly aggregated pGlu-modified ABri and ADan peptides in plaque cores and central vascular deposits in brains of FBD and FDD patients, respectively, were also positive for AB76-2 and Thio-S staining, which was absent in the periphery of AB77-immunoreactive deposits. These results are suggestive for a sequential maturation process of amyloid plaques leading to the assumption that N-terminally modified ABri and ADan peptides probably behave like pGlu-Aβ, meaning a role in

plaque maturation or seeding. This could be explained by the observation that unmodified ADan is deposited first (Fig. 3.9) and it can be assumed that ADan undergoes a conversion to pGlu-ADan over time in the ADanPP7 mouse model. Nevertheless, it was shown by Western-blotting that AB76-2 also cross-reacts with non-modified ABri (and to a lesser extent ADan) peptides (Fig. 3.4). Therefore, it cannot be completely ruled out whether AB76-2 immunoreactivity of plaque cores is caused by high concentrations of non-modified peptides instead of the detection of pGlu-modified peptides. Comparative analyses were also more complicated due to the different antibody affinities. However, it has been demonstrated that pGlu-Aβ containing plaques increase continuously with age in APP/PS1KI mice, whereas the amounts of non-truncated Aβ deposits beginning with an aspartate at amino acid one simultaneously decreases (Wirths et al. 2010a). This confirms a sequential maturation process in ABri or ADan plaques. Human AD brains between Braak stages IV-VI also carried approximately 20 % elevated pGlu-modified Aβ levels in cored plaques, whereas diffuse plaques harbored consistently low levels (Guntert et al. 2006). Therefore, it is currently hypothesized that N-truncated and pGlu-modified Aβ drives plaque maturation or is involved in seeding plaque formation. Compared to the findings in this study, plaque-maturating properties of pGlu-modified amyloid peptides would further reflect a basic characteristic pathological feature shared by AD as well as FBD and FDD.

4.1.3 Enhanced Aggregation Propensity of N-terminally modified ABri, ADan and CTF23 Peptides

The pGlu-modification of Aβ provides an enhanced aggregation propensity (He and Barrow 1999, Schilling et al. 2006) and an increased stability towards proteolytic degradation (Kuo et al. 1998). At pH 4.0, where ABri and ADan peptides are well soluble, N-terminally located pGlu-modifications of these peptides also resulted in strongly enhanced aggregation profiles (Schlenzig et al. 2009). In the current thesis, pGlu-modified ABri also harbored enhanced aggregation kinetics at physiological pH 7.0 with a much more rapid formation of intermediate oligomers and fibrils (Fig. 3.1a), which partially confirms earlier reports from Schlenzig et al. These observations were further corroborated by Western-blot data (Fig. 3.4), in which both freshly dissolved synthetic pGlu-modified ABri and ADan exhibited an increased tendency to form higher molecular weight aggregates exceeding the aggregation propensity of their non-modified counterparts. It has been shown that ABri peptides rapidly

form oligomeric species *in vitro* (El-Agnaf et al. 2001), whereas no such oligomerization was observed with the wild-type peptide CTF23, suggesting that C-terminal extension, which mediates an increased hydrophobicity, plays an important role in oligomerization and the formation of fibrils. Furthermore, formation of a single intramolecular disulfide bridge, which is crucial for sorting of pro-proteins and neuropeptides from the *trans*-Golgi network into a regulated secretory pathway (Choi et al. 2004), harbors also an important impact on ABri oligomerization as treatment with dithiothreitol (DTT) led to a disappearance of ABri aggregates (El-Agnaf et al. 2001). Interestingly, ThT assays revealed almost no aggregation behavior of unmodified CTF23 supporting its non-amyloidogenic characteristics as a signaling peptide, which probably promotes neurite outgrowth (Choi et al. 2004). In contrast, the pGlu-modified counterpart immediately started to form oligomeric assemblies (Fig. 3.1c), indicating that the pGlu-modification has a drastic influence on the biochemical characteristics of CTF23 by possibly making it more hydrophobic. That the formation of a N-terminal lactam ring strongly increases the hydrophobicity has been already shown for Aβ (He and Barrow 1999). This suggests that the pGlu-modification not only enhances the aggregation propensity of amyloidogenic peptides, but also converts a non-aggregating peptide, like CTF23, into an amyloidogenic species, whereas the aggregation peak is putatively limited by the shorter C-terminus compared to ABri.

4.1.4 Different Impacts on Cell Viability of pGlu-modified ABri, ADan and CTF23 Peptides

Former studies have been shown that N-truncated and pGlu-modified Aβ peptides induce apoptosis and necrosis, and exhibit an increased toxicity compared to full-length Aβ in cell-based assays (Russo et al. 2002, Acero et al. 2009). The application of pGlu-modified ABri and ADan peptides and the expression of the ABri1Q-34 transgene also led to a higher cytotoxicity in SH-SY5Y and a reduced cell growth in Hek293 cells, respectively (Fig. 3.2). This suggests that the post-translational pGlu-modification represents a general mechanism to promote toxicity of amyloid peptides. Interestingly, non-modified and to a lesser extent pGlu-modified wild-type CTF23 had the opposite effect in terms of strongly increased cell viability reflected in enhanced cell growth and reduced LDH-release in multiple human cell lines (Fig. 3.3). This could be an indicator for hypothetical functions of low molecular weight CTF23 as a transcription factor, anti-oxidant or as an intra- or intercellular signaling peptide,

since it has been shown that CTF23 enters the Golgi network and gets secreted via vesicles (Choi et al. 2004). Notably, it seemed that the CTF23 mediated effect occurred in a cell specific manner. CTF23 application had no influence on oligodendroglioma cells, but mostly improved neuroblastoma viability that possibly indicates the existence of specific receptors, especially in neuronal cells. That CTF23 is axonally transported was further confirmed by the identification of AB77-positive structures in AD and non-demented control brains as well as in brains of AD mouse models and controls (Fig. 3.15 and 3.16). Importantly, it seemed that both human and murine CTF23 gets redistributed from an equally intraperikaryal and axonal distribution pattern in controls to an accumulated pattern in dystrophic neurites, axon hillocks and extracellular plaques surrounded by activated astrocytes under AD pathological conditions. This suggests that the axonally transported CTF23 probably failed to reach its target compartments, leading to further disequilibrium of cell homeostasis in brains affected by AD.

4.1.5   ADan Peptides accumulate in Synapses of an Established Mouse Model for Familial Danish Dementia

In the present study, it has been shown that ADan peptides broadly co-localize intracellularly with synaptophysin and to a lesser extent with MAP2 in the hippocampus of ADanPP7 mice (Fig. 3.14). This suggests that ADan mainly accumulates in pre-synaptic terminals and further supports that C-terminal BRI2 fragments, generated after furin cleavage, are axonally transported. This observation is confirmed by *in vitro* analyses, in which ABri peptides were detected both intracellularly and in the medium, whereas ADan peptides accumulated predominantly in intracellular compartments (Kim et al. 2002). However, both amyloid peptides were secreted to a much lesser extent than the short wild-type CTF23. This is putatively associated with the elongated C-termini of ABri and ADan and, hence, linked to their increased aggregation propensity. Intracellular aggregated ADan peptides in synaptic terminals may impair synaptic transmission, causing neuronal damage and neurodegeneration, resulting in cognitive decline in FDD. This mechanism is comparable to AD. There is accumulating evidence revealing that soluble oligomeric species, especially soluble $A\beta_{42}$, but not plaque-associated $A\beta$ assemblies correlate best with the cognitive dysfunction in AD (Mclean et al. 1999, Benilova et al. 2012). These $A\beta$ oligomers are preferentially formed intracellularly within neuronal processes and synapses rather than

extracellularly (Takahashi et al. 2004, Walsh et al. 2000). Furthermore, intraneuronal Aβ rather than extracellular plaque pathology correlates with neuron loss in the hippocampus (Casas et al. 2004), frontal cortex (Christensen et al. 2008) and cholinergic system (Christensen et al. 2010a) of APP/PS1KI transgenic mice for AD.

4.1.6 Generation and Initial Characterization of a Novel Mouse Model for Familial Danish Dementia

Despite a couple of research efforts, pathophysiological changes of FBD and FDD could not be replicated in animal models in a satisfactory manner. A mouse model expressing the mutant British form of BRI2 under the control of the prion-protein promoter showed BRI2 accumulation in neurons, but it was only detected in membranes in close proximity to the nucleus instead of endosomal vesicles (Pickford et al. 2006). This suggests that the protein is localized in the endoplasmatic reticulum and Golgi apparatus lacking any secretion, whereupon no ABri peptides were found in this model. Therefore, it was supposed that the BRI2 processing by murine, endogenous furin is not sufficient for the generation of high amounts of amyloidogenic ABri. However, adenovirus-mediated over-expression of furin still could not achieve traceable amounts of ABri peptides (Pickford et al. 2006). Another transgenic model expressing the Danish mutant form of BRI2 under the control of the murine prion-protein promoter generated small amounts of ADan peptides in the brain and vessel walls. But besides a mild motor phenotype in old animals, no further behavioral deficits were described (Vidal et al. 2009). The same holds true for ADanPP7 mice, which were used in this thesis for the characterization of the novel generated pGlu-ADan detecting antibodies AB77 and AB76-2. Although these mice exhibit age-dependent ADan deposition throughout the brain with associated amyloid angiopathy, increased anxiety and memory impairment initially occurred in 18- to 20-month-old mice (Coomaraswamy et al. 2010). Due to low levels of produced amyloids in most models for FBD and FDD and the non-considered aspect of pGlu-modified ABri and ADan peptides, a transgenic mouse model was generated, which exclusively over-expresses the ADan sequence. The transgene started with a glutamine instead of a glutamate at position one and was combined with the thyrotropin-releasing hormone sequence (TRH-ADan1Q-34) embedded in the Thy1-promoter cassette (as described in (Wirths et al. 2009, Alexandru et al. 2011)) (see also Fig. 3.17). The TRH-fusion to the transgene should provide the transmission of ADan1Q-34 into the *trans*-Golgi

network, where it should be converted into pGlu-ADan1-34 by QC-mediated catalysis and packed into vesicles of the secretory pathway. The murine Thy1-promoter sequence was chosen for a neuron-specific expression of the transgene as described before (Wirths et al. 2009, Alexandru et al. 2011).

4.1.6.1 ADan1Q-34 Transgenic Mice harbor Substantial Amounts of Intraneuronal ADan Peptides

The ADanPP7 mouse model (Coomaraswamy et al. 2010) develops extracellular ADan amyloid lesions in several brain regions like hippocampus, cerebellum and frontal cortex as well as vascular deposits recapitulating very well the human FDD neuropathology. In contrast, ADan1Q-34 transgenic mice (particularly lines OW20, OW23 and OW24) showed abundant intracellular ADan expression in neuronal perikarya and processes in multiple brain regions, especially in CA1 neurons and mossy fibers of the hippocampus, layer IV and V of the cortex as well as in Purkinje cells of the cerebellum without any indication of age-dependent extracellular or vascular deposition at the analyzed time points (Fig. 3.19, Tab. 3.1). The reason for those drastic differences in both mouse models might be due to the use of different expression cassettes. The ADanPP7 mouse model expresses the full-length mutant BRI2 form of FDD under the control of the Syrian Hamster prion-promoter, whereas the Thy1-promoter was used in the ADan1Q-34 model. The region and cell specific expression pattern of the novel generated mice correlates very well with the Thy1.2 expression pattern that has been described earlier (Caroni 1997). Caroni examined 17 transgenic mouse lines expressing either GAP-43 or CAP-23, in which transgenes were constitutively produced by neurons in adult mice with no obvious age-dependent changes in expression patterns. The same holds true for OW20, OW23 and OW24 mice, where founders at 6 to 8 months of age as well as their offspring at 1 and 6 months constantly express the transgene in the hippocampal formation, cerebellum and cortex. Additionally, almost no ADan was detected in the olfactory bulb, which is further concordant to Caroni´s description of the Thy1 expression pattern. The finding that ADan was exclusively present intraneuronally in ADan1Q-34 transgenic mice suggests that ADan peptides accumulate in neuronal compartments as it has been shown for murine neuroblastoma cells transfected with Danish mutant BRI2 (Kim et al. 2002). Although ADan distribution in the novel generated model does not reflect the situation in human FDD, it is a promising model to

examine the toxic effects of intracellular pGlu-ADan on neuronal survival *in vivo*, since any side-effects by e.g. cleavage products from over-expressed full-length BRI2 or expression by other cell types like glia can be excluded as confounding factors.

4.1.6.2   Enhanced Inflammatory Processes in ADan1Q-34 Transgenic Mice

Neuroinflammation marked as astro- and microgliosis is a major pathological hallmark shared by AD, FDD and also ADanPP7 mice, where in all cases microglia and astrocytes surround congophilic amyloid deposits, which are associated with dystrophic neurites (Itagaki et al. 1989, Holton et al. 2002, Rostagno et al. 2005, Coomaraswamy et al. 2010). Under normal conditions, astrocytic activity is important for e.g. neuronal nutrition, ion exchange, modification of neurotransmitters and maintenance of the blood-brain-barrier, while microglia remove cytotoxic material via phagocytosis. Under pathological conditions as in AD brains, neuroinflammatory processes become chronically active, leading to detrimental effects, accelerated amyloid deposition and dysfunction in amyloid clearance (Nagele et al. 2003, Hickman et al. 2008). AD mouse models also harbor severe astrocytosis that coincides with extracellular Aβ deposits (Games et al. 1995, Irizarry et al. 1997, Casas et al. 2004). However, strong astrogliosis occurred in absence of classical neuritic plaque deposits in the TBA42 mouse model expressing abundantly $A\beta_{pGlu3-42}$ in CA1 hippocampal neurons (Wittnam et al. 2012). Both astrocytosis (Fig. 3.20) and microgliosis (Fig. 3.21) using GFAP and Iba1 antibodies, respectively, were mainly detected in hippocampal structures as well as in the cerebellum of 6-month-old ADan1Q-34 transgenic mice compared to a 10-month-old wild-type animal. These regions also showed abundant intracellular ADan-immunoreactivity, suggesting an activation of inflammatory processes as a result of high amyloid peptide amounts in absence of extracellular plaques. This might be an indicator for neuroinflammation associated neurodegeneration as it has been shown in several AD mouse models (Games et al. 1995, Hsiao et al. 1996, Sturchler-Pierrat et al. 1997).

4.1.6.3   ADan1Q-34 Transgenic Mice develop Behavioral Deficits

In several AD mouse models, motor impairment has been reported, which coincides with amyloid pathology and axonopathy, that is indicative for neuronal degeneration in the spinal cord and a dysfunction of the cerebellum (Wirths et al. 2008, Seo et al. 2010, Jawhar et al. 2012, Wittnam et al. 2012). Indeed, FDD patients develop cerebellar ataxia, but unlike FBD

and to lesser extent AD, it induces no spastic tetraparesis (Strömgren et al. 1970, Holton et al. 2002). ADan1Q-34 transgenic mice harbored no indications for motor impairment as measured in string suspension and balance beam tasks at 6 months of age (Fig. 3.22), although intracellular ADan has been found in cerebellar nuclei, Purkinje cells and partially in granule cells (Fig. 3.19), whereas the ADan expression pattern in the spinal cord still needs to be analyzed. Transgenic mice possibly develop no cerebellar ataxia anyway, which could be explained by the lack of vasculopathy in the cerebellum, cerebral cortex and white matter that occurs in FDD patients (Strömgren 1981). Nevertheless, another possible reason for missing motor impairment could be the young age of the analyzed mice, since even 5XFAD mice, harboring severe amyloid pathology coinciding with impaired working memory and drastic motor deficits, show first significant motor disabilities at 9 months of age (Jawhar et al. 2012). Therefore, it cannot be ruled out that ADan1Q-34 mice develop motor impairment at later stages.

In AD patients, opposite neuropsychiatric symptoms were described in several studies with either apathy and increased anxiety or disinhibition and restlessness (Frisoni et al. 1999, Chung and Cummings 2000, Lyketsos et al. 2002). Multiple AD mouse models, like Tg2576 (Lalonde et al. 2003a), PS1$_{A246E}$ (Lalonde et al. 2003b), APP$_{Sw}$/PS1$_{\Delta E9}$ (Lalonde et al. 2005), 5XFAD (Jawhar et al. 2012), APP/PS1KI (Cotel et al. 2012) and TBA42 (Wittnam et al. 2012), mimic a reduced anxiety, whereas in other models, such as APP23 (Lalonde et al. 2002) or APP$_{Sw}$/PS1$_{A246E}$ (Puoliväli et al. 2002), no changes or a slightly increased anxiety behavior were observed. Interestingly, ADan transgenic animals at 6 months of age showed a significantly increased anxiety, but also a slightly decreased exploratory behavior, especially mice from lines OW23 and OW24, as evaluated by the elevated plus maze test (Fig. 3.23). This reflects the behavioral changes observed in some AD mouse models and human cases.

Furthermore, 6-month-old animals of line OW23 had initial problems in recalling their spatial reference memories as evaluated by the Morris water maze task (Fig. 3.25). OW23 and OW24 mice harbored also a drastically impaired working memory as measured by the cross maze test (Fig. 3.24). Several studies demonstrated that the hippocampus can be subdivided into dorsal and ventral regions with functional differences. Accordingly, lesions of the hippocampal ventral part resulted in behavioral disinhibition and anxiety changes, whereas a damaged dorsal compartment mainly affected spatial learning and memory

(Bannerman et al. 2004). In ADan1Q-34 transgenic mice, the entire hippocampus and cortical layers IV/V were predominantly affected by intracellular ADan deposits, suggesting ADan induced detrimental effects on these brain areas that probably resulted in an altered anxiety behavior and an impaired spatial reference memory. In conclusion, the ADan1Q-34 mouse model for FDD exhibits behavioral changes mimicking clinical symptoms of FDD and AD patients. This leads to the assumption that although different amyloid peptides are deposited, similar biochemical properties of Aβ and ADan are responsible for distinct clinical and pathological phenotypes.

4.1.7   Conclusions of Project I

In the context of this project, it could be shown that abundant deposits of pGlu-modified ABri/ADan peptides are present in human FBD/FDD cases as well as in a mouse model for FDD, respectively, using the novel antibodies AB77 and AB76-2. Here, pGlu-modified ABri and ADan peptides are putatively involved in amyloid seeding and plaque maturation. ADan aggregates have been detected in synaptic compartments of the ADanPP7 mouse model suggesting an involvement in deficits of neuronal transmission.

In addition, it has been shown that pGlu-ABri exhibits a more rapid aggregation profile than unmodified ABri under physiological conditions and that ABri/ADan peptides act more toxic *in vitro*, when they carry the pGlu-modification. Notably, the pGlu-modification even renders the non-amyloidogenic, wild-type CTF23 into an aggregating peptide species that had less beneficial effects on cell viability than non-modified CTF23. It could be further demonstrated that wild-type CTF23 becomes intracellularly redistributed under AD pathological conditions.

A promising, novel mouse model for FDD was generated that exclusively expresses ADan peptides. This model develops an impaired working and spatial reference memory as well as an increased anxiety behavior already at 6 months of age, reflecting FDD and AD pathology. Although the neuropathological pattern in these mice not corresponds to human FDD, the presence of abundant intracellular ADan and gliosis make this model well suitable to study the toxic effects of ADan on neuronal integrity.

In conclusion, FBD, FDD and AD show striking similarities regarding biochemical properties of different amyloid peptides that share the same post-translational modification. Therefore, it can be hypothesized that pGlu-carrying amyloidogenic peptides possibly trigger

degenerative processes, which might represent a general pathological mechanism that is responsible for neuron loss in neurodegenerative diseases.

4.2 Project II: Aβ triggers Murine ApoE Fragmentation in Transgenic Mouse Models for Alzheimer's Disease

ApoE fragmentation is supposed to be an explanation for ApoEs´ characteristics as the strongest genetic risk factor for developing AD. Due to its unique biochemical properties, ApoE4 is most vulnerable for proteolytical processing compared to ApoE3 or ApoE2 isoforms (Weisgraber 1990, Huang et al. 2004, Mahley et al. 2006). A mass of studies have shown that ApoE4 and related fragments influence Aβ pathology. It has been reported that lipid-poor ApoE4 rather than ApoE3 enhances Aβ production in rat neuronal cells over-expressing human APP$_{695}$ (Ye et al. 2005). This suggests that ApoE4 modulates APP processing and Aβ production via LDL receptor-related protein pathway as well as by its domain interaction, since blocking both abolished Aβ production. Furthermore, it has been demonstrated that ApoE4 affects Aβ deposition and clearance *in vivo* and *in vitro*. Aβ formed insoluble, high-molecular-weight complexes more rapidly, which precipitate as fibers with higher density and massive amyloid monofibril matrix, when it was bound to ApoE4 instead of ApoE3 (Ma et al. 1994, Sanan et al. 1994, Wisniewski et al. 1994). Moreover, APP$_{V717F}$ transgenic mice expressing human ApoE4 in neurons (instead of endogenous, murine ApoE) showed less efficient Aβ clearance than mice harboring human ApoE3 (Holtzman et al. 2000). However, since it has been shown that AD patients with ApoE3 also produce more fragments than non-demented controls with the same genotype (Huang et al. 2004) and due to the high affinity of ApoE binding to Aβ peptides (Strittmatter et al. 1993), it is very likely that Aβ might influence ApoE's biochemical characteristics, especially influencing its metabolism and biological function. Therefore, in the context of this project, several AD mouse models, generating different amounts of Aβ peptides, as well as murine neuroblastoma cells were investigated regarding the proteolysis of endogenous or over-expressed murine ApoE (mApoE). Furthermore, it was analyzed whether intra- or extracellular Aβ peptides differ in their ability to induce human ApoE fragmentation *in vitro*. A novel AD mouse model (5XFAD/PS19) has been also generated and characterized, expressing human mutant APP, PS1 and tau, to investigate whether hyperphosphorylated tau influences Aβ pathology in

5XFAD mice or vice versa and which role proteolyzed ApoE might play in the amyloid cascade.

4.2.1 Intracellular Aβ triggers Proteolysis of Human ApoE

Isoform-specific ApoE proteolysis has been demonstrated in human brain tissue, in which controls as well as AD cases carrying the ApoE4 genotype harbor more ApoE fragments compared to ApoE3 carriers, which also correlates with intracellular Aβ accumulation (Huang et al. 2001, Huang et al. 2004, Christensen et al. 2010b). The present study confirms the previous findings by showing more detectable N-terminal ApoE fragments with comparable fragment sizes in sAD cases compared to non-demented controls, whereas full-length ApoE remained unaltered (Fig. 3.26). However, the ApoE genotype was unknown, therefore it cannot be completely ruled out that the increased ApoE fragmentation in sAD cases compared to controls is only caused by different genotypes. In contrast to the observations of Huang and colleagues, strongly elevated levels of C-terminal 10 to 15 kDa ApoE fragments were detected in sAD brains that were further increased in a fAD case carrying mutant APP$_{I716F}$, which affects the γ-secretase cleavage producing high amounts of intraneuronal Aβ$_{42}$ (Lichtenthaler et al. 1999a).

While the effect of ApoE and its fragments on the accumulation and deposition of Aβ peptides was investigated in numerous studies, almost nothing is known about if and how Aβ peptides in turn influence ApoE proteolysis. In the present work, SH-SY5Y neuroblastoma cells carrying human ApoE3 were stably transfected with different APP constructs, such as full-length wild-type APP$_{751}$ or APP C-terminal fragments (SPA4CTΔcyto) (Lichtenthaler et al. 1997, Fossgreen et al. 1998), which leads to varying intracellular Aβ levels. APP- and SPA4CTΔcyto over-expressing cells showed a marked increase in overall cellular ApoE levels and enhanced ApoE fragmentation compared to Mock control (Fig. 3.27c), with highest levels in SPA4CTΔcyto-transfected cells, which harbored highest intraneuronal Aβ amounts. In contrast, further *in vitro* experiments have shown that exogenous treatment of synthetic Aβ$_{1-42}$ on human Ntera2 teratocarcinoma cells led to a marked increase in cellular full-length ApoE levels (Fig. 3.27a-b). However, there was no evidence of enhanced ApoE proteolysis compared to untreated Ntera2 cells. These data suggest that ApoE fragmentation is putatively driven by intracellular Aβ, whereas extracellular Aβ provokes ApoE expression, likely reflecting a protective mechanism to clear amyloids.

4.2.2 Murine ApoE becomes fragmented under Amyloid Burden

This is the first study reporting a proteolytical processing of endogenous mApoE *in vitro* and *in vivo*. ApoE fragmentation has been previously described, however, only in mice over-expressing either human ApoE isoforms or C-terminally truncated human ApoE4 variants (He and Klionsky 2009, Brecht et al. 2004). In the current work, abundant endogenous mApoE fragments were detected in a variety of different AD mouse models, including APP/PS1KI (Fig. 3.28), 5XFAD (Fig. 3.30) and APP/PS1-21 (Fig. 3.31), that directly correlate with Aβ load in an age-dependent manner. The major detected fragments of approximately 29 kDa, 25 kDa and 10 to 15 kDa correspond to human data (Fig. 3.26) and to previous reports employing human brains or transgenic mice expressing human ApoE (Harris et al. 2003, Brecht et al. 2004). This suggests that mApoE fragments are generated in a similar way as their human counterparts. Interestingly, comparative analyses of the amino sequences of mouse and human ApoE revealed a 70 % homology with nearly identical α-helical regions, leading to similar secondary protein structures. Moreover, mApoE harbors the same amino acid residues as the human ApoE4 allele at corresponding positions, suggesting that ApoE4 represents an ancestral form of the other human ApoE isoforms (Rajavashisth et al. 1985, Mahley and Rall 1999). Under normal conditions, mApoE is probably not as vulnerable as human ApoE4 for proteolysis, which is likely due to the presence of a threonine instead of an arginine at position 61, resulting in a hindered interaction with glutamate at position 255 (Weisgraber 1994). This probably leads to a biochemical human ApoE3-like behavior of mApoE, without domain interaction and therefore to less ApoE fragmentation. However, the main portion of fragmented mApoE was present in SDS-soluble brain fractions of several AD mouse models that also contained aggregated, insoluble Aβ deposits, suggesting that mApoE proteolysis is associated with oligomeric or fibrillar Aβ assemblies. In addition, ApoE fragmentation was induced in murine Neuro2a neuroblastoma cells (Fig. 3.32) over-expressing mApoE by co-transfection with C-terminal APP fragments, such as SPA4CT and SPA4CT/Δcyto, producing high amounts of intracellular Aβ (Venkataramani et al. 2010). These findings combined with lacking ApoE fragmentation in 16-month-old 3xTg mice (Fig. 3.33b), which harbor age-dependent APP accumulation but low levels of intraneuronal Aβ (Wirths et al. 2012), further corroborate the assumption that ApoE fragmentation might be driven by intracellular Aβ.

Immunofluorescent staining revealed that ApoE and related fragments are localized in extracellular amyloid plaques and intracellularly in Aβ containing dystrophic neurites of APP/PS1KI mice, as well as in neuronal somata of APP/PS1KI and 5XFAD animals (Fig. 3.29). Therefore, mApoE fragmentation is probably linked directly to intracellular amyloid burden. The amounts of mApoE fragments were increased accompanied by elevated Aβ levels, whereas no such correlation has been found for the toxic APP cleavage product C99. Furthermore, initial prominent ApoE fragments with a size of 10 to 15 kDa were detected that represent possible C-terminal fragments according to their molecular weight, which correspond to the human data using a C-terminal specific ApoE antibody. It has been found that ApoE fragmentation is crucial for amyloid deposition in human AD cases as well as in AD mouse models expressing human ApoE (Namba et al. 1991, Näslund et al. 1995, Aizawa et al. 1997). Since full-length and N-terminally truncated mApoE was detected in hippocampi of APP/PS1KI brains already at 2 months of age, it is suggested that ApoE proteolysis is triggered by intraneuronal Aβ accumulation and further promotes Aβ deposition. This assumption is further supported, as it has been found that over-expression of human ApoE4 in murine Neuro2a neuroblastoma cells led to the generation of toxic C-terminal ApoE fragments, which reflect the same pattern as observed in AD transgenic mouse models investigated in the current study. These fragments have been demonstrated to stabilize Aβ hexamers and to inhibit fibril formation in contrast to full-length and N-terminal ApoE fragments (Wellnitz et al. 2005).

Interestingly, the generation of mApoE fragments was not restricted to AD mouse models and Aβ pathology, since ADanPP7 mice, harboring an age-dependent ADan amyloidosis, also showed an increase in mApoE proteolysis. This further supports that the similar biochemical properties of Aβ and ADan result in analog cellular effects in AD and FDD, respectively.

4.2.3 Murine ApoE Fragments may impair Neuronal Plasticity in AD Mouse Models

Under physiological conditions, ApoE is important for maintaining synapto-dendritic connections and stimulates neuritic outgrowth. However, ApoE4-targeted replacement mice show significantly reduced long-term potentiation compared to wild-type or ApoE3-targeted

replacement mice, suggesting that ApoE-dependent isoform characteristics modulate the susceptibility to memory impairment (Trommer et al. 2004).

In the present study, it could be shown that endogenous, murine full-length and fragmented ApoE were mainly present in synaptosomal compartments of brains from 5XFAD (Fig. 3.34) and APP/PS1KI mice (Fig. 3.35) that coincide with highest amounts of Aβ and C99 levels. In good agreement, it has been recently shown that increased ApoE levels lead to intracellular accumulation of Aβ in synapses (Arold et al. 2012). Murine ApoE was mainly found in microsomal instead of synaptosomal fractions of wild-type and APP$_{he}$ mouse, which produce no or only low levels of Aβ and lower ApoE amounts compared to APP/PS1KI or 5XFAD mice. The APP/PS1KI mouse model harbors a severe phenotype with early intraneuronal Aβ accumulations in the hippocampus and cortical layers correlating with abundant neuron loss at later stages (Casas et al. 2004, Christensen et al. 2008). Extensive changes in synaptic transmission with reductions in long-term potentiation have been also reported for this model, accompanied by decreased pre- and post-synaptic marker levels already at 6 months of age (Breyhan et al. 2009). Interestingly, this is the same time-point, in which full-length as well as N- and C-terminal mApoE fragments were prominently detected in synaptic compartments. This indicates that ApoE proteolysis may impair the synaptic transmission in concert with intracellular aggregated Aβ that likely triggers the neuropathological cascade. Thereby, possible mechanisms could be the ability of oligomeric Aβ to inhibit hippocampal long-term potentiation via activation of caspases (Jo et al. 2011) or to facilitate long-term depression by disrupting neuronal glutamate uptake (Li et al. 2009). In this regard, especially low-molecular weight Aβ species ranging from dimers to hexamers, which are stabilized by C-terminal ApoE fragments (Wellnitz et al. 2005), might play an important role.

Remarkably, APP/PS1KI mice at 2 months of age had significantly more post-synaptic compartments, as measured by PSD95 signal intensity, than age-matched wild-type or PS1KI$_{ho}$ mice, whereas PSD95 levels in APP/PS1KI mice were indistinguishable at 6 months and significantly decreased in 10-month-old animals compared to the other genotypes (Fig. 3.39-3.41). There is accumulating evidence that hyperactivity followed by hypoactivity of hippocampal neurons increases the risk for developing AD. It has been shown that hippocampal hyperactivity is related to early MCI brain atrophy in humans (Putcha et al. 2011) and silent seizures, resulting from over-excitation and compensatory inhibition,

126

occurred in cortical and hippocampal networks of human APP transgenic mice (Palop et al. 2007). Furthermore, it has been demonstrated that neuronal hyperactivity, which is boosted by soluble Aβ, precedes amyloid deposition in the hippocampus of APP23/PS45 transgenic mice (Busche et al. 2012). Along with the observations of the recent study, it can be assumed that ApoE fragments *per se* or in concert with Aβ may disturb synaptic transmission and further promote Aβ deposition in synapses, leading to a loss of synapto-dendritic connections.

4.2.4   Oxidative Stress accelerates ApoE Fragmentation

Increased inflammation and oxidative stress appear to be key features contributing to AD pathology. In the context of this thesis, it could be shown that 5XFAD and APP/PS1KI mice harbored prominent accumulation of ApoE fragments accompanied by high amounts of Aβ peptides in synaptosomal fractions, in which a major portion of mitochondria was detected using CoxIV antibody. CoxIV is a marker for the cytochrome c oxidase, which is a hetero-oligomeric enzyme localized to the inner mitochondrial membrane, regulating mitochondrial metabolism (Kadenbach et al. 2000). It has been shown that a deficiency of this enzyme accelerates aging and stimulates the production of reactive oxygen species (ROS) that correlate with a variety of human disorders (Barrientos et al. 2002). Furthermore, ApoE fragments associated with Aβ and also Aβ alone are putatively involved in a disrupted mitochondrial metabolism, leading to the production of ROS and promoting neuronal death (Keller et al. 2000, Butterfield et al. 2002). In the present work it could be shown, that human SH-SY5Y neuroblastoma cells over-expressing the SPA4CT construct with high amounts of intracellular Aβ (Lichtenthaler et al. 1997, Venkataramani et al. 2010) also produce fragmented ApoE (Fig. 3.37). Cell viability assays revealed that these cells are seriously affected by oxidative stress, since their proliferation rate could be restored after the application of the ROS scavenger N-acetyl-L-Cysteine (NAC). Interestingly, the reduction of oxidative stress also diminished ApoE proteolysis leading to significantly reduced levels of ApoE fragments, suggesting that oxidative stress in turn promotes ApoE proteolysis. It has been shown that, in contrast to non-synaptic mitochondria, synaptic mitochondria showed larger amounts of age dependent Aβ accumulation and earlier mitochondrial dysfunction, including an impaired respiratory function and activity of the cytochrome c oxidase. Furthermore, increased mitochondrial oxidative stress was demonstrated in APP over-

expressing mice, suggesting that synaptic mitochondria are more susceptible to Aβ induced damages (Du et al. 2010). Therefore, it can be assumed that Aβ associated ApoE fragmentation is accelerated in synaptic mitochondria and further promotes synaptic dysfunction mediated by oxidative stress in AD as well as AD mouse models.

4.2.5 Aβ and ApoE Fragments correspond to Axonopathy and Disturbed Autophagy in the APP/PS1KI Mouse Model

Studies on human AD cases and AD mouse models suggest that axonal transport deficits are enhanced under pathological conditions and they are linked to cholinergic disconnection and extracellular Aβ deposition (Roy et al. 2005, Smith et al. 2007, Minoshima and Cross 2008). Axonal transport deficits result in axonopathy in AD, which is characterized by abnormally swollen axons containing numerous aggregated proteins. APP is one of those proteins accumulating in dystrophic neurites and is therefore a valuable marker for pathological transport deficits (Cras et al. 1991, Coleman 2005). Immunohistochemistry using pT688 antibody detecting phosphorylated APP demonstrated a significant increase in dystrophic neurites with each copy of mutant PS1 in the APP/PS1KI mouse model, with highest amounts of swollen axons in homozygous mice (Fig. 3.38). Western-blot analyses of these mice revealed that APP levels remained the same, whereas Aβ was strongly increased with higher PS1 gene dose in double transgenic APP/PS1KI compared to single transgenic APP$_{he}$ mice (Fig. 3.36). This suggests that Aβ accumulates independently from APP in dystrophic neurites in these mice. It has been already demonstrated that intraneuronal Aβ accumulates within axonal swellings of double transgenic APP$_{SwLon}$/PS1$_{M146L}$ and APP/PS1KI mice (Wirths et al. 2006, Wirths et al. 2007b). In good agreement, it can be assumed that high Aβ levels in dystrophic neurites of APP/PS1KI mice further accelerate the axonal pathology in this mouse model.

It has been shown that Aβ peptides impair the axonal transport of mitochondria (Rui et al. 2006) and that a blockage of axonal transport precedes Aβ generation. This is putatively due to increased axonal processing of APP by an increased exposure to the γ-secretase complex during the prolonged transport (Stokin et al. 2005). That Aβ is produced locally in swollen axons is further supported by the detection of a substantial co-accumulation of APP, BACE1 and the γ-secretase compound PS1 in swollen axons of pigs, in which brain injury was induced experimentally (Chen et al. 2004). Besides the accumulation

of Aβ producing enzymes, impaired autophagy might also contribute to Aβ aggregation in swollen axons, since at least one subtype of autophagic vacuoles (AVs), which are enriched in axonal swellings, contains Aβ peptides and also PS1-dependent γ-secretase activity (Yu et al. 2005). In addition, a loss or the reduction of PS1 function led to a dysfunction of the autophagic system by enriched autophagosomes (Neely et al. 2011). Former studies revealed that behavioral deficits and marked axonal degeneration are associated with numerous axonal swellings in APP/PS1KI mice (Wirths et al. 2007b, Wirths et al. 2008), raising the question if impaired autophagy contributes to the AD-like pathology in these mice. Biochemical analyses of crude synaptosomal fractions of aged APP/PS1KI mice revealed a drastic decrease of the post-synaptic density protein 95 in combination with abnormally elevated levels of the autophagy substrate LC3-II compared to age-matched wild-type animals (Fig. 3.41). Furthermore, lysosomal LC3- and autophagosomal Cathepsin D- containing vesicles had a clotted, accumulated morphology and co-localized broadly with APP/Aβ accumulations in CA1 neurons of these mice as demonstrated by immunofluorescent staining (Fig. 3.42). This indicates that autophagic processes are disturbed by abnormally increased numbers of AVs, leading to intraneuronal Aβ aggregation, which likely contributes to axonopathy and synaptic loss in APP/PS1KI mice. Interestingly, it has been demonstrated that the aspartic protease Cathepsin D is a candidate enzyme for ApoE proteolysis by processing lipid-free and lipidated ApoE to C- and N-terminal fragments. ApoE fragments generated by Cathepsin D showed the same Western-blot pattern as ApoE fragments seen in humans, and they were also associated with a subset of plaques and tangles (Zhou et al. 2006c). Together with the recent findings, it can be hypothesized that endogenous mApoE might be further processed by abnormally accumulated Cathepsin D in AV-containing axonal swellings, which is induced by high intracellular Aβ levels.

Several studies reported that the expression of human ApoE4 *per se* also drastically affects the axonal transport leading to degenerated axons (Mahley et al. 2006). It has been shown that the fragmentation of human ApoE4 was strongly increased in mice expressing neuron-specific enolase (NSE)-ApoE4 following excitotoxic injury by kainic acid treatment (Brecht et al. 2004). The expression of ApoE4 in targeted replacement mice also led to a reduced excitatory synaptic transmission and dendritic arborization (Wang et al. 2005). Moreover, neuronal expression of full-length human ApoE4 induced an axonopathy phenotype in transgenic mice, showing impaired axonal transport and degeneration, where

axonal swellings contained aggregated vesicles and other compounds like synaptophysin, neurofilaments and mitochondria (Tesseur et al. 2000a). Holtzman and colleagues demonstrated that plaque-associated neuritic dystrophy completely disappeared in transgenic mice over-expressing human mutant APP$_{V717F}$ after knocking-out endogenous ApoE (Holtzman et al. 2000), suggesting also reciprocal pathological interactions between ApoE and its fragments with Aβ. Therefore, the observed axonopathy phenotype accompanied by synapse loss in APP/PS1KI mice might result from mApoE fragmentation by the conversion of full-length into fragmented ApoE. However, another possible mechanism how mApoE fragments are involved in the neurodegeneration in APP/PS1KI mice might be an impaired delivery of cholesterol and phospholipids to neuronal compartments by the conversion of a functional full-length ApoE to non-functional ApoE fragments. This might lead to a failed maintenance of synapto-dendritic connections as it is known for human ApoE4 (Wang et al. 2005).

4.2.6 Impact of Human Mutant Tau on Amyloid Pathology and Aβ-induced Proteolysis of Murine ApoE in 5XFAD Mice

Tauopathy is widespread in a variety of neurodegenerative diseases like e.g. frontotemporal dementia (FTD) with Parkinsonism, FBD, FDD and AD. Mutations in the *MAPT* gene on chromosome 17, encoding the microtubule associated protein tau, result in tau aggregation and neurodegeneration that cause FTD (Lee et al. 2001). In contrast, as no mutations in *MAPT* are known for fAD leading to hyperphosphorylated tau, *MAPT* mutations related to FTD have to be employed to model tau phosphorylation in AD mouse models. In the present thesis, PS19 mice over-expressing MAPT$_{P301S}$ (Yoshiyama et al. 2007) were crossed with the 5XFAD mouse model harboring five mutations for fAD (Oakley et al. 2006), resulting in a drastically accelerated pathology in trigenic mice. The novel generated 5XFAD/PS19 model recapitulates a broad variety of pathological alterations occurring in AD and provides a good possibility to investigate mutual influences of Aβ and tau in consideration of proteolytically processed, endogenous mApoE.

4.2.6.1 Analyses of 5XFAD/PS19 Mice support the Amyloid Hypothesis with Aβ's Role Upstream from Tau Pathology

So far, the function of tau in the amyloid cascade remains still controversial regarding its role either acting upstream or downstream from Aβ pathology. It has been shown that neurofibrillary changes develop preferentially prior amyloid deposits in human AD brains with Braak stages I to II (Braak and Braak 1997). Another study even claims that tau is able to change APP metabolism by reduced BACE1 levels in 5XFAD/tau-knockout mice, resulting in a moderate reduction of amyloid plaque load and concomitant synapse as well as neuron loss (Leroy et al. 2012). However, 16-month-old double transgenic mice, harboring human mutant APP$_{Sw}$ and tau$_{G272V/P301L/R406W}$ transgenes, developed drastically increased amyloid burden compared to single transgenic APP$_{Sw}$ animals (Ribe et al. 2005). Ribe and colleagues concluded therefore that tau might influence amyloid production and/or clearance by lysosomal dysfunction evoked by tau transgenic mice.

However, the crucial position of tau in the amyloid cascade has been previously addressed in a plethora of AD mouse models, suggesting multiple modes of interaction without indicating evidence for an upstream role of tau. A study led by Götz and colleagues has shown that transgenic mice over-expressing human mutant tau$_{P301L}$ developed fivefold elevated amounts of NFT-like structures in perikarya of the amygdala after injection of fibrillar Aβ$_{42}$ (Götz et al. 2001). Moreover, injection of amyloid containing brain extracts from aged APP23 mice, carrying APP$_{Sw}$, into the cerebrum of tau$_{P301L}$ transgenic mice resulted in accelerated tau pathology in the hippocampus, amygdala and entorhinal cortex, whereas infusion of brain extracts from aged tau over-expressing mice did not significantly alter tau pathology. Interestingly, crossing these tau-expressing mice with APP23 animals led also to higher amounts of hyperphosphorylated tau that occurred in areas with highest Aβ load, whereas amyloid deposits were not changed (Bolmont et al. 2007). The findings from the novel generated 5XFAD/PS19 mice further corroborate the amyloid cascade hypothesis, affirming that Aβ peptides represent an initial trigger underlying further pathological alterations in AD (Hardy and Allsop 1991). No significant changes of amyloid plaque pathology and APP levels and its metabolites, C99 and Aβ, were detected in the hippocampi of either 3- or 9-month-old 5XFAD/PS19 animals compared to 5XFAD littermates in immunohistochemical approaches or by Western-blotting of whole brain lysates using antibodies 24311 and IC16, respectively (Fig. 3.43 and Fig. 3.47). These results suggest no

pivotal role for tau in triggering Aβ production. In contrast, tau pathology was substantially aggravated in brains of 9-month-old triple transgenic 5XFAD/PS19 mice compared to age-matched single transgenic PS19 animals (Fig. 3.44 and Fig. 3.47). Triple transgenic animals showed also an earlier onset of tau aggregation that was preceded by substantial amounts of extracellular Aβ deposits. These findings corroborate previous studies, in which mutant APP transgenic mice were crossed with mice expressing mutant tau, resulting in alterations of tau conformational states, without any changes of APP metabolism or plaque pathology (Lewis et al. 2001, Terwel et al. 2008, Grueninger et al. 2010, Hurtado et al. 2010). Furthermore, the observed precedence of amyloid plaques prior the onset of tau conformational changes in 5XFAD/PS19 mice confirms the findings by Oddo and colleagues, using the 3xTG mouse model carrying human APP_{Sw} and tau_{P301L} on a $PS1_{M146V}$ knock-in background (Oddo et al. 2003). These mice show age-dependent amyloidosis and tau hyperphosphorylation with initial MC1- and AT8-immunoreactivity at the age of 12 to 15 months, whereas extracellular Aβ plaques occurred already at 6 months of age. Moreover, the reduction of the APP cleaving enzyme BACE in double transgenic mice, expressing human mutant APP_{E693G} and human wild-type tau, led to decreased levels of soluble Aβ, tau phosphorylation and tau's mislocalization in synapses (Chabrier et al. 2012). A possible direct link of Aβ and tau interaction is provided by a study from Terwel and colleagues, showing that enhanced tau phosphorylation is mediated by Aβ-driven GSK-3β activation in transgenic mice, harboring human mutant APP and tau (Terwel et al. 2008).

4.2.6.2 Neuronal Integrity Impairment, Hippocampal Atrophy and Inflammation are aggravated in 5XFAD/PS19 Mice

5XFAD/PS19 mice showed hippocampal shrinkage, significantly aggravated diminishment of synapto-dendritic connections (Fig. 3.45), as well as drastically elevated astrocytosis (Fig. 3.46) compared to PS19 and 5XFAD parental lines, suggesting a clear impairment of neuronal integrity associated with increased tau pathology. Immunostaining using β3-tubulin antibody revealed a drastic decrease of apical dendrites in the stratum radiatum of the hippocampus in 9-month-old 5XFAD/PS19 animals, whereas PS19 and 5XFAD littermates seemed to be not affected (Fig. 3.45). Under physiological conditions, tau is intraneuronally distributed with a spatial gradient, meaning higher concentrations in axons than in somato-dendritic compartments (Buée et al. 2000). However, it has been demonstrated that tau gets

aberrantly mislocalized to dendritic spines by hyperphosphorylation, resulting in a decreased expression of AMPA- and NMDA-receptors and an impaired synaptic transmission (Hoover et al. 2010). In addition, intracerebral injection of adeno-associated viral (AAV) mutant tau$_{P301L}$ in transgenic mice expressing the yellow fluorescent protein, led to a drastic degradation of apical dendrites of hippocampal CA1 neurons accompanied by accumulated, enlarged autophagic vacuoles and activated astrocytes (Jaworski et al. 2011). The appearance of hyperphosphorylated tau in apical dendrites in the hippocampus of 5XFAD/PS19 mice already at 3 months of age indicates that tau gets also mislocalized in somato-dendritic compartments in this mouse model. Furthermore, missorted tau might induce dendritic diminishment, since the affected tau-immunostained processes disappeared in aged animals (Fig. 3.44f, h), corresponding to a reduced amount of β3-tubulin-stained dendrites (Fig. 3.45f) and hippocampal atrophy. However, it has been reported that PS19 mice harbor reduced levels of endoplasmatic reticulum-specific proteins in dendrites already at 3 months of age, as well as hippocampal shrinkage of approximately 25 % and 45 % at 9 and 12 months of age, respectively, compared to non-transgenic controls (Yoshiyama et al. 2007). Therefore, it cannot be excluded that PS19 transgenic mice also develop distorted apical dendrites in the hippocampal stratum radiatum in later ages, since tau pathology in 5XFAD/PS19 animals started earlier as well. Furthermore, immunostaining using synaptic markers like synapsin-1 further confirms tau's toxic function in damaging neuronal arborizations. Aged trigenic 5XFAD/PS19 mice harbored drastically reduced synapses in the hippocampal CA3 mossy fiber pathway compared to aged-matched 5XFAD and PS19 mice, whereas the latter also had significantly less synapses than 5XFAD littermates (Fig. 3.45). That the PS19 mouse model develops degenerated mossy fibers has been already demonstrated in a previous study, showing reduced neurofilament-staining in the same region (Yoshiyama et al. 2007). The aggravated synaptic loss in the mossy fiber pathway in combination with drastically decreased apical dendrites in hippocampi of 5XFAD/PS19 suggests that the presence of human mutant APP and PS1, leading to high levels of Aβ, accelerates the degeneration of neuronal processes, which is putatively induced by early tau conformational changes.

5XFAD mice harbor chronic inflammation represented as micro- and astrogliosis that increases proportionally with Aβ$_{42}$ levels (Oakley et al. 2006). Interestingly, *in vitro* data suggest that astrocytes are crucial for Aβ-mediated toxicity and hyperphosphorylation of tau

in neurons (Garwood et al. 2011). Furthermore, the application of conditioned medium from astrocytes, incubated with soluble Aβ peptides, induced tau phosphorylation and neuronal death of cultured hippocampal neurons (Saez et al. 2006). In the present work, 5XFAD mice also showed an increased inflammatory response in the cortex and thalamus compared to PS19 mice. However, the amounts of activated astrocytes were significantly elevated in 5XFAD/PS19 animals compared to the other genotypes (Fig. 3.46). This indicates that Aβ induced hyperphosphorylation of tau triggers astrocytosis and *vice versa* resulting in a subsequent aggravation of the phenotype.

Moreover, quantification of hippocampal CA1 neurons revealed a significant loss coinciding with overall hippocampal atrophy in 5XFAD/PS19 mice compared to PS19 and 5XFAD littermates at 9 months of age, with single transgenic PS19 animals showing a tendency towards reduced CA1 neuron number (Fig. 3.45). This finding is in good agreement with the demonstrated hippocampal atrophy in PS19 mice, described in a previous study (Yoshiyama et al. 2007). Notably, the 5XFAD model harbors neuron loss in the fifth cortical layer at 12 months of age, however, CA1 neurons, in which no intracellular Aβ is detectable, are not affected (Jawhar et al. 2012). These data suggest that the co-expression of Aβ and tau aggravates the hippocampal atrophy as well as CA1 neuron loss in 5XFAD/PS19 mice, probably by Aβ-triggered tau hyperphosphorylation and toxicity. Similar findings were observed in previous studies dealing with transgenic mice over-expressing human mutant APP. Injection of AVV-coupled mutant tau into the entorhinal cortex of TASTPM mice, expressing human mutant APP_{Sw} and $PS1_{M146V}$, induced hyperphosphorylated tau pathology combined with neuritic dystrophy, neuron loss in the hippocampal CA1 region and entorhinal cortex, as well as increased inflammatory response, whereas no changes in Aβ pathology were observed (Dassie et al. 2013). Furthermore, a study using the same PS19 mouse model revealed that crossing these mice with the PDAPP mice, carrying human mutant APP_{V717F}, resulted in the formation of NFT-like structures and increased premature death rate, without any significant changes in amyloid pathology (Hurtado et al. 2010). Here, Hurtado and colleagues demonstrated that PS19-PDAPP mice also develop neuron loss compared to PDAPP animals, but they did not consider the neuronal reduction in PS19 animals alone, which has been previously shown by Yoshiyama and colleagues (Yoshiyama et al. 2007).

4.2.6.3 Aβ-induced ApoE Proteolysis is a Possible Upstream Event of Tau Hyperphosphorylation in 5XFAD/PS19 Mice

As discussed above, 5XFAD/PS19 mice showed severe tau pathology that is putatively driven by Aβ peptides. It has been shown that cytoskeletal abnormalities in terms of the formation of NFTs in neurons are caused by the neuron-specific effect of ApoE4 on tau phosphorylation. Whereas ApoE3 binds irreversible to non-phosphorylated tau, ApoE4 is not able to interact, leading to enhanced hyperphosphorylation of tau in neurons (Strittmatter et al. 1994, Tesseur et al. 2000b, Brecht et al. 2004). Accordingly, enhanced tau phosphorylation was only seen in transgenic mice carrying human ApoE4 in neurons but not in glial cells, using cell type-specific promoters. Moreover, these animals showed age-dependent tau hyperphosphorylation, which correlates with ApoE4 expression levels, accompanied by increased astrogliosis and pathological ubiquitin inclusions, resulting in motor impairment, muscle atrophy and pre-mature death (Tesseur et al. 2000b). A subsequent study demonstrated that neuronally expressed ApoE4 also induces axonal degeneration in ApoE4-transgenic mice (Tesseur et al. 2000a). Due to its unique biochemical properties, ApoE4 is more susceptible to form molten globules and reactive intermediates than ApoE2 or ApoE3. These intermediates have been reported to enhance ApoE's vulnerability for proteolysis and cellular translocation (Mahley et al. 2006). The neurotoxic action of ApoE was assigned to the translocation of ApoE fragments into the cytosol, where they interact with mitochondria and components of the cytoskeleton (Chang et al. 2005). Chang and colleagues demonstrated that full-length ApoE was, as expected, present in components of the secretory pathway in Neuro2a cells transfected with human full-length ApoE4. In contrast, Neuro2a cultures over-expressing the C-terminally truncated ApoE4$_{1-272}$ fragment harbored mislocalized ApoE4 in the cytoplasm, where they formed filamentous inclusions. Previous studies reported that ApoE fragments form complexes with tau, inducing its hyperphosphorylation and the generation of NFT-like inclusions (Huang et al. 2001, Harris et al. 2003). This is suggestive of a crucial function of ApoE in the progression of AD pathology by disrupting the cytoskeletal stability and axonal trafficking. Using Western-blot analysis, brains of trigenic 5XFAD/PS19 mice exhibited a fragmentation pattern of endogenous mApoE that was indistinguishable from those observed in 5XFAD littermates (Fig. 3.47c-d). However, compared to PS19 single transgenic mice, both 5XFAD and 5XFAD/PS19 animals generated significantly higher amounts of total and fragmented

mApoE, whereas APP, C99 and Aβ amounts in 5XFAD and 5XFAD/PS19 mice remained the same (Fig. 3.47a, d), confirming the immunohistochemical data (Fig. 3.43). Furthermore, the observed aggravation of tau pathology in 5XFAD/PS19 compared to PS19 littermates using AT8 antibody (Fig. 3.44) were further corroborated by Western-blot data using MC1 and CP13 antibodies, showing enhanced tau phosphorylation in triple transgenic mice (Fig. 3.47b, d). This leads to the assumption that fragmented mApoE possibly interacts with tau in the cytoplasm, leading to an acceleration of NFT-like pathology and promotes the reduction of neuronal processes, which was seen in synapsin-1 and β3-tubulin immunostainings of 5XFAD/PS19 brains (Fig. 3.45a-l). A possible mechanism might be the direct activation of the glycogen synthase kinase-3 (GSK-3) by ApoE fragments that phosphorylates tau at serine-202, as it has been demonstrated for Neuro2a cells over-expressing C-terminally truncated ApoE4$_{\Delta272-299}$ (Zhou et al. 2006a). Interestingly, it has been shown that Aβ peptides also activate GSK in cultured AD mouse brain slices (Pena-Ortega et al. 2012) and rat hippocampal cultures (Takashima et al. 1998, Takashima 2006). Therefore, with regard to the amyloid cascade it can be hypothesized that Aβ acts in concert with mApoE fragments as an inducer and enhancer of tau phosphorylation by the activation of GSK-3, representing a possible initiator of the pathological cascade driving AD progression.

4.2.7   Conclusions of Project II

In the course of this project, it could be shown that – like in human AD brains – murine, endogenous ApoE becomes proteolytically processed, generating 10 to 15 kDa C-terminal as well as approximately 25 and 29 kDa N-terminal fragments that correlate with amyloid loads in different AD mouse models and an FDD mouse model.

    In vitro experiments using human and murine cells suggest that intracellular Aβ peptides induce and/or trigger human and murine ApoE proteolysis, whereas extracellular Aβ only enhances full-length ApoE expression without any fragmentation.

    Young APP/PS1KI animals mainly produced C-terminal ApoE fragments in their brains with increased amounts of N-terminal fragments at older ages, indicating that ApoE processing might be a crucial early event that triggers AD progression by provoking Aβ deposition.

    Furthermore, in contrast to wild-type animals, full-length and fragmented mApoE, co-localizing with Aβ, was mainly detected in synaptic compartments of AD mouse models.

These mice showed reduced synapto-dendritic connections, suggesting that ApoE and related fragments are mislocalized to synapses under pathological conditions. Here, it can be assumed that ApoE fragments act in concert with Aβ leading to an impaired synaptic transmission that provokes memory decline in AD.

Synaptic dysfunction might be the result of oxidative stress, since the main portion of mitochondria were co-localized with Aβ and ApoE fragments in synaptic compartments of AD mouse models. *In vitro* data have demonstrated that oxidative stress correlates with Aβ-induced ApoE fragmentation, since the reduction of ROS diminished ApoE fragments and rescued the viability of SPA4CT-expressing cells.

Moreover, it could be shown that synapse loss and axonopathy in APP/PS1KI mice are associated with accumulated ApoE fragments and Aβ peptides, coinciding with impaired autophagic processes.

The novel 5XFAD/PS19 mouse model develops a variety of AD pathological hallmarks like amyloid pathology, NFT-like structures, astrocytosis, reduced synapto-dendritic connections, neuron loss and hippocampal atrophy. Using this model it can be assumed that Aβ and ApoE fragments trigger tau hyperphosphorylation, leading to an aggravated AD pathology.

In conclusion, while extracellular Aβ only enhances full-length ApoE expression, intracellular Aβ might be able to induce ApoE proteolysis in humans and even in AD mouse models harboring endogenous ApoE. These fragments reflect the same pattern as seen in human AD and possibly act directly toxic or aggravate the Aβ-caused pathology in AD (Fig. 4.1).
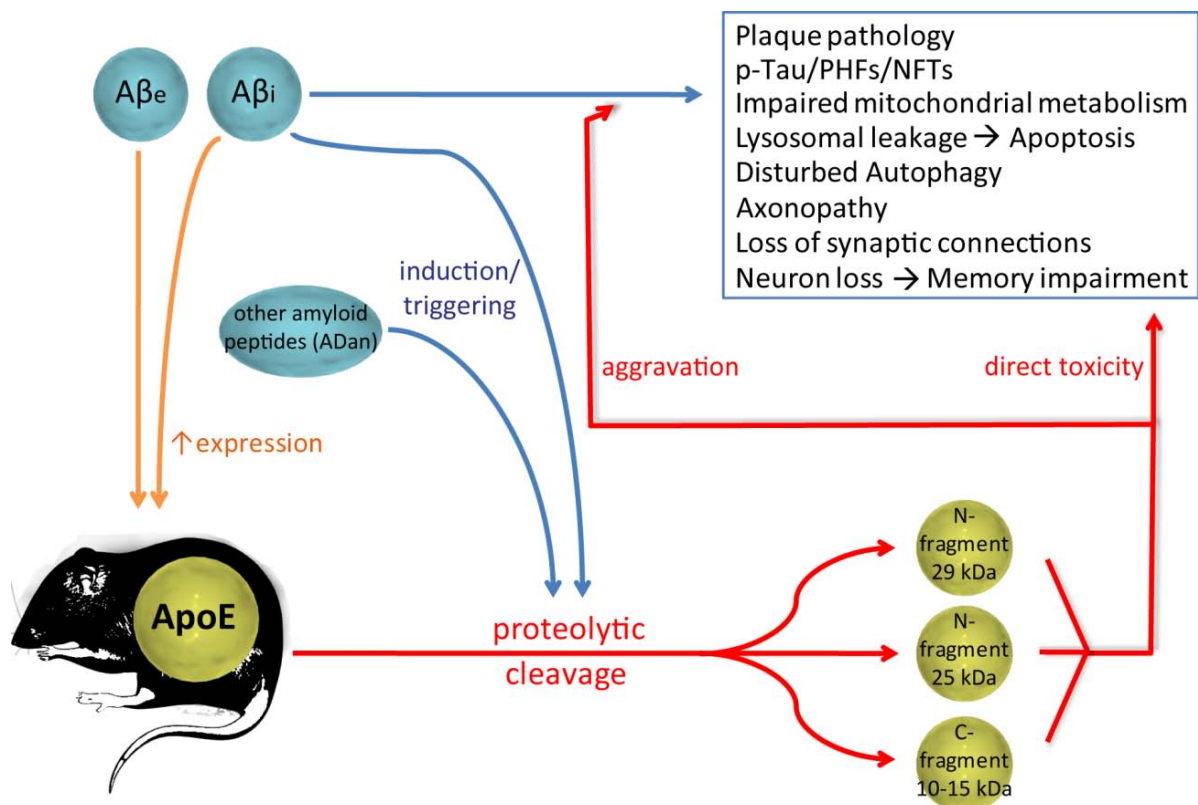
Figure 4.1. Scheme summarizing possible interactions between Aβ peptides, murine ApoE and tau in AD mouse models. Intracellular (Aβi) and/or extracellular Aβ (Aβe) peptides enhance the expression of murine ApoE, whereas Aβi and other amyloid peptides might further induce/trigger ApoE processing, resulting in the production of several fragments. These ApoE fragments may act toxic *per se* or aggravate Aβ-driven AD pathology.

5 Summary and Conclusions

In the first part of this thesis, it was investigated if the pGlu-modification changes the aggregation kinetics and enhances the toxicity of ABri and Dan peptides and which role they play regarding neuronal integrity *in vitro* and *in vivo*. Mutations in the BRI2 gene cause rare neurodegenerative diseases referred to as familial British dementia (FBD) and familial Danish dementia (FDD) (Vidal et al. 1999, Vidal et al. 2000). These disorders are both associated with neurodegeneration and extensive amyloid deposition in the central nervous system (Holton et al. 2001, Holton et al. 2002). FBD and FDD are distinguished from Alzheimer's disease (AD) and other dementing disorders by plaque deposition in the cerebellum and an accompanying cerebellar ataxia. In both lesions, 34-amino acid long peptides are generated (ABri/ADan), which share homology in their first 22 amino acids and completely differ at their C-termini (Ghiso et al. 2006). Amyloidogenic ABri and ADan peptides are mainly present as dimers, and exhibit to 60 % a post-translational pGlu-modification at position one (Ghiso et al. 2006).

So far, nothing was known about the immunohistochemical profile of pGlu-modified ABri and ADan peptides in brain tissue. Novel antibodies (AB77 and AB76-2) were generated that recognize the pGlu-modification at the N-terminus of ABri, ADan and CTF23 peptides, which are processed from non-mutant BRI2. In immunohistochemical approaches using AB77 and AB76-2, abundant pGlu-modified ABri and ADan peptides were detected in parenchymal and vascular deposits in human brain tissue of patients suffering from FBD and FDD, respectively, as well as age-dependent accumulation of pGlu-ADan in an FDD mouse model (ADanPP7). In addition, it was demonstrated that ADan aggregates intracellularly in synapses of the ADanPP7 mouse model suggesting an impairment of synaptic transmission that causes neuronal damage and neurodegeneration, resulting in cognitive decline in FDD as it has been shown for Aβ peptides in AD.

Thioflavin-T assays at physiological pH 7.0 revealed that in the case of ABri, the pGlu-modification leads to a more rapid aggregation profile than non-modified ABri, with both ABri and ADan peptides harboring an increased cytotoxicity when carrying a pGlu-modification at position one. Furthermore, the pGlu-modification even renders the non-aggregating CTF23 into an amyloidogenic peptide species that had less positive effects on

cell viability than unmodified CTF23, which is intracellularly redistributed under AD pathological conditions.

A novel, promising mouse model for FDD was generated and initially characterized that over-expresses ADan1Q-34 under the control of the neuron-specific Thy1-promoter. Pilot experiments have shown that, already at 6 months of age, these animals harbored deficits in working and spatial reference memory as well as an increased anxiety behavior reflecting some aspects of FDD and AD pathology. Furthermore, abundant intracellular ADan peptides were detected in different brain regions with high expression levels in the hippocampus and isocortex coinciding with astro- and microgliosis. As this model only expresses ADan, possible side-effects can be ruled out that probably originate from the over-expression of the precursor making this model suitable to investigate the toxic effects of ADan on neuronal integrity.

The second part of this thesis investigates the role of Apolipoprotein E (ApoE) fragments in the progression of AD pathology. In humans, three different ApoE isoforms exist, with ApoE4 being the most important genetic risk factor for AD, resulting in a younger average age of onset with a more rapid disease progression (Corder et al. 1993). ApoE4 is more susceptible to proteolysis and ApoE fragments have been shown to promote tau hyperphosphorylation and to facilitate mitochondrial dysfunction, which is accompanied by oxidative stress (Mahley et al. 2006). A plethora of studies deals with the effect of ApoE and its fragments on Aβ deposition and clearance, but it is completely unknown if Aβ in turn triggers ApoE fragmentation and the responsible mechanism behind it. Therefore, the influence of Aβ on human and murine ApoE expression and its proteolytical fragmentation was investigated *in vitro* and *in vivo* using cell-based, immunohistochemical and Western-blot assays.

To the author's knowledge, this is the first report demonstrating that endogenous murine ApoE becomes proteolytically processed with major fragment sizes of 10 to 15 kDa, which are putatively C-terminal fragments, as well as approximately 25 and 29 kDa representing possible N-terminal fragments in different AD mouse models. These fragments reflect the same pattern as observed in human brain tissue.

Transfected SH-SY5Y cells, which generate high amounts of intracellular Aβ, produced human ApoE fragments corresponding to human brains, whereas exogenous Aβ treatment on Ntera2 cells resulted in elevated full-length ApoE levels without any fragmentation.

Interestingly, the amount of ApoE fragments in human and mouse brains depended on amyloid load and increased with age in AD mouse models as well as in ADanPP7 mice developing age-dependent ADan amyloidosis, with 3xTG animals carrying low levels of intracellular Aβ not showing any fragmentation. This suggests that there could be another similarity between AD and FDD regarding ApoE proteolysis initiated by amyloid peptides in both dementias.

Corresponding to human data, young APP/PS1KI mice exhibited predominantly putative C-terminal ApoE fragments that are assigned to stabilize toxic Aβ oligomers and inhibit fibril formation (Wellnitz et al. 2005). Therefore, it can be hypothesized that the amyloid-associated processing of ApoE might reflect a critical early event in disease progression.

Full-length and murine ApoE fragments accumulate in synapses of 5XFAD and APP/PS1KI mice, in contrast to wild-type animals, coinciding with highest Aβ levels suggesting that ApoE gets mislocalized to synapses. This indicates that synaptosomal ApoE fragments act in concert with Aβ, resulting probably in reduced synapto-dendritic connections and impaired synaptic transmission.

Synaptic compartments of APP/PS1KI and 5XFAD mice contained highest amounts of mitochondria accompanied by accumulated Aβ peptides and murine ApoE fragments. Scavenging reactive oxygen species by N-acetyl-L-Cysteine application reduced ApoE proteolysis and restored the cell viability of SH-SY5Y cells producing high amounts of intracellular Aβ, without altering full-length ApoE levels and endogenous APP metabolism. Therefore, it may be assumed that intracellular accumulation of Aβ and ApoE fragments trigger oxidative stress, which in turn drives ApoE proteolysis, leading to synaptic dysfunction.

It could be further shown, that the axonopathy phenotype and the observed synapse loss in the APP/PS1KI model correlates best with the PS1 gene dose and Aβ load, but also with the amounts of fragmented murine ApoE. It is likely that ApoE fragments and Aβ accumulate independently from APP in axons and induce a disturbed trafficking leading to axonal degeneration.

Under physiological conditions, ApoE controls the microtubule stability by binding to tau protein (Lovestone et al. 1996). Disturbances in cytoskeletal structures are caused by hyperphosphorylation of tau forming intraneuronal NFTs in neurons that is triggered by the

neuron-specific effect of ApoE4 (Huang et al. 2004). The novel generated 5XFAD/PS19 mouse model recapitulates a variety of AD pathological hallmarks including amyloid plaque pathology, tau hyperphosphorylation, chronic inflammation, reduction of synapto-dendritic connections, neuron loss and hippocampal atrophy. Supporting the amyloid cascade hypothesis, AD-like pathology was drastically aggravated in trigenic mice that combine high Aβ levels and mutant tau. Furthermore, ApoE fragments were equally detected in 5XFAD and 5XFAD/PS19 mice, whereas ApoE proteolysis was almost lacking in PS19 mice confirming that this processing is induced by Aβ. This result also demonstrates that Aβ-induced ApoE proteolysis represents an upstream event, with a possible interaction of Aβ and ApoE fragments in triggering tau hyperphosphorylation leading to an aggravated AD pathology.

In conclusion, ApoE fragmentation is putatively linked directly to intraneuronal amyloid deposits, whereas extracellular Aβ leads to enhanced expression of full-length ApoE, representing a possible protective mechanism towards amyloid clearance. The fragmentation pattern of murine ApoE in dementia mouse and cell models recapitulates the human situation and might play a crucial role in AD pathology progression.

6 Bibliography

Acero, G., Manoutcharian, K., Vasilevko, V., Munguia, M. E., Govezensky, T., Coronas, G., Luz-Madrigal, A., Cribbs, D. H. & Gevorkian, G. 2009. Immunodominant epitope and properties of pyroglutamate-modified Abeta-specific antibodies produced in rabbits. *J Neuroimmunol,* 213**,** 39-46.

Aizawa, Y., Fukatsu, R., Takamaru, Y., Tsuzuki, K., Chiba, H., Kobayashi, K., Fujii, N. & Takahata, N. 1997. Amino-terminus truncated apolipoprotein E is the major species in amyloid deposits in Alzheimer's disease-affected brains: a possible role for apolipoprotein E in Alzheimer's disease. *Brain Res,* 768**,** 208-14.

Akiyama, H., Kondo, H., Arai, T., Ikeda, K., Kato, M., Iseki, E., Schwab, C. & Mcgeer, P. L. 2004. Expression of BRI, the normal precursor of the amyloid protein of familial British dementia, in human brain. *Acta Neuropathol,* 107**,** 53-8.

Alexandru, A., Jagla, W., Graubner, S., Becker, A., Bauscher, C., Kohlmann, S., Sedlmeier, R., Raber, K. A., Cynis, H., Ronicke, R., Reymann, K. G., Petrasch-Parwez, E., Hartlage-Rubsamen, M., Waniek, A., Rossner, S., Schilling, S., Osmand, A. P., Demuth, H. U. & Von Horsten, S. 2011. Selective hippocampal neurodegeneration in transgenic mice expressing small amounts of truncated Abeta is induced by pyroglutamate-Abeta formation. *J Neurosci,* 31**,** 12790-801.

Allinson, T. M., Parkin, E. T., Turner, A. J. & Hooper, N. M. 2003. ADAMs family members as amyloid precursor protein alpha-secretases. *J Neurosci Res,* 74**,** 342-52.

Anderson, J. P., Esch, F. S., Keim, P. S., Sambamurti, K., Lieberburg, I. & Robakis, N. K. 1991. Exact cleavage site of Alzheimer amyloid precursor in neuronal PC-12 cells. *Neurosci Lett,* 128**,** 126-8.

Andrews, P. W., Damjanov, I., Simon, D., Banting, G. S., Carlin, C., Dracopoli, N. C. & Fogh, J. 1984. Pluripotent embryonal carcinoma clones derived from the human teratocarcinoma cell line Tera-2. Differentiation in vivo and in vitro. *Lab Invest,* 50**,** 147-62.

Annaert, W. & De Strooper, B. 2002. A cell biological perspective on Alzheimer's disease. *Annu Rev Cell Dev Biol,* 18**,** 25-51.

Aoki, K., Uchihara, T., Sanjo, N., Nakamura, A., Ikeda, K., Tsuchiya, K. & Wakayama, Y. 2003. Increased expression of neuronal apolipoprotein E in human brain with cerebral infarction. *Stroke,* 34**,** 875-80.

Apelt, J. & Schliebs, R. 2001. Beta-amyloid-induced glial expression of both pro- and anti-inflammatory cytokines in cerebral cortex of aged transgenic Tg2576 mice with Alzheimer plaque pathology. *Brain Res,* 894**,** 21-30.

Arendash, G. W., King, D. L., Gordon, M. N., Morgan, D., Hatcher, J. M., Hope, C. E. & Diamond, D. M. 2001. Progressive, age-related behavioral impairments in transgenic mice carrying both mutant amyloid precursor protein and presenilin-1 transgenes. *Brain Res.,* 891**,** 42-53.

Arnold, S. E., Hyman, B. T., Flory, J., Damasio, A. R. & Van Hoesen, G. W. 1991. The topographical and neuroanatomical distribution of neurofibrillary tangles and neuritic plaques in the cerebral cortex of patients with Alzheimer's disease. *Cereb Cortex.,* 1**,** 103-16.

Arold, S., Sullivan, P., Bilousova, T., Teng, E., Miller, C. A., Poon, W. W., Vinters, H. V., Cornwell, L. B., Saing, T., Cole, G. M. & Gylys, K. H. 2012. Apolipoprotein E level and cholesterol are associated with reduced synaptic amyloid beta in Alzheimer's disease and apoE TR mouse cortex. *Acta Neuropathol,* 123**,** 39-52.

Arriagada, P. V., Growdon, J. H., Hedley-Whyte, E. T. & Hyman, B. T. 1992. Neurofibrillary tangles but not senile plaques parallel duration and severity of Alzheimer's disease. *Neurology,* 42**,** 631-9.

Artavanis-Tsakonas, S., Rand, M. D. & Lake, R. J. 1999. Notch signaling: cell fate control and signal integration in development. *Science,* 284**,** 770-6.

Aruoma, O. I., Halliwell, B., Hoey, B. M. & Butler, J. 1989. The antioxidant action of N-acetylcysteine: its reaction with hydrogen peroxide, hydroxyl radical, superoxide, and hypochlorous acid. *Free Radic Biol Med,* 6**,** 593-7.

Bäckman, L., Jones, S., Berger, A. K., Laukka, E. J. & Small, B. J. 2004. Multiple cognitive deficits during the transition to Alzheimer's disease. *J Intern Med,* 256**,** 195-204.

Bailey, J. A., Maloney, B., Ge, Y. W. & Lahiri, D. K. 2011. Functional activity of the novel Alzheimer's amyloid beta-peptide interacting domain (AbetaID) in the APP and BACE1 promoter sequences and implications in activating apoptotic genes and in amyloidogenesis. *Gene,* 488**,** 13-22.

Bannerman, D. M., Rawlins, J. N., Mchugh, S. B., Deacon, R. M., Yee, B. K., Bast, T., Zhang, W. N., Pothuizen, H. H. & Feldon, J. 2004. Regional dissociations within the hippocampus--memory and anxiety. *Neurosci Biobehav Rev,* 28**,** 273-83.

Bao, F., Arai, H., Matsushita, S., Higuchi, S. & Sasaki, H. 1996. Expression of apolipoprotein E in normal and diverse neurodegenerative disease brain. *Neuroreport,* 7**,** 1733-9.

Bard, F., Cannon, C., Barbour, R., Burke, R. L., Games, D., Grajeda, H., Guido, T., Hu, K., Huang, J., Johnson-Wood, K., Khan, K., Kholodenko, D., Lee, M., Lieberburg, I., Motter, R., Nguyen, M., Soriano, F., Vasquez, N., Weiss, K., Welch, B., Seubert, P., Schenk, D. & Yednock, T. 2000. Peripherally administered antibodies against amyloid beta-peptide enter the central nervous system and reduce pathology in a mouse model of Alzheimer disease. *Nat Med,* 6**,** 916-9.

Barrientos, A., Barros, M. H., Valnot, I., Rotig, A., Rustin, P. & Tzagoloff, A. 2002. Cytochrome oxidase in health and disease. *Gene,* 286**,** 53-63.

Baruch-Suchodolsky, R. & Fischer, B. 2009. Abeta40, either soluble or aggregated, is a remarkably potent antioxidant in cell-free oxidative systems. *Biochemistry,* 48**,** 4354-70.

Beaven, S. W. & Tontonoz, P. 2006. Nuclear receptors in lipid metabolism: targeting the heart of dyslipidemia. *Annu Rev Med,* 57**,** 313-29.

Beffert, U., Cohn, J. S., Petit-Turcotte, C., Tremblay, M., Aumont, N., Ramassamy, C., Davignon, J. & Poirier, J. 1999. Apolipoprotein E and beta-amyloid levels in the hippocampus and frontal cortex of Alzheimer's disease subjects are disease-related and apolipoprotein E genotype dependent. *Brain Res,* 843**,** 87-94.

Bellosta, S., Nathan, B. P., Orth, M., Dong, L. M., Mahley, R. W. & Pitas, R. E. 1995. Stable expression and secretion of apolipoproteins E3 and E4 in mouse neuroblastoma cells produces differential effects on neurite outgrowth. *J Biol Chem,* 270**,** 27063-71.

Benilova, I., Karran, E. & De Strooper, B. 2012. The toxic Abeta oligomer and Alzheimer's disease: an emperor in need of clothes. *Nat Neurosci,* 15**,** 349-57.

Bibel, M., Richter, J., Schrenk, K., Tucker, K. L., Staiger, V., Korte, M., Goetz, M. & Barde, Y. A. 2004. Differentiation of mouse embryonic stem cells into a defined neuronal lineage. *Nat Neurosci,* 7**,** 1003-9.

Biedler, J. L., Helson, L. & Spengler, B. A. 1973. Morphology and growth, tumorigenicity, and cytogenetics of human neuroblastoma cells in continuous culture. *Cancer Res,* 33**,** 2643-52.

Blennow, K., De Leon, M. J. & Zetterberg, H. 2006. Alzheimer's disease. *Lancet,* 368**,** 387-403.

Bogoyevitch, M. A., Boehm, I., Oakley, A., Ketterman, A. J. & Barr, R. K. 2004. Targeting the JNK MAPK cascade for inhibition: basic science and therapeutic potential. *Biochim Biophys Acta,* 1697**,** 89-101.

Bolmont, T., Clavaguera, F., Meyer-Luehmann, M., Herzig, M. C., Radde, R., Staufenbiel, M., Lewis, J., Hutton, M., Tolnay, M. & Jucker, M. 2007. Induction of tau pathology by intracerebral infusion of amyloid-beta -containing brain extract and by amyloid-beta deposition in APP x Tau transgenic mice. *Am J Pathol,* 171**,** 2012-20.

Braak, E., Griffing, K., Arai, K., Bohl, J., Bratzke, H. & Braak, H. 1999. Neuropathology of Alzheimer's disease: what is new since A. Alzheimer? *Eur Arch Psychiatry Clin Neurosci,* 249 Suppl 3**,** 14-22.

Braak, H. & Braak, E. 1991. Neuropathological stageing of Alzheimer-related changes. *Acta Neuropathol (Berl),* 82**,** 239-59.

Braak, H. & Braak, E. 1995. Staging of Alzheimer's disease-related neurofibrillary changes. *Neurobiol Aging,* 16**,** 271-8; discussion 278-84.

Braak, H. & Braak, E. 1997. Frequency of stages of Alzheimer-related lesions in different age categories. *Neurobiol Aging,* 18**,** 351-7.

Brecht, W. J., Harris, F. M., Chang, S., Tesseur, I., Yu, G. Q., Xu, Q., Dee Fish, J., Wyss-Coray, T., Buttini, M., Mucke, L., Mahley, R. W. & Huang, Y. 2004. Neuron-specific apolipoprotein e4 proteolysis is associated with increased tau phosphorylation in brains of transgenic mice. *J Neurosci,* 24**,** 2527-34.

Breyhan, H., Wirths, O., Duan, K., Marcello, A., Rettig, J. & Bayer, T. A. 2009. APP/PS1KI bigenic mice develop early synaptic deficits and hippocampus atrophy. *Acta Neuropathol,* 117**,** 677-685.

Buée, L., Bussiere, T., Buee-Scherrer, V., Delacourte, A. & Hof, P. R. 2000. Tau protein isoforms, phosphorylation and role in neurodegenerative disorders. *Brain Res Brain Res Rev,* 33**,** 95-130.

Buntinx, M., Vanderlocht, J., Hellings, N., Vandenabeele, F., Lambrichts, I., Raus, J., Ameloot, M., Stinissen, P. & Steels, P. 2003. Characterization of three human oligodendroglial cell lines as a model to study oligodendrocyte injury: morphology and oligodendrocyte-specific gene expression. *J Neurocytol,* 32**,** 25-38.

Busby, W. H., Jr., Quackenbush, G. E., Humm, J., Youngblood, W. W. & Kizer, J. S. 1987. An enzyme(s) that converts glutaminyl-peptides into pyroglutamyl-peptides. Presence in pituitary, brain, adrenal medulla, and lymphocytes. *J Biol Chem,* 262**,** 8532-6.

Busche, M. A., Chen, X., Henning, H. A., Reichwald, J., Staufenbiel, M., Sakmann, B. & Konnerth, A. 2012. Critical role of soluble amyloid-beta for early hippocampal hyperactivity in a mouse model of Alzheimer's disease. *Proc Natl Acad Sci U S A,* 109**,** 8740-5.

Butterfield, D. A., Castegna, A., Lauderback, C. M. & Drake, J. 2002. Evidence that amyloid beta-peptide-induced lipid peroxidation and its sequelae in Alzheimer's disease brain contribute to neuronal death. *Neurobiol Aging,* 23**,** 655-64.

Buttini, M., Orth, M., Bellosta, S., Akeefe, H., Pitas, R. E., Wyss-Coray, T., Mucke, L. & Mahley, R. W. 1999. Expression of human apolipoprotein E3 or E4 in the brains of Apoe-/-mice: isoform-specific effects on neurodegeneration. *J Neurosci,* 19**,** 4867-80.

Buttini, M., Yu, G. Q., Shockley, K., Huang, Y., Jones, B., Masliah, E., Mallory, M., Yeo, T., Longo, F. M. & Mucke, L. 2002. Modulation of Alzheimer-like synaptic and cholinergic deficits in transgenic mice by human apolipoprotein E depends on isoform, aging, and overexpression of amyloid beta peptides but not on plaque formation. *J Neurosci,* 22**,** 10539-48.

Cao, G., Bales, K. R., Demattos, R. B. & Paul, S. M. 2007. Liver X receptor-mediated gene regulation and cholesterol homeostasis in brain: relevance to Alzheimer's disease therapeutics. *Curr Alzheimer Res,* 4**,** 179-84.

Cao, X. & Sudhof, T. C. 2001. A transcriptionally [correction of transcriptively] active complex of APP with Fe65 and histone acetyltransferase Tip60. *Science,* 293**,** 115-20.

Carlesimo, G. A. & Oscar-Berman, M. 1992. Memory deficits in Alzheimer's patients: a comprehensive review. *Neuropsychol Rev,* 3**,** 119-69.

Caroni, P. 1997. Overexpression of growth-associated proteins in the neurons of adult transgenic mice. *J Neurosci Methods,* 71**,** 3-9.

Casas, C., Sergeant, N., Itier, J. M., Blanchard, V., Wirths, O., Van Der Kolk, N., Vingtdeux, V., Van De Steeg, E., Ret, G., Canton, T., Drobecq, H., Clark, A., Bonici, B., Delacourte, A., Benavides, J., Schmitz, C., Tremp, G., Bayer, T. A., Benoit, P. & Pradier, L. 2004. Massive CA1/2 neuronal loss with intraneuronal and N-terminal truncated Abeta42 accumulation in a novel Alzheimer transgenic model. *Am J Pathol,* 165**,** 1289-300.

Cataldo, A. M., Peterhoff, C. M., Troncoso, J. C., Gomez-Isla, T., Hyman, B. T. & Nixon, R. A. 2000. Endocytic pathway abnormalities precede amyloid beta deposition in sporadic Alzheimer's disease and Down syndrome: differential effects of APOE genotype and presenilin mutations. *Am J Pathol,* 157**,** 277-86.

Chabrier, M. A., Blurton-Jones, M., Agazaryan, A. A., Nerhus, J. L., Martinez-Coria, H. & Laferla, F. M. 2012. Soluble abeta promotes wild-type tau pathology in vivo. *J Neurosci,* 32**,** 17345-50.

Chang, S., Ran Ma, T., Miranda, R. D., Balestra, M. E., Mahley, R. W. & Huang, Y. 2005. Lipid- and receptor-binding regions of apolipoprotein E4 fragments act in concert to cause mitochondrial dysfunction and neurotoxicity. *Proc Natl Acad Sci U S A,* 102**,** 18694-9.

Chen, X. H., Siman, R., Iwata, A., Meaney, D. F., Trojanowski, J. Q. & Smith, D. H. 2004. Long-term accumulation of amyloid-beta, beta-secretase, presenilin-1, and caspase-3 in damaged axons following brain trauma. *Am J Pathol,* 165**,** 357-71.

Chetelat, G., Villemagne, V. L., Bourgeat, P., Pike, K. E., Jones, G., Ames, D., Ellis, K. A., Szoeke, C., Martins, R. N., O'keefe, G. J., Salvado, O., Masters, C. L. & Rowe, C. C. 2010. Relationship between atrophy and beta-amyloid deposition in Alzheimer disease. *Ann Neurol,* 67**,** 317-24.

Choi, S. I., Vidal, R., Frangione, B. & Levy, E. 2004. Axonal transport of British and Danish amyloid peptides via secretory vesicles. *Faseb J,* 18**,** 373-5.

Christensen, D. Z., Bayer, T. A. & Wirths, O. 2010a. Intracellular Abeta triggers neuron loss in the cholinergic system of the APP/PS1KI mouse model of Alzheimer's disease. *Neurobiol Aging,* 31**,** 1153-1163.

Christensen, D. Z., Kraus, S. L., Flohr, A., Cotel, M. C., Wirths, O. & Bayer, T. A. 2008. Transient intraneuronal Abeta rather than extracellular plaque pathology correlates with neuron loss in the frontal cortex of APP/PS1KI mice. *Acta Neuropathol,* 116**,** 647-55.

Christensen, D. Z., Schneider-Axmann, T., Lucassen, P. J., Bayer, T. A. & Wirths, O. 2010b. Accumulation of intraneuronal Abeta correlates with ApoE4 genotype. *Acta Neuropathol,* 119**,** 555-566.

Chung, J. A. & Cummings, J. L. 2000. Neurobehavioral and neuropsychiatric symptoms in Alzheimer's disease: characteristics and treatment. *Neurol Clin,* 18**,** 829-46.

Citron, M., Oltersdorf, T., Haass, C., Mcconlogue, L., Hung, A. Y., Seubert, P., Vigo-Pelfrey, C., Lieberburg, I. & Selkoe, D. J. 1992. Mutation of the beta-amyloid precursor protein in familial Alzheimer's disease increases beta-protein production. *Nature,* 360**,** 672-4.

Citron, M., Westaway, D., Xia, W., Carlson, G., Diehl, T., Levesque, G., Johnson-Wood, K., Lee, M., Seubert, P., Davis, A., Kholodenko, D., Motter, R., Sherrington, R., Perry, B., Yao, H., Strome, R., Lieberburg, I., Rommens, J., Kim, S., Schenk, D., Fraser, P., St George Hyslop, P. & Selkoe, D. J. 1997. Mutant presenilins of Alzheimer's disease increase production of 42-residue amyloid beta-protein in both transfected cells and transgenic mice. *Nat Med,* 3**,** 67-72.

Colangelo, V., Schurr, J., Ball, M. J., Pelaez, R. P., Bazan, N. G. & Lukiw, W. J. 2002. Gene expression profiling of 12633 genes in Alzheimer hippocampal CA1: transcription and neurotrophic factor down-regulation and up-regulation of apoptotic and pro-inflammatory signaling. *J Neurosci Res,* 70**,** 462-73.

Coleman, M. 2005. Axon degeneration mechanisms: commonality amid diversity. *Nat Rev Neurosci,* 6**,** 889-98.

Coomaraswamy, J., Kilger, E., Wolfing, H., Schafer, C., Kaeser, S. A., Wegenast-Braun, B. M., Hefendehl, J. K., Wolburg, H., Mazzella, M., Ghiso, J., Goedert, M., Akiyama, H., Garcia-Sierra, F., Wolfer, D. P., Mathews, P. M. & Jucker, M. 2010. Modeling familial Danish dementia in mice supports the concept of the amyloid hypothesis of Alzheimer's disease. *Proc Natl Acad Sci U S A,* 107**,** 7969-74.

Corder, E. H., Saunders, A. M., Strittmatter, W. J., Schmechel, D. E., Gaskell, P. C., Small, G. W., Roses, A. D., Haines, J. L. & Pericak-Vance, M. A. 1993. Gene dose of apolipoprotein E type 4 allele and the risk of Alzheimer's disease in late onset families. *Science,* 261**,** 921-3.

Cotel, M. C., Jawhar, S., Christensen, D. Z., Bayer, T. A. & Wirths, O. 2012. Environmental enrichment fails to rescue working memory deficits, neuron loss, and neurogenesis in APP/PS1KI mice. *Neurobiol Aging,* 33**,** 96-107.

Cras, P., Kawai, M., Lowery, D., Gonzalez-Dewhitt, P., Greenberg, B. & Perry, G. 1991. Senile plaque neurites in Alzheimer disease accumulate amyloid precursor protein. *Proc Natl Acad Sci U S A,* 88**,** 7552-6.

Cynis, H., Scheel, E., Saido, T. C., Schilling, S. & Demuth, H. U. 2008. Amyloidogenic Processing of Amyloid Precursor Protein: Evidence of a Pivotal Role of Glutaminyl Cyclase in Generation of Pyroglutamate-Modified Amyloid-beta. *Biochemistry,* 47**,** 7405-13.

Cynis, H., Schilling, S., Bodnar, M., Hoffmann, T., Heiser, U., Saido, T. C. & Demuth, H. U. 2006. Inhibition of glutaminyl cyclase alters pyroglutamate formation in mammalian cells. *Biochim Biophys Acta,* 1764**,** 1618-25.

D'arrigo, C., Tabaton, M. & Perico, A. 2009. N-terminal truncated pyroglutamyl beta amyloid peptide Abetapy3-42 shows a faster aggregation kinetics than the full-length Abeta1-42. *Biopolymers,* 91**,** 861-73.

Dafnis, I., Stratikos, E., Tzinia, A., Tsilibary, E. C., Zannis, V. I. & Chroni, A. 2011. An apolipoprotein E4 fragment can promote intracellular accumulation of amyloid peptide beta 42. *J Neurochem,* 115**,** 873-84.

Dassie, E., Andrews, M. R., Bensadoun, J. C., Cacquevel, M., Schneider, B. L., Aebischer, P., Wouters, F. S., Richardson, J. C., Hussain, I., Howlett, D. R., Spillantini, M. G. &

Fawcett, J. W. 2013. Focal expression of adeno-associated viral-mutant tau induces widespread impairment in an APP mouse model. *Neurobiol Aging, 34,* 1355-68.

Davis, J., Cribbs, D. H., Cotman, C. W. & Van Nostrand, W. E. 1999. Pathogenic amyloid beta-protein induces apoptosis in cultured human cerebrovascular smooth muscle cells. *Amyloid,* 6**,** 157-64.

De Vos, K. J., Grierson, A. J., Ackerley, S. & Miller, C. C. 2008. Role of axonal transport in neurodegenerative diseases. *Annu Rev Neurosci,* 31**,** 151-73.

Deleersnijder, W., Hong, G., Cortvrindt, R., Poirier, C., Tylzanowski, P., Pittois, K., Van Marck, E. & Merregaert, J. 1996. Isolation of markers for chondro-osteogenic differentiation using cDNA library subtraction. Molecular cloning and characterization of a gene belonging to a novel multigene family of integral membrane proteins. *J Biol Chem,* 271**,** 19475-82.

Dergunov, A. D., Smirnova, E. A., Merched, A., Visvikis, S., Siest, G., Yakushkin, V. V. & Tsibulsky, V. 2000. Conformation of apolipoprotein E both in free and in lipid-bound form may determine the avidity of triglyceride-rich lipoproteins to the LDL receptor: structural and kinetic study. *Biochim Biophys Acta,* 1484**,** 14-28.

Detoledo-Morrell, L., Stoub, T. R., Bulgakova, M., Wilson, R. S., Bennett, D. A., Leurgans, S., Wuu, J. & Turner, D. A. 2004. MRI-derived entorhinal volume is a good predictor of conversion from MCI to AD. *Neurobiol Aging,* 25**,** 1197-203.

Dong, L. M. & Weisgraber, K. H. 1996. Human apolipoprotein E4 domain interaction. Arginine 61 and glutamic acid 255 interact to direct the preference for very low density lipoproteins. *J Biol Chem,* 271**,** 19053-7.

Dong, L. M., Wilson, C., Wardell, M. R., Simmons, T., Mahley, R. W., Weisgraber, K. H. & Agard, D. A. 1994. Human apolipoprotein E. Role of arginine 61 in mediating the lipoprotein preferences of the E3 and E4 isoforms. *J Biol Chem,* 269**,** 22358-65.

Du, H., Guo, L., Yan, S., Sosunov, A. A., Mckhann, G. M. & Yan, S. S. 2010. Early deficits in synaptic mitochondria in an Alzheimer's disease mouse model. *Proc Natl Acad Sci U S A,* 107**,** 18670-5.

Duce, J. A., Tsatsanis, A., Cater, M. A., James, S. A., Robb, E., Wikhe, K., Leong, S. L., Perez, K., Johanssen, T., Greenough, M. A., Cho, H. H., Galatis, D., Moir, R. D., Masters, C. L., Mclean, C., Tanzi, R. E., Cappai, R., Barnham, K. J., Ciccotosto, G. D., Rogers, J. T. & Bush, A. I. 2010. Iron-export ferroxidase activity of beta-amyloid precursor protein is inhibited by zinc in Alzheimer's disease. *Cell,* 142**,** 857-67.

Duyckaerts, C., Delatour, B. & Potier, M. C. 2009. Classification and basic pathology of Alzheimer disease. *Acta Neuropathol,* 118**,** 5-36.

Dyrks, T., Dyrks, E., Masters, C. & Beyreuther, K. 1992. Membrane inserted APP fragments containing the beta A4 sequence of Alzheimer's disease do not aggregate. *FEBS Lett,* 309**,** 20-4.

Dyrks, T., Weidemann, A., Multhaup, G., Salbaum, J. M., Lemaire, H. G., Kang, J., Muller-Hill, B., Masters, C. L. & Beyreuther, K. 1988. Identification, transmembrane orientation and biogenesis of the amyloid A4 precursor of Alzheimer's disease. *Embo J,* 7**,** 949-57.

El-Agnaf, O. M., Sheridan, J. M., Sidera, C., Siligardi, G., Hussain, R., Haris, P. I. & Austen, B. M. 2001. Effect of the disulfide bridge and the C-terminal extension on the oligomerization of the amyloid peptide ABri implicated in familial British dementia. *Biochemistry,* 40**,** 3449-57.

Fenderson, B. A., Andrews, P. W., Nudelman, E., Clausen, H. & Hakomori, S. 1987. Glycolipid core structure switching from globo- to lacto- and ganglio-series during retinoic acid-

induced differentiation of TERA-2-derived human embryonal carcinoma cells. *Dev Biol,* 122**,** 21-34.

Fischer, W. H. & Spiess, J. 1987. Identification of a mammalian glutaminyl cyclase converting glutaminyl into pyroglutamyl peptides. *Proc Natl Acad Sci U S A,* 84**,** 3628-32.

Fisher, C. A. & Ryan, R. O. 1999. Lipid binding-induced conformational changes in the N-terminal domain of human apolipoprotein E. *J Lipid Res,* 40**,** 93-9.

Fleischer, A., Ayllon, V., Dumoutier, L., Renauld, J. C. & Rebollo, A. 2002. Proapoptotic activity of ITM2B(s), a BH3-only protein induced upon IL-2-deprivation which interacts with Bcl-2. *Oncogene,* 21**,** 3181-9.

Folstein, M. F., Folstein, S. E. & Mchugh, P. R. 1975. "Mini-mental state". A practical method for grading the cognitive state of patients for the clinician. *J Psychiatr Res,* 12**,** 189-98.

Förstl, H. & Kurz, A. 1999. Clinical features of Alzheimer's disease. *Eur Arch Psychiatry Clin Neurosci,* 249**,** 288-90.

Fossgreen, A., Bruckner, B., Czech, C., Masters, C. L., Beyreuther, K. & Paro, R. 1998. Transgenic Drosophila expressing human amyloid precursor protein show gamma-secretase activity and a blistered-wing phenotype. *Proc Natl Acad Sci U S A,* 95**,** 13703-8.

Fotinopoulou, A., Tsachaki, M., Vlavaki, M., Poulopoulos, A., Rostagno, A., Frangione, B., Ghiso, J. & Efthimiopoulos, S. 2005. BRI2 interacts with amyloid precursor protein (APP) and regulates amyloid beta (Abeta) production. *J Biol Chem,* 280**,** 30768-72.

Frank, E. M. 1994. Effect of Alzheimer's disease on communication function. *J S C Med Assoc,* 90**,** 417-23.

Frisoni, G. B., Rozzini, L., Gozzetti, A., Binetti, G., Zanetti, O., Bianchetti, A., Trabucchi, M. & Cummings, J. L. 1999. Behavioral syndromes in Alzheimer's disease: description and correlates. *Dement Geriatr Cogn Disord,* 10**,** 130-8.

Games, D., Adams, D., Alessandrini, R., Barbour, R., Berthelette, P., Blackwell, C., Carr, T., Clemens, J., Donaldson, T., Gillespie, F. & Et Al. 1995. Alzheimer-type neuropathology in transgenic mice overexpressing V717F beta-amyloid precursor protein. *Nature,* 373**,** 523-7.

Garringer, H. J., Murrell, J., D'adamio, L., Ghetti, B. & Vidal, R. 2010. Modeling familial British and Danish dementia. *Brain Struct Funct,* 214**,** 235-44.

Garwood, C. J., Pooler, A. M., Atherton, J., Hanger, D. P. & Noble, W. 2011. Astrocytes are important mediators of Abeta-induced neurotoxicity and tau phosphorylation in primary culture. *Cell Death Dis,* 2**,** e167.

Ghetti, B., Tagliavini, F., Masters, C. L., Beyreuther, K., Giaccone, G., Verga, L., Farlow, M. R., Conneally, P. M., Dlouhy, S. R., Azzarelli, B. & Et Al. 1989. Gerstmann-Straussler-Scheinker disease. II. Neurofibrillary tangles and plaques with PrP-amyloid coexist in an affected family. *Neurology,* 39**,** 1453-61.

Ghiso, J., Rostagno, A., Tomidokoro, Y., Lashley, T., Bojsen-Moller, M., Braendgaard, H., Plant, G., Holton, J., Lal, R., Revesz, T. & Frangione, B. 2006. Genetic alterations of the BRI2 gene: familial British and Danish dementias. *Brain Pathol,* 16**,** 71-9.

Giaccone, G., Mangieri, M., Capobianco, R., Limido, L., Hauw, J. J., Haik, S., Fociani, P., Bugiani, O. & Tagliavini, F. 2008. Tauopathy in human and experimental variant Creutzfeldt-Jakob disease. *Neurobiol Aging,* 29**,** 1864-73.

Giaccone, G., Tagliavini, F., Verga, L., Frangione, B., Farlow, M. R., Bugiani, O. & Ghetti, B. 1990. Neurofibrillary tangles of the Indiana kindred of Gerstmann-Straussler-Scheinker disease share antigenic determinants with those of Alzheimer disease. *Brain Res,* 530**,** 325-9.

Gibson, G., El-Agnaf, O. M., Anwar, Z., Sidera, C., Isbister, A. & Austen, B. M. 2005. Structure and neurotoxicity of novel amyloids derived from the BRI gene. *Biochem Soc Trans,* 33**,** 1111-2.

Götz, J., Chen, F., Van Dorpe, J. & Nitsch, R. M. 2001. Formation of neurofibrillary tangles in P301l tau transgenic mice induced by Abeta 42 fibrils. *Science,* 293**,** 1491-5.

Graham, F. L., Smiley, J., Russell, W. C. & Nairn, R. 1977. Characteristics of a human cell line transformed by DNA from human adenovirus type 5. *J Gen Virol,* 36**,** 59-74.

Griffiths, R. A., Mortimer, T. F., Oppenheimer, D. R. & Spalding, J. M. 1982. Congophilic angiopathy of the brain: a clinical and pathological report on two siblings. *J Neurol Neurosurg Psychiatry,* 45**,** 396-408.

Grueninger, F., Bohrmann, B., Czech, C., Ballard, T. M., Frey, J. R., Weidensteiner, C., Von Kienlin, M. & Ozmen, L. 2010. Phosphorylation of Tau at S422 is enhanced by Abeta in TauPS2APP triple transgenic mice. *Neurobiol Dis,* 37**,** 294-306.

Guntert, A., Dobeli, H. & Bohrmann, B. 2006. High sensitivity analysis of amyloid-beta peptide composition in amyloid deposits from human and PS2APP mouse brain. *Neuroscience,* 143**,** 461-75.

Gyure, K. A., Durham, R., Stewart, W. F., Smialek, J. E. & Troncoso, J. C. 2001. Intraneuronal abeta-amyloid precedes development of amyloid plaques in Down syndrome. *Arch Pathol Lab Med,* 125**,** 489-92.

Haass, C., Hung, A. Y., Schlossmacher, M. G., Teplow, D. B. & Selkoe, D. J. 1993. beta-Amyloid peptide and a 3-kDa fragment are derived by distinct cellular mechanisms. *J Biol Chem,* 268**,** 3021-4.

Haass, C., Hung, A. Y., Selkoe, D. J. & Teplow, D. B. 1994. Mutations associated with a locus for familial Alzheimer's disease result in alternative processing of amyloid beta-protein precursor. *J Biol Chem,* 269**,** 17741-8.

Haass, C., Kaether, C., Thinakaran, G. & Sisodia, S. 2012. Trafficking and Proteolytic Processing of APP. *Cold Spring Harb Perspect Med,* 2**,** a006270.

Haass, C., Koo, E. H., Mellon, A., Hung, A. Y. & Selkoe, D. J. 1992. Targeting of cell-surface beta-amyloid precursor protein to lysosomes: alternative processing into amyloid-bearing fragments. *Nature,* 357**,** 500-3.

Haass, C. & Selkoe, D. J. 2007. Soluble protein oligomers in neurodegeneration: lessons from the Alzheimer's amyloid beta-peptide. *Nat Rev Mol Cell Biol,* 8**,** 101-12.

Han, S. H., Einstein, G., Weisgraber, K. H., Strittmatter, W. J., Saunders, A. M., Pericak-Vance, M., Roses, A. D. & Schmechel, D. E. 1994. Apolipoprotein E is localized to the cytoplasm of human cortical neurons: a light and electron microscopic study. *J Neuropathol Exp Neurol,* 53**,** 535-44.

Hardy, J. & Allsop, D. 1991. Amyloid deposition as the central event in the aetiology of Alzheimer's disease. *Trends Pharmacol Sci,* 12**,** 383-8.

Harigaya, Y., Saido, T. C., Eckman, C. B., Prada, C. M., Shoji, M. & Younkin, S. G. 2000. Amyloid beta protein starting pyroglutamate at position 3 is a major component of the amyloid deposits in the Alzheimer's disease brain. *Biochem Biophys Res Commun,* 276**,** 422-7.

Harris, F. M., Brecht, W. J., Xu, Q., Tesseur, I., Kekonius, L., Wyss-Coray, T., Fish, J. D., Masliah, E., Hopkins, P. C., Scearce-Levie, K., Weisgraber, K. H., Mucke, L., Mahley, R. W. & Huang, Y. 2003. Carboxyl-terminal-truncated apolipoprotein E4 causes Alzheimer's disease-like neurodegeneration and behavioral deficits in transgenic mice. *Proc Natl Acad Sci U S A,* 100**,** 10966-71.

Hartman, R. E., Wozniak, D. F., Nardi, A., Olney, J. W., Sartorius, L. & Holtzman, D. M. 2001. Behavioral phenotyping of GFAP-apoE3 and -apoE4 transgenic mice: apoE4 mice show profound working memory impairments in the absence of Alzheimer's-like neuropathology. *Exp Neurol,* 170**,** 326-44.

Hartmann, T. 1999. Intracellular biology of Alzheimer's disease amyloid beta peptide. *Eur Arch Psychiatry Clin Neurosci,* 249**,** 291-8.

Hatters, D. M., Budamagunta, M. S., Voss, J. C. & Weisgraber, K. H. 2005. Modulation of apolipoprotein E structure by domain interaction: differences in lipid-bound and lipid-free forms. *J Biol Chem,* 280**,** 34288-95.

He, C. & Klionsky, D. J. 2009. Regulation mechanisms and signaling pathways of autophagy. *Annu Rev Genet,* 43**,** 67-93.

He, W. & Barrow, C. J. 1999. The A beta 3-pyroglutamyl and 11-pyroglutamyl peptides found in senile plaque have greater beta-sheet forming and aggregation propensities in vitro than full-length A beta. *Biochemistry.,* 38**,** 10871-7.

Hecimovic, S., Wang, J., Dolios, G., Martinez, M., Wang, R. & Goate, A. M. 2004. Mutations in APP have independent effects on Abeta and CTFgamma generation. *Neurobiol Dis,* 17**,** 205-18.

Heston, L. L. & Mastri, A. R. 1977. The genetics of Alzheimer's disease: associations with hematologic malignancy and Down's syndrome. *Arch Gen Psychiatry,* 34**,** 976-981.

Hickman, S. E., Allison, E. K. & El Khoury, J. 2008. Microglial dysfunction and defective beta-amyloid clearance pathways in aging Alzheimer's disease mice. *J Neurosci,* 28**,** 8354-60.

Hirsch-Reinshagen, V., Maia, L. F., Burgess, B. L., Blain, J. F., Naus, K. E., Mcisaac, S. A., Parkinson, P. F., Chan, J. Y., Tansley, G. H., Hayden, M. R., Poirier, J., Van Nostrand, W. & Wellington, C. L. 2005. The absence of ABCA1 decreases soluble ApoE levels but does not diminish amyloid deposition in two murine models of Alzheimer disease. *J Biol Chem,* 280**,** 43243-56.

Holmes, C., Boche, D., Wilkinson, D., Yadegarfar, G., Hopkins, V., Bayer, A., Jones, R. W., Bullock, R., Love, S., Neal, J. W., Zotova, E. & Nicoll, J. A. 2008. Long-term effects of Abeta42 immunisation in Alzheimer's disease: follow-up of a randomised, placebo-controlled phase I trial. *Lancet,* 372**,** 216-23.

Holton, J. L., Ghiso, J., Lashley, T., Rostagno, A., Guerin, C. J., Gibb, G., Houlden, H., Ayling, H., Martinian, L., Anderton, B. H., Wood, N. W., Vidal, R., Plant, G., Frangione, B. & Revesz, T. 2001. Regional distribution of amyloid-Bri deposition and its association with neurofibrillary degeneration in familial British dementia. *Am J Pathol,* 158**,** 515-26.

Holton, J. L., Lashley, T., Ghiso, J., Braendgaard, H., Vidal, R., Guerin, C. J., Gibb, G., Hanger, D. P., Rostagno, A., Anderton, B. H., Strand, C., Ayling, H., Plant, G., Frangione, B., Bojsen-Moller, M. & Revesz, T. 2002. Familial Danish dementia: a novel form of cerebral amyloidosis associated with deposition of both amyloid-Dan and amyloid-beta. *J Neuropathol Exp Neurol,* 61**,** 254-67.

Holtzman, D. M. 2004. In vivo effects of ApoE and clusterin on amyloid-beta metabolism and neuropathology. *J Mol Neurosci,* 23**,** 247-54.

Holtzman, D. M., Bales, K. R., Tenkova, T., Fagan, A. M., Parsadanian, M., Sartorius, L. J., Mackey, B., Olney, J., Mckeel, D., Wozniak, D. & Paul, S. M. 2000. Apolipoprotein E isoform-dependent amyloid deposition and neuritic degeneration in a mouse model of Alzheimer's disease. *Proc Natl Acad Sci U S A,* 97**,** 2892-7.

Hoover, B. R., Reed, M. N., Su, J., Penrod, R. D., Kotilinek, L. A., Grant, M. K., Pitstick, R., Carlson, G. A., Lanier, L. M., Yuan, L. L., Ashe, K. H. & Liao, D. 2010. Tau mislocalization to dendritic spines mediates synaptic dysfunction independently of neurodegeneration. *Neuron,* 68**,** 1067-81.

Hsiao, K. K., Chapman, P., Nilsen, S., Eckman, C., Harigaya, Y., Younkin, S., Yang, F. & Cole, G. 1996. Correlative memory deficits, Abeta elevation and amyloid plaques in transgenic mice. *Science,* 274**,** 99-102.

Huang, Y., Liu, X. Q., Wyss-Coray, T., Brecht, W. J., Sanan, D. A. & Mahley, R. W. 2001. Apolipoprotein E fragments present in Alzheimer's disease brains induce neurofibrillary tangle-like intracellular inclusions in neurons. *Proc Natl Acad Sci U S A,* 98**,** 8838-43.

Huang, Y., Weisgraber, K. H., Mucke, L. & Mahley, R. W. 2004. Apolipoprotein E: diversity of cellular origins, structural and biophysical properties, and effects in Alzheimer's disease. *J Mol Neurosci,* 23**,** 189-204.

Hung, A. Y., Koo, E. H., Haass, C. & Selkoe, D. J. 1992. Increased expression of beta-amyloid precursor protein during neuronal differentiation is not accompanied by secretory cleavage. *Proc Natl Acad Sci U S A,* 89**,** 9439-43.

Hurtado, D. E., Molina-Porcel, L., Iba, M., Aboagye, A. K., Paul, S. M., Trojanowski, J. Q. & Lee, V. M. 2010. A{beta} accelerates the spatiotemporal progression of tau pathology and augments tau amyloidosis in an Alzheimer mouse model. *Am J Pathol,* 177**,** 1977-88.

Igbavboa, U., Sun, G. Y., Weisman, G. A., He, Y. & Wood, W. G. 2009. Amyloid beta-protein stimulates trafficking of cholesterol and caveolin-1 from the plasma membrane to the Golgi complex in mouse primary astrocytes. *Neuroscience,* 162**,** 328-38.

Iglesias, J., Abernethy, V. E., Wang, Z., Lieberthal, W., Koh, J. S. & Levine, J. S. 1999. Albumin is a major serum survival factor for renal tubular cells and macrophages through scavenging of ROS. *Am J Physiol,* 277**,** F711-22.

Ihara, Y., Morishima-Kawashima, M. & Nixon, R. 2012. The ubiquitin-proteasome system and the autophagic-lysosomal system in Alzheimer disease. *Cold Spring Harb Perspect Med,* 2**,** a006361.

Irizarry, M. C., Mcnamara, M., Fedorchak, K., Hsiao, K. & Hyman, B. T. 1997. APPSw transgenic mice develop age-related A beta deposits and neuropil abnormalities, but no neuronal loss in CA1. *J Neuropathol Exp Neurol,* 56**,** 965-73.

Itagaki, S., Mcgeer, P. L., Akiyama, H., Zhu, S. & Selkoe, D. 1989. Relationship of microglia and astrocytes to amyloid deposits of Alzheimer disease. *J Neuroimmunol,* 24**,** 173-82.

Ittner, L. M. & Götz, J. 2011. Amyloid-beta and tau - a toxic pas de deux in Alzheimer's disease. *Nat Rev Neurosci,* 12**,** 67-72.

Iwata, N., Tsubuki, S., Takaki, Y., Watanabe, K., Sekiguchi, M., Hosoki, E., Kawashima-Morishima, M., Lee, H. J., Hama, E., Sekine-Aizawa, Y. & Saido, T. C. 2000. Identification of the major Abeta1-42-degrading catabolic pathway in brain parenchyma: suppression leads to biochemical and pathological deposition. *Nat Med,* 6**,** 143-50.

Jack, C. R., Jr., Shiung, M. M., Weigand, S. D., O'brien, P. C., Gunter, J. L., Boeve, B. F., Knopman, D. S., Smith, G. E., Ivnik, R. J., Tangalos, E. G. & Petersen, R. C. 2005. Brain atrophy rates predict subsequent clinical conversion in normal elderly and amnestic MCI. *Neurology,* 65**,** 1227-31.

Jagust, W. 2006. Positron emission tomography and magnetic resonance imaging in the diagnosis and prediction of dementia. *Alzheimers Dement,* 2**,** 36-42.

Jalava, A. M., Heikkila, J., Akerlind, G., Pettit, G. R. & Akerman, K. E. 1990. Effects of bryostatins 1 and 2 on morphological and functional differentiation of SH-SY5Y human neuroblastoma cells. *Cancer Res,* 50**,** 3422-8.

Jawhar, S., Trawicka, A., Jenneckens, C., Bayer, T. A. & Wirths, O. 2012. Motor deficits, neuron loss, and reduced anxiety coinciding with axonal degeneration and intraneuronal Abeta aggregation in the 5XFAD mouse model of Alzheimer's disease. *Neurobiol Aging,* 33**,** 196.e29-40.

Jawhar, S., Wirths, O. & Bayer, T. A. 2011a. Pyroglutamate amyloid-beta (Abeta): a hatchet man in Alzheimer disease. *J Biol Chem,* 286**,** 38825-32.

Jawhar, S., Wirths, O., Schilling, S., Graubner, S., Demuth, H. U. & Bayer, T. A. 2011b. Overexpression of glutaminyl cyclase, the enzyme responsible for pyroglutamate abeta formation, induces behavioral deficits and glutaminyl cyclase knock-out rescues the behavioral phenotype in 5XFAD mice. *J Biol Chem,* 286**,** 4454-60.

Jaworski, T., Lechat, B., Demedts, D., Gielis, L., Devijver, H., Borghgraef, P., Duimel, H., Verheyen, F., Kugler, S. & Van Leuven, F. 2011. Dendritic degeneration, neurovascular defects, and inflammation precede neuronal loss in a mouse model for tau-mediated neurodegeneration. *Am J Pathol,* 179**,** 2001-15.

Jelicic, M., Bonebakker, A. E. & Bonke, B. 1995. Implicit memory performance of patients with Alzheimer's disease: a brief review. *Int Psychogeriatr,* 7**,** 385-92.

Jellinger, K. A. 2004. Head injury and dementia. *Curr Opin Neurol,* 17**,** 719-23.

Ji, Z. S., Miranda, R. D., Newhouse, Y. M., Weisgraber, K. H., Huang, Y. & Mahley, R. W. 2002. Apolipoprotein E4 potentiates amyloid beta peptide-induced lysosomal leakage and apoptosis in neuronal cells. *J Biol Chem,* 277**,** 21821-8.

Jiang, Q., Lee, C. Y., Mandrekar, S., Wilkinson, B., Cramer, P., Zelcer, N., Mann, K., Lamb, B., Willson, T. M., Collins, J. L., Richardson, J. C., Smith, J. D., Comery, T. A., Riddell, D., Holtzman, D. M., Tontonoz, P. & Landreth, G. E. 2008. ApoE promotes the proteolytic degradation of Abeta. *Neuron,* 58**,** 681-93.

Jiang, Y., Mullaney, K. A., Peterhoff, C. M., Che, S., Schmidt, S. D., Boyer-Boiteau, A., Ginsberg, S. D., Cataldo, A. M., Mathews, P. M. & Nixon, R. A. 2010. Alzheimer's-related endosome dysfunction in Down syndrome is Abeta-independent but requires APP and is reversed by BACE-1 inhibition. *Proc Natl Acad Sci U S A,* 107**,** 1630-5.

Jo, J., Whitcomb, D. J., Olsen, K. M., Kerrigan, T. L., Lo, S.-C., Bru-Mercier, G., Dickinson, B., Scullion, S., Sheng, M., Collingridge, G. & Cho, K. 2011. A[beta]1-42 inhibition of LTP is mediated by a signaling pathway involving caspase-3, Akt1 and GSK-3[beta]. *Nat Neurosci,* 14**,** 545-7.

Joachim, C. L., Morris, J. H. & Selkoe, D. J. 1989. Diffuse senile plaques occur commonly in the cerebellum in Alzheimer's disease. *Am J Pathol,* 135**,** 309-19.

Jonsson, T., Atwal, J. K., Steinberg, S., Snaedal, J., Jonsson, P. V., Bjornsson, S., Stefansson, H., Sulem, P., Gudbjartsson, D., Maloney, J., Hoyte, K., Gustafson, A., Liu, Y., Lu, Y., Bhangale, T., Graham, R. R., Huttenlocher, J., Bjornsdottir, G., Andreassen, O. A., Jonsson, E. G., Palotie, A., Behrens, T. W., Magnusson, O. T., Kong, A., Thorsteinsdottir, U., Watts, R. J. & Stefansson, K. 2012. A mutation in APP protects against Alzheimer's disease and age-related cognitive decline. *Nature,* 488**,** 96-9.

Kadenbach, B., Huttemann, M., Arnold, S., Lee, I. & Bender, E. 2000. Mitochondrial energy metabolism is regulated via nuclear-coded subunits of cytochrome c oxidase. *Free Radic Biol Med,* 29**,** 211-21.

Kaether, C., Haass, C. & Steiner, H. 2006. Assembly, trafficking and function of gamma-secretase. *Neurodegener Dis,* 3**,** 275-83.

Kang, J., Lemaire, H. G., Unterbeck, A., Salbaum, J. M., Masters, C. L., Grzeschik, K. H., Multhaup, G., Beyreuther, K. & Muller-Hill, B. 1987. The precursor of Alzheimer's disease amyloid A4 protein resembles a cell-surface receptor. *Nature,* 325**,** 733-736.

Kang, J. E., Lim, M. M., Bateman, R. J., Lee, J. J., Smyth, L. P., Cirrito, J. R., Fujiki, N., Nishino, S. & Holtzman, D. M. 2009. Amyloid-beta dynamics are regulated by orexin and the sleep-wake cycle. *Science,* 326**,** 1005-7.

Keller, J. N., Lauderback, C. M., Butterfield, D. A., Kindy, M. S., Yu, J. & Markesbery, W. R. 2000. Amyloid beta-peptide effects on synaptosomes from apolipoprotein E-deficient mice. *J Neurochem,* 74**,** 1579-86.

Kim, J., Miller, V. M., Levites, Y., West, K. J., Zwizinski, C. W., Moore, B. D., Troendle, F. J., Bann, M., Verbeeck, C., Price, R. W., Smithson, L., Sonoda, L., Wagg, K., Rangachari, V., Zou, F., Younkin, S. G., Graff-Radford, N., Dickson, D., Rosenberry, T. & Golde, T. E. 2008. BRI2 (ITM2b) inhibits abeta deposition in vivo. *J Neurosci,* 28**,** 6030-6.

Kim, S. H., Creemers, J. W., Chu, S., Thinakaran, G. & Sisodia, S. S. 2002. Proteolytic processing of familial British dementia-associated BRI variants: evidence for enhanced intracellular accumulation of amyloidogenic peptides. *J Biol Chem,* 277**,** 1872-7.

Kim, S. H., Wang, R., Gordon, D. J., Bass, J., Steiner, D. F., Lynn, D. G., Thinakaran, G., Meredith, S. C. & Sisodia, S. S. 1999. Furin mediates enhanced production of fibrillogenic ABri peptides in familial British dementia. *Nat Neurosci,* 2**,** 984-8.

Klebe, R. J. & Ruddle, F. H. 1969. Neuroblastoma: cell culture analysis of a differentiating stem cell system. *J Cell Biol,* 43.

Klionsky, D. J. 2010. The autophagy connection. *Dev Cell,* 19**,** 11-2.

Koo, E. H., Sisodia, S. S., Archer, D. R., Martin, L. J., Weidemann, A., Beyreuther, K., Fischer, P., Masters, C. L. & Price, D. L. 1990. Precursor of amyloid protein in Alzheimer disease undergoes fast anterograde axonal transport. *Proc Natl Acad Sci U S A,* 87**,** 1561-5.

Kuo, Y. M., Webster, S., Emmerling, M. R., De Lima, N. & Roher, A. E. 1998. Irreversible dimerization/tetramerization and post-translational modifications inhibit proteolytic degradation of A beta peptides of Alzheimer's disease. *Biochim Biophys Acta,* 1406**,** 291-8.

Kurochkin, I. V. & Goto, S. 1994. Alzheimer's beta-amyloid peptide specifically interacts with and is degraded by insulin degrading enzyme. *FEBS Lett,* 345**,** 33-7.

Kurz, T., Terman, A., Gustafsson, B. & Brunk, U. T. 2008. Lysosomes and oxidative stress in aging and apoptosis. *Biochim Biophys Acta,* 1780**,** 1291-303.

Ladu, M. J., Pederson, T. M., Frail, D. E., Reardon, C. A., Getz, G. S. & Falduto, M. T. 1995. Purification of apolipoprotein E attenuates isoform-specific binding to beta-amyloid. *J Biol Chem,* 270**,** 9039-42.

Lai, A., Sisodia, S. S. & Trowbridge, I. S. 1995. Characterization of sorting signals in the beta-amyloid precursor protein cytoplasmic domain. *J Biol Chem,* 270**,** 3565-73.

Lalonde, R., Dumont, M., Staufenbiel, M., Sturchler-Pierrat, C. & Strazielle, C. 2002. Spatial learning, exploration, anxiety, and motor coordination in female APP23 transgenic mice with the Swedish mutation. *Brain Res.,* 956**,** 36-44.

Lalonde, R., Kim, H. D., Maxwell, J. A. & Fukuchi, K. 2005. Exploratory activity and spatial learning in 12-month-old APP(695)SWE/co+PS1/DeltaE9 mice with amyloid plaques. *Neurosci Lett.,* 390**,** 87-92.

Lalonde, R., Lewis, T. L., Strazielle, C., Kim, H. & Fukuchi, K. 2003a. Transgenic mice expressing the betaAPP695SWE mutation: effects on exploratory activity, anxiety, and motor coordination. *Brain Res,* 977**,** 38-45.

Lalonde, R., Qian, S. & Strazielle, C. 2003b. Transgenic mice expressing the PS1-A246E mutation: effects on spatial learning, exploration, anxiety, and motor coordination. *Behav Brain Res.,* 138**,** 71-9.

Lashley, T., Revesz, T., Plant, G., Bandopadhyay, R., Lees, A. J., Frangione, B., Wood, N. W., De Silva, R., Ghiso, J., Rostagno, A. & Holton, J. L. 2008. Expression of BRI2 mRNA and protein in normal human brain and familial British dementia: its relevance to the pathogenesis of disease. *Neuropathol Appl Neurobiol,* 34**,** 492-505.

Latil, A., Chene, L., Mangin, P., Fournier, G., Berthon, P. & Cussenot, O. 2003. Extensive analysis of the 13q14 region in human prostate tumors: DNA analysis and quantitative expression of genes lying in the interval of deletion. *Prostate,* 57**,** 39-50.

Lauderback, C. M., Kanski, J., Hackett, J. M., Maeda, N., Kindy, M. S. & Butterfield, D. A. 2002. Apolipoprotein E modulates Alzheimer's Abeta(1-42)-induced oxidative damage to synaptosomes in an allele-specific manner. *Brain Res,* 924**,** 90-7.

Lee, H. G., Perry, G., Moreira, P. I., Garrett, M. R., Liu, Q., Zhu, X., Takeda, A., Nunomura, A. & Smith, M. A. 2005. Tau phosphorylation in Alzheimer's disease: pathogen or protector? *Trends Mol Med,* 11**,** 164-9.

Lee, J. H., Yu, W. H., Kumar, A., Lee, S., Mohan, P. S., Peterhoff, C. M., Wolfe, D. M., Martinez-Vicente, M., Massey, A. C., Sovak, G., Uchiyama, Y., Westaway, D., Cuervo, A. M. & Nixon, R. A. 2010. Lysosomal proteolysis and autophagy require presenilin 1 and are disrupted by Alzheimer-related PS1 mutations. *Cell,* 141**,** 1146-58.

Lee, V. M., Goedert, M. & Trojanowski, J. Q. 2001. Neurodegenerative tauopathies. *Annu Rev Neurosci,* 24**,** 1121-59.

Leroy, K., Ando, K., Laporte, V., Dedecker, R., Suain, V., Authelet, M., Heraud, C., Pierrot, N., Yilmaz, Z., Octave, J. N. & Brion, J. P. 2012. Lack of Tau Proteins Rescues Neuronal Cell Death and Decreases Amyloidogenic Processing of APP in APP/PS1 Mice. *Am J Pathol,* 181**,** 1928-40.

Levy, E., Carman, M. D., Fernandez-Madrid, I. J., Power, M. D., Lieberburg, I., Van Duinen, S. G., Bots, G. T., Luyendijk, W. & Frangione, B. 1990. Mutation of the Alzheimer's disease amyloid gene in hereditary cerebral hemorrhage, Dutch type. *Science,* 248**,** 1124-6.

Lewis, J., Dickson, D. W., Lin, W. L., Chisholm, L., Corral, A., Jones, G., Yen, S. H., Sahara, N., Skipper, L., Yager, D., Eckman, C., Hardy, J., Hutton, M. & Mcgowan, E. 2001. Enhanced neurofibrillary degeneration in transgenic mice expressing mutant tau and APP. *Science,* 293**,** 1487-91.

Li, S., Hong, S., Shepardson, N. E., Walsh, D. M., Shankar, G. M. & Selkoe, D. 2009. Soluble oligomers of amyloid Beta protein facilitate hippocampal long-term depression by disrupting neuronal glutamate uptake. *Neuron,* 62**,** 788-801.

Lichtenthaler, S. F., Ida, N., Multhaup, G., Masters, C. L. & Beyreuther, K. 1997. Mutations in the transmembrane domain of APP altering gamma-secretase specificity. *Biochemistry,* 36**,** 15396-403.

Lichtenthaler, S. F., Multhaup, G., Masters, C. L. & Beyreuther, K. 1999a. A novel substrate for analyzing Alzheimer's disease gamma-secretase. *FEBS Lett,* 453**,** 288-92.

Lichtenthaler, S. F., Wang, R., Grimm, H., Uljon, S. N., Masters, C. L. & Beyreuther, K. 1999b. Mechanism of the cleavage specificity of Alzheimer's disease gamma-secretase

identified by phenylalanine-scanning mutagenesis of the transmembrane domain of the amyloid precursor protein. *Proc Natl Acad Sci U S A,* 96**,** 3053-8.

Lister, R. G. 1987. The use of a plus-maze to measure anxiety in the mouse. *Psychopharmacology (Berl),* 92**,** 180-5.

Love, S. & Duchen, L. W. 1982. Familial cerebellar ataxia with cerebrovascular amyloid. *J Neurol Neurosurg Psychiatry,* 45**,** 271-3.

Lovestone, S., Anderton, B. H., Hartley, C., Jensen, T. G. & Jorgensen, A. L. 1996. The intracellular fate of apolipoprotein E is tau dependent and apoe allele-specific. *Neuroreport,* 7**,** 1005-8.

Lyketsos, C. G., Lopez, O., Jones, B., Fitzpatrick, A. L., Breitner, J. & Dekosky, S. 2002. Prevalence of neuropsychiatric symptoms in dementia and mild cognitive impairment: results from the cardiovascular health study. *Jama,* 288**,** 1475-83.

Ma, J., Yee, A., Brewer, H. B., Jr., Das, S. & Potter, H. 1994. Amyloid-associated proteins alpha 1-antichymotrypsin and apolipoprotein E promote assembly of Alzheimer beta-protein into filaments. *Nature,* 372**,** 92-4.

Mahley, R. W., Hui, D. Y., Innerarity, T. L. & Beisiegel, U. 1989. Chylomicron remnant metabolism. Role of hepatic lipoprotein receptors in mediating uptake. *Arteriosclerosis,* 9**,** I14-8.

Mahley, R. W. & Rall, S. C., Jr. 1999. Is epsilon4 the ancestral human apoE allele? *Neurobiol Aging,* 20**,** 429-30.

Mahley, R. W., Weisgraber, K. H. & Huang, Y. 2006. Apolipoprotein E4: a causative factor and therapeutic target in neuropathology, including Alzheimer's disease. *Proc Natl Acad Sci U S A,* 103**,** 5644-51.

Maloney, B. & Lahiri, D. K. 2011. The Alzheimer's amyloid beta-peptide (Abeta) binds a specific DNA Abeta-interacting domain (AbetaID) in the APP, BACE1, and APOE promoters in a sequence-specific manner: characterizing a new regulatory motif. *Gene,* 488**,** 1-12.

Maretzky, T., Reiss, K., Ludwig, A., Buchholz, J., Scholz, F., Proksch, E., De Strooper, B., Hartmann, D. & Saftig, P. 2005. ADAM10 mediates E-cadherin shedding and regulates epithelial cell-cell adhesion, migration, and beta-catenin translocation. *Proc Natl Acad Sci U S A,* 102**,** 9182-7.

Marquez-Sterling, N. R., Lo, A. C., Sisodia, S. S. & Koo, E. H. 1997. Trafficking of cell-surface beta-amyloid precursor protein: evidence that a sorting intermediate participates in synaptic vesicle recycling. *J Neurosci,* 17**,** 140-51.

Martin, L., Fluhrer, R. & Haass, C. 2009. Substrate requirements for SPPL2b-dependent regulated intramembrane proteolysis. *J Biol Chem,* 284**,** 5662-70.

Martin, L., Fluhrer, R., Reiss, K., Kremmer, E., Saftig, P. & Haass, C. 2008. Regulated Intramembrane Proteolysis of Bri2 (Itm2b) by ADAM10 and SPPL2a/SPPL2b. *J Biol Chem,* 283**,** 1644-52.

Matsuda, S., Giliberto, L., Matsuda, Y., Davies, P., Mcgowan, E., Pickford, F., Ghiso, J., Frangione, B. & D'adamio, L. 2005. The Familial Dementia BRI2 Gene Binds the Alzheimer Gene Amyloid-β Precursor Protein and Inhibits Amyloid-β Production. *J Biol Chem,* 280**,** 28912-28916.

Matsuda, S., Giliberto, L., Matsuda, Y., Mcgowan, E. M. & D'adamio, L. 2008. BRI2 inhibits amyloid beta-peptide precursor protein processing by interfering with the docking of secretases to the substrate. *J Neurosci,* 28**,** 8668-76.

Mattsson, N., Zetterberg, H., Hansson, O., Andreasen, N., Parnetti, L., Jonsson, M., Herukka, S. K., Van Der Flier, W. M., Blankenstein, M. A., Ewers, M., Rich, K., Kaiser, E.,

Verbeek, M., Tsolaki, M., Mulugeta, E., Rosen, E., Aarsland, D., Visser, P. J., Schroder, J., Marcusson, J., De Leon, M., Hampel, H., Scheltens, P., Pirttila, T., Wallin, A., Jonhagen, M. E., Minthon, L., Winblad, B. & Blennow, K. 2009. CSF biomarkers and incipient Alzheimer disease in patients with mild cognitive impairment. *Jama,* 302**,** 385-93.

Mayeux, R. 2003. Epidemiology of neurodegeneration. *Annu Rev Neurosci,* 26**,** 81-104.

Mclean, C. A., Cherny, R. A., Fraser, F. W., Fuller, S. J., Smith, M. J., Beyreuther, K., Bush, A. I. & Masters, C. L. 1999. Soluble pool of Abeta amyloid as a determinant of severity of neurodegeneration in Alzheimer's disease. *Ann Neurol,* 46**,** 860-6.

Mead, S., James-Galton, M., Revesz, T., Doshi, R. B., Harwood, G., Pan, E. L., Ghiso, J., Frangione, B. & Plant, G. 2000. Familial British dementia with amyloid angiopathy: early clinical, neuropsychological and imaging findings. *Brain,* 123**,** 975-91.

Meyer-Luehmann, M., Coomaraswamy, J., Bolmont, T., Kaeser, S., Schaefer, C., Kilger, E., Neuenschwander, A., Abramowski, D., Frey, P., Jaton, A. L., Vigouret, J. M., Paganetti, P., Walsh, D. M., Mathews, P. M., Ghiso, J., Staufenbiel, M., Walker, L. C. & Jucker, M. 2006. Exogenous induction of cerebral beta-amyloidogenesis is governed by agent and host. *Science,* 313**,** 1781-4.

Minoshima, S. & Cross, D. 2008. In vivo imaging of axonal transport using MRI: aging and Alzheimer's disease. *Eur J Nucl Med Mol Imaging,* 35 Suppl 1**,** S89-92.

Miravalle, L., Tokuda, T., Chiarle, R., Giaccone, G., Bugiani, O., Tagliavini, F., Frangione, B. & Ghiso, J. 2000. Substitutions at codon 22 of Alzheimer's abeta peptide induce diverse conformational changes and apoptotic effects in human cerebral endothelial cells. *J Biol Chem,* 275**,** 27110-6.

Mirra, S. S., Heyman, A., Mckeel, D., Sumi, S. M., Crain, B. J., Brownlee, L. M., Vogel, F. S., Hughes, J. P., Van Belle, G. & Berg, L. 1991. The Consortium to Establish a Registry for Alzheimer's Disease (CERAD). Part II. Standardization of the neuropathologic assessment of Alzheimer's disease. *Neurology,* 41**,** 479-86.

Miyata, M. & Smith, J. D. 1996. Apolipoprotein E allele-specific antioxidant activity and effects on cytotoxicity by oxidative insults and beta-amyloid peptides. *Nat Genet,* 14**,** 55-61.

Morales, R., Duran-Aniotz, C., Castilla, J., Estrada, L. D. & Soto, C. 2011. De novo induction of amyloid-beta deposition in vivo. *Mol Psychiatry,* 4**,** 120.

Morfini, G. A., Burns, M., Binder, L. I., Kanaan, N. M., Lapointe, N., Bosco, D. A., Brown, R. H., Jr., Brown, H., Tiwari, A., Hayward, L., Edgar, J., Nave, K. A., Garberrn, J., Atagi, Y., Song, Y., Pigino, G. & Brady, S. T. 2009. Axonal transport defects in neurodegenerative diseases. *J Neurosci,* 29**,** 12776-86.

Morris, R. 1984. Developments of a water-maze procedure for studying spatial learning in the rat. *J Neurosci Methods.,* 11**,** 47-60.

Morrow, J. A., Hatters, D. M., Lu, B., Hochtl, P., Oberg, K. A., Rupp, B. & Weisgraber, K. H. 2002. Apolipoprotein E4 forms a molten globule. A potential basis for its association with disease. *J Biol Chem,* 277**,** 50380-5.

Mortimer, J. A., Snowdon, D. A. & Markesbery, W. R. 2003. Head circumference, education and risk of dementia: findings from the Nun Study. *J Clin Exp Neuropsychol,* 25**,** 671-9.

Moya, K. L., Benowitz, L. I., Schneider, G. E. & Allinquant, B. 1994. The amyloid precursor protein is developmentally regulated and correlated with synaptogenesis. *Dev Biol,* 161**,** 597-603.

Murakami, N., Yamaki, T., Iwamoto, Y., Sakakibara, T., Kobori, N., Fushiki, S. & Ueda, S. 1998. Experimental brain injury induces expression of amyloid precursor protein, which may be related to neuronal loss in the hippocampus. *J Neurotrauma,* 15**,** 993-1003.

Nagele, R. G., D'andrea, M. R., Lee, H., Venkataraman, V. & Wang, H. Y. 2003. Astrocytes accumulate A beta 42 and give rise to astrocytic amyloid plaques in Alzheimer disease brains. *Brain Res,* 971**,** 197-209.

Namba, Y., Tomonaga, M., Kawasaki, H., Otomo, E. & Ikeda, K. 1991. Apolipoprotein E immunoreactivity in cerebral amyloid deposits and neurofibrillary tangles in Alzheimer's disease and kuru plaque amyloid in Creutzfeldt-Jakob disease. *Brain Res,* 541**,** 163-6.

Näslund, J., Thyberg, J., Tjernberg, L. O., Wernstedt, C., Karlstrom, A. R., Bogdanovic, N., Gandy, S. E., Lannfelt, L., Terenius, L. & Nordstedt, C. 1995. Characterization of stable complexes involving apolipoprotein E and the amyloid beta peptide in Alzheimer's disease brain. *Neuron,* 15**,** 219-28.

Neely, K., Green, K. & Laferla, F. 2011. Presenilin is necessary for efficient proteolysis through the autophagy-lysosome system in a gamma-secretase-independent manner. *J Neurosci,* 31**,** 2781-91.

Nitsch, R. M., Slack, B. E., Wurtman, R. J. & Growdon, J. H. 1992. Release of Alzheimer amyloid precursor derivatives stimulated by activation of muscarinic acetylcholine receptors. *Science,* 258**,** 304-7.

Nixon, R. A. 2007. Autophagy, amyloidogenesis and Alzheimer disease. *J Cell Sci,* 120**,** 4081-91.

Nixon, R. A. & Yang, D. S. 2011. Autophagy failure in Alzheimer's disease-locating the primary defect. *Neurobiol Dis,* 43**,** 38-45.

Nupponen, N. N., Hyytinen, E. R., Kallioniemi, A. H. & Visakorpi, T. 1998. Genetic alterations in prostate cancer cell lines detected by comparative genomic hybridization. *Cancer Genet Cytogenet,* 101**,** 53-7.

Nussbaum, J. M., Schilling, S., Cynis, H., Silva, A., Swanson, E., Wangsanut, T., Tayler, K., Wiltgen, B., Hatami, A., Ronicke, R., Reymann, K., Hutter-Paier, B., Alexandru, A., Jagla, W., Graubner, S., Glabe, C. G., Demuth, H. U. & Bloom, G. S. 2012. Prion-like behaviour and tau-dependent cytotoxicity of pyroglutamylated amyloid-beta. *Nature,* 485**,** 651-5.

Oakley, H., Cole, S. L., Logan, S., Maus, E., Shao, P., Craft, J., Guillozet-Bongaarts, A., Ohno, M., Disterhoft, J., Van Eldik, L., Berry, R. & Vassar, R. 2006. Intraneuronal beta-amyloid aggregates, neurodegeneration, and neuron loss in transgenic mice with five familial Alzheimer's disease mutations: potential factors in amyloid plaque formation. *J Neurosci.,* 26**,** 10129-40.

Oddo, S., Caccamo, A., Shepherd, J. D., Murphy, M. P., Golde, T. E., Kayed, R., Metherate, R., Mattson, M. P., Akbari, Y. & Laferla, F. M. 2003. Triple-transgenic model of Alzheimer's disease with plaques and tangles: intracellular Abeta and synaptic dysfunction. *Neuron,* 39**,** 409-21.

Olmsted, J. B., Carlson, K., Klebe, R., Ruddle, F. & Rosenbaum, J. 1970. Isolation of microtubule protein from cultured mouse neuroblastoma cells. *Proc Natl Acad Sci U S A,* 65**,** 129-36.

Overly, C. C. & Hollenbeck, P. J. 1996. Dynamic organization of endocytic pathways in axons of cultured sympathetic neurons. *J Neurosci,* 16**,** 6056-64.

Palop, J. J., Chin, J., Roberson, E. D., Wang, J., Thwin, M. T., Bien-Ly, N., Yoo, J., Ho, K. O., Yu, G. Q., Kreitzer, A., Finkbeiner, S., Noebels, J. L. & Mucke, L. 2007. Aberrant excitatory

neuronal activity and compensatory remodeling of inhibitory hippocampal circuits in mouse models of Alzheimer's disease. *Neuron,* 55**,** 697-711.

Pan, D. & Rubin, G. M. 1997. Kuzbanian controls proteolytic processing of Notch and mediates lateral inhibition during Drosophila and vertebrate neurogenesis. *Cell,* 90**,** 271-80.

Pena-Ortega, F., Solis-Cisneros, A., Ordaz, B., Balleza-Tapia, H. & Javier Lopez-Guerrero, J. 2012. Amyloid beta 1-42 inhibits entorhinal cortex activity in the beta-gamma range: role of GSK-3. *Curr Alzheimer Res,* 9**,** 857-63.

Pennanen, C., Kivipelto, M., Tuomainen, S., Hartikainen, P., Hanninen, T., Laakso, M. P., Hallikainen, M., Vanhanen, M., Nissinen, A., Helkala, E. L., Vainio, P., Vanninen, R., Partanen, K. & Soininen, H. 2004. Hippocampus and entorhinal cortex in mild cognitive impairment and early AD. *Neurobiol Aging,* 25**,** 303-10.

Perrin, R. J., Fagan, A. M. & Holtzman, D. M. 2009. Multimodal techniques for diagnosis and prognosis of Alzheimer's disease. *Nature,* 461**,** 916-22.

Pickford, F., Coomaraswamy, J., Jucker, M. & Mcgowan, E. 2006. Modeling familial British dementia in transgenic mice. *Brain Pathol,* 16**,** 80-5.

Pike, C. J., Overman, M. J. & Cotman, C. W. 1995. Amino-terminal deletions enhance aggregation of beta-amyloid peptides in vitro. *J Biol Chem.,* 270**,** 23895-8.

Pitas, R. E., Boyles, J. K., Lee, S. H., Foss, D. & Mahley, R. W. 1987. Astrocytes synthesize apolipoprotein E and metabolize apolipoprotein E-containing lipoproteins. *Biochim Biophys Acta,* 917**,** 148-61.

Pittois, K., Deleersnijder, W. & Merregaert, J. 1998. cDNA sequence analysis, chromosomal assignment and expression pattern of the gene coding for integral membrane protein 2B. *Gene,* 217**,** 141-149.

Plant, G. T., Revesz, T., Barnard, R. O., Harding, A. E. & Gautier-Smith, P. C. 1990. Familial cerebral amyloid angiopathy with nonneuritic amyloid plaque formation. *Brain,* 113**,** 721-47.

Postina, R., Schroeder, A., Dewachter, I., Bohl, J., Schmitt, U., Kojro, E., Prinzen, C., Endres, K., Hiemke, C., Blessing, M., Flamez, P., Dequenne, A., Godaux, E., Van Leuven, F. & Fahrenholz, F. 2004. A disintegrin-metalloproteinase prevents amyloid plaque formation and hippocampal defects in an Alzheimer disease mouse model. *J Clin Invest,* 113**,** 1456-64.

Priller, C., Bauer, T., Mitteregger, G., Krebs, B., Kretzschmar, H. A. & Herms, J. 2006. Synapse formation and function is modulated by the amyloid precursor protein. *J Neurosci,* 26**,** 7212-21.

Puoliväli, J., Wang, J., Heikkinen, T., Heikkilä, M., Tapiola, T., Van Groen, T. & Tanila, H. 2002. Hippocampal A beta 42 levels correlate with spatial memory deficit in APP and PS1 double transgenic mice. *Neurobiol Dis,* 9**,** 339-47.

Putcha, D., Brickhouse, M., O'keefe, K., Sullivan, C., Rentz, D., Marshall, G., Dickerson, B. & Sperling, R. 2011. Hippocampal hyperactivation associated with cortical thinning in Alzheimer's disease signature regions in non-demented elderly adults. *J Neurosci,* 31**,** 17680-8.

Qiu, W. Q., Walsh, D. M., Ye, Z., Vekrellis, K., Zhang, J., Podlisny, M. B., Rosner, M. R., Safavi, A., Hersh, L. B. & Selkoe, D. J. 1998. Insulin-degrading enzyme regulates extracellular levels of amyloid beta-protein by degradation. *J Biol Chem,* 273**,** 32730-8.

Raber, J., Huang, Y. & Ashford, J. W. 2004. ApoE genotype accounts for the vast majority of AD risk and AD pathology. *Neurobiol Aging,* 25**,** 641-50.

Raber, J., Wong, D., Yu, G. Q., Buttini, M., Mahley, R. W., Pitas, R. E. & Mucke, L. 2000. Apolipoprotein E and cognitive performance. *Nature,* 404**,** 352-4.

Radde, R., Bolmont, T., Kaeser, S. A., Coomaraswamy, J., Lindau, D., Stoltze, L., Calhoun, M. E., Jaggi, F., Wolburg, H., Gengler, S., Haass, C., Ghetti, B., Czech, C., Holscher, C., Mathews, P. M. & Jucker, M. 2006. Abeta42-driven cerebral amyloidosis in transgenic mice reveals early and robust pathology. *EMBO Rep,* 7**,** 940-6.

Rademakers, R. & Rovelet-Lecrux, A. 2009. Recent insights into the molecular genetics of dementia. *Trends Neurosci,* 32**,** 451-61.

Rajavashisth, T. B., Kaptein, J. S., Reue, K. L. & Lusis, A. J. 1985. Evolution of apolipoprotein E: mouse sequence and evidence for an 11-nucleotide ancestral unit. *Proc Natl Acad Sci U S A,* 82**,** 8085-9.

Reiss, K., Maretzky, T., Ludwig, A., Tousseyn, T., De Strooper, B., Hartmann, D. & Saftig, P. 2005. ADAM10 cleavage of N-cadherin and regulation of cell-cell adhesion and beta-catenin nuclear signalling. *Embo J,* 24**,** 742-52.

Report 2011. World Alzheimer Report (2011). Alzheimer's Disease International.

Revesz, T., Ghiso, J., Lashley, T., Plant, G., Rostagno, A., Frangione, B. & Holton, J. L. 2003. Cerebral amyloid angiopathies: a pathologic, biochemical, and genetic view. *J Neuropathol Exp Neurol,* 62**,** 885-98.

Revesz, T., Holton, J. L., Doshi, B., Anderton, B. H., Scaravilli, F. & Plant, G. T. 1999. Cytoskeletal pathology in familial cerebral amyloid angiopathy (British type) with non-neuritic amyloid plaque formation. *Acta Neuropathol,* 97**,** 170-6.

Revesz, T., Holton, J. L., Lashley, T., Plant, G., Frangione, B., Rostagno, A. & Ghiso, J. 2009. Genetics and molecular pathogenesis of sporadic and hereditary cerebral amyloid angiopathies. *Acta Neuropathol,* 118**,** 115-30.

Ribe, E. M., Perez, M., Puig, B., Gich, I., Lim, F., Cuadrado, M., Sesma, T., Catena, S., Sanchez, B., Nieto, M., Gomez-Ramos, P., Moran, M. A., Cabodevilla, F., Samaranch, L., Ortiz, L., Perez, A., Ferrer, I., Avila, J. & Gomez-Isla, T. 2005. Accelerated amyloid deposition, neurofibrillary degeneration and neuronal loss in double mutant APP/tau transgenic mice. *Neurobiol Dis.,* 20**,** 814-22. .

Ross, R. A., Spengler, B. A. & Biedler, J. L. 1983. Coordinate morphological and biochemical interconversion of human neuroblastoma cells. *J Natl Cancer Inst,* 71**,** 741-7.

Rostagno, A., Revesz, T., Lashley, T., Tomidokoro, Y., Magnotti, L., Braendgaard, H., Plant, G., Bojsen-Moller, M., Holton, J., Frangione, B. & Ghiso, J. 2002. Complement activation in chromosome 13 dementias. Similarities with Alzheimer's disease. *J Biol Chem,* 277**,** 49782-90.

Rostagno, A., Tomidokoro, Y., Lashley, T., Ng, D., Plant, G., Holton, J., Frangione, B., Revesz, T. & Ghiso, J. 2005. Chromosome 13 dementias. *Cell Mol Life Sci,* 62**,** 1814-25.

Roy, S., Zhang, B., Lee, V. M. & Trojanowski, J. Q. 2005. Axonal transport defects: a common theme in neurodegenerative diseases. *Acta Neuropathol (Berl),* 109**,** 5-13.

Rui, Y., Tiwari, P., Xie, Z. & Zheng, J. Q. 2006. Acute Impairment of Mitochondrial Trafficking by beta-Amyloid Peptides in Hippocampal Neurons. *J Neurosci.,* 26**,** 10480-10487.

Russo, C., Violani, E., Salis, S., Venezia, V., Dolcini, V., Damonte, G., Benatti, U., D'arrigo, C., Patrone, E., Carlo, P. & Schettini, G. 2002. Pyroglutamate-modified amyloid beta-peptides--AbetaN3(pE)--strongly affect cultured neuron and astrocyte survival. *J Neurochem.,* 82**,** 1480-9.

Saez, E. T., Pehar, M., Vargas, M. R., Barbeito, L. & Maccioni, R. B. 2006. Production of nerve growth factor by beta-amyloid-stimulated astrocytes induces p75NTR-dependent tau

hyperphosphorylation in cultured hippocampal neurons. *J Neurosci Res,* 84**,** 1098-106.

Saido, T. C., Iwatsubo, T., Mann, D. M., Shimada, H., Ihara, Y. & Kawashima, S. 1995. Dominant and differential deposition of distinct beta-amyloid peptide species, A beta N3(pE), in senile plaques. *Neuron,* 14**,** 457-66.

Sanan, D. A., Weisgraber, K. H., Russell, S. J., Mahley, R. W., Huang, D., Saunders, A., Schmechel, D., Wisniewski, T., Frangione, B., Roses, A. D. & Et Al. 1994. Apolipoprotein E associates with beta amyloid peptide of Alzheimer's disease to form novel monofibrils. Isoform apoE4 associates more efficiently than apoE3. *J Clin Invest,* 94**,** 860-9.

Sanchez-Pulido, L., Devos, D. & Valencia, A. 2002. BRICHOS: a conserved domain in proteins associated with dementia, respiratory distress and cancer. *Trends Biochem Sci,* 27**,** 329-32.

Saul, A., Lashley, T., Revesz, T., Holton, J., Ghiso, J. A., Coomaraswamy, J. & Wirths, O. 2013. Abundant pyroglutamate-modified ABri and ADan peptides in extracellular and vascular amyloid deposits in familial British and Danish dementias. *Neurobiol Aging,* 34**,** 1416-25.

Savva, G. M., Wharton, S. B., Ince, P. G., Forster, G., Matthews, F. E. & Brayne, C. 2009. Age, neuropathology, and dementia. *N Engl J Med,* 360**,** 2302-9.

Scheuner, D., Eckman, C., Jensen, M., Song, X., Citron, M., Suzuki, N., Bird, T. D., Hardy, J., Hutton, M., Kukull, W., Larson, E., Levy-Lahad, E., Viitanen, M., Peskind, E., Poorkaj, P., Schellenberg, G., Tanzi, R., Wasco, W., Lannfelt, L., Selkoe, D. & Younkin, S. 1996. Secreted amyloid beta-protein similar to that in the senile plaques of Alzheimer's disease is increased in vivo by the presenilin 1 and 2 and APP mutations linked to familial Alzheimer's disease. *Nat Med,* 2**,** 864-70.

Schilling, S., Lauber, T., Schaupp, M., Manhart, S., Scheel, E., Bohm, G. & Demuth, H. U. 2006. On the seeding and oligomerization of pGlu-amyloid peptides (in vitro). *Biochemistry,* 45**,** 12393-9.

Schilling, S., Zeitschel, U., Hoffmann, T., Heiser, U., Francke, M., Kehlen, A., Holzer, M., Hutter-Paier, B., Prokesch, M., Windisch, M., Jagla, W., Schlenzig, D., Lindner, C., Rudolph, T., Reuter, G., Cynis, H., Montag, D., Demuth, H. U. & Rossner, S. 2008. Glutaminyl cyclase inhibition attenuates pyroglutamate Abeta and Alzheimer's disease-like pathology. *Nat Med,* 14**,** 1106-11.

Schlenzig, D., Manhart, S., Cinar, Y., Kleinschmidt, M., Hause, G., Willbold, D., Funke, S. A., Schilling, S. & Demuth, H. U. 2009. Pyroglutamate formation influences solubility and amyloidogenicity of amyloid peptides. *Biochemistry,* 48**,** 7072-8.

Schroeter, M. L., Stein, T., Maslowski, N. & Neumann, J. 2009. Neural correlates of Alzheimer's disease and mild cognitive impairment: a systematic and quantitative meta-analysis involving 1351 patients. *Neuroimage,* 47**,** 1196-206.

Selkoe, D. J. 2001. Alzheimer's disease: genes, proteins, and therapy. *Physiol Rev,* 81**,** 741-66.

Seo, J. S., Leem, Y. H., Lee, K. W., Kim, S. W., Lee, J. K. & Han, P. L. 2010. Severe motor neuron degeneration in the spinal cord of the Tg2576 mouse model of Alzheimer disease. *J Alzheimers Dis,* 21**,** 263-76.

Sigurdsson, E. M., Scholtzova, H., Mehta, P. D., Frangione, B. & Wisniewski, T. 2001. Immunization with a nontoxic/nonfibrillar amyloid-beta homologous peptide reduces Alzheimer's disease-associated pathology in transgenic mice. *Am J Pathol,* 159**,** 439-47.

Sinha, M., Bhowmick, P., Banerjee, A. & Chakrabarti, S. 2012. Antioxidant role of amyloid beta protein in cell-free and biological systems: implication for the pathogenesis of Alzheimer disease. *Free Radic Biol Med,* 3**,** 01170-7.

Sisodia, S. S. 1992. Beta-amyloid precursor protein cleavage by a membrane-bound protease. *Proc Natl Acad Sci U S A,* 89**,** 6075-9.

Sisodia, S. S., Koo, E. H., Beyreuther, K., Unterbeck, A. & Price, D. L. 1990. Evidence that beta-amyloid protein in Alzheimer's disease is not derived by normal processing. *Science,* 248**,** 492-5.

Sleegers, K., Lambert, J. C., Bertram, L., Cruts, M., Amouyel, P. & Van Broeckhoven, C. 2010. The pursuit of susceptibility genes for Alzheimer's disease: progress and prospects. *Trends Genet,* 26**,** 84-93.

Small, G. W., Ercoli, L. M., Silverman, D. H., Huang, S. C., Komo, S., Bookheimer, S. Y., Lavretsky, H., Miller, K., Siddarth, P., Rasgon, N. L., Mazziotta, J. C., Saxena, S., Wu, H. M., Mega, M. S., Cummings, J. L., Saunders, A. M., Pericak-Vance, M. A., Roses, A. D., Barrio, J. R. & Phelps, M. E. 2000. Cerebral metabolic and cognitive decline in persons at genetic risk for Alzheimer's disease. *Proc Natl Acad Sci U S A,* 97**,** 6037-42.

Smith, K. D., Kallhoff, V., Zheng, H. & Pautler, R. G. 2007. In vivo axonal transport rates decrease in a mouse model of Alzheimer's disease. *Neuroimage,* 35**,** 1401-8.

Soscia, S. J., Kirby, J. E., Washicosky, K. J., Tucker, S. M., Ingelsson, M., Hyman, B., Burton, M. A., Goldstein, L. E., Duong, S., Tanzi, R. E. & Moir, R. D. 2010. The Alzheimer's disease-associated amyloid beta-protein is an antimicrobial peptide. *PLoS ONE,* 5**,** e9505.

Steiner, D. F. 1998. The proprotein convertases. *Curr Opin Chem Biol,* 2**,** 31-9.

Stokin, G. B., Lillo, C., Falzone, T. L., Brusch, R. G., Rockenstein, E., Mount, S. L., Raman, R., Davies, P., Masliah, E., Williams, D. S. & Goldstein, L. S. 2005. Axonopathy and transport deficits early in the pathogenesis of Alzheimer's disease. *Science,* 307**,** 1282-8.

Strittmatter, W. J., Saunders, A. M., Schmechel, D., Pericak-Vance, M., Enghild, J., Salvesen, G. S. & Roses, A. D. 1993. Apolipoprotein E: high-avidity binding to beta-amyloid and increased frequency of type 4 allele in late-onset familial Alzheimer disease. *Proc Natl Acad Sci U S A,* 90**,** 1977-81.

Strittmatter, W. J., Weisgraber, K. H., Goedert, M., Saunders, A. M., Huang, D., Corder, E. H., Dong, L. M., Jakes, R., Alberts, M. J., Gilbert, J. R. & Et Al. 1994. Hypothesis: microtubule instability and paired helical filament formation in the Alzheimer disease brain are related to apolipoprotein E genotype. *Exp Neurol,* 125**,** 163-71; discussion 172-4.

Strömgren, E. 1981. Heredopathia ophthalmo-oto-encephalica. *In:* Vinken Pj & Bruyn Gw (eds.) *Handbook of clinical neurology.* Amsterdam: North-Holland Publishing Company.

Strömgren, E., Dalby, A., Dalby, M. A. & Ranheim, B. 1970. Cataract, deafness, cerebellar ataxia, psychosis and dementia--a new syndrome. *Acta Neurol Scand,* 46**,** Suppl 43:261+.

Sturchler-Pierrat, C., Abramowski, D., Duke, M., Wiederhold, K. H., Mistl, C., Rothacher, S., Ledermann, B., Burki, K., Frey, P., Paganetti, P. A., Waridel, C., Calhoun, M. E., Jucker, M., Probst, A., Staufenbiel, M. & Sommer, B. 1997. Two amyloid precursor protein transgenic mouse models with Alzheimer disease-like pathology. *Proc Natl Acad Sci U S A,* 94**,** 13287-92.

Sunderland, T., Hill, J. L., Mellow, A. M., Lawlor, B. A., Gundersheimer, J., Newhouse, P. A. & Grafman, J. H. 1989. Clock drawing in Alzheimer's disease. A novel measure of dementia severity. *J Am Geriatr Soc,* 37**,** 725-9.

Suzuki, N., Cheung, T. T., Cai, X. D., Odaka, A., Otvos, L., Jr., Eckman, C., Golde, T. E. & Younkin, S. G. 1994. An increased percentage of long amyloid beta protein secreted by familial amyloid beta protein precursor (beta APP717) mutants. *Science,* 264**,** 1336-40.

Sykes, P. A., Watson, S. J., Temple, J. S. & Bateman, R. C., Jr. 1999. Evidence for tissue-specific forms of glutaminyl cyclase. *FEBS Lett,* 455**,** 159-61.

Tabaton, M. & Piccini, A. 2005. Role of water-soluble amyloid-beta in the pathogenesis of Alzheimer's disease. *Int J Exp Pathol,* 86**,** 139-45.

Tabaton, M., Zhu, X., Perry, G., Smith, M. A. & Giliberto, L. 2010. Signaling effect of amyloid-beta(42) on the processing of AbetaPP. *Exp Neurol,* 221**,** 18-25.

Takahashi, R. H., Almeida, C. G., Kearney, P. F., Yu, F., Lin, M. T., Milner, T. A. & Gouras, G. K. 2004. Oligomerization of Alzheimer's beta-amyloid within processes and synapses of cultured neurons and brain. *J Neurosci,* 24**,** 3592-9.

Takashima, A. 2006. GSK-3 is essential in the pathogenesis of Alzheimer's disease. *J Alzheimers Dis,* 9**,** 309-17.

Takashima, A., Honda, T., Yasutake, K., Michel, G., Murayama, O., Murayama, M., Ishiguro, K. & Yamaguchi, H. 1998. Activation of tau protein kinase I/glycogen synthase kinase-3beta by amyloid beta peptide (25-35) enhances phosphorylation of tau in hippocampal neurons. *Neurosci Res,* 31**,** 317-23.

Tampellini, D., Magrane, J., Takahashi, R. H., Li, F., Lin, M. T., Almeida, C. G. & Gouras, G. K. 2007. Internalized antibodies to the Abeta domain of APP reduce neuronal Abeta and protect against synaptic alterations. *J Biol Chem,* 282**,** 18895-906.

Terman, A. & Brunk, U. T. 2006. Oxidative stress, accumulation of biological 'garbage', and aging. *Antioxid Redox Signal,* 8**,** 197-204.

Terwel, D., Muyllaert, D., Dewachter, I., Borghgraef, P., Croes, S., Devijver, H. & Van Leuven, F. 2008. Amyloid activates GSK-3beta to aggravate neuronal tauopathy in bigenic mice. *Am J Pathol,* 172**,** 786-98.

Tesseur, I., Van Dorpe, J., Bruynseels, K., Bronfman, F., Sciot, R., Van Lommel, A. & Van Leuven, F. 2000a. Prominent axonopathy and disruption of axonal transport in transgenic mice expressing human apolipoprotein E4 in neurons of brain and spinal cord. *Am J Pathol,* 157**,** 1495-510.

Tesseur, I., Van Dorpe, J., Spittaels, K., Van Den Haute, C., Moechars, D. & Van Leuven, F. 2000b. Expression of human apolipoprotein E4 in neurons causes hyperphosphorylation of protein tau in the brains of transgenic mice. *Am J Pathol,* 156**,** 951-64.

Thinakaran, G. & Koo, E. H. 2008. Amyloid precursor protein trafficking, processing, and function. *J Biol Chem,* 283**,** 29615-9.

Tokuda, T., Calero, M., Matsubara, E., Vidal, R., Kumar, A., Permanne, B., Zlokovic, B., Smith, J. D., Ladu, M. J., Rostagno, A., Frangione, B. & Ghiso, J. 2000. Lipidation of apolipoprotein E influences its isoform-specific interaction with Alzheimer's amyloid beta peptides. *Biochem J,* 348**,** 359-65.

Tomidokoro, Y., Lashley, T., Rostagno, A., Neubert, T. A., Bojsen-Moller, M., Braendgaard, H., Plant, G., Holton, J., Frangione, B., Revesz, T. & Ghiso, J. 2005. Familial Danish dementia: co-existence of Danish and Alzheimer amyloid subunits (ADan AND A{beta}) in the absence of compact plaques. *J Biol Chem,* 280**,** 36883-94.

Tomidokoro, Y., Tamaoka, A., Holton, J. L., Lashley, T., Frangione, B., Revesz, T., Rostagno, A. & Ghiso, J. 2010. Pyroglutamate formation at the N-termini of ABri molecules in familial British dementia is not restricted to the central nervous system. *Hirosaki Igaku,* 61**,** S262-S269.

Trommer, B. L., Shah, C., Yun, S. H., Gamkrelidze, G., Pasternak, E. S., Ye, G. L., Sotak, M., Sullivan, P. M., Pasternak, J. F. & Ladu, M. J. 2004. ApoE isoform affects LTP in human targeted replacement mice. *Neuroreport,* 15**,** 2655-8.

Tsachaki, M., Ghiso, J. & Efthimiopoulos, S. 2008. BRI2 as a central protein involved in neurodegeneration. *Biotechnol J,* 3**,** 1548-54.

Turner, P. R., O'connor, K., Tate, W. P. & Abraham, W. C. 2003. Roles of amyloid precursor protein and its fragments in regulating neural activity, plasticity and memory. *Prog Neurobiol,* 70**,** 1-32.

Uchihara, T., Duyckaerts, C., He, Y., Kobayashi, K., Seilhean, D., Amouyel, P. & Hauw, J. J. 1995. ApoE immunoreactivity and microglial cells in Alzheimer's disease brain. *Neurosci Lett,* 195**,** 5-8.

Vassar, R., Bennett, B. D., Babu-Khan, S., Kahn, S., Mendiaz, E. A., Denis, P., Teplow, D. B., Ross, S., Amarante, P., Loeloff, R., Luo, Y., Fisher, S., Fuller, J., Edenson, S., Lile, J., Jarosinski, M. A., Biere, A. L., Curran, E., Burgess, T., Louis, J. C., Collins, F., Treanor, J., Rogers, G. & Citron, M. 1999. Beta-secretase cleavage of Alzheimer's amyloid precursor protein by the transmembrane aspartic protease BACE. *Science,* 286**,** 735-41.

Venkataramani, V., Rossner, C., Iffland, L., Schweyer, S., Tamboli, I., Walter, J., Wirths, O. & Bayer, T. A. 2010. The histone deacetylase inhibitor valproic acid inhibits cancer cell proliferation via down-regulation of the Alzheimer amyloid precursor protein. *J Biol Chem,* 285**,** 10678-10689.

Vidal, R., Barbeito, A. G., Miravalle, L. & Ghetti, B. 2009. Cerebral amyloid angiopathy and parenchymal amyloid deposition in transgenic mice expressing the Danish mutant form of human BRI2. *Brain Pathol,* 19**,** 58-68.

Vidal, R., Calero, M., Revesz, T., Plant, G., Ghiso, J. & Frangione, B. 2001. Sequence, genomic structure and tissue expression of Human BRI3, a member of the BRI gene family. *Gene,* 266**,** 95-102.

Vidal, R., Frangione, B., Rostagno, A., Mead, S., Revesz, T., Plant, G. & Ghiso, J. 1999. A stop-codon mutation in the BRI gene associated with familial British dementia. *Nature,* 399**,** 776-81.

Vidal, R., Revesz, T., Rostagno, A., Kim, E., Holton, J. L., Bek, T., Bojsen-Moller, M., Braendgaard, H., Plant, G., Ghiso, J. & Frangione, B. 2000. A decamer duplication in the 3' region of the BRI gene originates an amyloid peptide that is associated with dementia in a Danish kindred. *Proc Natl Acad Sci U S A,* 97**,** 4920-5.

Vincent, B. & Smith, J. D. 2001. Astrocytes down-regulate neuronal beta-amyloid precursor protein expression and modify its processing in an apolipoprotein E isoform-specific manner. *Eur J Neurosci,* 14**,** 256-66.

Vorhees, C. V. & Williams, M. T. 2006. Morris water maze: procedures for assessing spatial and related forms of learning and memory. *Nat Protoc,* 1**,** 848-58.

Wahrle, S. E., Jiang, H., Parsadanian, M., Legleiter, J., Han, X., Fryer, J. D., Kowalewski, T. & Holtzman, D. M. 2004. ABCA1 is required for normal central nervous system ApoE levels and for lipidation of astrocyte-secreted apoE. *J Biol Chem,* 279**,** 40987-93.

Walsh, D. M., Tseng, B. P., Rydel, R. E., Podlisny, M. B. & Selkoe, D. J. 2000. The oligomerization of amyloid beta-protein begins intracellularly in cells derived from human brain. *Biochemistry,* 39**,** 10831-9.

Wang, C., Wilson, W. A., Moore, S. D., Mace, B. E., Maeda, N., Schmechel, D. E. & Sullivan, P. M. 2005. Human apoE4-targeted replacement mice display synaptic deficits in the absence of neuropathology. *Neurobiol Dis,* 18**,** 390-8.

Wang, Y. & Ha, Y. 2004. The X-ray structure of an antiparallel dimer of the human amyloid precursor protein E2 domain. *Mol Cell,* 15**,** 343-53.

Watts, J. C., Giles, K., Grillo, S. K., Lemus, A., Dearmond, S. J. & Prusiner, S. B. 2011. Bioluminescence imaging of Abeta deposition in bigenic mouse models of Alzheimer's disease. *Proc Natl Acad Sci U S A,* 108**,** 2528-33.

Weisgraber, K. H. 1990. Apolipoprotein E distribution among human plasma lipoproteins: role of the cysteine-arginine interchange at residue 112. *J Lipid Res,* 31**,** 1503-11.

Weisgraber, K. H. 1994. Apolipoprotein E: structure-function relationships. *Adv Protein Chem,* 45**,** 249-302.

Weller, R. O., Massey, A., Newman, T. A., Hutchings, M., Kuo, Y. M. & Roher, A. E. 1998. Cerebral amyloid angiopathy: amyloid beta accumulates in putative interstitial fluid drainage pathways in Alzheimer's disease. *Am J Pathol,* 153**,** 725-33.

Wellnitz, S., Friedlein, A., Bonanni, C., Anquez, V., Goepfert, F., Loetscher, H., Adessi, C. & Czech, C. 2005. A 13 kDa carboxy-terminal fragment of ApoE stabilizes Abeta hexamers. *J Neurochem,* 94**,** 1351-60.

Winton, M. J., Lee, E. B., Sun, E., Wong, M. M., Leight, S., Zhang, B., Trojanowski, J. Q. & Lee, V. M. 2011. Intraneuronal APP, Not Free A{beta} Peptides in 3xTg-AD Mice: Implications for Tau versus A{beta}-Mediated Alzheimer Neurodegeneration. *J Neurosci,* 31**,** 7691-9.

Wirths, O. & Bayer, T. A. 2008. Early intraneuronal beta-amyloid pathology: Do transgenic mice represent valid model systems? *The Open Aging Journal,* 2**,** 7-12.

Wirths, O. & Bayer, T. A. 2010. Neuron loss in transgenic mouse models of Alzheimer's disease. *Int J Alzheimers Dis,* 2010**,** 723782.

Wirths, O., Bethge, T., Marcello, A., Harmeier, A., Jawhar, S., Lucassen, P. J., Multhaup, G., Brody, D. L., Esparza, T., Ingelsson, M., Kalimo, H., Lannfelt, L. & Bayer, T. A. 2010a. Pyroglutamate Abeta pathology in APP/PS1KI mice, sporadic and familial Alzheimer's disease cases. *J Neural Transm,* 117**,** 85-96.

Wirths, O., Breyhan, H., Cynis, H., Schilling, S., Demuth, H. U. & Bayer, T. A. 2009. Intraneuronal pyroglutamate-Abeta 3-42 triggers neurodegeneration and lethal neurological deficits in a transgenic mouse model. *Acta Neuropathol,* 118**,** 487-496.

Wirths, O., Breyhan, H., Schafer, S., Roth, C. & Bayer, T. A. 2008. Deficits in working memory and motor performance in the APP/PS1ki mouse model for Alzheimer's disease. *Neurobiol Aging,* 29**,** 891-901.

Wirths, O., Dins, A. & Bayer, T. A. 2012. AbetaPP accumulation and/or intraneuronal amyloid-beta accumulation? The 3xTg-AD mouse model revisited. *J Alzheimers Dis,* 28**,** 897-904.

Wirths, O., Erck, C., Martens, H., Harmeier, A., Geumann, C., Jawhar, S., Kumar, S., Multhaup, G., Walter, J., Ingelsson, M., Degerman-Gunnarsson, M., Kalimo, H., Huitinga, I., Lannfelt, L. & Bayer, T. A. 2010b. Identification of low molecular weight pyroglutamate abeta oligomers in Alzheimer disease: a novel tool for therapy and diagnosis. *J Biol Chem,* 285**,** 41517-24.

Wirths, O., Multhaup, G. & Bayer, T. A. 2004. A modified beta-amyloid hypothesis: intraneuronal accumulation of the beta-amyloid peptide - the first step of a fatal cascade. *J Neurochem,* 91**,** 513-20.

Wirths, O., Thelen, K. M., Lutjohann, D., Falkai, P. & Bayer, T. A. 2007a. Altered cholesterol metabolism in APP695-transfected neuroblastoma cells. *Brain Res,* 1152**,** 209-14.

Wirths, O., Weis, J., Kayed, R., Saido, T. C. & Bayer, T. A. 2007b. Age-dependent axonal degeneration in an Alzheimer mouse model. *Neurobiol Aging,* 28**,** 1689-1699.

Wirths, O., Weis, J., Szczygielski, J., Multhaup, G. & Bayer, T. A. 2006. Axonopathy in an APP/PS1 transgenic mouse model of Alzheimer's disease. *Acta Neuropathol,* 111**,** 312-9.

Wisniewski, T., Castano, E. M., Golabek, A., Vogel, T. & Frangione, B. 1994. Acceleration of Alzheimer's fibril formation by apolipoprotein E in vitro. *Am J Pathol,* 145**,** 1030-5.

Wittnam, J. L., Portelius, E., Zetterberg, H., Gustavsson, M. K., Schilling, S., Koch, B., Demuth, H. U., Blennow, K., Wirths, O. & Bayer, T. A. 2012. Pyroglutamate amyloid beta (Abeta) aggravates behavioral deficits in transgenic amyloid mouse model for Alzheimer disease. *J Biol Chem,* 287**,** 8154-62.

Worster-Drought, C., Hill, T. R. & Mcmenemey, W. H. 1933. Familial Presenile Dementia with Spastic Paralysis. *J Neurol Psychopathol,* 14**,** 27-34.

Xu, Q., Bernardo, A., Walker, D., Kanegawa, T., Mahley, R. W. & Huang, Y. 2006. Profile and regulation of apolipoprotein E (ApoE) expression in the CNS in mice with targeting of green fluorescent protein gene to the ApoE locus. *J Neurosci,* 26**,** 4985-94.

Yang, D. S., Stavrides, P., Mohan, P. S., Kaushik, S., Kumar, A., Ohno, M., Schmidt, S. D., Wesson, D., Bandyopadhyay, U., Jiang, Y., Pawlik, M., Peterhoff, C. M., Yang, A. J., Wilson, D. A., St George-Hyslop, P., Westaway, D., Mathews, P. M., Levy, E., Cuervo, A. M. & Nixon, R. A. 2011. Reversal of autophagy dysfunction in the TgCRND8 mouse model of Alzheimer's disease ameliorates amyloid pathologies and memory deficits. *Brain,* 134**,** 258-77.

Yao, Z. X. & Papadopoulos, V. 2002. Function of beta-amyloid in cholesterol transport: a lead to neurotoxicity. *Faseb J,* 16**,** 1677-9.

Ye, S., Huang, Y., Mullendorff, K., Dong, L., Giedt, G., Meng, E. C., Cohen, F. E., Kuntz, I. D., Weisgraber, K. H. & Mahley, R. W. 2005. Apolipoprotein (apo) E4 enhances amyloid beta peptide production in cultured neuronal cells: apoE structure as a potential therapeutic target. *Proc Natl Acad Sci U S A,* 102**,** 18700-5.

Yoshiyama, Y., Higuchi, M., Zhang, B., Huang, S. M., Iwata, N., Saido, T. C., Maeda, J., Suhara, T., Trojanowski, J. Q. & Lee, V. M. 2007. Synapse loss and microglial activation precede tangles in a P301S tauopathy mouse model. *Neuron,* 53**,** 337-51.

Yu, W. H., Cuervo, A. M., Kumar, A., Peterhoff, C. M., Schmidt, S. D., Lee, J. H., Mohan, P. S., Mercken, M., Farmery, M. R., Tjernberg, L. O., Jiang, Y., Duff, K., Uchiyama, Y., Naslund, J., Mathews, P. M., Cataldo, A. M. & Nixon, R. A. 2005. Macroautophagy--a novel Beta-amyloid peptide-generating pathway activated in Alzheimer's disease. *J Cell Biol,* 171**,** 87-98.

Zheng, H. & Koo, E. H. 2006. The amyloid precursor protein: beyond amyloid. *Mol Neurodegener,* 1**,** 5.

Zhou, J., Chen, J. & Feng, Y. 2006a. Effect of truncated-ApoE4 overexpression on tau phosphorylation in cultured N2a cells. *J Huazhong Univ Sci Technolog Med Sci,* 26**,** 272-4.

Zhou, S., Zhou, H., Walian, P. J. & Jap, B. K. 2006b. The discovery and role of CD147 as a subunit of gamma-secretase complex. *Drug News Perspect,* 19**,** 133-8.

Zhou, W., Scott, S. A., Shelton, S. B. & Crutcher, K. A. 2006c. Cathepsin D-mediated proteolysis of apolipoprotein E: possible role in Alzheimer's disease. *Neuroscience,* 143**,** 689-701.

Zlokovic, B. V., Deane, R., Sallstrom, J., Chow, N. & Miano, J. M. 2005. Neurovascular pathways and Alzheimer amyloid beta-peptide. *Brain Pathol,* 15**,** 78-83.

Zou, K., Gong, J. S., Yanagisawa, K. & Michikawa, M. 2002. A novel function of monomeric amyloid beta-protein serving as an antioxidant molecule against metal-induced oxidative damage. *J Neurosci,* 22**,** 4833-41.

Curriculum vitae

Name:	Anika Saul
Email:	anika_saul@yahoo.de
Place of birth:	Heilbad Heiligenstadt, Germany
Date of birth:	21.03.1986
Citizenship:	German

Education

2009 – 2013	University Medical Center Göttingen, Germany Department of Molecular Psychiatry Ph.D. thesis
2009 – 2013	Georg-August-University, Göttingen, Germany International Ph.D. program "Molecular Medicine"
2004 – 2009	Biology studies at the Georg-August-University, Göttingen, Germany Degree: Diploma (grade: very good)
1996 – 2004	Gymnasium „Johann Georg Lingemann", Heilbad Heiligenstadt, Germany Degree: Abitur

Publications

Conference contributions

Saul A., Martinelli G.P. & Reischig T. (2009): Evidence for nitric oxide/cyclic guanosine monophosphate (NO/cGMP) signalling in circadian clock neurons of the cockroach *Leucophaea maderae.* In: Bähr, M. & Zerr, I. (eds.) Proceedings of the 8th Göttingen meeting of the German Neuroscience Society/32nd Göttingen neurobiology conference, Germany.

Reischig T. & **Saul A.** (2008): Nitric oxide/cyclic guanosine monophosphate (NO/cGMP) signalling in the circadian rhythm generating mechanism of the cockroach *Leucophaea maderae.* 6th FENS Forum of European Neuroscience, FENS. Genf, Switzerland.

Saul A., Lashley T., Revesz T., Ghiso J., Coomaraswamy J., Bayer T.A. & Wirths O. (2011): Analysis of pyroglutamate-modified amyloid peptides in Familial British and Familial Danish dementia. 10th International Conference AD/PD[TM]. Barcelona, Spain.

Wirths O., Bayer T.A. & **Saul A.** (2013): ApoE Fragmentation is linked to Neuritic Dystrophy in Transgenic Mouse Models of Alzheimer's Disease. 11th International Conference AD/PD[TM]. Florenz, Italy.

Journal articles

Saul, A., Lashley, T., Revesz, T., Holton, J., Ghiso, J. A., Coomaraswamy, J. & Wirths, O. 2013. Abundant pyroglutamate-modified ABri and ADan peptides in extracellular and vascular amyloid deposits in familial British and Danish dementias. *Neurobiol Aging*, 34, 1416-25.

Härtig, W., **Saul, A.**, Kacza, J., Grosche, J., Goldhammer, S., Michalski, D. & Wirths, O. 2013. Immunolesion-induced loss of cholinergic projection neurons promotes beta-amyloidosis and tau hyperphosphorylation in the hippocampus of triple-transgenic mice. *Neuropathol Appl Neurobiol*, 9, 12050.

Saul, A., Sprenger, F., Bayer, T. A. & Wirths, O. 2013. Accelerated tau pathology with synaptic and neuronal loss in a novel triple transgenic mouse model of Alzheimer's disease. *Neurobiol Aging*, 5, 201-7.

Göttingen, April 2013